(2)

NAVAL POSTGRADUATE SCHOOL
Monterey, California

THESIS

DETERMINATION OF SPEAR-1 ROCKET BODY POTENTIAL DURING HIGH-VOLTAGE EXPERIMENTS

by

Thurston Van Horn

June 1990

Thesis Advisor: R. C. Olsen

Unclassified

SECURITY CLASSIFICATION OF THIS PAGE

REPORT DOCUMENTATION PAGE

Form Approved OMB No. 0704-0188

1. REPORT SECURITY CLASSIFICATION: Unclassified	1b. RESTRICTIVE MARKINGS
2a. SECURITY CLASSIFICATION AUTHORITY	3. DISTRIBUTION/AVAILABILITY OF REPORT: Approved for public release; distribution is unlimited
2b. DECLASSIFICATION/DOWNGRADING SCHEDULE	
4. PERFORMING ORGANIZATION REPORT NUMBER(S)	5. MONITORING ORGANIZATION REPORT NUMBER(S)
6a. NAME OF PERFORMING ORGANIZATION: Naval Postgraduate School; 6b. OFFICE SYMBOL (If applicable): 39	7a. NAME OF MONITORING ORGANIZATION: Naval Postgraduate School
6c. ADDRESS (City, State, and ZIP Code): Monterey, CA 93943-5000	7b. ADDRESS (City, State, and ZIP Code): Monterey, CA 93943-5000
8a. NAME OF FUNDING/SPONSORING ORGANIZATION; 8b. OFFICE SYMBOL (If applicable)	9. PROCUREMENT INSTRUMENT IDENTIFICATION NUMBER
8c. ADDRESS (City, State, and ZIP Code)	10. SOURCE OF FUNDING NUMBERS: PROGRAM ELEMENT NO. / PROJECT NO. / TASK NO. / WORK UNIT ACCESSION NO.

11. TITLE (Include Security Classification)
Determination of SPEAR-1 Rocket Body Potential During High-Voltage Experiments

12. PERSONAL AUTHOR(S)
Thurston Van Horn

13a. TYPE OF REPORT	13b. TIME COVERED	14. DATE OF REPORT (Year, Month, Day)	15. PAGE COUNT
Master's Thesis	FROM _____ TO _____	June 1990	

16. SUPPLEMENTARY NOTATION
The views expressed in this thesis are those of the author and do not reflect the official policy or position of the Department of Defense or the U.S. Government.

17. COSATI CODES			18. SUBJECT TERMS (Continue on reverse if necessary and identify by block number)
FIELD	GROUP	SUB-GROUP	
			SPEAR-1, Spacecraft Charging, Altitude Effects, Geomagnetic Orientation Effects, Electrostatic Analyzer, Attitude Control System Gas Emissions. Theses. (RH)

19. ABSTRACT (Continue on reverse if necessary and identify by block number)

The Space Power Experiment Aboard Rockets (SPEAR) 1 payload was launched on December 13, 1987. It had a primary objective of providing guidelines in designing high-voltage (HV) systems for use in Low-Earth Orbit (LEO). The experiment consisted of 24 HV bias operations using two 20 cm diameter spheres attached to the rocket by booms. The SPEAR-1 rocket charged to substantial negative potentials during the flight when the spheres were biased positive with respect to the rocket. This thesis uses the electrostatic analyzer ion data to determine the charging response of the rocket body. The peak potential was reached during a 45 kV sphere bias sequence resulting in a -17.4 kV rocket body potential at 361 km altitude. The rocket body potential varied between 7 and 38 percent of sphere potential. Geomagnetic orientation, vice altitude, had greater effect on rocket body potential. The flight data also indicated that neutral gas emissions from the rocket attitude control system (ACS) triggered transient discharge currents that effectively grounded the rocket body potential. ACS firings resulted in an order of magnitude change in the rocket body potential.

20. DISTRIBUTION/AVAILABILITY OF ABSTRACT	21. ABSTRACT SECURITY CLASSIFICATION	
X UNCLASSIFIED/UNLIMITED ☐ SAME AS RPT. ☐ DTIC USERS	Unclassified	
22a. NAME OF RESPONSIBLE INDIVIDUAL: Richard C. Olsen	22b. TELEPHONE (Include Area Code): (408) 646-2019	22c. OFFICE SYMBOL: PH/Os

DD Form 1473, JUN 86 — Previous editions are obsolete — SECURITY CLASSIFICATION OF THIS PAGE: Unclassified

Approved for public release; distribution is unlimited.

Determination of SPEAR-1 Rocket Body Potential During High-Voltage Experiments

by

Thurston Van Horn
Captain, United States Army
B.S., U.S. Military Academy, 1979

Submitted in partial fulfillment of the requirements for the degree of

MASTER OF SCIENCE IN PHYSICS

from the

NAVAL POSTGRADUATE SCHOOL
June 1990

Author: Thurston Van Horn
Thurston Van Horn

Approved by:
R. C. Olsen, Thesis Advisor

S. Gnanalingham, Second Reader

K. E. Woehler, Chairman,
Department of Physics

ABSTRACT

The Space Power Experiment Aboard Rockets (SPEAR) 1 payload was launched on December 13, 1987. It had a primary objective of providing guidelines in designing high-voltage (HV) systems for use in Low-Earth Orbit (LEO). The experiment consisted of 24 HV bias operations using two 20 cm diameter spheres attached to the rocket by booms. The SPEAR-1 rocket charged to substantial negative potentials during the flight when the spheres were biased positive with respect to the rocket. This thesis uses the electrostatic analyzer ion data to determine the charging response of the rocket body. The peak potential was reached during a 45 kV sphere bias sequence resulting in a -17.4 kV rocket body potential at 361 km altitude. The rocket body potential varied between 7 and 38 percent of sphere potential. Geomagnetic orientation, vice altitude, had greater effect on rocket body potential. The flight data also indicated that neutral gas emissions from the rocket attitude control system (ACS) triggered transient discharge currents that effectively grounded the rocket body potential. ACS firings resulted in an order of magnitude change in the rocket body potential.

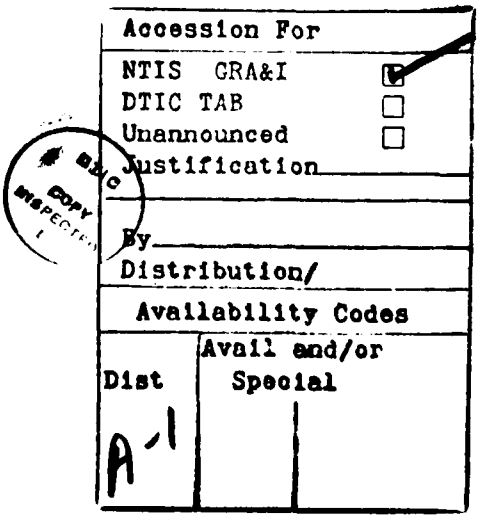

TABLE OF CONTENTS

LIST OF TABLES

LIST OF FIGURES

ACKNOWLEDGMENTS

The author expresses his appreciation to Professor R. C. Olsen, whose scholarly advice and expertise in graphical computer analysis made this work possible.

The author also wishes to thank Dr. Roy Torbert, Dr. Craig Kletzing, and Mr. David Rau (UNH), who provided the SPEAR particle detectors and information on the particle detector operation. Mr. Gerald Larson (UAH) provided useful software aid early in the project.

The principal investigator for SPEAR-1 was Dr. W. John Raitt (Utah State University). Support for this work was provided by DNA.

I. BACKGROUND

A. OVERVIEW

During the past decade, the trend in the design and development of satellites and other space-based platforms has been to design large vehicles with high power requirements. Interest in the charging of vehicles in the lower ionosphere has increased because of the desire to use this type of space vehicle in Low Earth Orbit (LEO).The planned space station and space platforms for use in the Strategic Defense Initiative are two applications of high-voltage pulsed power systems desired for use in LEO.

In order to gain some scientific data that could be used to provide guidelines in the design of high-voltage (HV) power systems, the Space Power Experiments Aboard Rockets (SPEAR) program began in December 1986. The SPEAR program was initiated by the Strategic Defense Initiative Office, Innovative Science and Technology Division, and was organized into three research groups:

1. Theoretical modeling
2. Ground-based laboratory (vacuum chamber)
3. Flight experiments utilizing sounding rockets to carry experiments into the LEO environment

The SPEAR program authorized two space flights, designated SPEAR-1 and SPEAR-2. SPEAR-1 was launched on December 13, 1987, and SPEAR-2 is currently scheduled for launch on July 16, 1990 [Ref. 1:p. 1]. This thesis uses the particle detector data from the SPEAR-1 experiment.

B. PREVIOUS RESULTS

Previous experiments performed in the lower ionosphere used an electron beam to study the processes that occur when high potentials are exposed to the space environment [Ref. 2:p. 1]. These experiments tended to complicate the interpretation of the process and could change the current collection characteristics of the beam-emitting vehicle [Ref. 2:p. 4].

A more recent experiment (conducted in December 1985) was the cooperative high-altitude rocket gun experiment (CHARGE) 2. This rocket had an electron beam-emitting mother payload electronically tethered to an ejected daughter payload. Its major goal was "...to measure payload charging and return currents during periods of electron emission." [Ref. 3:p. 2469] One result from CHARGE 2 indicated that an electrical discharge occurred in the vicinity of the daughter payload. The discharge was believed to be caused by nitrogen gas emissions from the daughter's combined thruster and rate control system (TRCS). [Ref. 3:p. 2469]

C. THE SPEAR-1 ROCKET

The short development time of the SPEAR-1 rocket (December 1986–December 1987) required a design philosophy which would keep the payload simple but sophisticated enough to accomplish its scientific objectives. The designers wanted to avoid the use of sophisticated microprocessor control and to utilize previously developed diagnostic instruments to reduce the development and component integration time.

> The major challenge was to develop a HV power supply capable of generating 10s of kV and delivering 10s of amperes for short periods while still conforming to the volume and weight restrictions imposed by the capabilities of a Black Brant 10 sounding rocket and the requirement to reach an apogee exceeding 300 km. [Ref. 1:p. 2]

This design philosophy resulted in a simple but very effective design for SPEAR-1. The experiment design included two spherical conductors that were separated from the rocket body by a fiberglass boom. Figure 1 shows a general configuration of the rocket instruments and subsystems [Ref. 1:fig. 3-1]. The two spheres were .2 m in diameter and were made from aluminum and plated with gold over nickel. A spherical design was chosen for the conductors in order to provide a means of comparison of current collection from a space plasma with known analytic models. [Ref. 2:p. 2].

The upper portion of the boom that separated the two spheres utilized a grading ring structure to ensure a uniform potential drop from the spheres to the main portion of the boom that was maintained at the rocket body potential. The rings prevented a large change in the potential occurring over a short distance, thereby keeping the voltage below the threshold for arcing. The grading rings were spun from aluminum sheet and nickel plated. When mounted on the fiberglass support, they comprised a series of 46 shallow, saucer-shaped rings connected together by resistors to provide the needed uniformity of potential. The total resistance provided by the grading ring structure was 1.1 MΩ to sphere 1 and 980 kΩ to sphere 2. The difference was due to the different lengths of the booms necessary to accommodate the spheres in their stowed, predeployment configuration. [Ref. 1:p. 4]

To accommodate the instruments and other subsystems necessary to conduct the experiment, the equipment was engineered into three

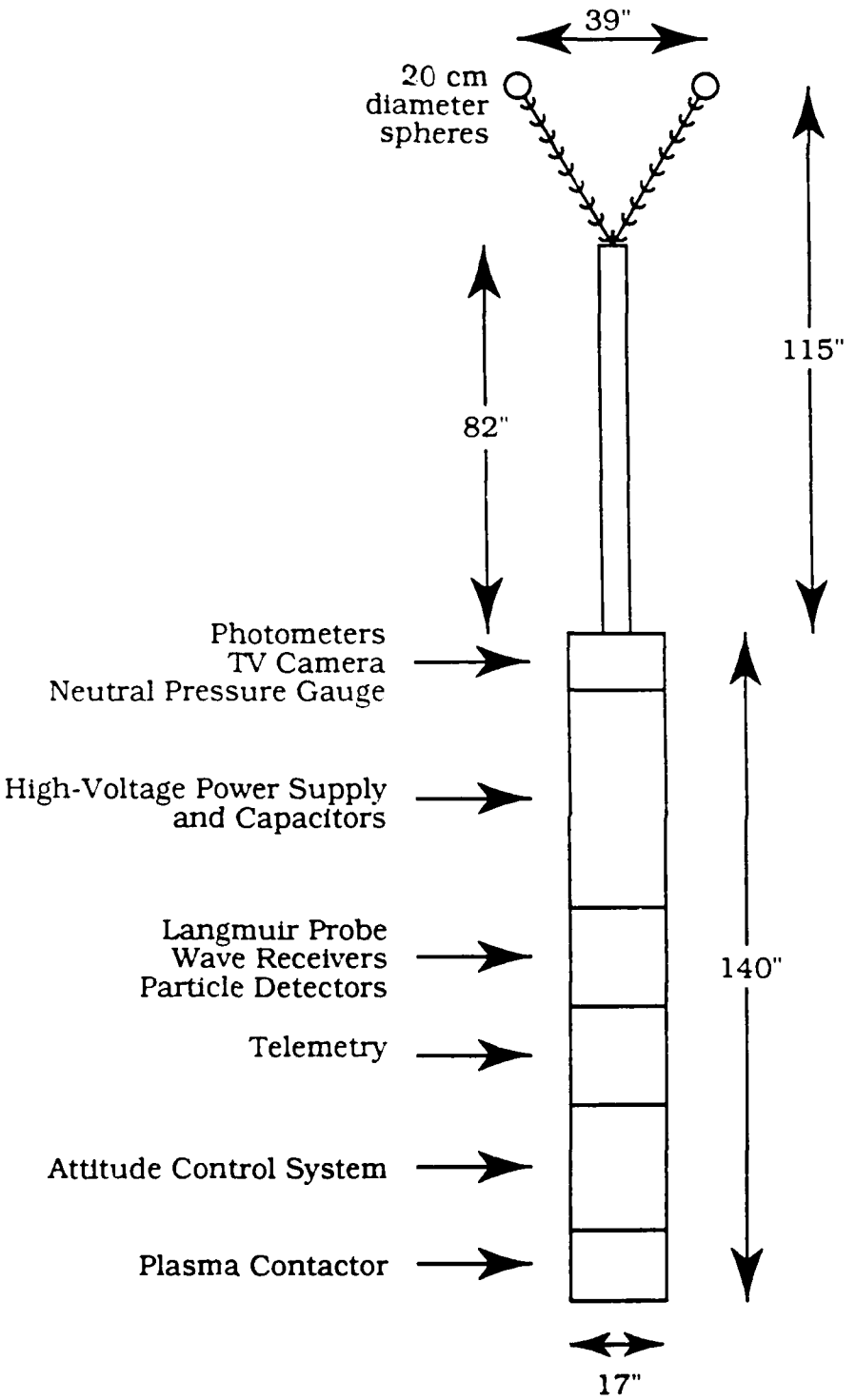

Figure 1. **SPEAR-1 Rocket Configuration**

sections. The first section housed the diagnostic equipment including photometers, low-light TV cameras, neutral pressure gage, the high-voltage power supply and capacitors, Langmuir probe, wave receivers, and the particle detectors. The specific instruments and data obtained for use in this thesis will be described in the next section. The high-voltage power supply and capacitors were sealed and filled with sulphur hexaflouride to maintain a pressure of one atmosphere for the duration of the flight. The surrounding diagnostic instruments were evacuated during the rocket ascent, exposing them to the ambient pressure.

The second section of the rocket body housed the attitude control system (ACS) and the telemetry section. The ACS was used to orient the spheres in three different positions relative to the geomagnetic field. The different orientations allowed magnetic effects of the HV interaction to be analyzed. Figure 2 shows the orientation of the spheres with respect to the geomagnetic field. The near-perpendicular orientation was from a line joining the spheres to the rocket body axis. [Ref. 2:fig. 4]

The third section of the rocket body consisted of a hollow cathode plasma contactor that used argon as the operating gas. The purpose of the plasma contactor was to clamp the rocket body potential near the plasma potential during the voltage bias operations. It was located at the end of the rocket away from the spheres to minimize any contamination to the sphere environment. The plate covering the plasma contactor was to have been pulled away after separation of the third stage booster. Unfortunately, the cover plate jammed during the separation, preventing

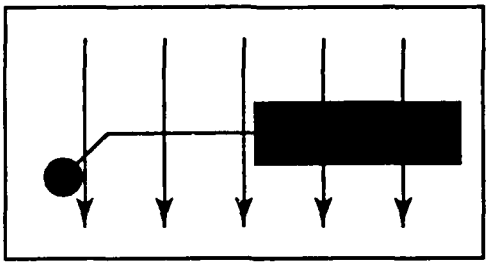

Position 1. Near Perpendicular

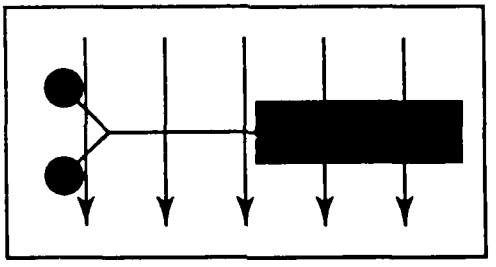

Position 2. V-Plane of Booms Parallel

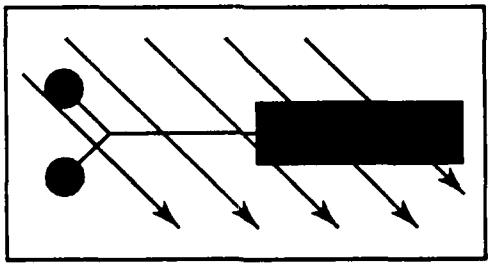

Position 3. Boom of Sphere 1 Parallel

Figure 2. **Geomagnetic Field Orientations**

the plasma source from being exposed to the ionosphere. Due to this failure, the rocket body charged to high negative potentials that generated sheaths that modified the charge sheaths of the spheres. This made comparisons with the previously mentioned analytic models less meaningful. [Ref. 2:p. 1]

D. THE INSTRUMENTS

The prime instrumentation for the SPEAR-1 experiment was the electronics which measured the currents and voltages on the spheres and booms [Ref. 1:p. 3]. The current and voltage measurements were supplemented by the other diagnostic instruments mentioned in the previous section.

The analysis conducted in this paper utilizes the data collected from the ion and electron detectors located on the rocket body. Four imaging ion and electron detectors were utilized to monitor the energetic ion and electron fluxes. The detectors measured particles with energies of 10 eV to 30 keV at several different view directions relative to the axes of the instruments. Previous rocket flights used detectors that were devoted to single pitch angles. This was a major shortcoming in that many pitch angles could not be measured. SPEAR-1 eliminated this problem by using a new design which measured 0- to 180-degree pitch angle simultaneously. These detectors were provided to the SPEAR project by Dr. Roy Torbert, University of Alabama, Huntsville. [Ref. 4]

The instrument spectra were generated by sweeping over the particle energy range in 32 steps, each step being held for 1 ms. This provided particle spectra with a 32 ms time resolution. A total of 26 telemetry

channels were assigned to the four particle detectors, which were arranged in two groups of two with their axes of symmetry viewing in opposite directions. Figure 3 shows a simple diagram of the particle detector orientation with respect to the rocket body. Within the detector, the sensor pads were assigned alphanumeric codes (4A, 4B, 5A, etc.) that identified each pad's position on the detector. Each of these positions corresponded to a particular view direction and was assigned one of the 26 channels. The fields of view of each look direction were approximately 5° in the polar and 10° in the azimuthal direction. The geometric factor of the detectors was 1.35×10^{-4} $cm^2 \bullet str \bullet eV/eV$, and their energy bandwidth was 11 percent [Ref. 1:p. 20; Ref. 5]. Figure 4 is a simple schematic of the detector just described. It shows a typical particle trajectory corresponding to the view direction of 56°. Particles entering from this direction pass through the view window and impact on the 5A sensor pad. [Ref. 4]

E. CHAMBER TESTS

To prepare for the SPEAR-1 flight, a series of vacuum chamber experiments was performed on mock-ups of the boom and rocket. The tests were conducted at the University of Maryland plasma chamber facility and the B-2 chamber at NASA-Lewis Plum Brook Station.

> The principal purpose of the test was to verify the high voltage engineering and ensure that no unexpected discharges or arcs occurred in the high voltage wiring that was exposed to the ambient vacuum environment. [Ref. 1:p. 16].

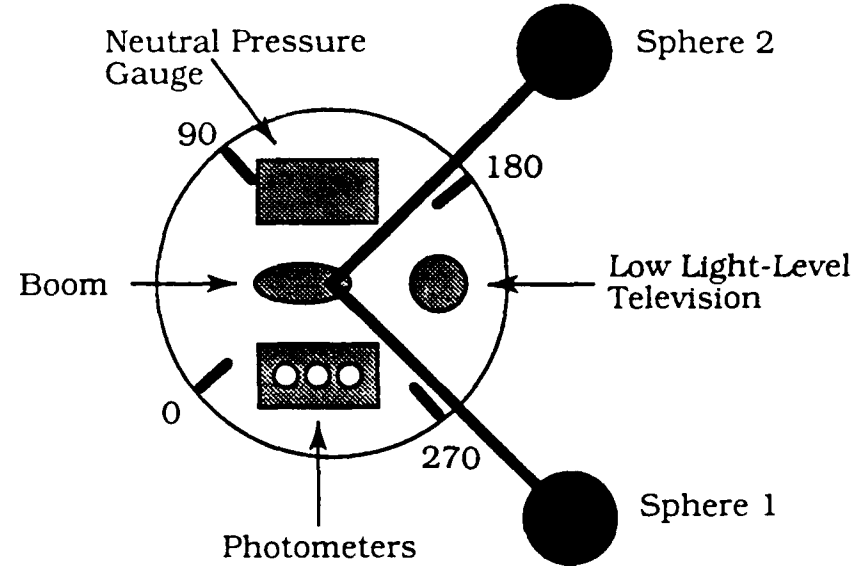

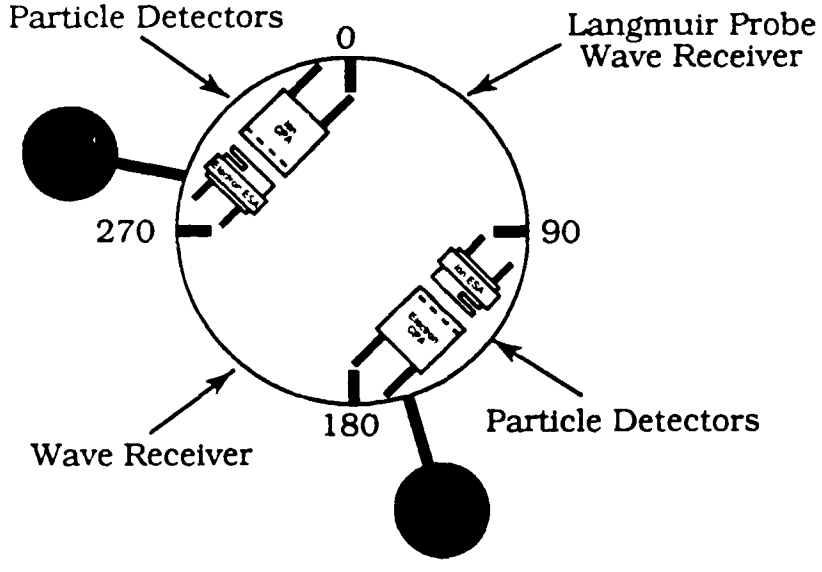

Figure 3. **Particle Detector Orientations**

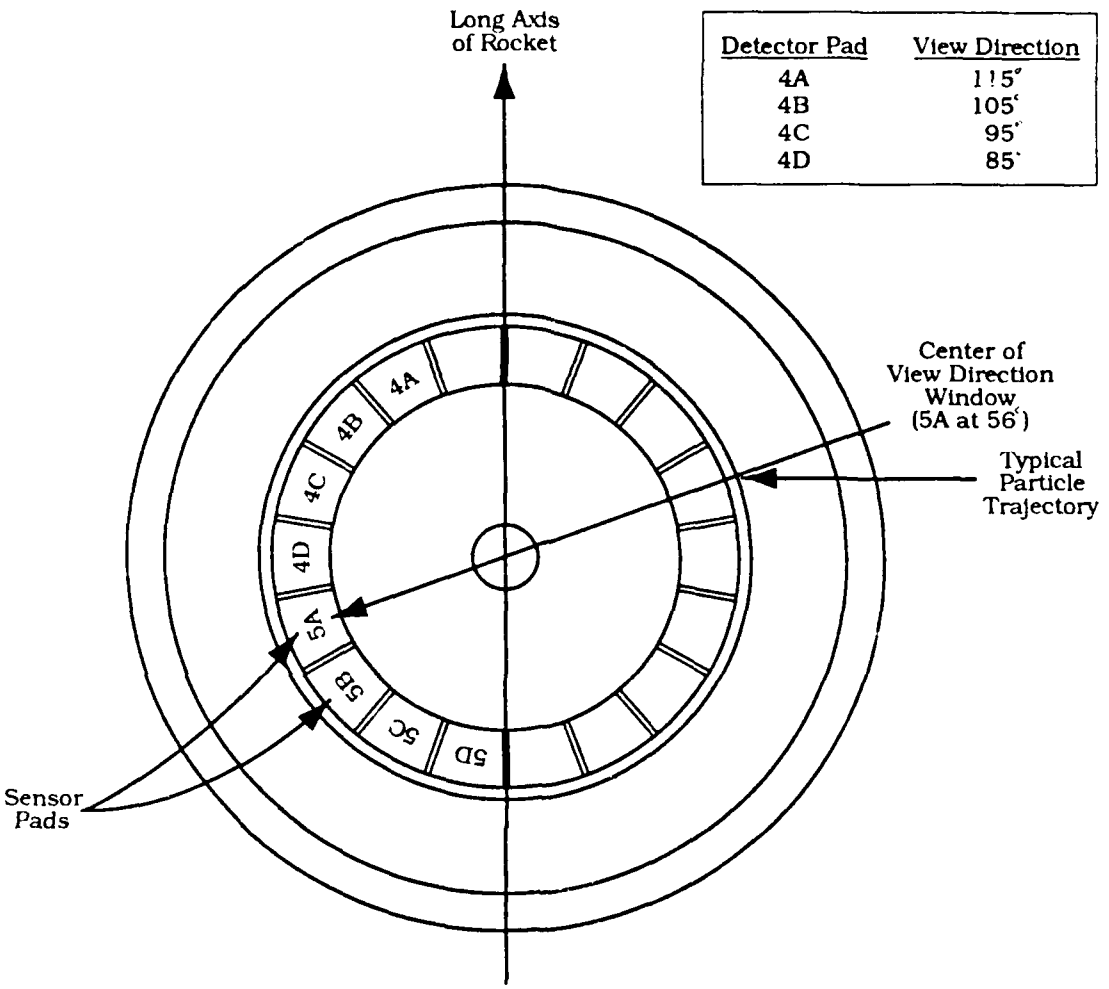

Figure 4. **Sensor Pad Orientation**

The chamber tests showed that a series of breakdowns occurred between the spheres and the walls of the vacuum chamber. "The presence of the chamber walls, coupled with the existence of a weak magnetic field, produced severe breakdowns at ionospheric plasma conditions, even at very low pressures of neutral gasses." [Ref. 6:p. 1389] The chamber tests showed that the experiment would survive arcing but did not provide a completely relevant scientific baseline for flight.

Additional research on the SPEAR-1 and other high-voltage tests shows that breakdowns are to be expected in vacuum chambers. "They indicate that in any large space simulation chambers, electrical breakdown is likely to occur whenever voltages of more than a few kilovolts are applied...." [Ref. 1:p. 6152]

F. FLIGHT OPERATIONS

SPEAR-1 was launched at 20:45 EST on December 13, 1987. The launch took place at the NASA Wallops Flight Facility in Virginia. A summary of key events during the flight sequence is provided in Table 1 [Ref. 1:p. 21]. As shown in Table 1, the rocket reached an apogee of 369 km at 350 seconds mission elapsed time (MET). The HV system was activated at +179 MET and then operated on its own timer. Twenty-four voltage bias operations were performed between 191 and 622 seconds. The bias operations are shown graphically in Figure 5. The voltage bias of sphere 1 is annotated above the trajectory and that of sphere 2 is below the trajectory. As shown in Figure 2, the ACS placed the spheres into three different orientations with respect to the geomagnetic field. These maneuvers and their respective orientations are also indicated in Figure 5. [Ref. 2:fig. 5]

G. FLIGHT RESULTS

SPEAR-1 was successful in its primary technical and programmatic goal—the successful application of bias voltages up to 45 kV between

TABLE 1

SPEAR-1 FLIGHT SEQUENCE

Event	Time (seconds)	Alt (km)	Function
1	-600	0.0	ACS External
2	-180	0.0	Uncage Gyro– Slew Launcher
3	-120	0.0	ACS Internal
4	0	0.0	Terrier Ignition
5	+4.4	0.7	Terrier Burn-Out
6	+12	3.0	Second-Stage Ignition
7	+44.4	28.6	Second-Stage Burn-Out
8	+88	80.2	Second-Stage Separation
9	+93	85.0	Third Stage Ignition
10	+110	113.2	Third Stage Burn-Out
11	+113	119.4	Third Stage & Payload Despin
12	+115	123.6	Third Stage Separation
13	+116	125.6	LP and Wave Receiver Doors Eject
14	+117	127.7	Particle Detector Doors Eject
15	+118	129.7	Wave Receiver Booms Deploy
16	+129	151.6	ACS Position 1
17	+149	188.7	Nose Cone Eject
18	+151	192.2	ACS Position 2
19	+160	207.6	Part Detector HV On
20	+171	225.5	HV Booms Deploy, NPG Uncover
21	+179	237.8	HV Experiment On
22	+350	369.2	Apogee
23	+403	358.5	Second-Stage Impact
24	+405	357.6	ACS Position 3
25	+518	251.7	ACS Position 4
26	+601	103.4	Payload Starts Re-Entry
27	+641	0.0	Payload Impact

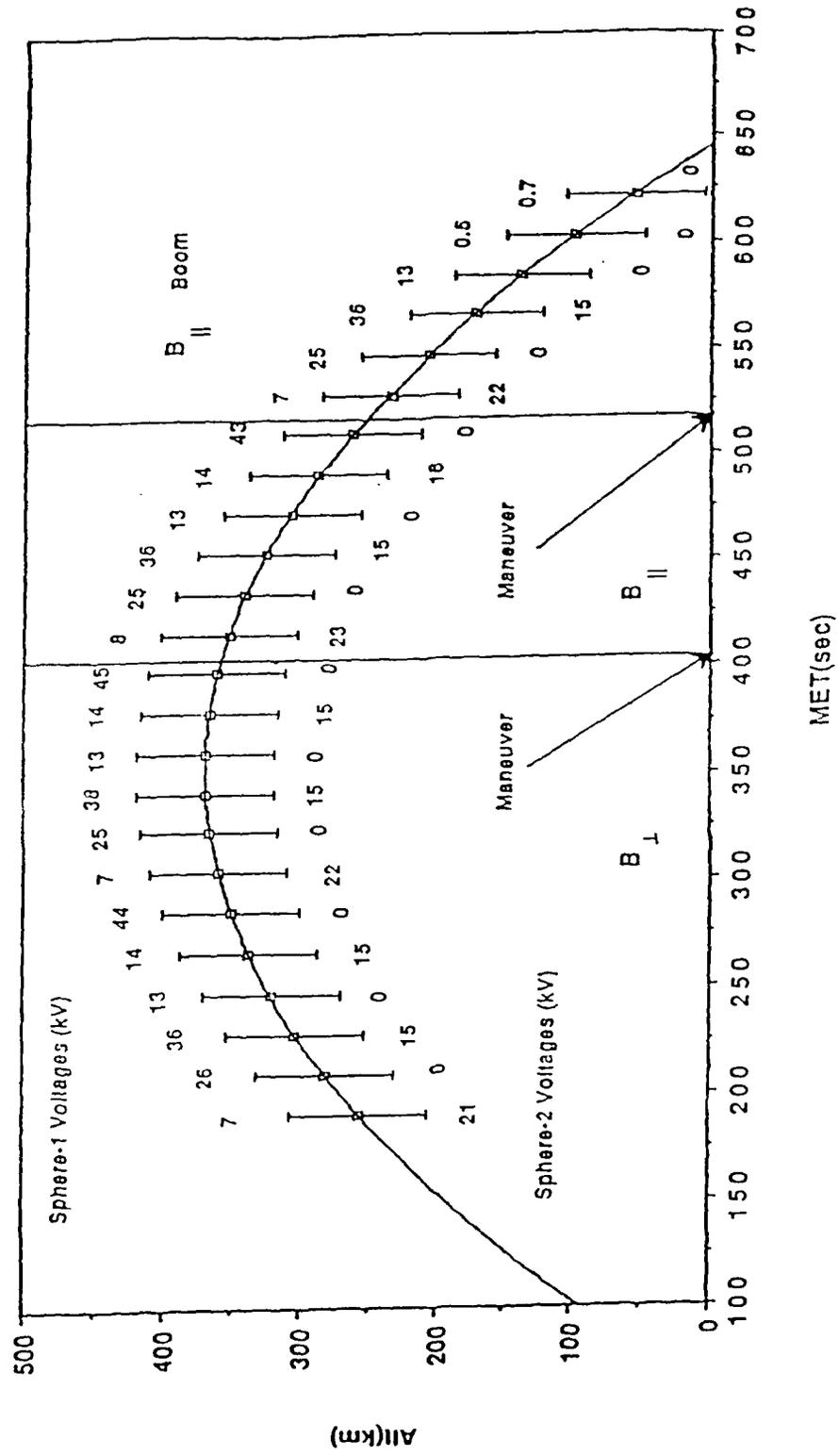

Figure 5. **Voltage Bias Operations**

sphere and rocket without arcing. The measured currents and voltages displayed an exponential decay expected for a classical discharge of a capacitor into a linear resistor. [Ref. 6:p. 1390]

This was a particularly important result because the previous vacuum chamber tests produced severe breakdowns at ionospheric plasma conditions. The responsible mechanism for the breakdowns in the vacuum chamber is understood to be the result of the entrapment of secondary electrons emitted by the walls when they are bombarded by the positive ions that are accelerated in the electric field established by the biassed spheres. These results demonstrate that substantial differences can occur between a vacuum chamber experiment and the corresponding space experiment. [Ref. 6:p. 1389]

The initial flight results also indicated that transient discharge currents could be triggered by vehicle gas release during ACS operations in the discharge cycle [Ref. 6:p. 1393]. Two of the voltage bias operations occurred during ACS thruster firings. The ACS thruster firings resulted in temporary enhancements to the current collected by the spheres. Figure 6 shows the capacitor voltage and plasma current versus time for two bias operations. The bias operation on the left occurred at 285 km without ACS activity. The one on the right occurred at 235 km and was affected by the ACS firings. The current enhancements can be seen as spikes in the plasma current. These current enhancements had very little effect on the measurement of the capacitor potential because the charge required to produce these spikes was small compared to the charge

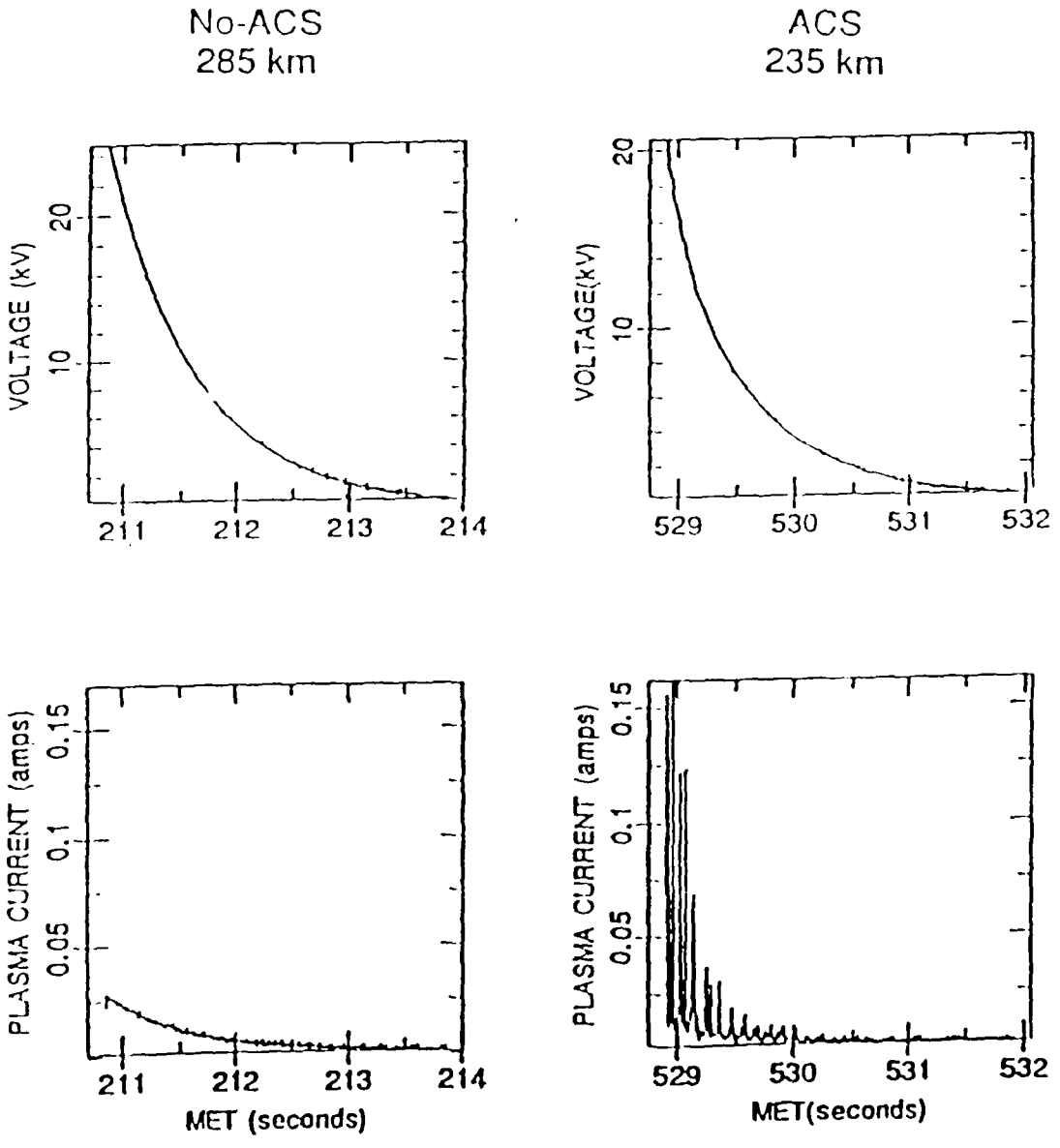

Figure 6. **ACS vs. Non-ACS Current and Voltage**

stored in the capacitor [Ref. 2:p. 6, fig. 16, 14]. A strong correlation was demonstrated between the ACS firings and the enhanced current spikes. Figure 7 shows the plasma currents and ACS firings versus time for the two bias operations that occurred during ACS firings. The top two panels correspond to the discharge cycle that began at 416.781 MET at an altitude of 352 km. The bottom two panels occurred at 529.900 MET at 235 km. (The slight misalignments of some of the current spikes with the ACS firings is believed to be a result of the slow sampling rate of the ACS data.) These figures show that ACS firing functioned as a plasma contactor and may effectively neutralize the rocket body potential. [Ref. 2:p. 6]

Determination of the potential of the spheres with respect to the environment was complicated by the failure of the plasma contactor mentioned previously. The measured potential was the voltage of the capacitor (i.e., the sphere-to-rocket potential). This would have been equal to the potential of sphere with respect to the ambient ionosphere if the plasma contactor had maintained the rocket body potential at the ionospheric potential. The failure of the plasma contactor resulted in the rocket body being charged to several kilovolts negative during each of the voltage bias operations. The initial studies of data from the electrostatic analyzer supported the conclusion that the rocket body was at a several kilovolt negative potential. [Ref. 1:p. 28]

The measured spectra of ions also indicated that the energization process was not just a straightforward acceleration from the ionosphere of thermal ions of an energy equal to the negative potential of the vehicle.

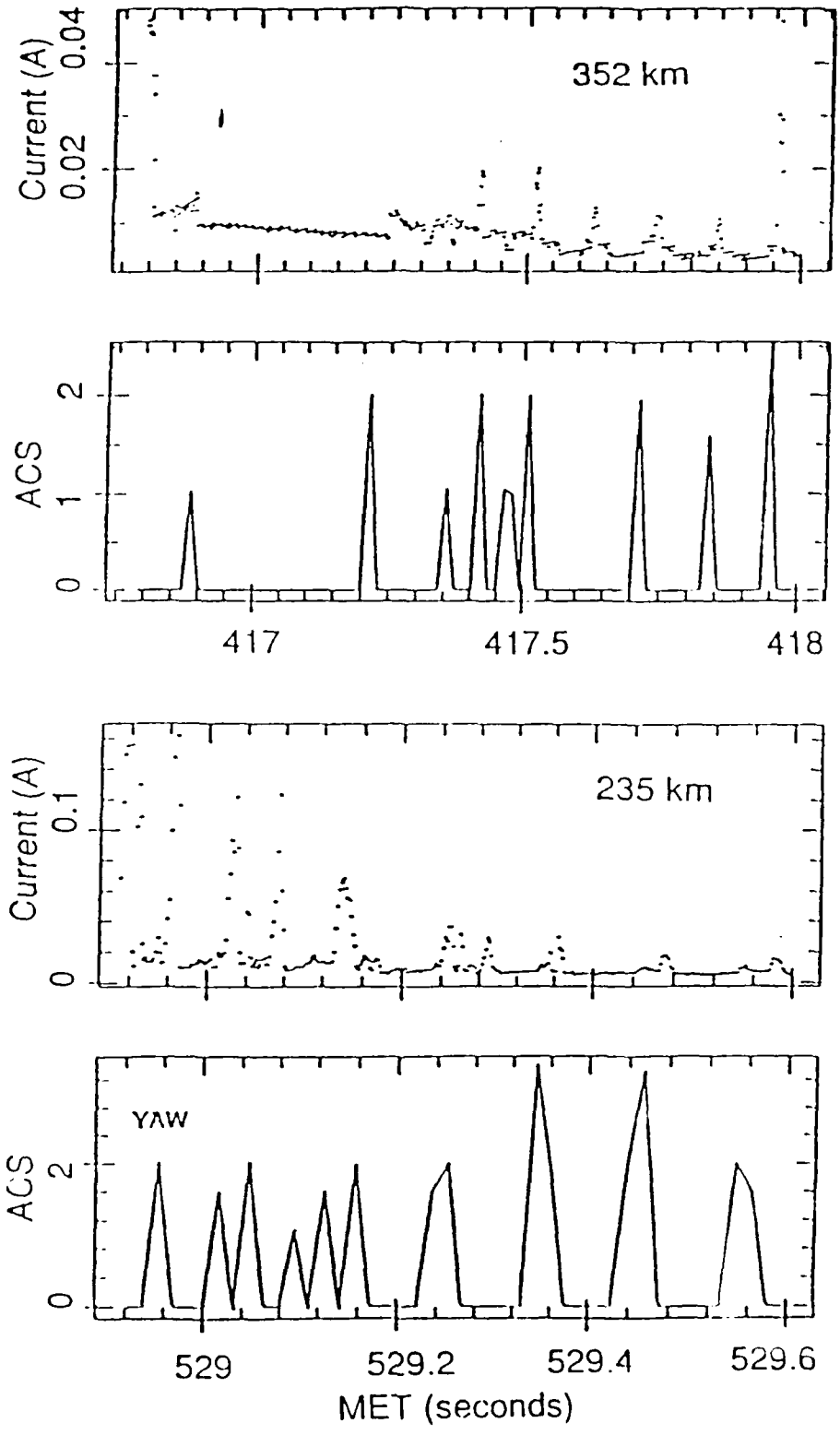

Figure 7. **ACS Current Effects**

Although a cutoff could be determined from the spectra, there was not always a narrow peak in the flux. This continuum of energies below the cutoff was considered to be "...the result of secondary ions produced as a result of the impact of the primary particles on the vehicle surface, and returned to the surface by the electric field due to the vehicle charge." [Ref. 1:p. 28]

Initial studies of the ion ESA data resulted in an upper and lower bound for estimates of the rocket body potential for one operation sequence. Modeling of the SPEAR charging pattern produced the results plotted in Figure 8 [Ref. 8]. The ESA-derived potential estimates are also indicated.

The preliminary analysis of the ESA data which resulted in Figure 8 was never continued due to funding constraints. A major purpose of the work done in this paper is to analyze the rocket body potential for all 24 discharge operations. The major new scientific goal is to obtain the rocket body potential during ACS firings, which has not been done. This is important because all high-power satellites or space platforms will use some type of ACS to maintain orbit.

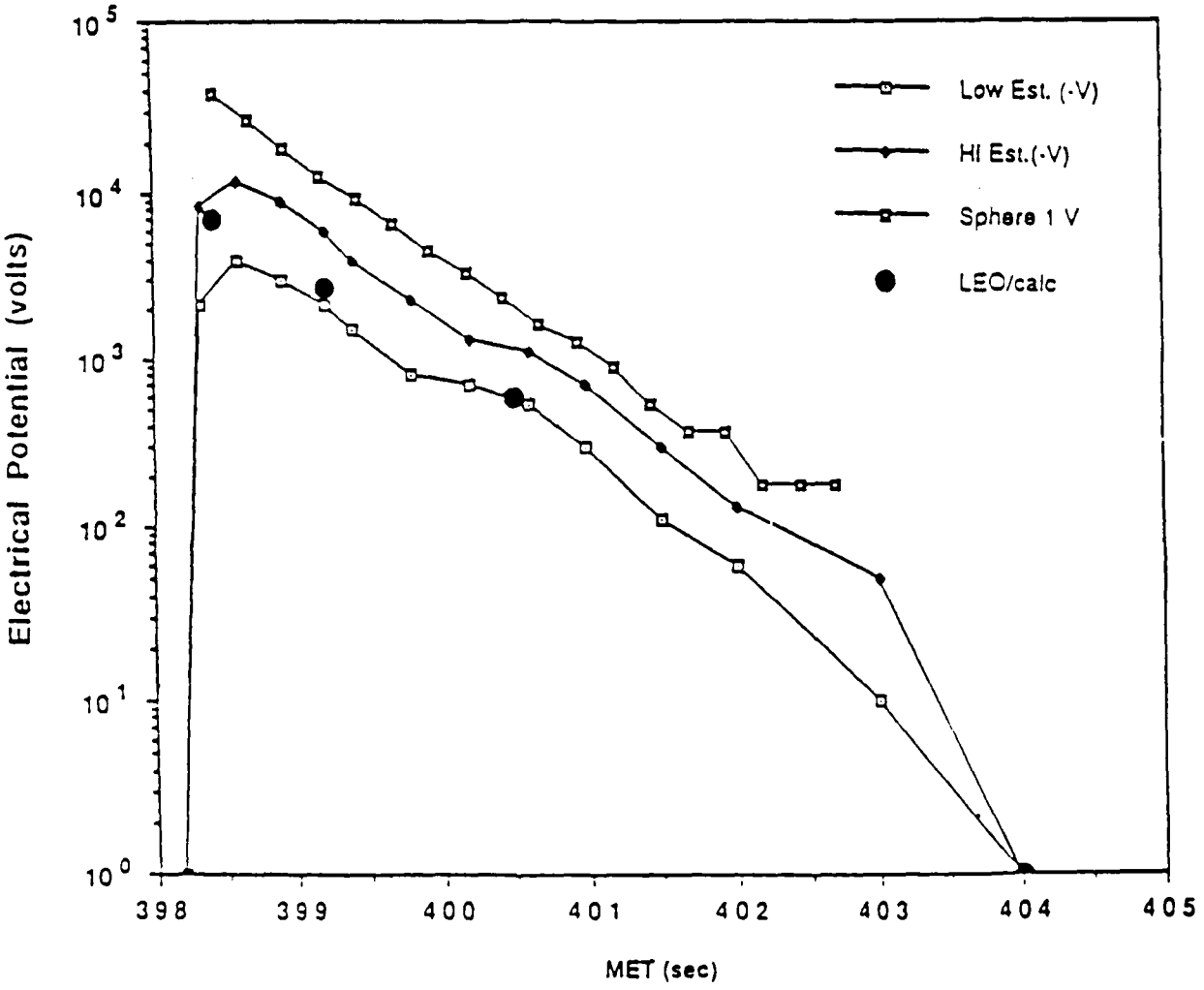

Figure 8. **SPEAR-1 Vehicle Potential and Sphere-1 Potential**

II. DATA REDUCTION

A. GENERAL

The rocket body potential was determined by interactive data analysis using graphical display techniques. The first step in this process was an analysis of all the data contained in the 26 channels allocated to the four particle detectors. All the data taken by the detectors had not been reviewed previously, so it was a primary aspect of this work. In addition, this made it possible to establish the context for the intermittent effects of the ACS firings.

The four particle detectors included one ion electrostatic analyzer (ESA), one electron ESA, one ion charged particle analyzer (CPA), and one electron CPA. These four instruments were allocated the specific channels shown in Table 2.

Since the rocket body charged to high negative potentials during the voltage bias operations, the ion ESA and CPA were expected to provide the most useful data for determining the charging peak. However, in order to provide a thorough data reduction, each channel was analyzed to determine:

1. Whether like channels provided consistent and similar results;
2. Whether a particular channel displayed unusual or interesting phenomena; and
3. Whether the channel operated properly and could provide constructive data for the analysis.

TABLE 2

ESA AND CPA CHANNELS

Channel		Channel	
1	e^- CPA 08	14	i^+ CPA 12
2	e^- ESA 2A	15	i^+ ESA 4C
3	e^- CPA 09	16	i^+ CPA 10
4	e^- ESA 2B	17	i^+ ESA 4D
5	e^- CPA 10	18	i^+ CPA 11
6	e^- ESA 2C	19	e^- CPA 11
7	N/C	20	e^- ESA 2D
8	e^- ESA 3C	21	e^- CPA 12
9	N/C	22	e^- ESA 3A
10	e^- ESA 3D	23	N/C
11	i^+ ESA 4A	24	e^- ESA 3B
12	i^+ CPA 08	25	i^+ ESA 4B
13	i^+ ESA 5A	26	i^+ CPA 09

The data from each channel was separated into 24 data files corresponding to the 24 discharge periods conducted during the experiment. Table 3 shows the MET at which each discharge began, the voltages applied to the spheres during each discharge, and the altitude at which the discharge occurred. Each discharge lasted approximately five seconds, so each data file was created using six seconds MET beginning at the discharge MET truncated to the nearest whole second.

B. COUNT RATE PLOTS

Plots of the count rate versus MET were the first graphical depiction of the data used in the analysis. These plots were useful because they provided a high time resolution picture of any phenomena occurring

TABLE 3

SPEAR-1 HV DISCHARGE TIMES VOLTAGES AND ALTITUDES

MET	SPEAR-1 HV Sequence		
	Peak Voltage		
	Sphere 1	Sphere 2	Alt (km)
191.927	7098	21400	257
210.851	25660	200	285
229.800	36400	15000	303
248.342	13470	200	321
267.202	13650	15330	337
286.102	43860	200	350
304.590	7098	21500	359
323.391	24570	800	365
342.251	37860	15000	369
360.727	13290	300	369
379.506	13650	14800	366
398.344	45320	200	361
416.781	8008	22700	352
435.549	25120	200	340
454.387	36220	14600	325
472.847	13100	200	307
491.624	13650	15500	287
510.449	43320	800	263
528.900	7098	21600	235
547.658	24570	900	206
566.465	36400	14600	172
584.900	13290	200	137*
603.658	546	800	97.7*
622.452	728	800	55.4*

without regard to the energy of the particles. These plots were used to identify particle phenomena and to establish the scale necessary to generate the energy vs. time spectrograms. Figure 9 shows a characteristic count rate plot for the ion ESA 5A. This operation began at 286.102 MET at an altitude of 350 km. The plot shows a peak count rate in excess of 10^6 occurring midway through the discharge. There is a very distinctive "hump" that occurs toward the end of the discharge. This phenomenon was evident in all of the ion ESA 5A count rate plots, and it will be shown later that it is due to low energy ions.

A third phenomenon visible during the first 1.5 seconds of the discharge is a modulation effect. The modulation is evident by tracing the peak count rate from the beginning of the discharge. Further analysis of this effect revealed that it is a result of a beat between the energy sweep rate and the rate of change of the potential.

C. ENERGY SPECTROGRAMS

Review of the particle detector data contained in the 26 channels continued by generating an energy spectrogram for each six-second MET corresponding to its particular voltage bias operation. As can be seen from Table 2, three detectors failed to provide data, so the analysis was reduced to 23 channels. Since the SPEAR-1 experiment included 24 voltage bias operations, this required the generation and analysis of 552 spectrograms.

Figures 10 and 11 show a characteristic spectrogram from the electron ESA 3A and the ion ESA 5A detectors. On both figures, the energy

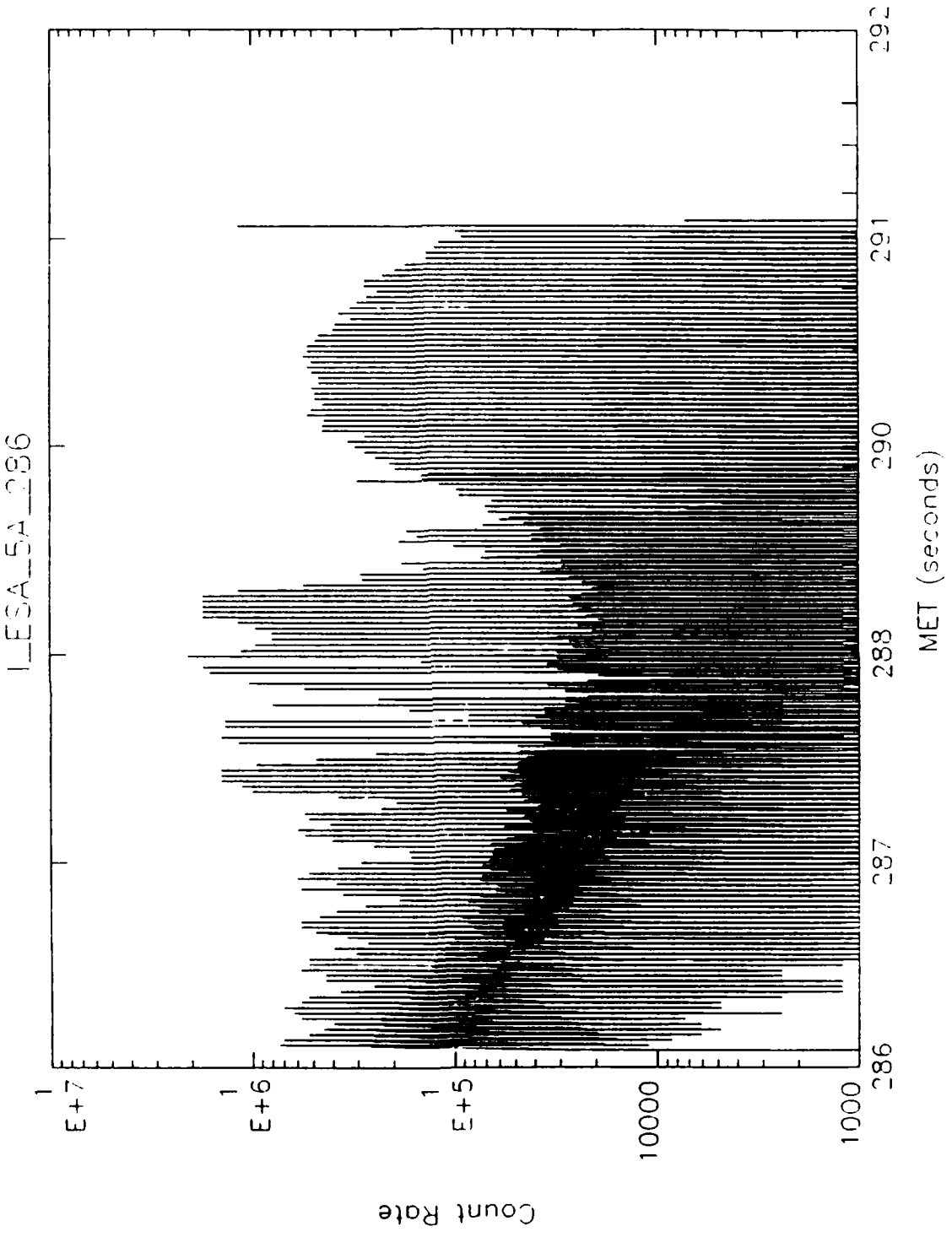

Figure 9. **Count Rate I-ESA-5A-286**

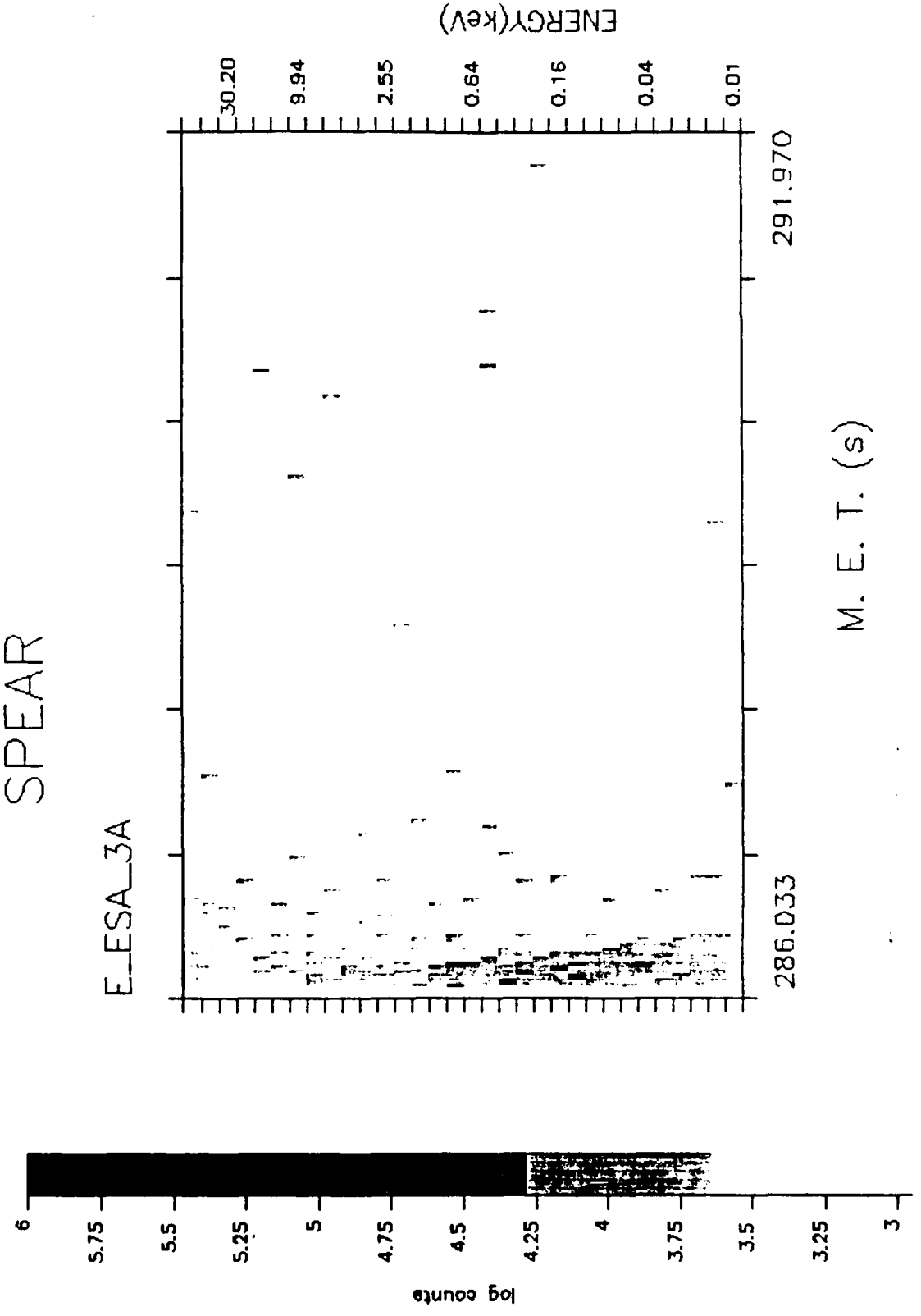

Figure 10. **Electron ESA 3A Spectrogram**

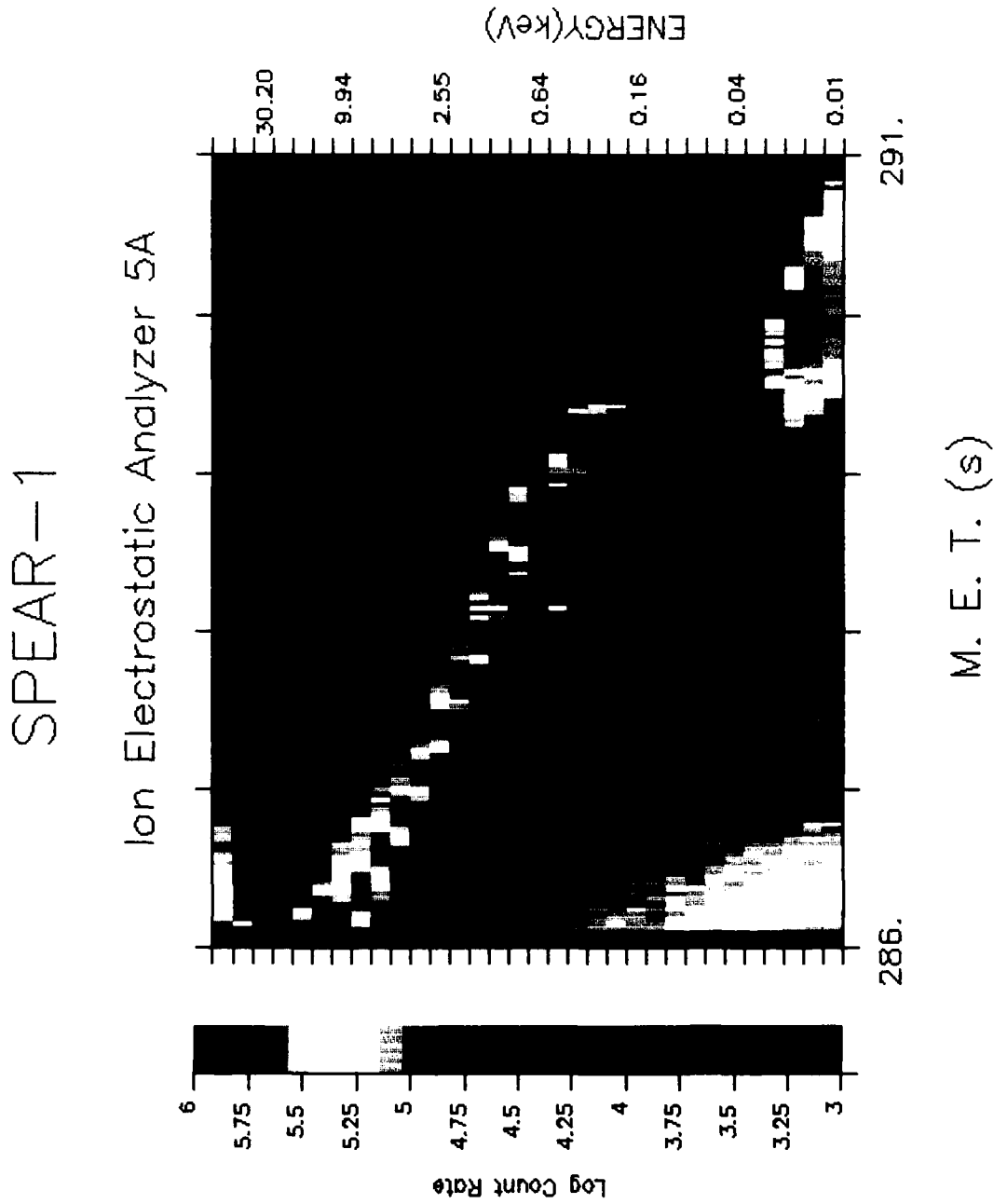

Figure 11. **Ion ESA 5A Spectrogram**

scale represents the 32 energy "bins" that were swept by the detector during the discharge period. Correspondence with the detector designer revealed that energy bins 1 and 2 (represented by the top two graduations on the scale) are not useful. These bins correspond to measurements taken while the high-voltage supply is recharging to its peak voltage (energy sweeps are from high to low energy) [Ref. 9]. The log of the count rate is represented by the shading on a scale from 3.0 to 6.0. This scale typically provided the best resolution for discriminating the peak counts of the energies.

The electron ESA 3A spectrogram (Figure 10) shows data that are typical of the data from the electron detector. This discharge operation began at 286 MET at an altitude of 350 km. The spectrogram depicts the count rate peaking at the mid-energies and falling off rapidly to lower energies within the first half-second of the discharge.

The ion ESA 5A detector (Figure 11) provided much more useful data. This spectrogram shows data from the same discharge (286 MET, 350 km). The spectrogram shows a definite peak count rate and corresponding energy for most of the discharge period. The last two seconds of the discharge are dominated by high counts of low-energy ions. This corresponds to the hump described earlier in the count rate plot (Figure 9). This latter phenomenon was only evident in the ion ESA 5A detector, which viewed "up" toward the spheres. The other four ion sensors looked "down," away from the spheres. Unfortunately, the other detectors (5B, 5C, and 5D) which had "up" view directions, failed to operate.

The distinct drops in count centered at 288 MET on the spectrogram are believed to be the result of neutral gas emissions from the ACS. These drops were evident in all of the other detectors for the same discharge operation.

The spectrograms generated on the computer screen and printed in hard copy for analysis were in color. The spectrograms provided in this report, with the exception of Figure 11, are in black and white due to reproduction restrictions. Spectrograms for the ion and electron CPAs were also printed and analyzed. The validity of the CPA data was questionable, so it was not used during the remainder of the analysis. [Ref. 10]

In addition, the initial review of all the spectrograms indicated that the last two discharge operations occurred during re-entry and resulted in little or no charging. This reduced the number of discharge operations to be analyzed to 22. A complete set of the 24 spectrograms for ion ESA 5A and ion ESA 4B are included in Appendix A and Appendix B, respectively.

D. CHARGING ANALYSIS

Review of the energy spectrograms indicated that detectors ion ESA 5A, ion ESA 4C, and ion ESA 4B would provide the best data for determining the charging peak. Initially, two methods were utilized to determine this peak. The first method was selecting the maximum count rate and its corresponding energy for each of the 32 ms sweeps in the five-second discharge cycle. This process was accomplished initially by selecting the peak count rate (and corresponding energy) by inspecting a

numerical table of the data. After several manual iterations, an interactive program was written to select the count rate via the computer cursor.

Figure 12 shows a sequence of count rate versus energy plots for the discharge operation that began at 210.851 MET. Data for each figure are approximately one second apart and are taken from the ion ESA 4C detector. The 32 tick marks on the plot represent the spectra generated by sweeping over the energy range in 1 ms intervals. They correspond to the 32 intervals that are on the vertical (energy) axes of the spectrograms.

The computer program selected and "boxed" the highest count rate for each sweep, but it also provided some flexibility for the analyst. As each sweep was analyzed, the analyst could accept the computer's selection, change the selection, or skip it completely. In addition, the "quality" of each selected data point was recorded as good or questionable. A brief description of charging peak characteristics is provided in Appendix E.

Figure 12a shows a peak at 6 kV and a diffuse spectrum at lower energies. The low energy peak (10-100 eV) is attributed to sputtering induced by the 6 keV O^+ beam (assumed) [Ref. 11]. The measurement at 40 keV represents energy bin 1 that occurs during the high-voltage supply reset, as discussed earlier.

At 211.914 seconds (Figure 12b), the peak is at approximately 2 keV and is more distinct. Figure 12c has a peak at 650 eV. This peak is broader and less distinct than 12a and 12b. Figure 12d shows a peak just below 300 eV. This sweep is typical of some of the more questionable

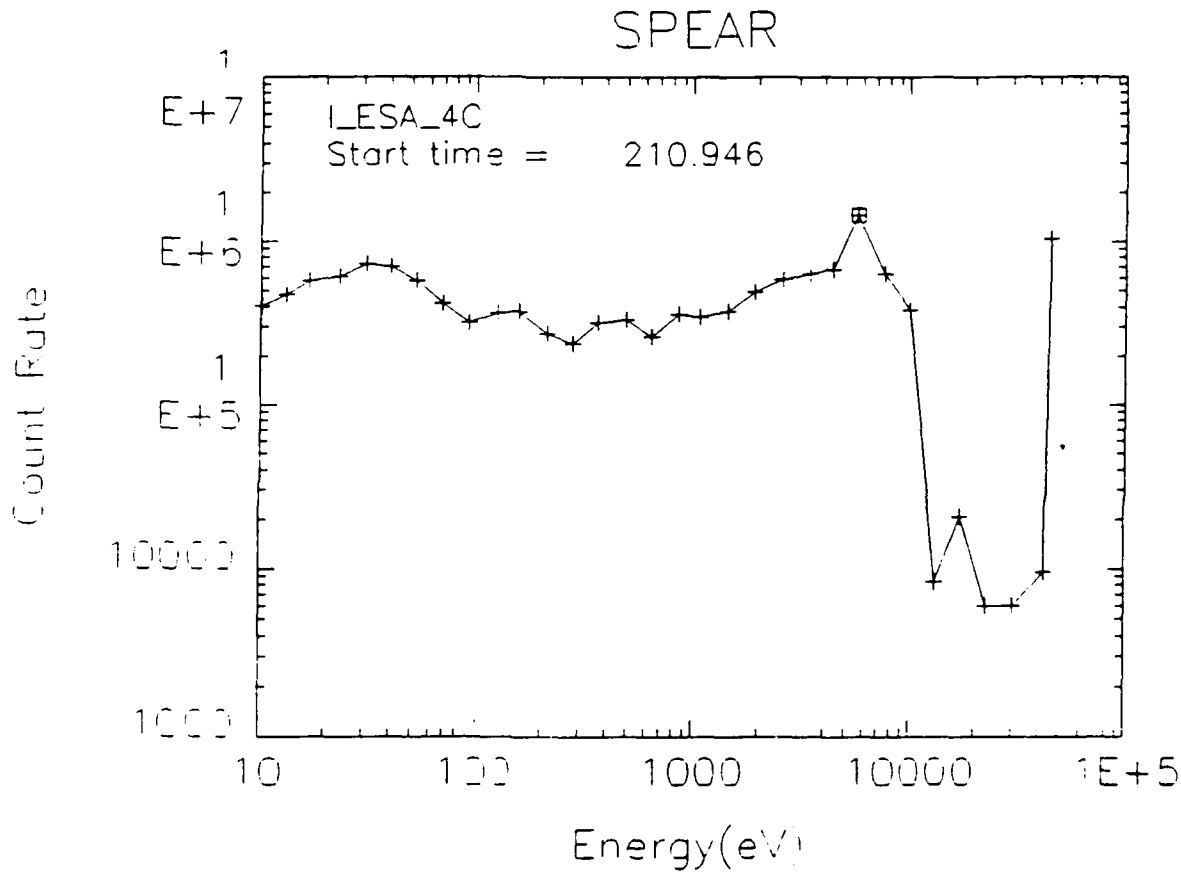

12a. 210.946 MET

Figure 12. **Ion ESA 4C Energy Sweeps**

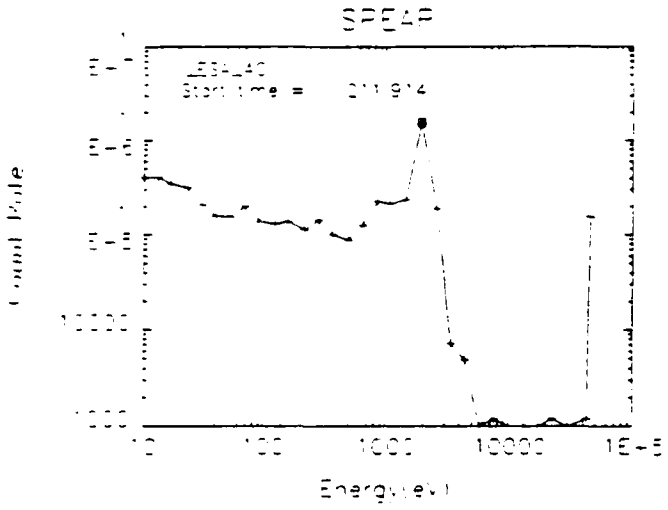

12b. **211.914 MET**

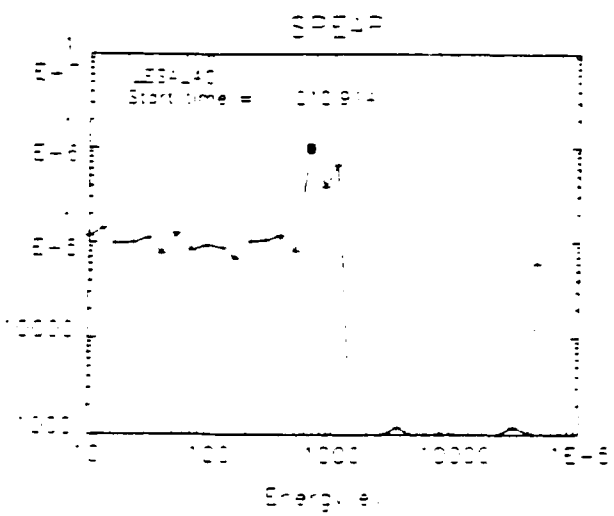

12c. **212.914 MET**

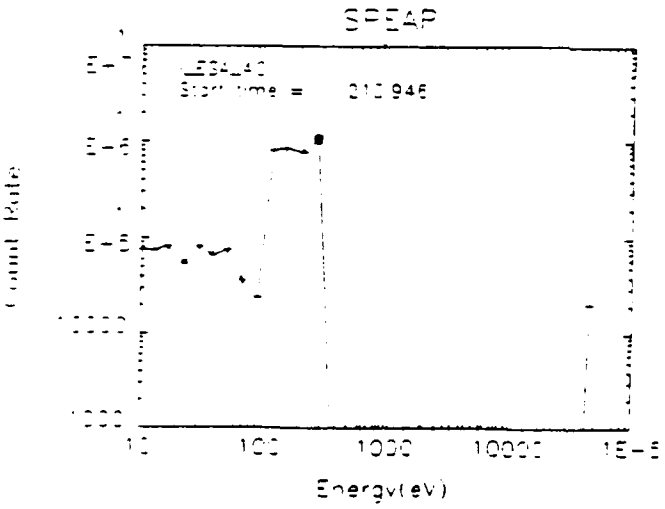

12d. **213.946 MET**

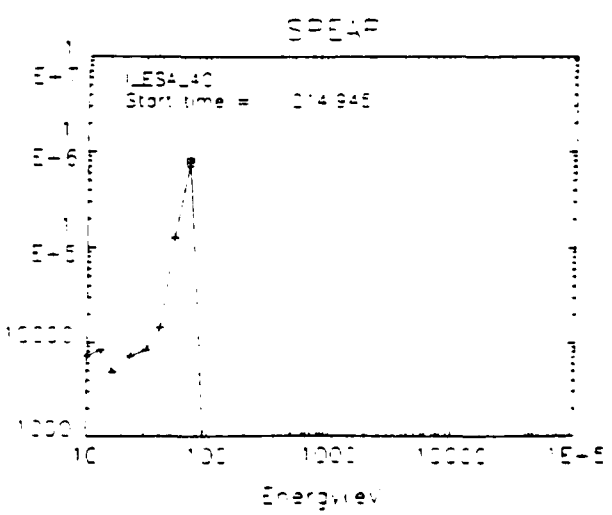

12e. **214.945 MET**

Figure 12. **Ion ESA 4C Energy Sweeps** (continued)

measurements. Individually, these plots could be difficult to analyze, but, when analyzed in conjunction with the energy spectrograms, they could be interpreted. Figure 12e at 214.945 seconds shows the peak at 70 eV. The sharper peak in count rate for the lower energies (<100 eV) was characteristic for the ion ESA 4C detector.

For the sequence represented by Figure 12 (a through e), 123 energy sweeps were generated, giving 123 data points for calculation of potentials. Of these data points, only two were considered questionable. Typically, less than five percent of the data points were questionable. Since three detectors were analyzed for each of the 22 usable discharge periods, approximately 8,000 of these plots were generated and analyzed.

The second analysis method used a distribution function (f) or phase space density given by

$$f = \frac{\text{count rate}}{E^2}$$

where E is the energy of the particle. This method also required the review of each 32 ms sweep. The measured ion was assumed to be O^+.

Figure 13 depicts a typical energy sweep using the phase space density. The diagonal line represents the one count level for a given energy. The computer boxed the energy that had the highest count rate, and it was left to the analyst to determine whether this peak also corresponded to the peak in the distribution function.

The distribution function shown in Figure 13 corresponds to the count rate plot given in Figure 12a. Comparison of Figures 12a and 13

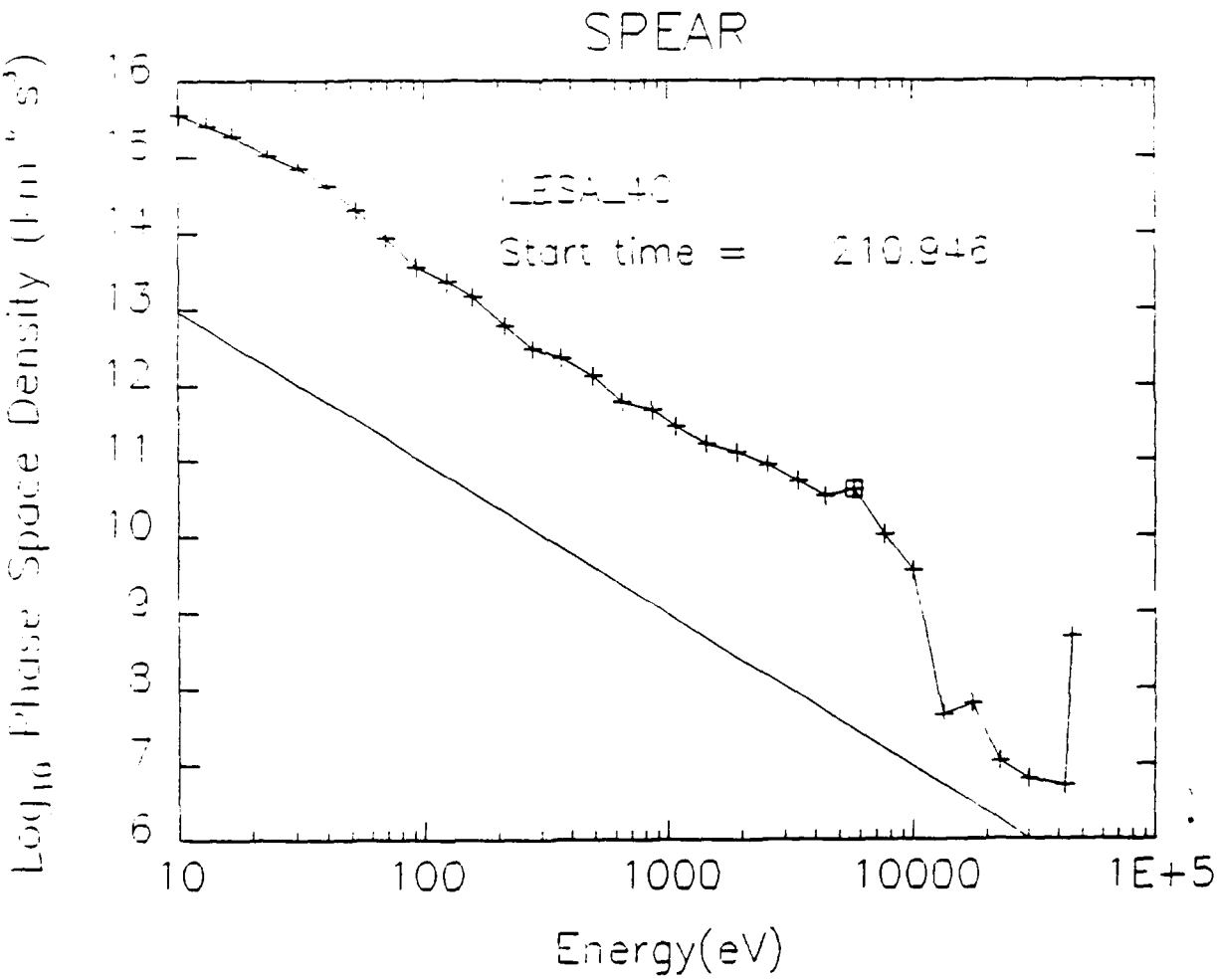

Figure 13. Ion ESA 4C (DF Method)

shows that visual determination of the distribution peak is much more difficult than that of the peak count rate and little additional information is gained.

Both methods were used for two discharge operations from each of the three detectors selected for use in the analysis. After confirming the consistency of the results using both methods, the maximum count rate method was used for the remainder of the analysis.

E. RESULTS OF ANALYSIS—ROCKET POTENTIAL

From the data points selected in the analysis, graphs of the selected energies/potentials (eV) versus MET were then plotted. Figure 14 shows a typical potential plot produced using the peak count rate method.

This plot is from the analyses of ion ESA 4B detector data for the first discharge operation that occurred at 191.927 MET at an altitude of 257 km. For this discharge operation, sphere 1 was biased to 7 keV and sphere 2 was biased to 21.4 keV. An important characteristic of this potential versus MET plot is that it is linear on a log-linear scale (e.g., exponential decay). This was the case in all plots of this type for all three detectors and agrees with behavior of the sphere potential versus time.

Three distinct drops in the potential are also very evident in this graph. These drops are of one or two orders of magnitude greater than the small, random deviations in the plot, which are due to uncertainties in the analysis.

Figure 15 depicts another discharge operation with data from the ion ESA 4B detector. This operation began at 398.344 MET at an altitude of

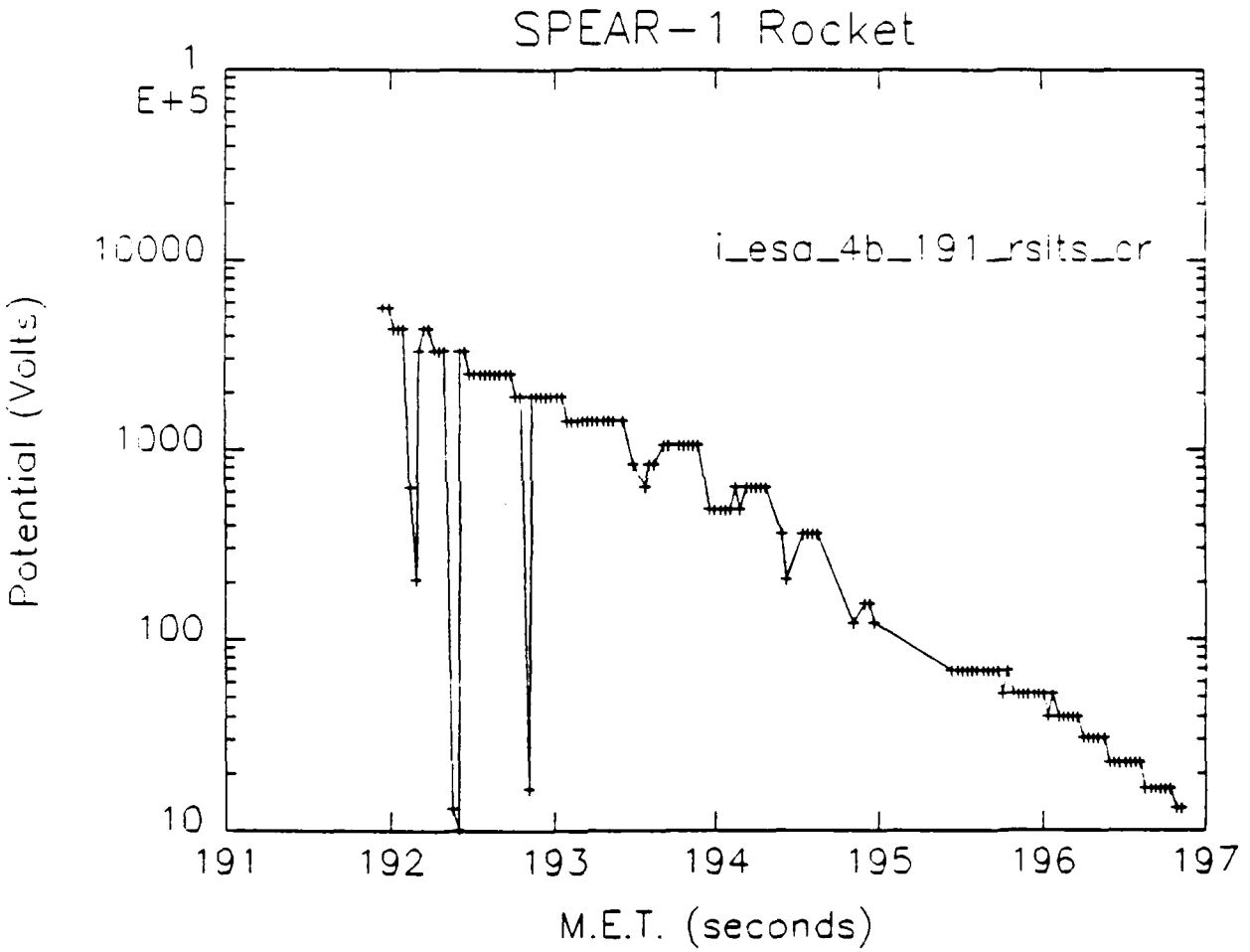

Figure 14. Peak Potential Plot (ESA 4B 191 MET)

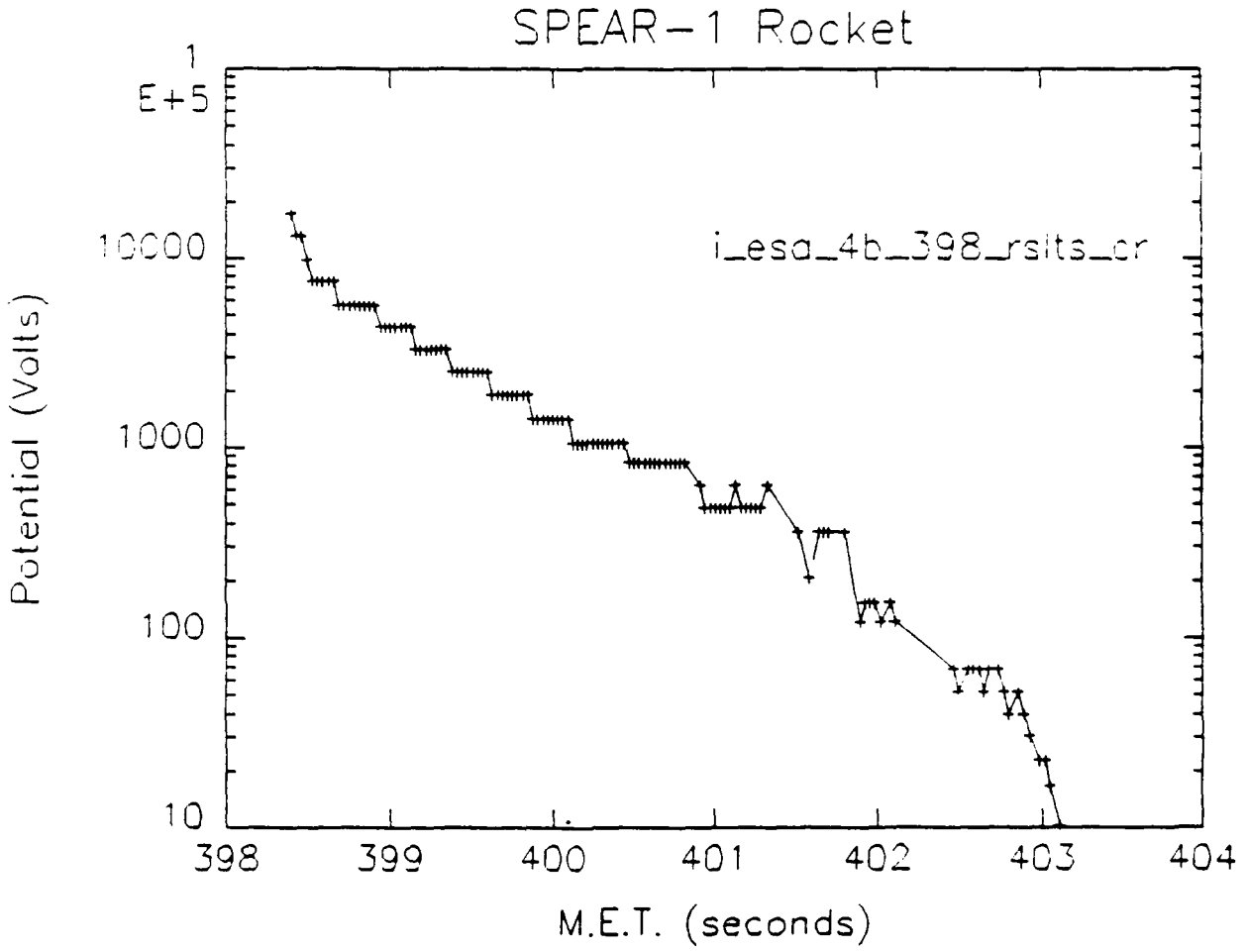

Figure 15. Peak Potential Plot (ESA 4B 398 MET)

361 km. Sphere 1 was biased to 45.3 keV, which was the highest potential applied during the entire experiment. Sphere 2 was left nominally uncharged at 200 eV.

The inferred potential plot is very well behaved (linear) initially, but becomes more erratic during the final two seconds of the discharge. It also indicates a potential that is two times greater than the potential shown in Figure 14. This corresponds to the potential being applied to the sphere during this operation being double the potential that was applied during the first discharge operation.

As discussed earlier, the rocket was reoriented during the experiment to analyze the geomagnetic effects. One of these ACS maneuvers occurred at approximately 405 MET, just prior to the discharge operation that began at 416.781 MET. Another ACS maneuver began at approximately 518 MET and was still occurring when a discharge operation began at 528.900 MET.

Figures 16 and 17 graphically portray the impact of these ACS maneuvers on the potential of the rocket body. Figure 16 shows considerable drops in the potential due to the ACS firing even though the maneuver had been completed. Figure 17 shows an even greater impact because the ACS jets were still firing. The wide dip (531.7–532.0) appears to be an artifact of processing due to lack of ion counts at all energies. Detector 4C suggested a higher potential during this period. A complete set of potential plots from the I ESA 4B detector is contained in Annex C.

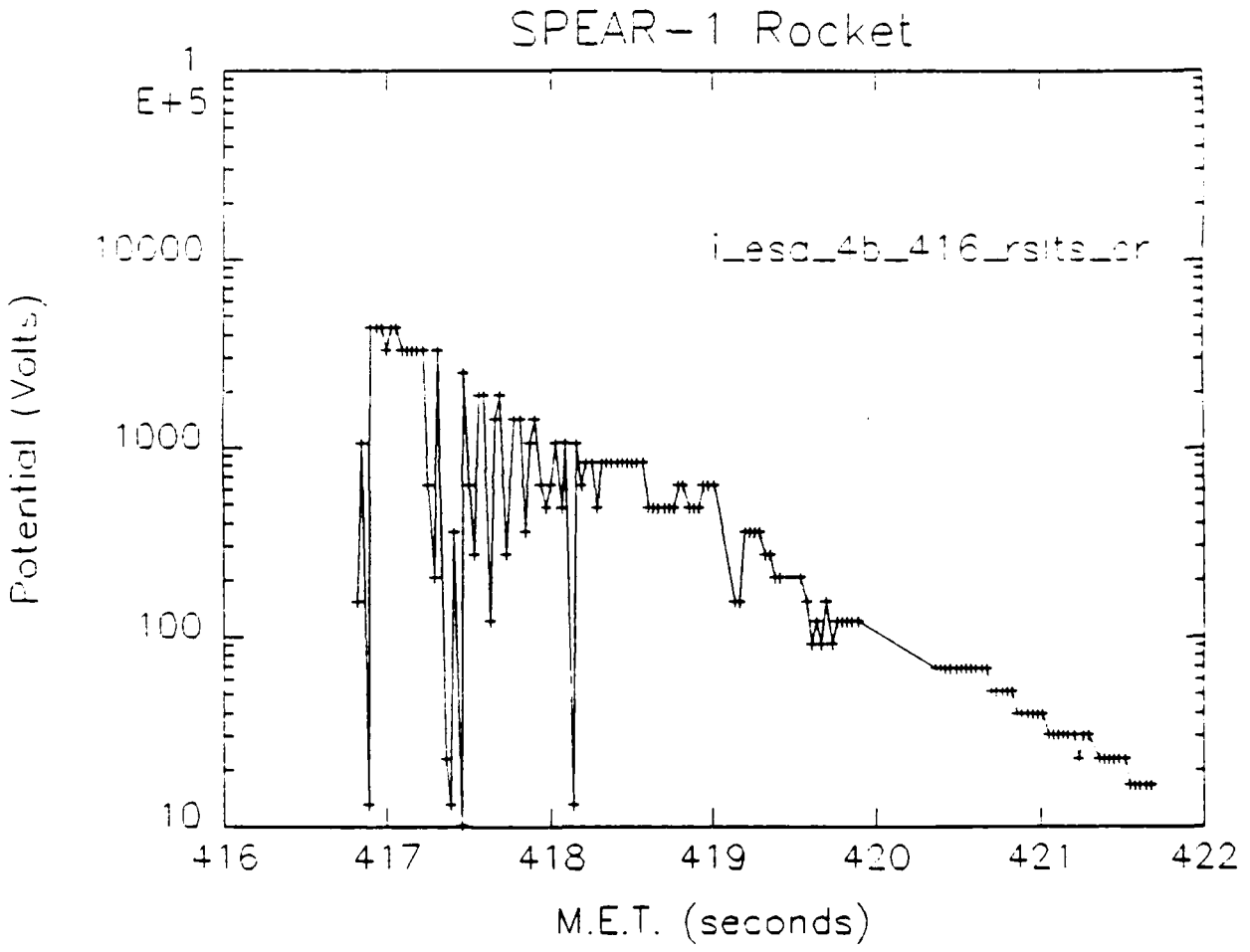

Figure 16. **Peak Potential Plot (ESA 4B 416 MET)**

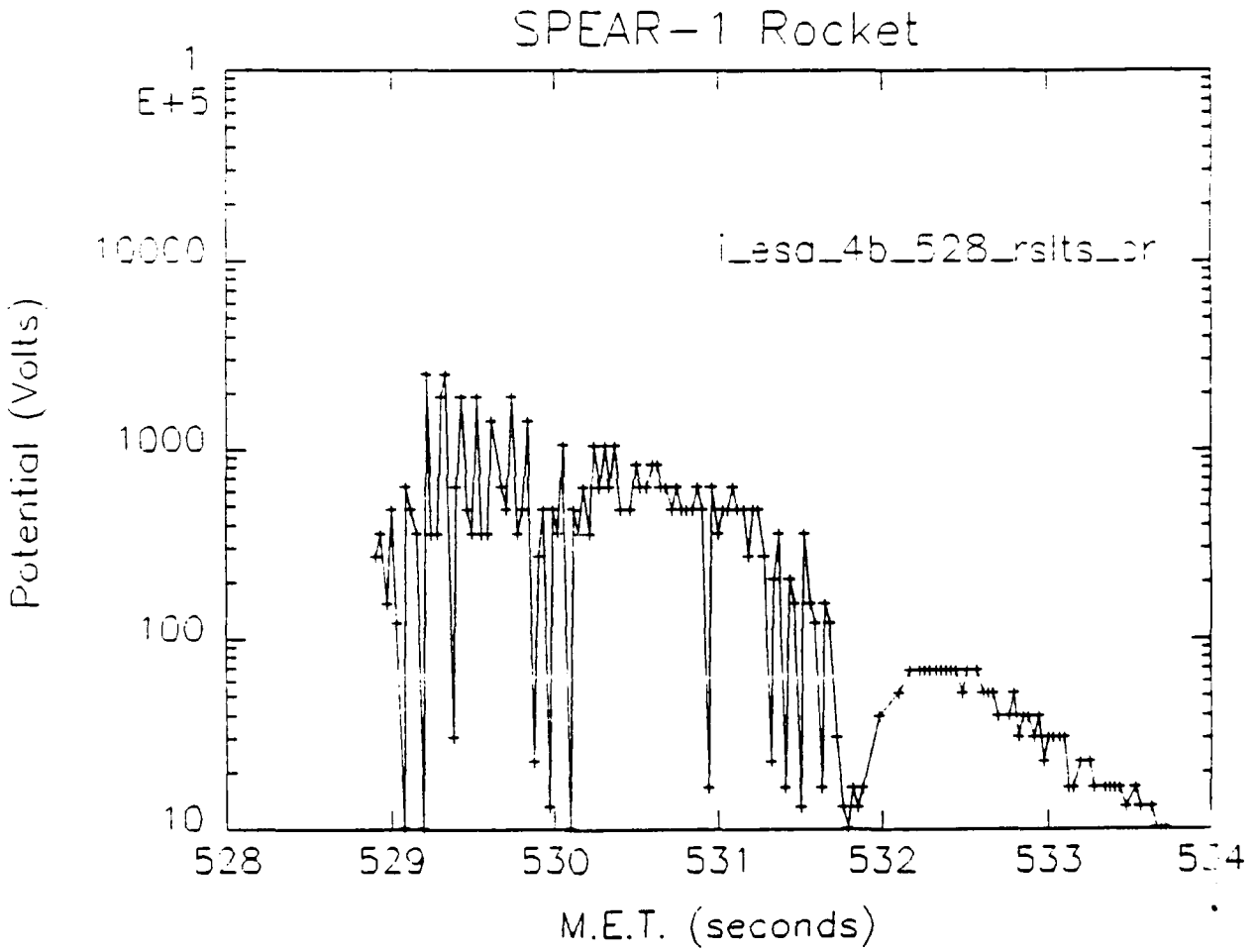

Figure 17. **Peak Potential Plot (ESA 4B 528 MET)**

Potential plots were created for the results obtained from each of the three detectors. Next, an interactive program was written to fit a curve to the data points to determine the time constants for the potential decay. Figure 18 depicts a typical result from this analysis. Several iterations of this process revealed that the data points could be divided into two groups and fitted independently of each other. The two curve fits that can be seen in Figure 18 were labeled HI and LO with their respective slopes. Data from the slopes computed for the ion ESA 4B detector is shown in Table 4. The analysis was repeated on the ion ESA 4C detector and a summary of these results is contained in Table 5.

The results from both detectors indicated that there was no significant variation in the slope with respect to the altitude of the rocket. As can be seen from Tables 4 and 5, the HI slope increased after the rocket was reoriented into position 2. The LO slope in both detectors showed very little change.

Since only two usable discharges occurred after position 3, no valid observation could be made. Data from the 191, 416, 454, and 528 MET discharges were not used in this analysis. Plots from these periods had significant potential drops due to gas releases that resulted in the curve fit being skewed.

F. ROCKET VS. SPHERE POTENTIAL

Since the particle detectors were housed in the rocket body, the potentials determined corresponded to the peak negative potentials that were induced on the rocket body due to failure of the plasma contactor.

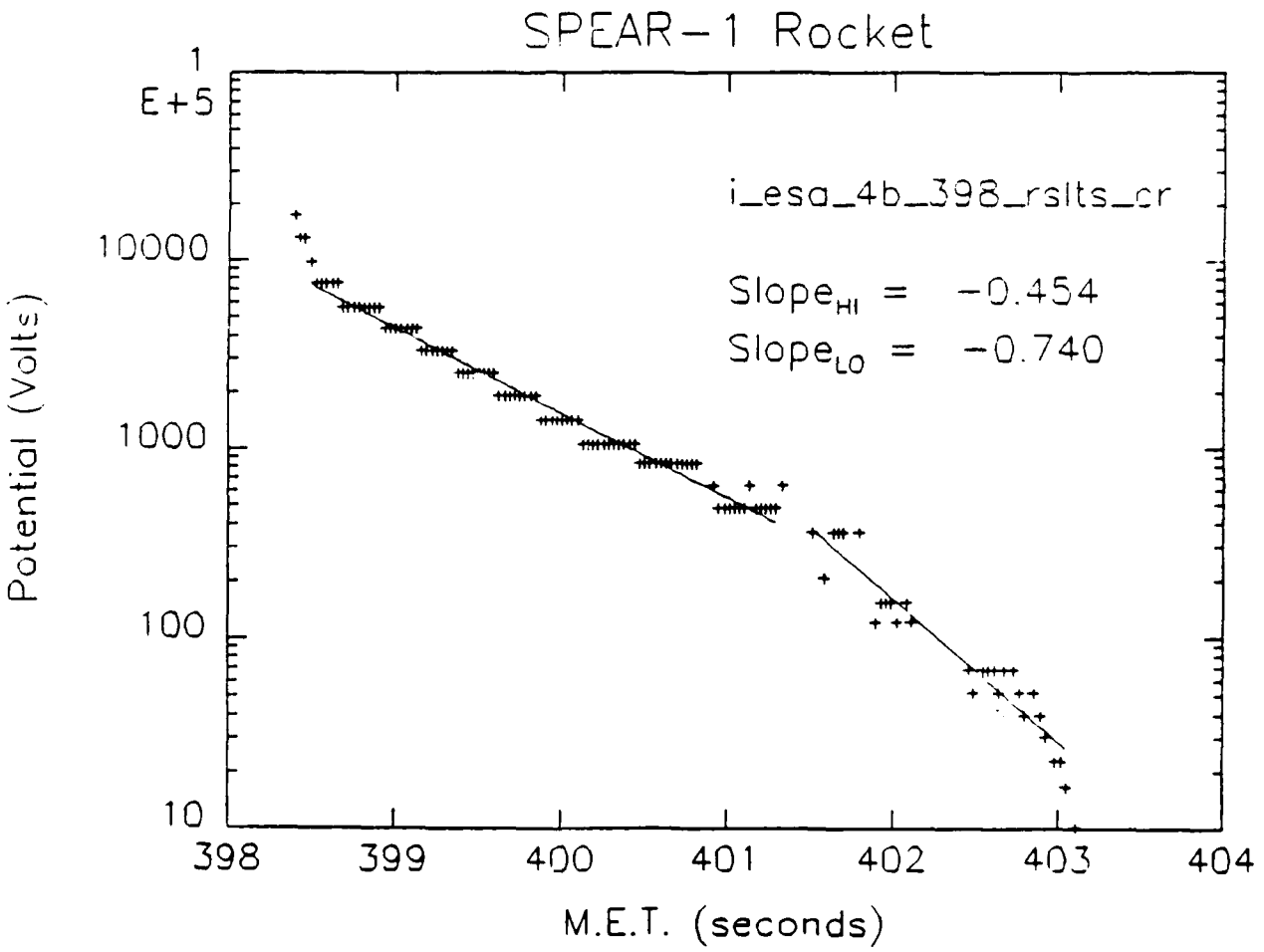

Figure 18. **Potential Curve Fit (ESA 4B 398 MET)**

TABLE 4

ION ESA 4B SLOPES

MET (sec)	ALT (km)	HI	LO
Position 1—Plane of Booms Perpendicular to Magnetic Field			
210	285	0.438	0.594
229	303	0.450	0.533
248	321	0.411	0.796
267	337	0.467	0.468
286	350	0.471	0.397
304	359	0.470	0.470
323	365	0.389	0.480
342	369	0.478	0.634
360	369	0.391	0.669
379	366	0.417	0.605
398	361	0.454	0.740
	$\bar{x}$ =	0.439	0.580
	σ =	0.031	0.118
Position 2—Plane of Booms Parallel to Magnetic Field			
435	340	0.544	0.440
472	325	0.485	0.630
491	307	0.555	0.654
510	263	0.593	0.540
		0.544	0.566
	σ =	0.038	0.084
Position 3—Boom 1 Parallel to Magnetic Field			
566	172	0.317	0.317
584	137	0.591	0.499

TABLE 5

ION ESA 4C SLOPE SUMMARY

			Slope HI	Slope LO
Position 1	$\bar{x}$	=	0.437	0.543
	σ	=	0.028	0.106
Position 2	$\bar{x}$	=	0.631	0.565
	σ	=	0.153	0.109

Consequently, the next graphical analysis conducted was a rocket potential versus sphere potential to compare the computed rocket potentials to the sphere potentials measured by the voltage sensors electronically connected to the spheres. Detector ion ESA 4B was selected for this analysis because it contained the best set of data points determined during the charging peak analysis. This comparative analysis was conducted for each discharge cycle. When one sphere was held at near-zero voltage, only the sphere having an induced voltage bias was compared. When both spheres had voltages applied, a graph was generated for each. Figures 19 and 20 show typical rocket versus sphere potential plots for cases where only one boom was biased greater than 10 keV.

Both figures show a linear relationship between the sphere potential and the rocket body potential. The drops in rocket potential notable in Figure 19 on the right side are similar to effects noted for gas emissions from the ACS (W. J. Raitt has suggested these may be due to outgassing on the booms early in the mission [Ref. 12]). Since the capacitance to the

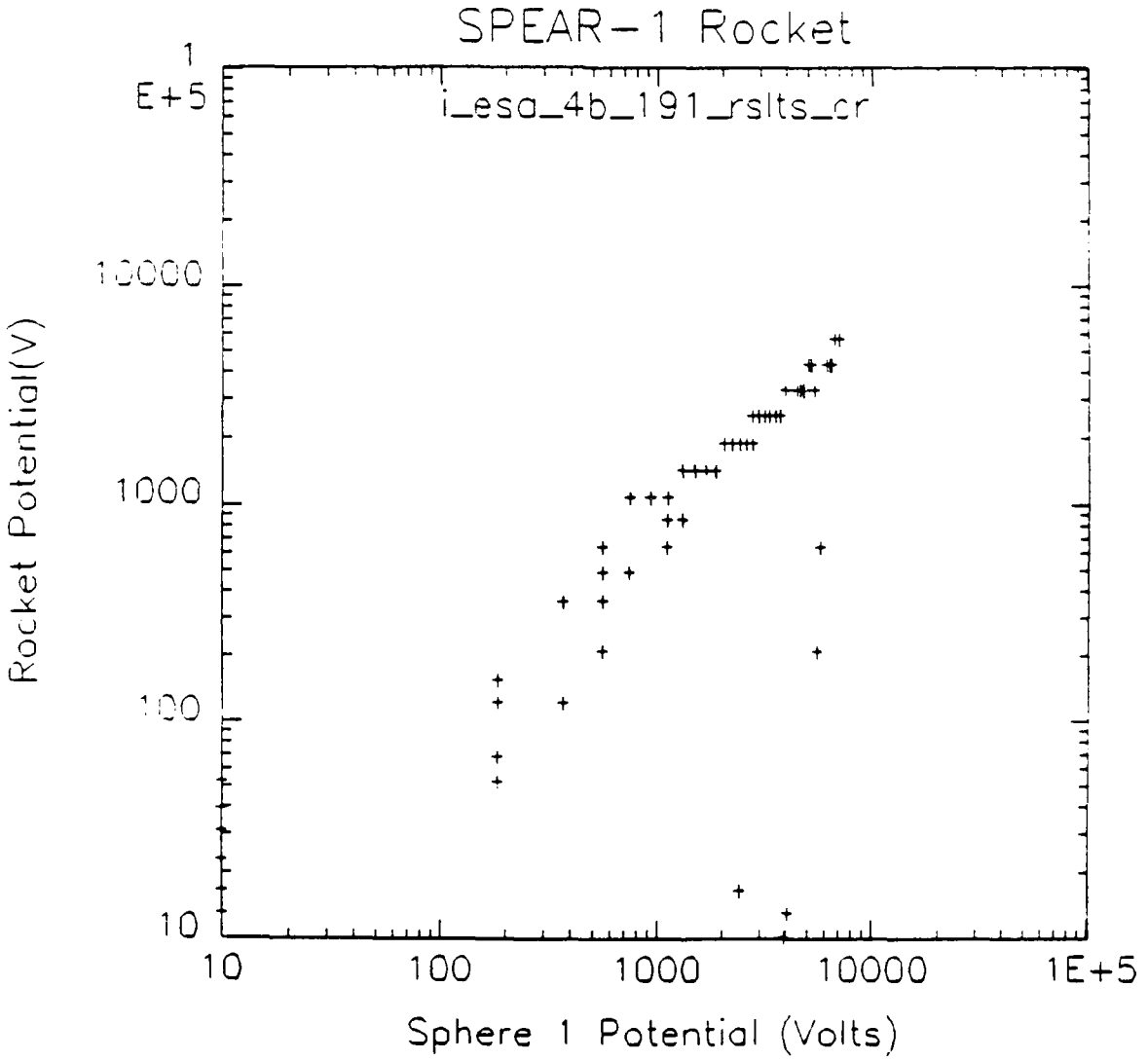

Figure 19. **Sphere vs. Rocket (ESA 4B 191 MET)**

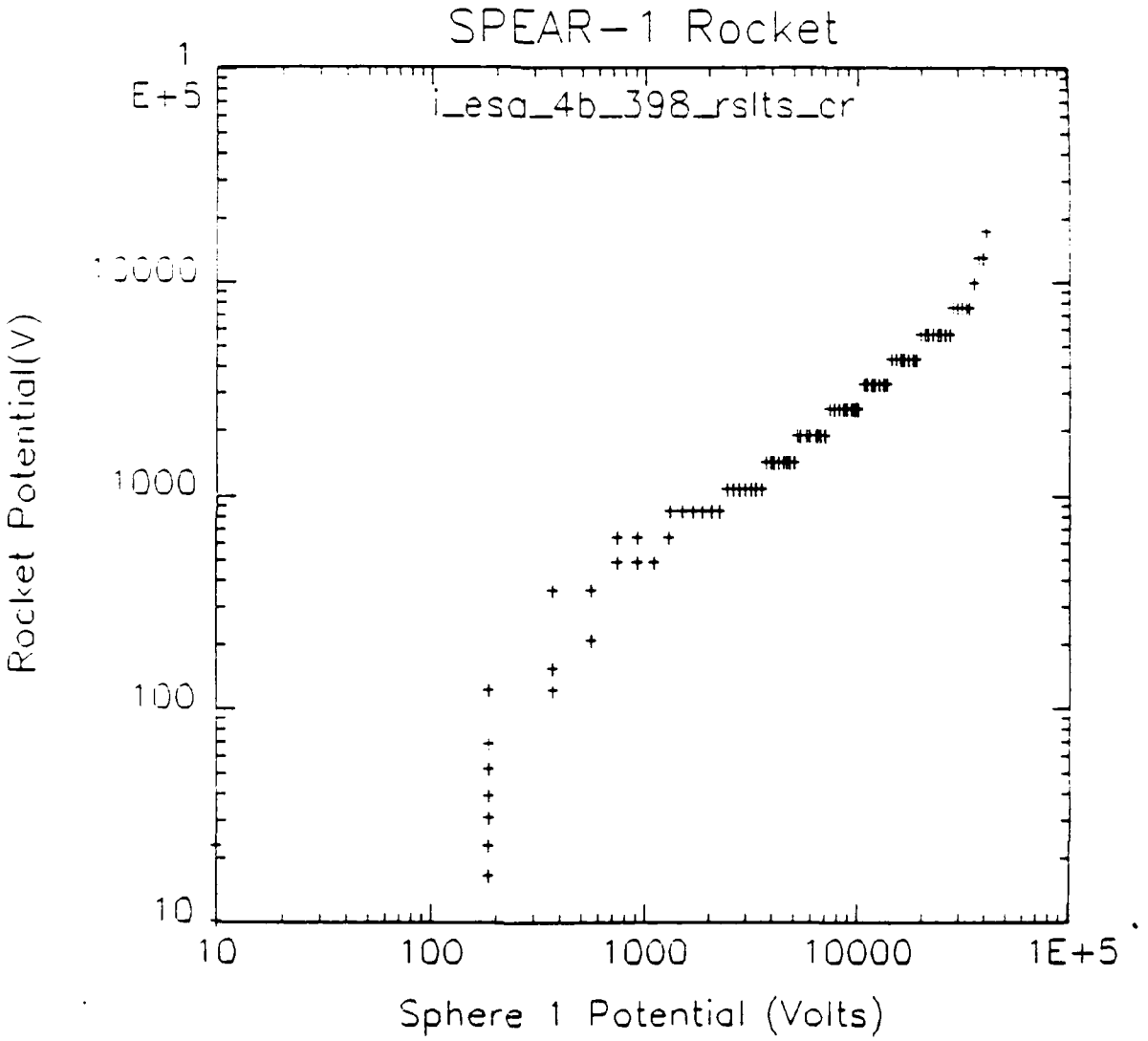

Figure 20. **Sphere vs. Rocket (ESA 4B 398 MET)**

sphere(s) to the rocket is much higher than the capacitance of the rocket body to space, these emissions discharge the rocket body but have no effect on the HV capacitor system.

Figure 20 also shows a deviation from linearity at the high potential end of the plot. This phenomenon was also noted in two other plots of this type. For each of these discharges, the bias applied to one of the spheres exceeded 40 kV. These were the three largest voltage bias sequences. None of the other discharge operations displayed this effect.

During this analysis, overlays were made of these plots to determine any effects from altitude or different rocket orientations. Figure 21 depicts the results from this analysis. The data points indicated by the symbol 5 are from the 398 MET discharge shown in Figure 20. With the exception of the deviation at the high potential end, this plot was representative of all the discharges that occurred while the rocket was in position 1. The data points indicated by a 7 are representative of the plots taken when the rocket was in position 2. The number 8 represents data from position 3. All other discharge data would simply plot on top of the numbers that corresponded to its particular orientation, regardless of the altitude.

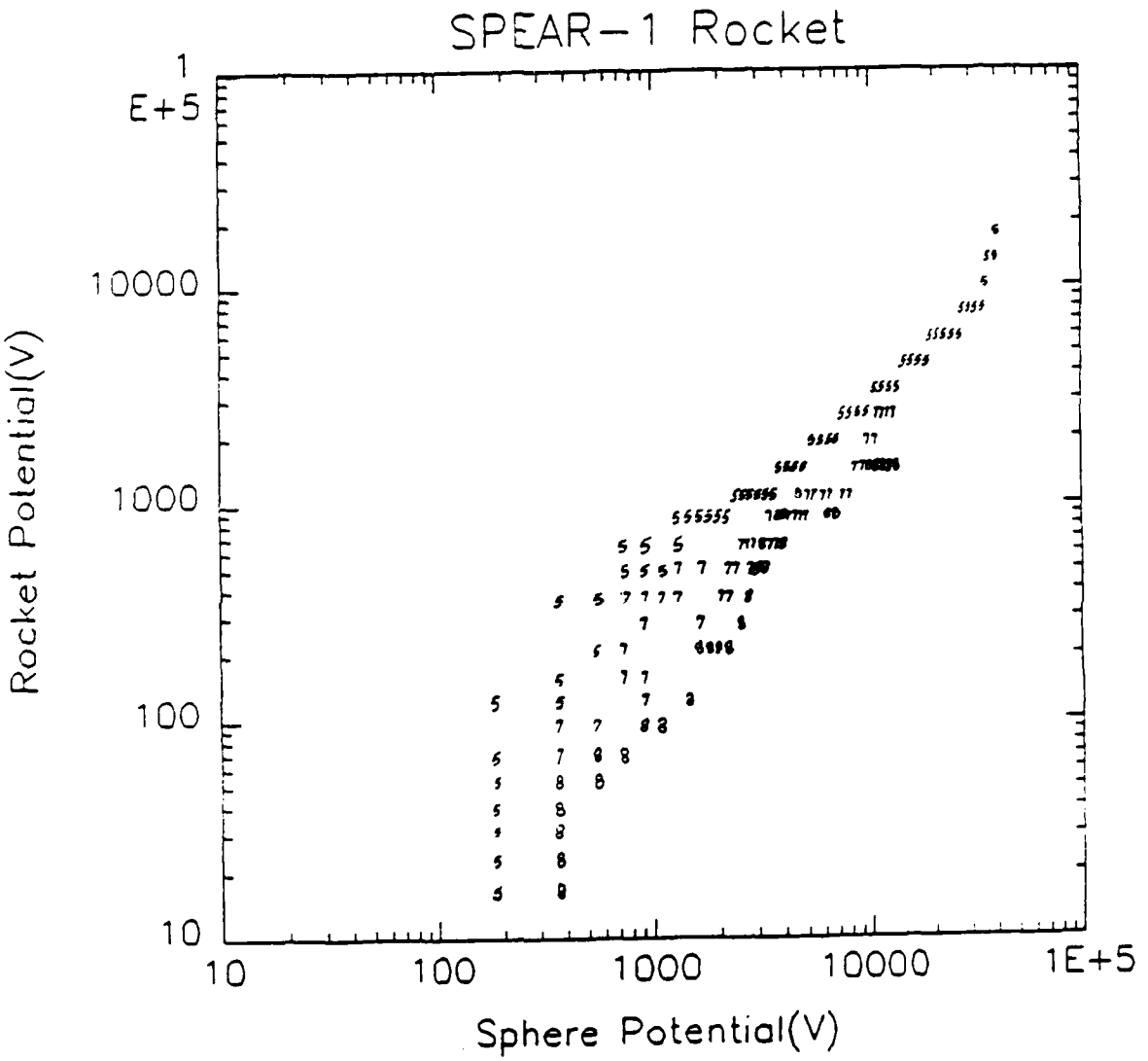

Figure 21. **Sphere vs. Rocket (Orientation Effects)**

III. SUMMARY

A. ROCKET POTENTIAL

The initial charging peak analysis conducted on the SPEAR-1 ESA data by the original investigators (Figure 8) gave high and low estimates for the rocket body potential. The data analyzed in this paper indicates that the rocket body potential was much closer to the higher estimate. The broad, and occasionally ambiguous, charging peaks now appear to be partly an artifact of missing the charging peak as it moves between energy channels.

There was an absence of a charging peak in ion ESA 5A for potentials below 500 V, though there were clear peaks in the "down" viewing ESAs. This appears to be a trajectory effect related to the shape of the sheath around the vehicle.

During the 398 MET discharge operation, sphere 1 was charged to 45.3 kV. The results from the analysis of this discharge period indicate that the rocket body charged to a peak of 17.4 kV. This rocket body potential was 38 percent of the sphere potential and represented the highest percentage of all the discharge operations. The 398, 286, and 510 MET discharges all displayed non-linear effects at high voltages. These discharges were the only operations that had one of the spheres biased in excess of 40 kV. A summary of the results is provided in Table 6.

TABLE 6

ROCKET BODY POTENTIALS

MET (sec)	**ALT** (km)	**Rocket Potential** (volts)	**Percent of Peak Sphere Potential**
191	257	5700	26
210	285	5700	27
229	303	9940	27
248	321	3350	24
267	337	4380	28
286	350	13200	30
304	359	5700	26
323	365	5700	23
342	369	7360	19
360	369	3350	25
379	366	4380	29
398	361	17400	38
416	352	4380	19*
435	340	5700	22
454	325	7630	21
472	307	2550	19
491	287	5700	36
510	263	9940	22
528	235	2250	11*
547	206	1920	7
566	172	1445	10
584	137	1445	10

*indicates a change in the rocket orientation with respect to the geomagnetic field

B. EFFECTS OF ACS GAS EMISSIONS

All of the graphs produced during this analysis support the earlier conclusion that gas emissions from the ACS effectively grounded the rocket body [Ref. 2:p. 6]. The discharge operations that occurred immediately after these ACS maneuvers typically showed an order of magnitude drop in the rocket body potential. This drop in potential was evident in other discharge operations, but only when the potential of the rocket had

a magnitude greater than 1 keV. No ACS discharge effects were noted when the rocket body potential was less than 50 eV.

C. ALTITUDE AND ORIENTATION EFFECTS

The results indicate that the orientation of the rocket with respect to the geomagnetic field was more critical than the altitude. This was demonstrated in Figure 21 and is supported by the results in Table 6. The near-perpendicular orientation had the higher percentages, and the third orientation (boom of sphere 1 parallel to geomagnetic field) had much lower percentages.

The rocket body potential was significantly reduced during the last two discharge operations. The 603 MET at an altitude of 98 km shows a peak potential of less than 50 eV. The 622 MET discharge gave no results, indicating that the instruments had "burned up" during the re-entry (see Appendices A and B).

IV. CONCLUSIONS

The data contained in this work provides a myriad of opportunities for further research. The energy spectrograms show numerous phenomena that merit explanation. Additional research needs to be done to correlate the ACS telemetry with the observed drops in the rocket body potential. In addition, a more-detailed analysis of the rocket body orientation and particle detector view directions with respect to the geomagnetic field needs to be conducted.

The results from this work also provide a baseline from which future rocket experiments (SPEAR-3) can orient their payload and sensor design. An increase in the number of energy steps from 32 to 64 with a 20–30 ms sweep period is needed. This increase, coupled with a mass analysis of the returned ions, would provide a much clearer picture of the rocket-space environment interaction.

The electrostatic analyzer provided the best source of data for this work. The CPA data was questionable and made no relevant contribution to the analysis. The CPA design should be deleted from future experiments.

The rocket ACS acted as a plasma contactor during firing. Unfortunately, the limited telemetry data for the ACS made correlations in ACS firings and rocket body potential more difficult. Future experiments should dedicate more telemetry for the ACS in order to

provide specific information on which gas jet(s) fired, how much gas was emitted, and more precise timing.

APPENDIX A

ION ESA 5A SPECTROGRAMS

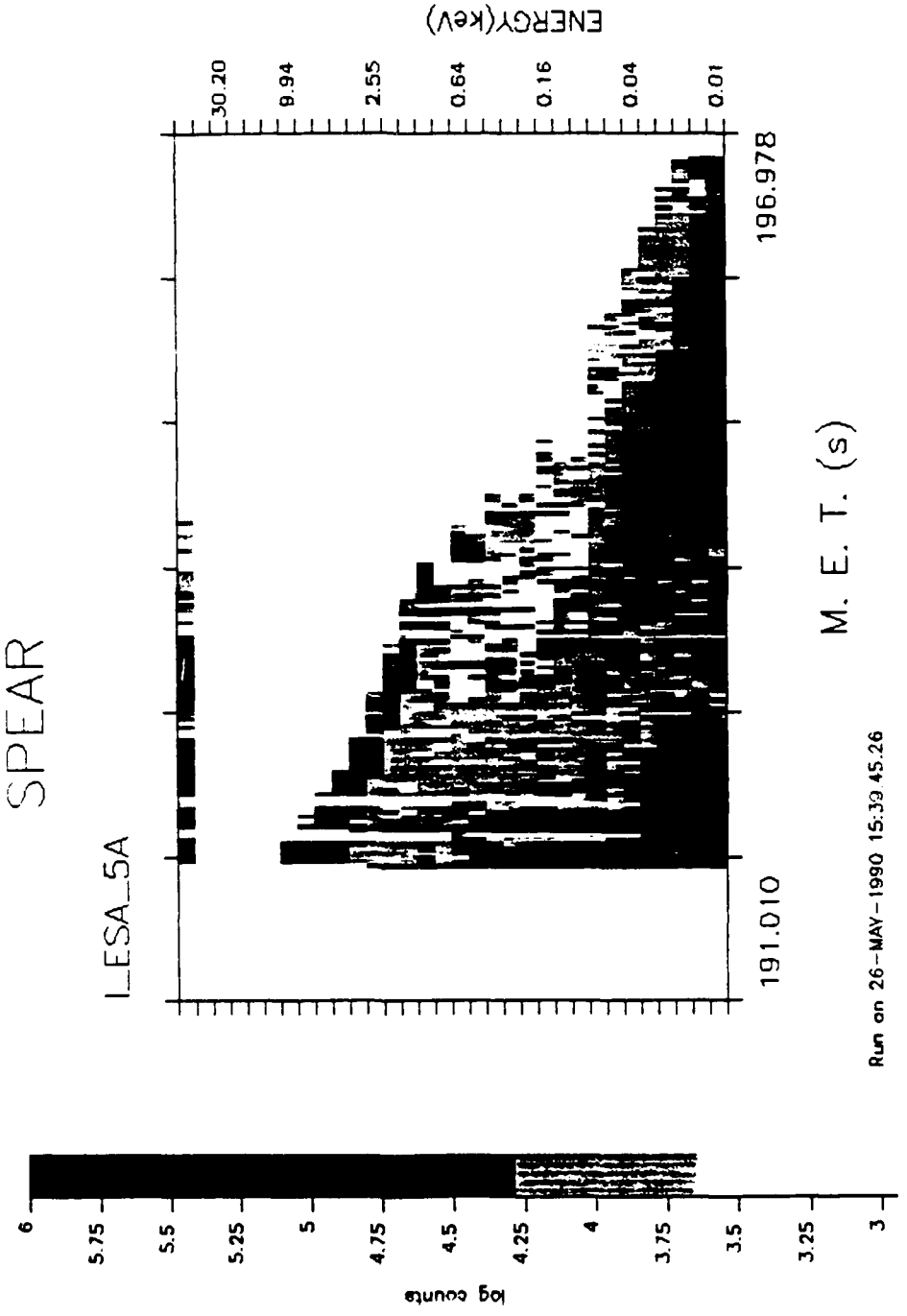

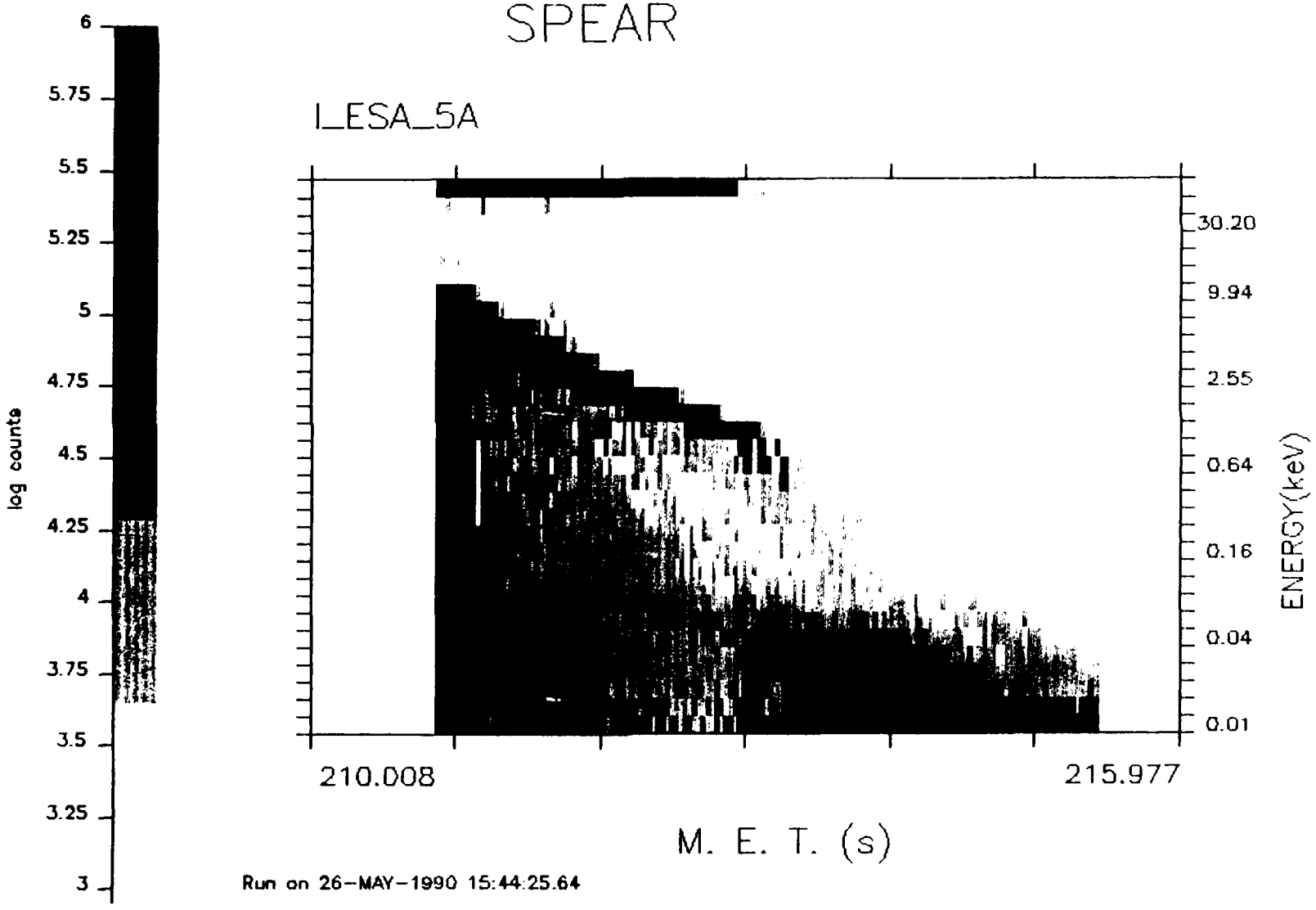
SPEAR
I_ESA_5A
log counts
6
5.75
5.5
5.25
5
4.75
4.5
4.25
4
3.75
3.5
3.25
3
30.20
9.94
2.55
0.64
0.16
0.04
0.01
ENERGY(keV)
210.008
215.977
M. E. T. (s)
Run on 26-MAY-1990 15:44:25.64

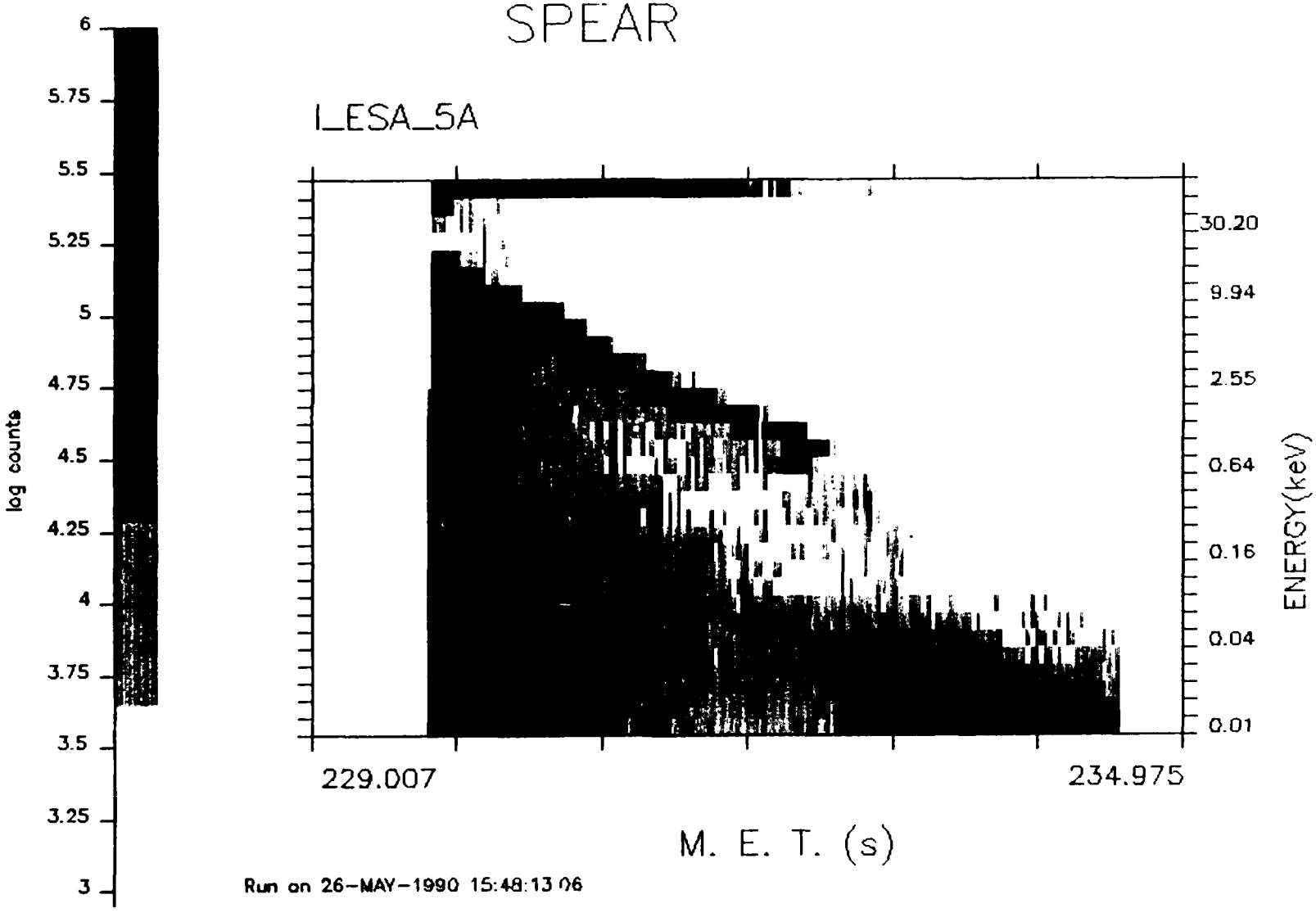
SPEAR
I_ESA_5A
log counts
6
5.75
5.5
5.25
5
4.75
4.5
4.25
4
3.75
3.5
3.25
3
30.20
9.94
2.55
0.64
0.16
0.04
0.01
ENERGY(keV)
229.007
234.975
M. E. T. (s)
Run on 26-MAY-1990 15:48:13.06

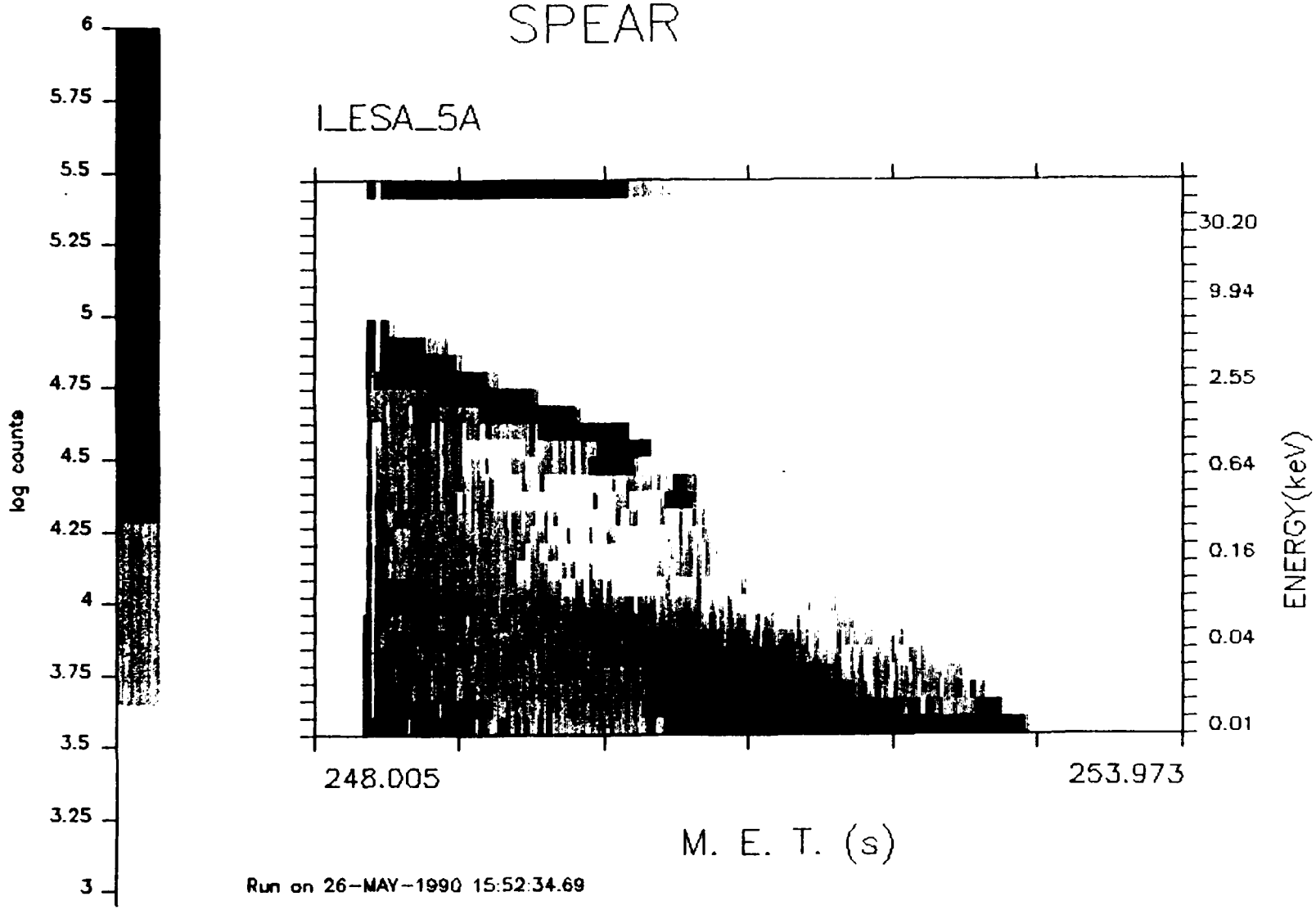
SPEAR
I_ESA_5A
log counts
6
5.75
5.5
5.25
5
4.75
4.5
4.25
4
3.75
3.5
3.25
3
30.20
9.94
2.55
0.64
0.16
0.04
0.01
ENERGY(keV)
248.005
253.973
M. E. T. (s)
Run on 26-MAY-1990 15:52:34.69

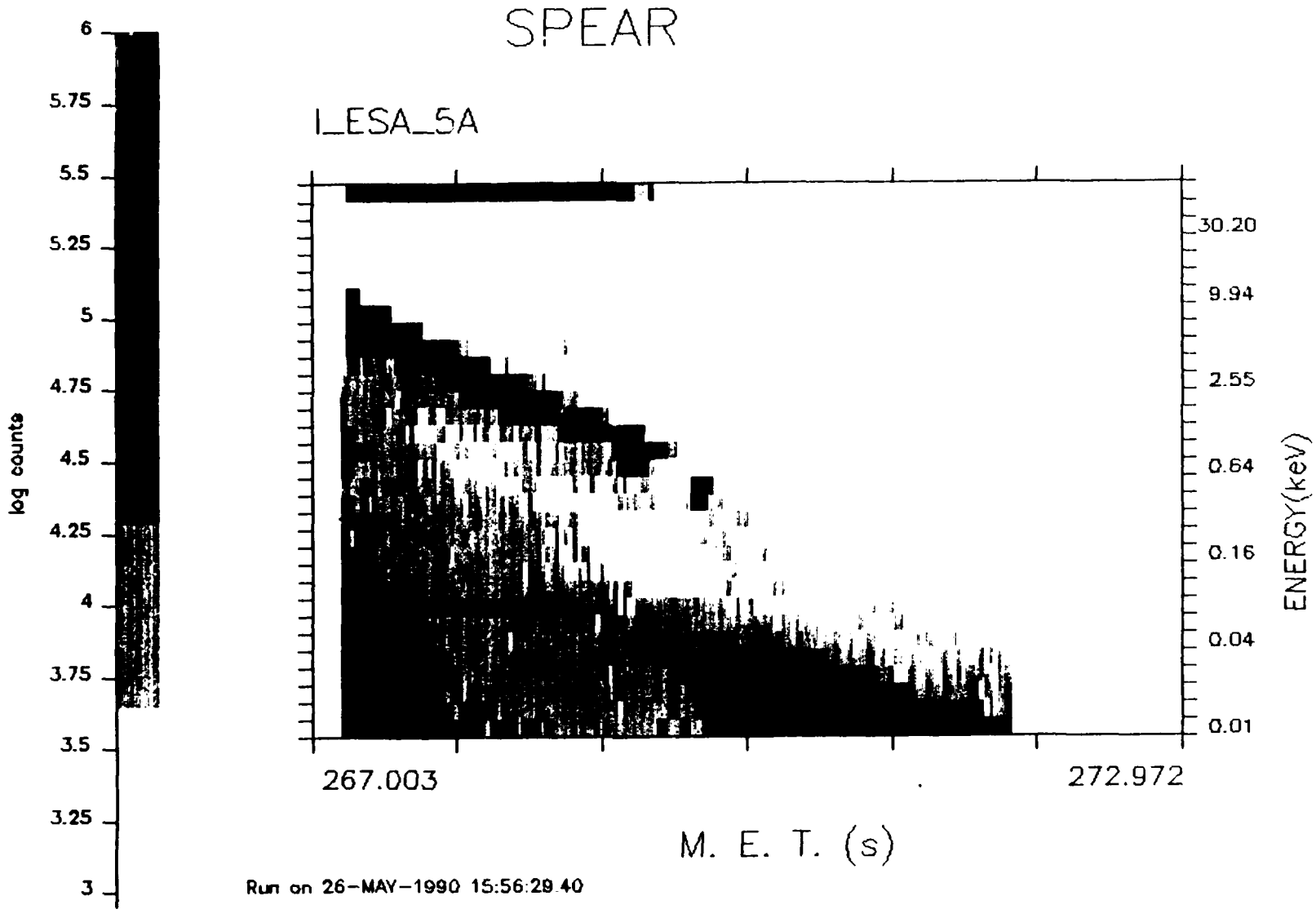
SPEAR
I_ESA_5A
log counts
6
5.75
5.5
5.25
5
4.75
4.5
4.25
4
3.75
3.5
3.25
3
30.20
9.94
2.55
0.64
0.16
0.04
0.01
ENERGY(keV)
267.003
272.972
M. E. T. (s)
Run on 26-MAY-1990 15:56:29.40

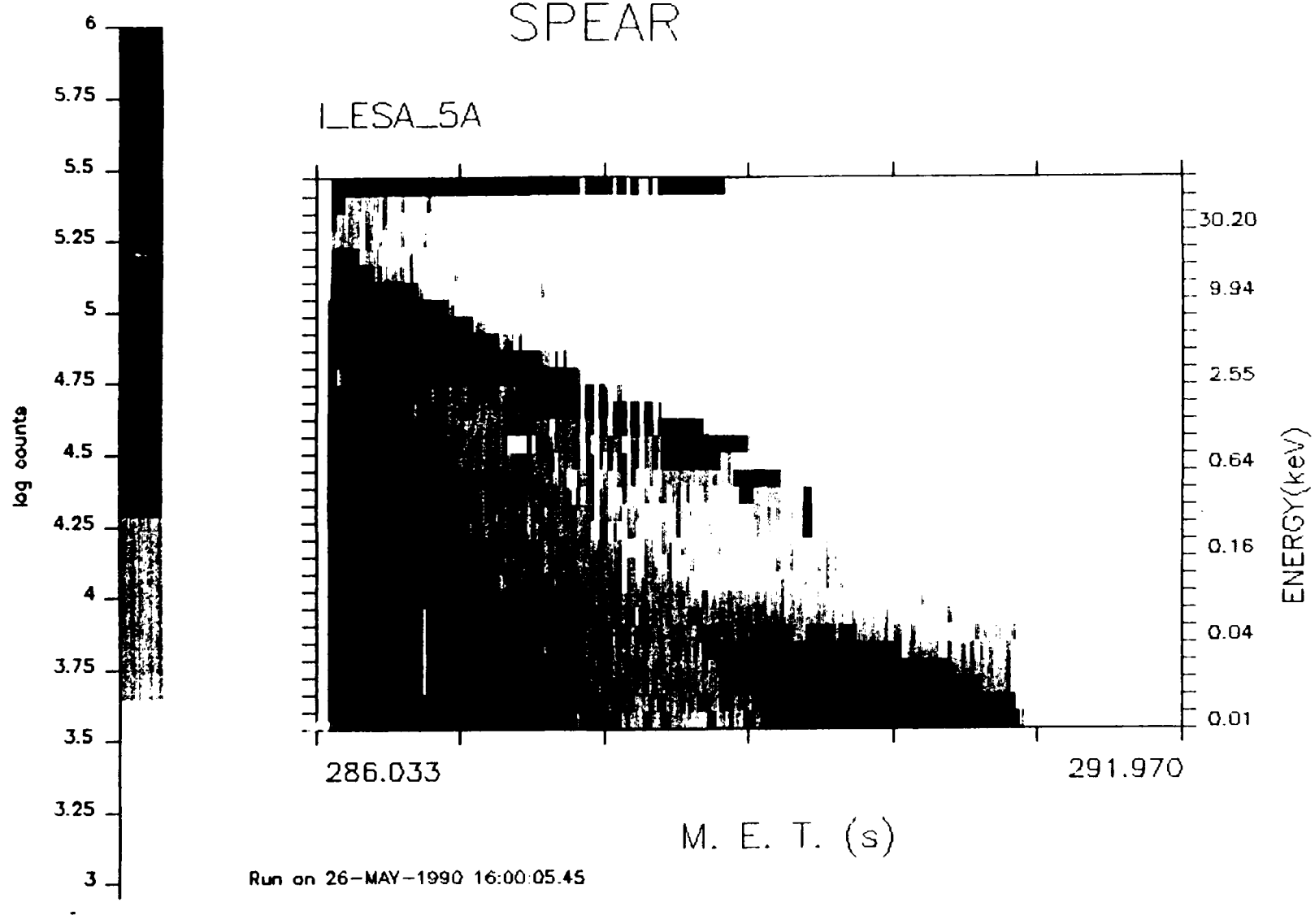
SPEAR
I_ESA_5A
log counts
6
5.75
5.5
5.25
5
4.75
4.5
4.25
4
3.75
3.5
3.25
3
30.20
9.94
2.55
0.64
0.16
0.04
0.01
ENERGY(keV)
286.033
291.970
M. E. T. (s)
Run on 26-MAY-1990 16:00:05.45

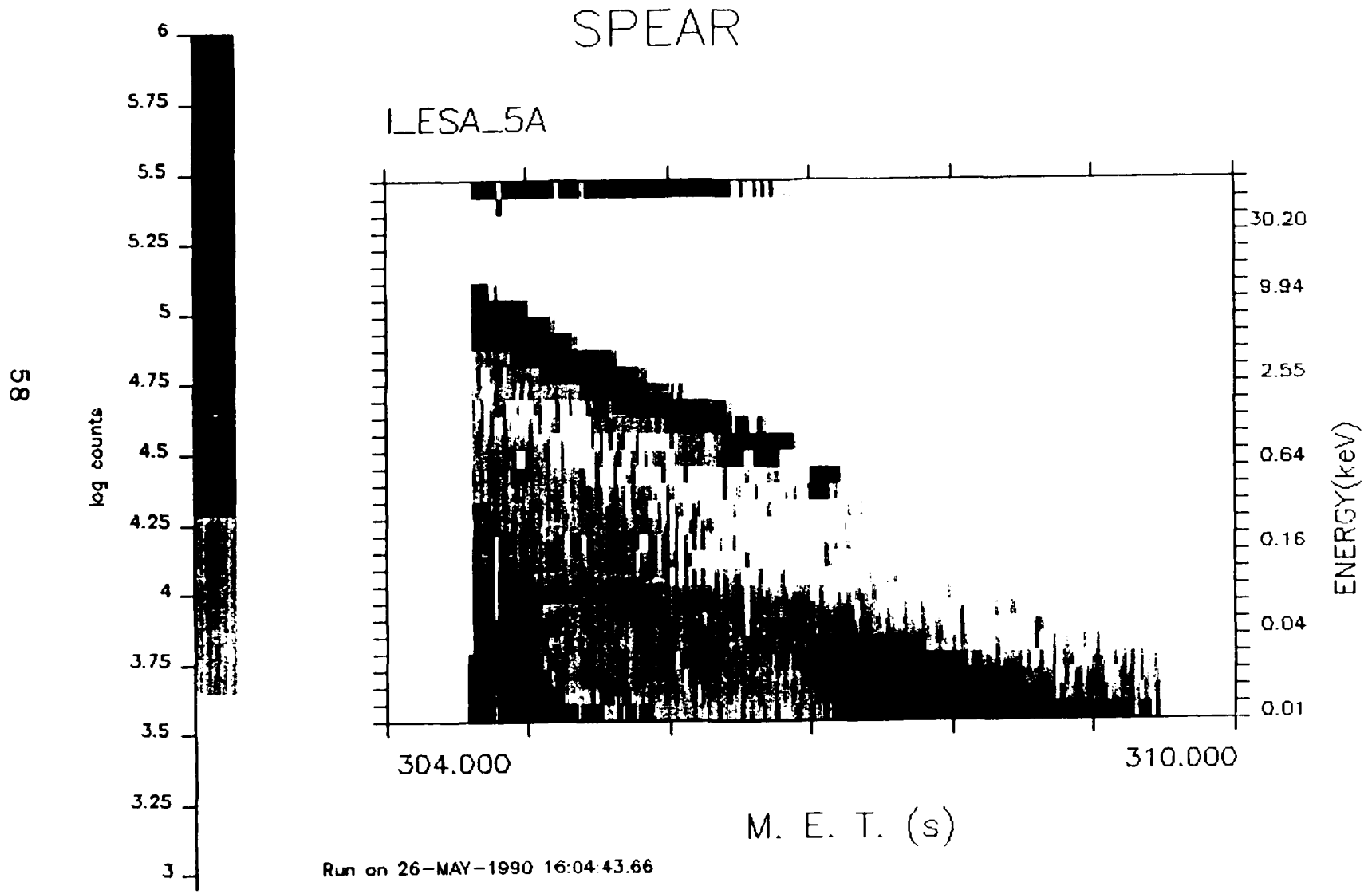
SPEAR
I_ESA_5A
6
5.75
5.5
5.25
5
4.75
4.5
4.25
4
3.75
3.5
3.25
3
log counts
30.20
9.94
2.55
0.64
0.16
0.04
0.01
ENERGY(keV)
304.000
310.000
M. E. T. (s)
Run on 26-MAY-1990 16:04:43.66

58

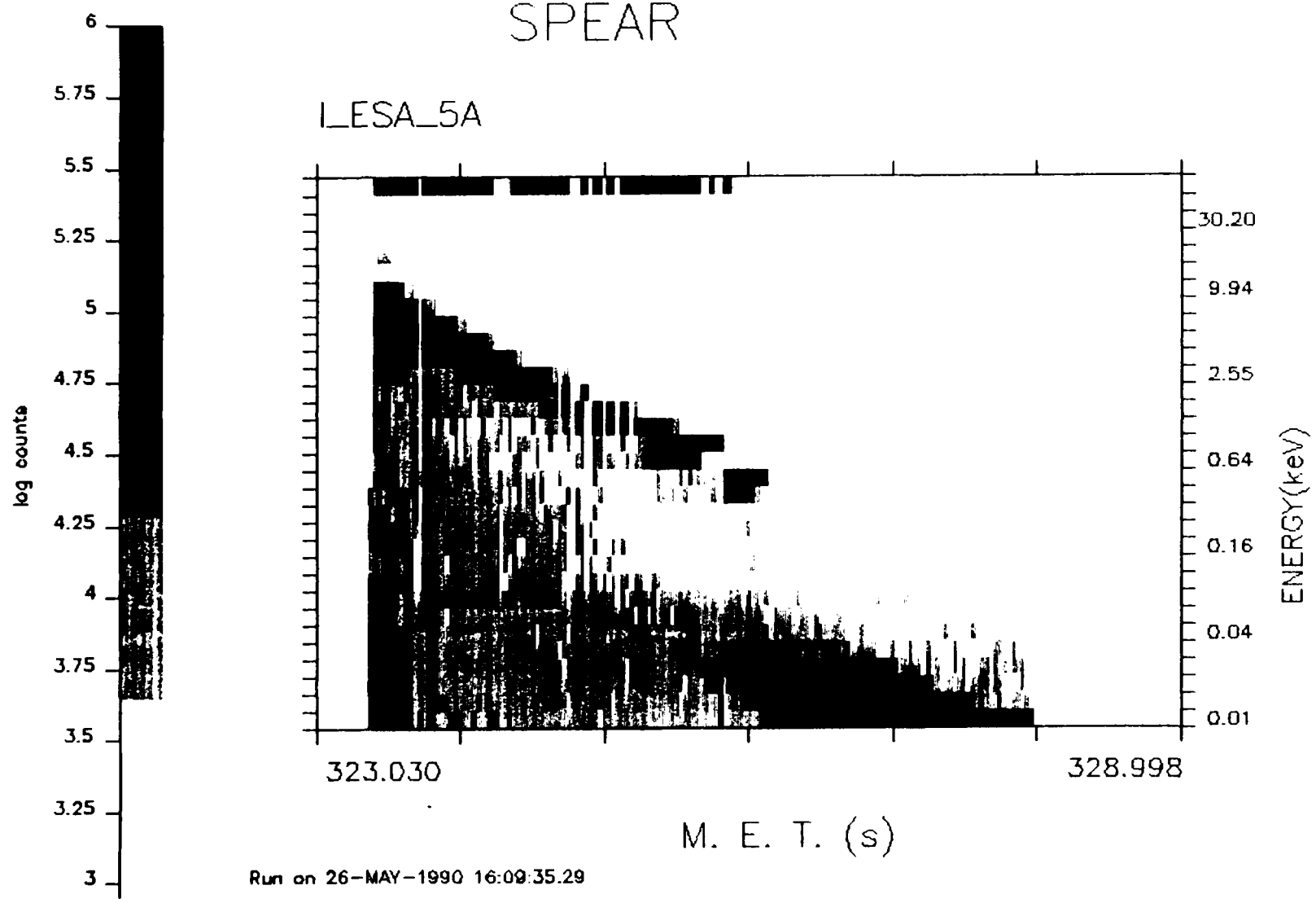
SPEAR
I_ESA_5A
log counts
6
5.75
5.5
5.25
5
4.75
4.5
4.25
4
3.75
3.5
3.25
3
30.20
9.94
2.55
0.64
0.16
0.04
0.01
ENERGY(keV)
323.030
328.998
M. E. T. (s)
Run on 26-MAY-1990 16:09:35.29

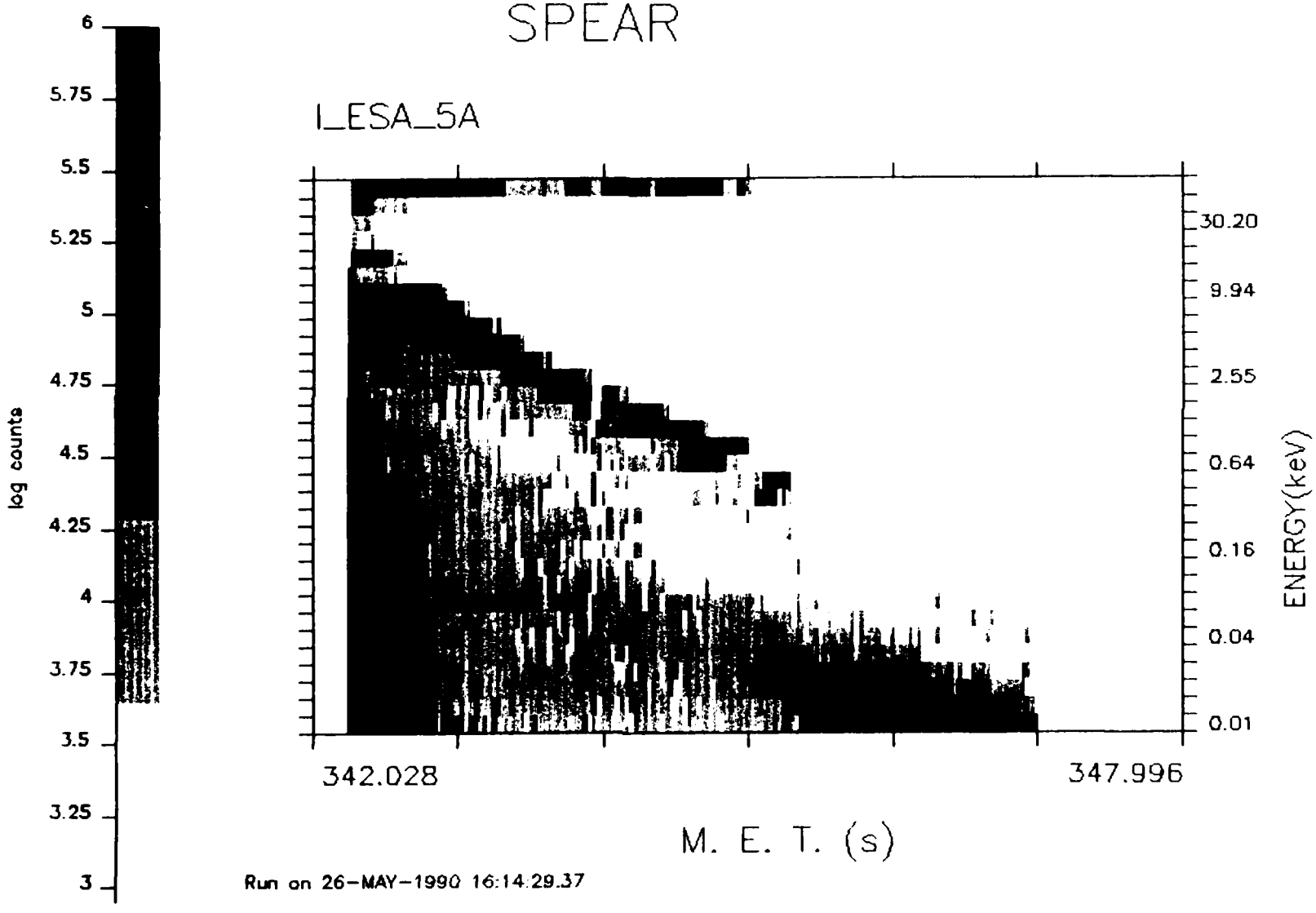
SPEAR
I_ESA_5A
6
5.75
5.5
5.25
5
4.75
4.5
4.25
4
3.75
3.5
3.25
3
log counts
30.20
9.94
2.55
0.64
0.16
0.04
0.01
ENERGY(keV)
342.028
347.996
M. E. T. (s)
Run on 26-MAY-1990 16:14:29.37

60

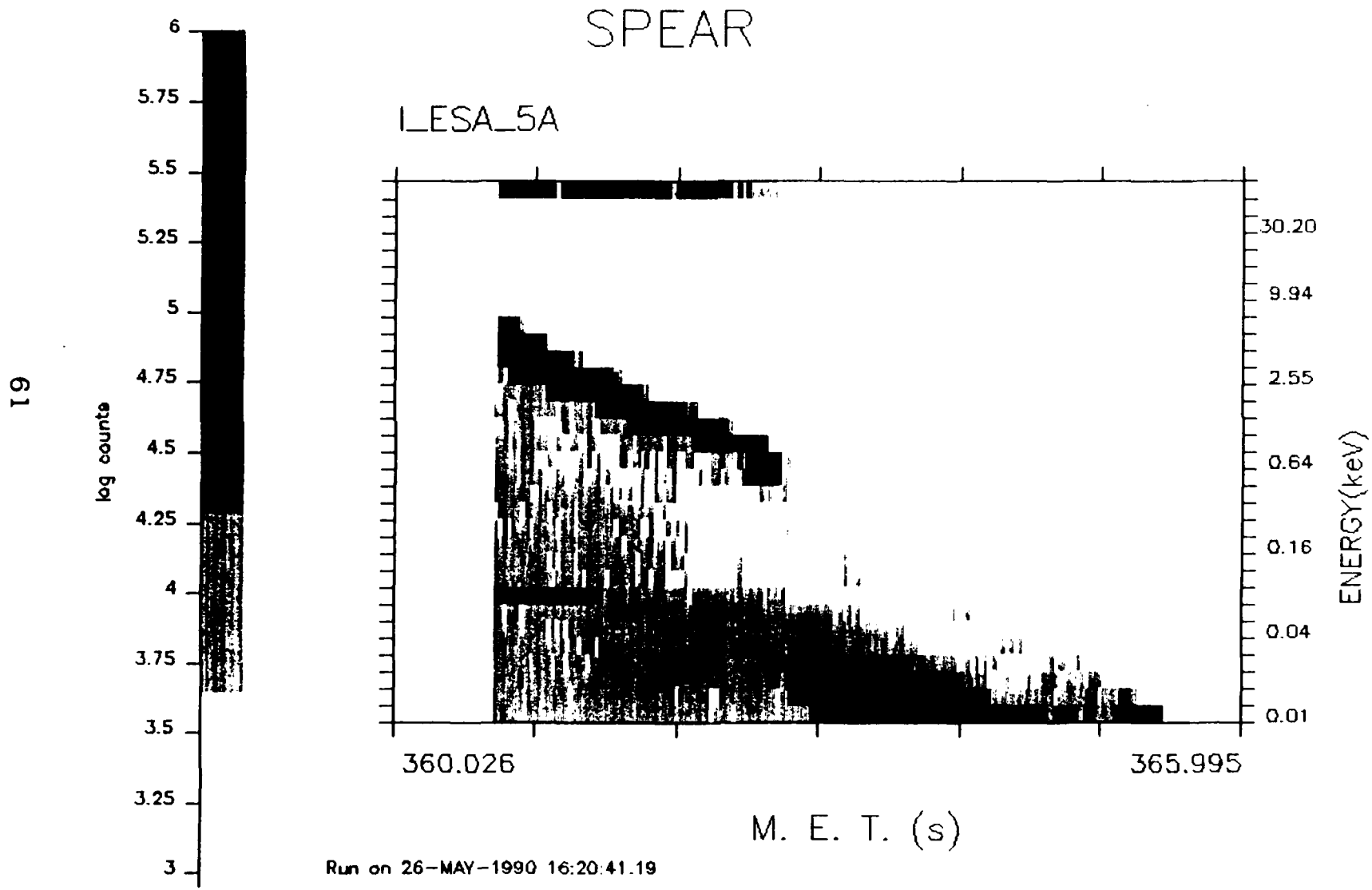
SPEAR
I_ESA_5A
6
5.75
5.5
5.25
5
4.75
4.5
4.25
4
3.75
3.5
3.25
3
log counts
30.20
9.94
2.55
0.64
0.16
0.04
0.01
ENERGY(keV)
360.026
365.995
M. E. T. (s)
Run on 26-MAY-1990 16:20:41.19

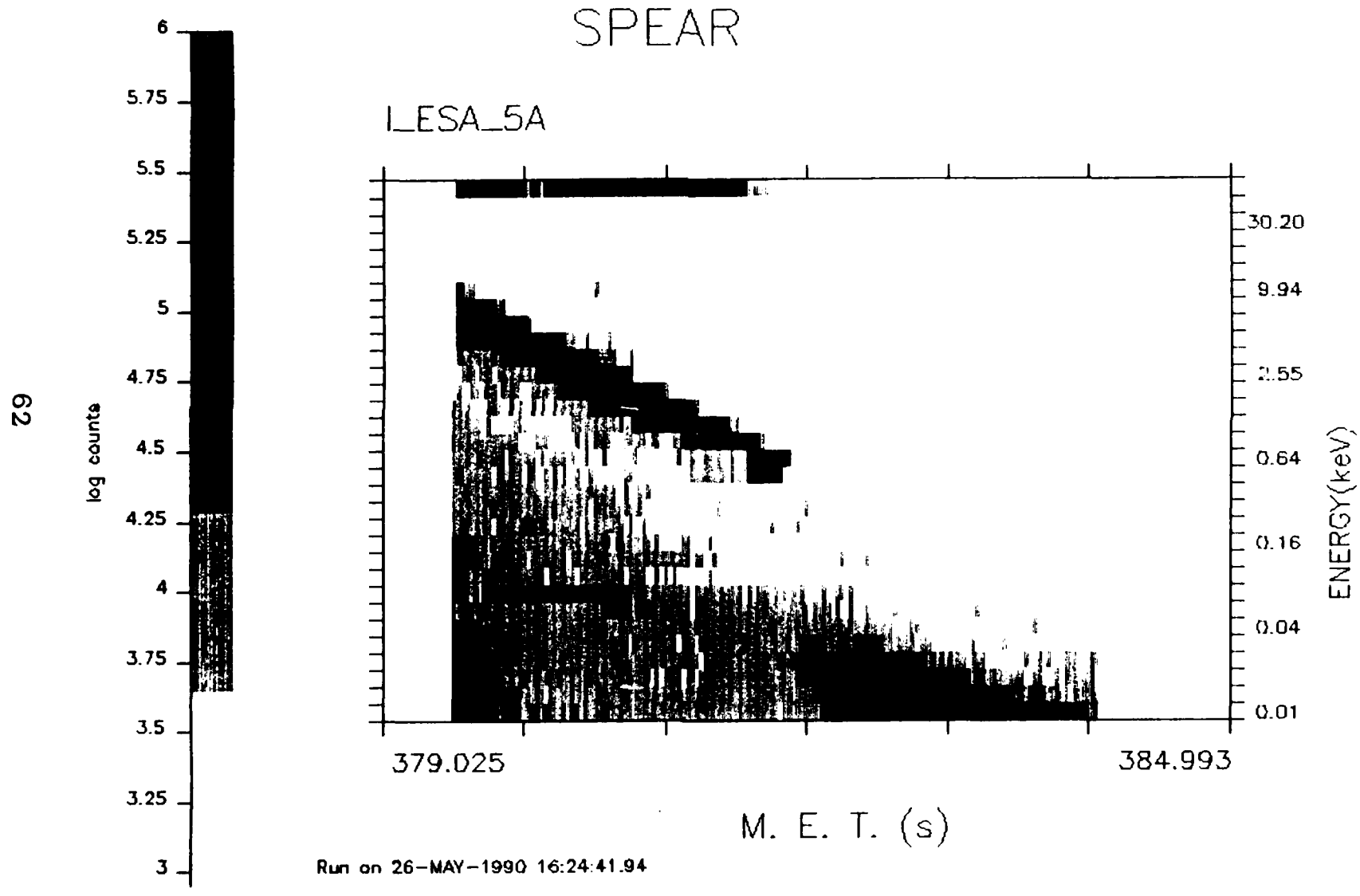
SPEAR
I_ESA_5A
62
log counts
6
5.75
5.5
5.25
5
4.75
4.5
4.25
4
3.75
3.5
3.25
3
30.20
9.94
2.55
0.64
0.16
0.04
0.01
ENERGY(keV)
379.025
384.993
M. E. T. (s)
Run on 26-MAY-1990 16:24:41.94

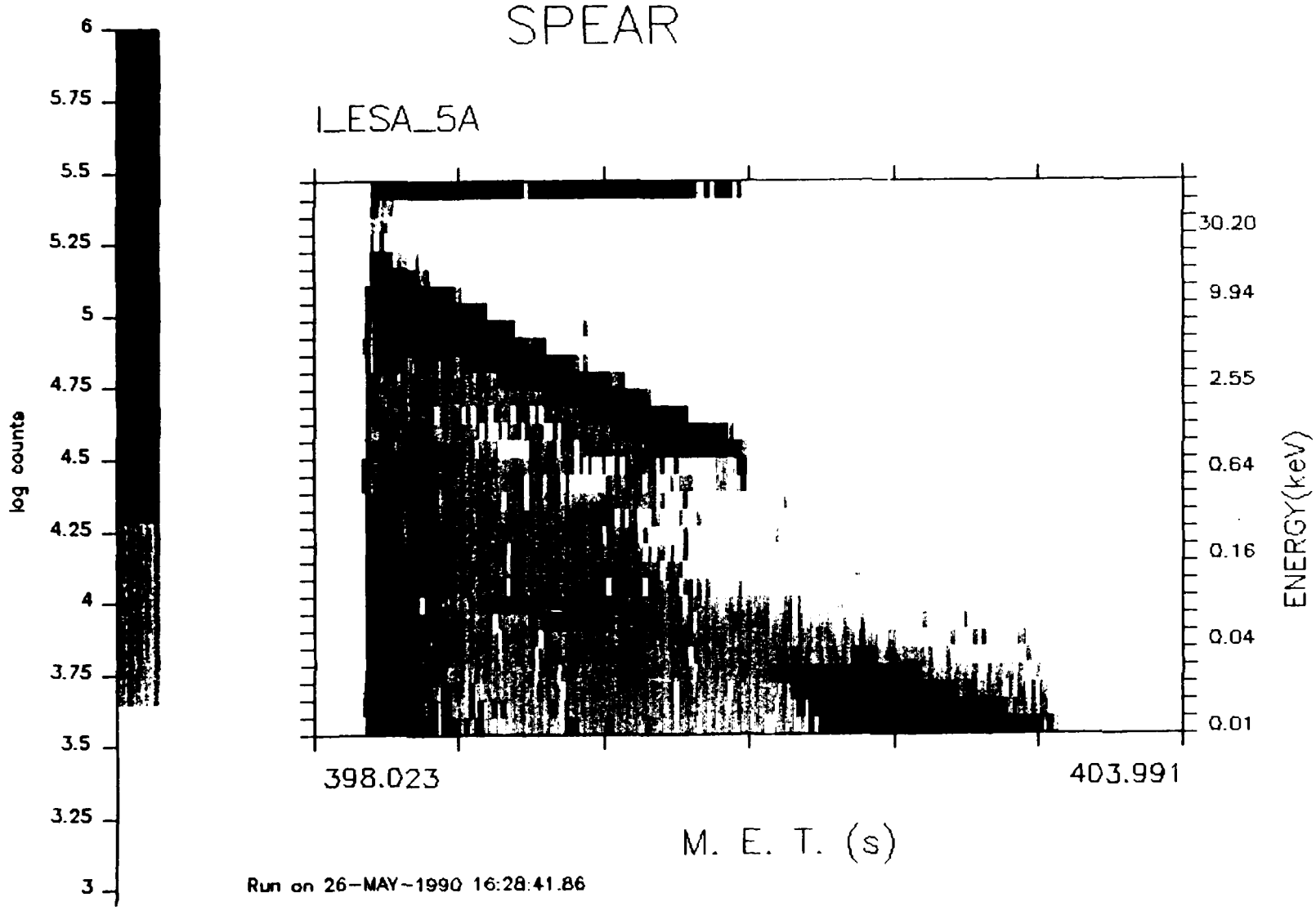
SPEAR
I_ESA_5A
log counts
6
5.75
5.5
5.25
5
4.75
4.5
4.25
4
3.75
3.5
3.25
3
30.20
9.94
2.55
0.64
0.16
0.04
0.01
ENERGY(keV)
398.023
403.991
M. E. T. (s)
Run on 26-MAY-1990 16:28:41.86

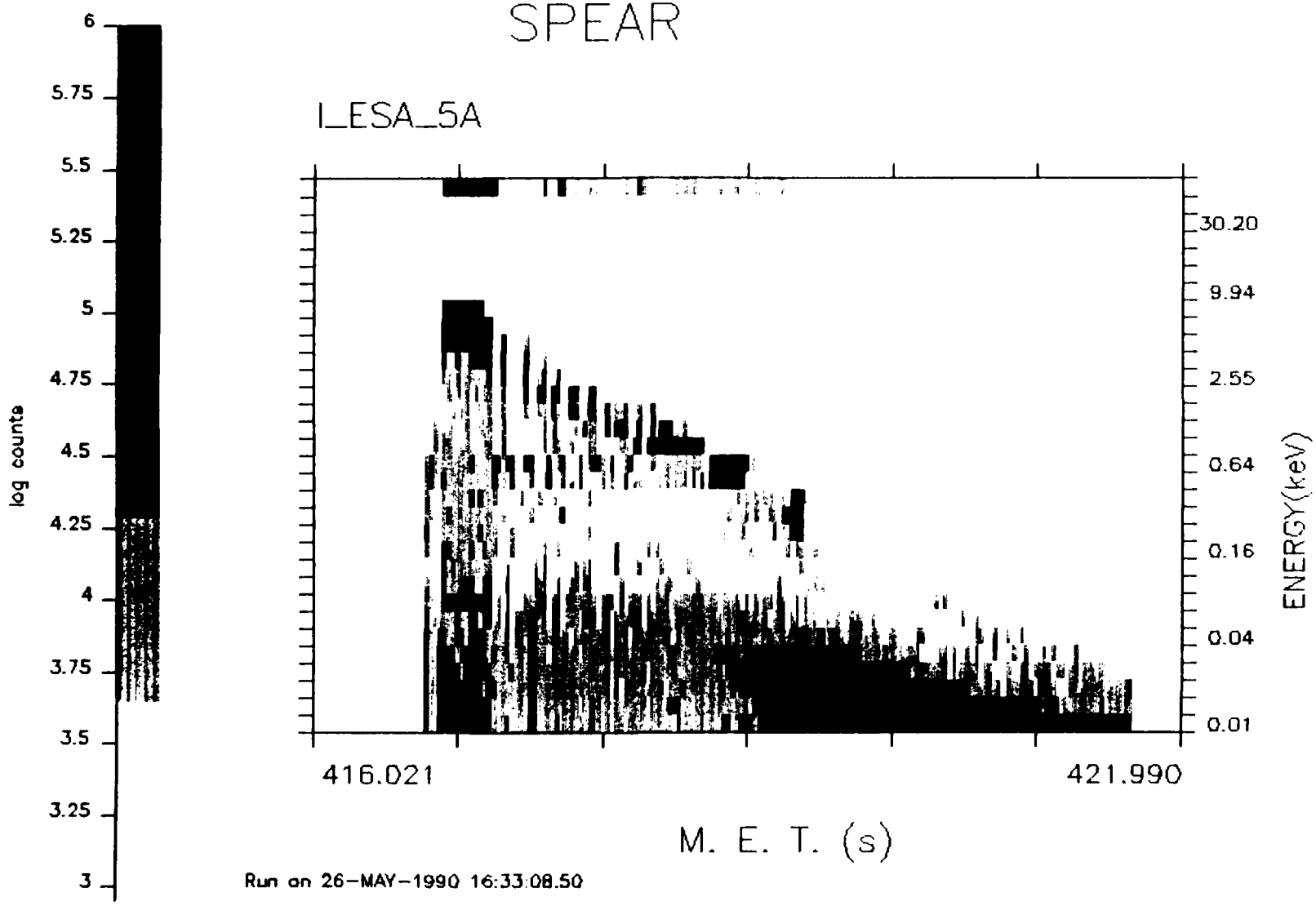
SPEAR
I_ESA_5A
log counts
6
5.75
5.5
5.25
5
4.75
4.5
4.25
4
3.75
3.5
3.25
3
30.20
9.94
2.55
0.64
0.16
0.04
0.01
ENERGY(keV)
416.021
421.990
M. E. T. (s)
Run on 26-MAY-1990 16:33:08.50

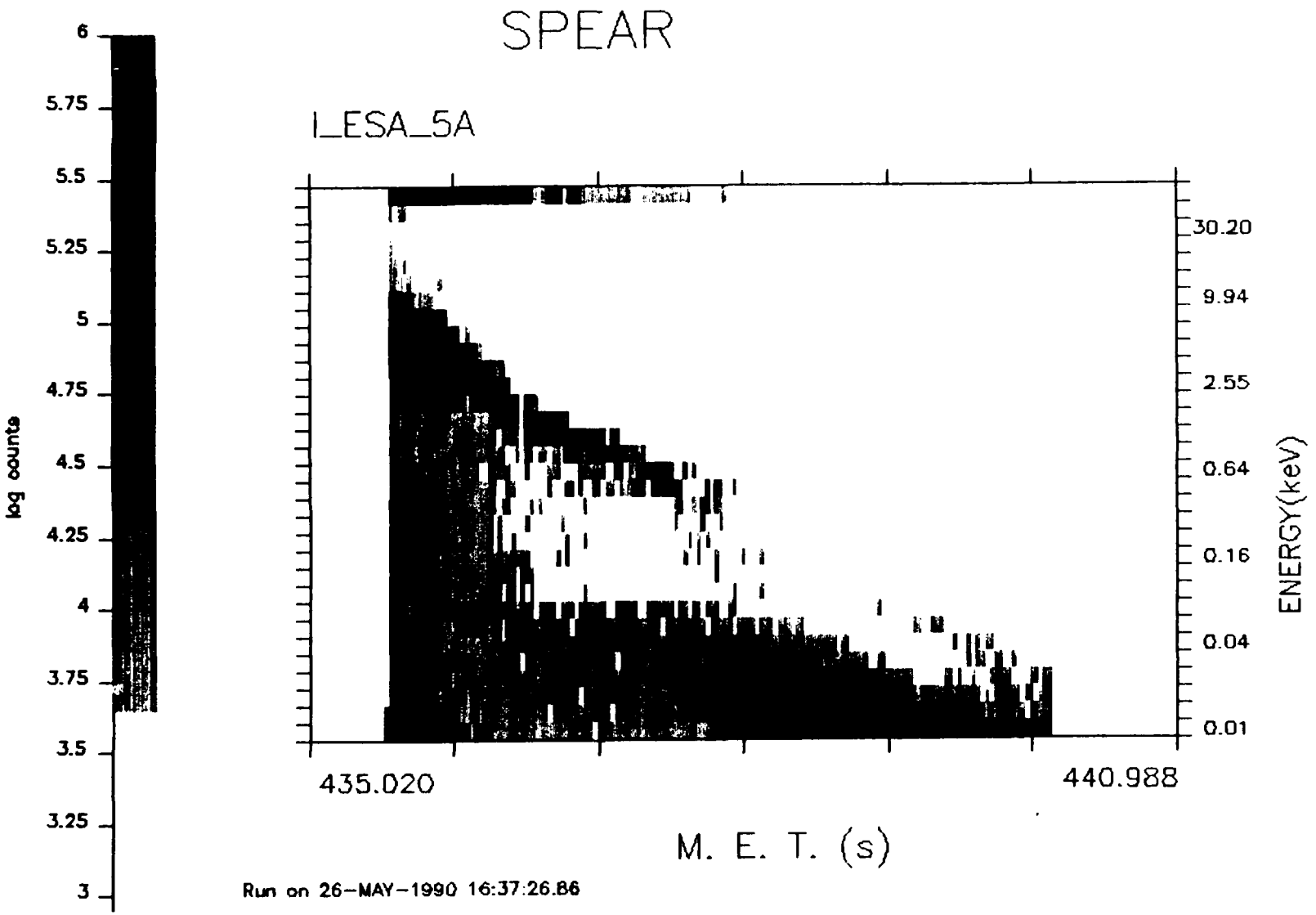
SPEAR
I_ESA_5A
log counts
6
5.75
5.5
5.25
5
4.75
4.5
4.25
4
3.75
3.5
3.25
3
30.20
9.94
2.55
0.64
0.16
0.04
0.01
ENERGY(keV)
435.020
440.988
M. E. T. (s)
Run on 26-MAY-1990 16:37:26.86

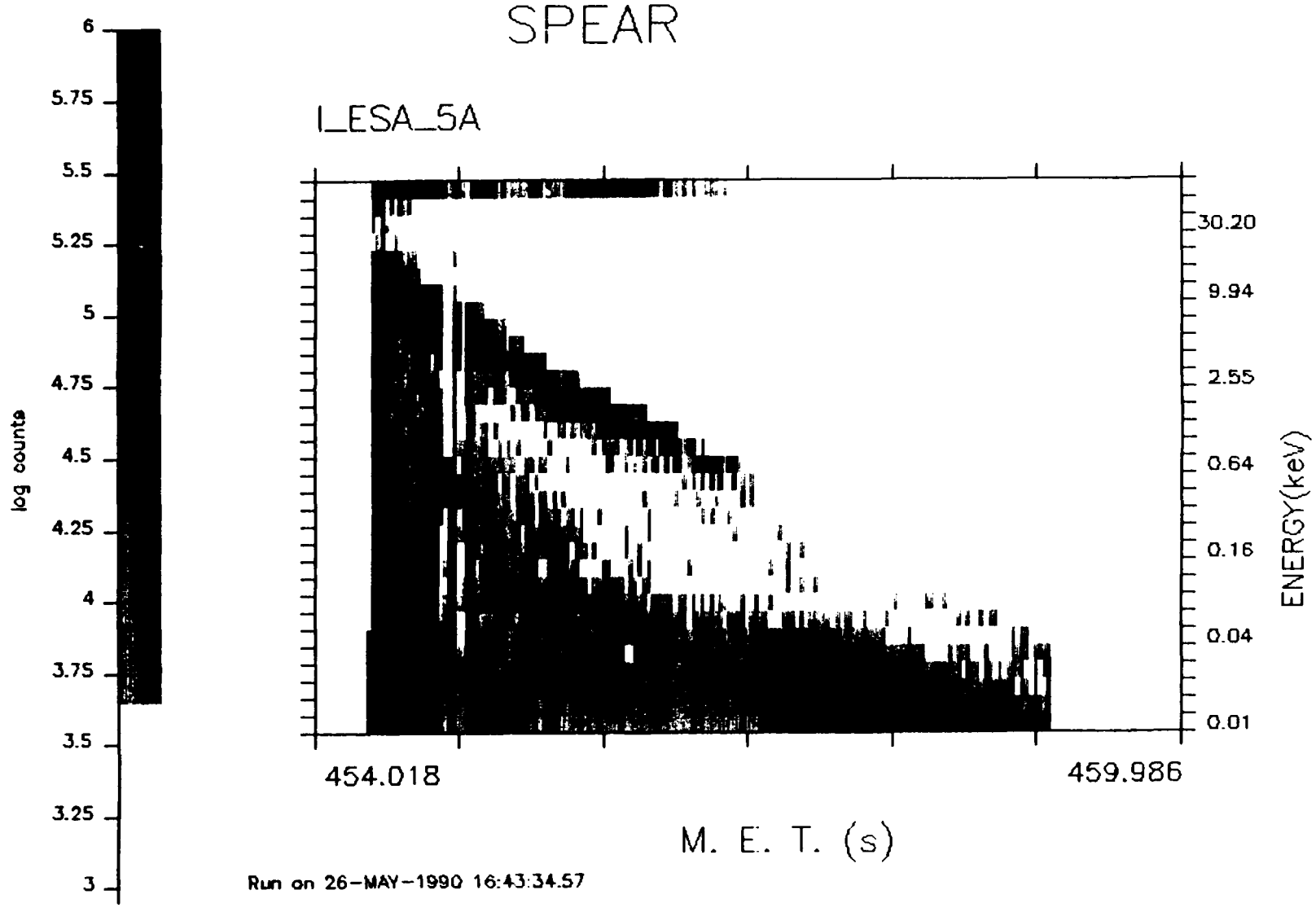
SPEAR
I_ESA_5A
log counts
6
5.75
5.5
5.25
5
4.75
4.5
4.25
4
3.75
3.5
3.25
3
30.20
9.94
2.55
0.64
0.16
0.04
0.01
ENERGY(keV)
454.018
459.986
M. E. T. (s)
Run on 26-MAY-1990 16:43:34.57

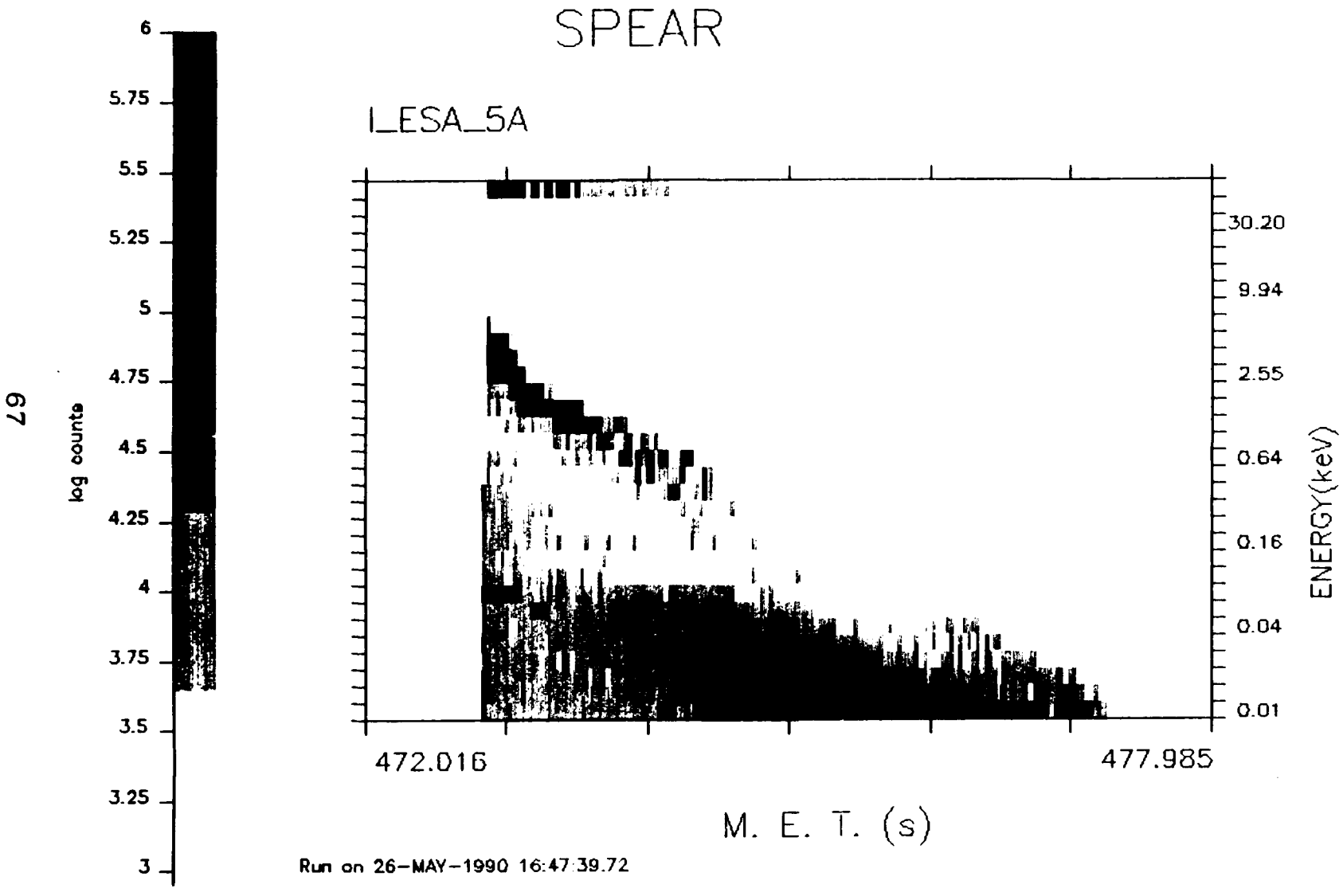
SPEAR
I_ESA_5A
log counts
6
5.75
5.5
5.25
5
4.75
4.5
4.25
4
3.75
3.5
3.25
3
30.20
9.94
2.55
0.64
0.16
0.04
0.01
ENERGY(keV)
472.016
477.985
M. E. T. (s)
Run on 26-MAY-1990 16:47:39.72

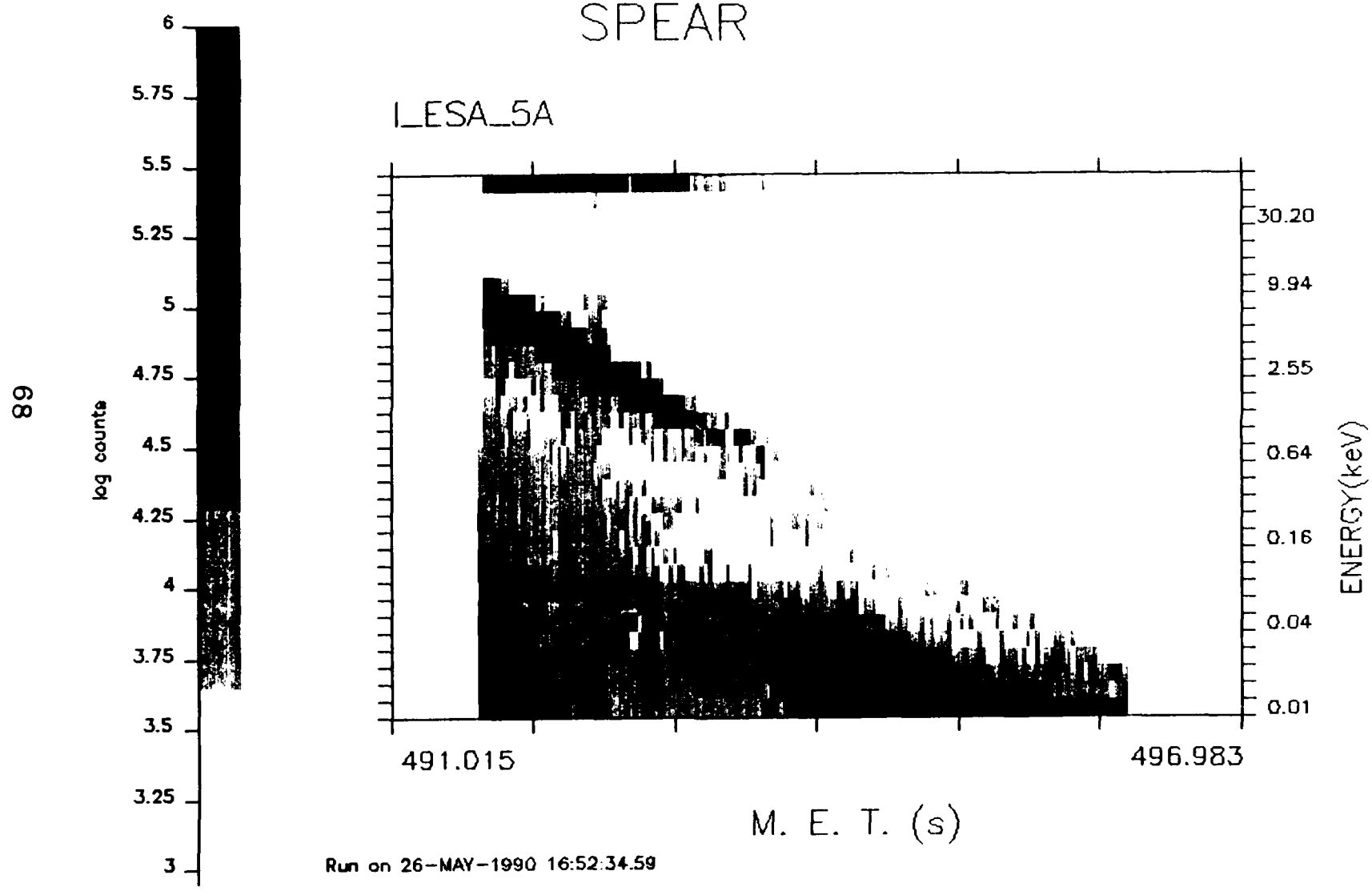
SPEAR
I_ESA_5A
6
5.75
5.5
5.25
5
4.75
4.5
4.25
4
3.75
3.5
3.25
3
log counts
30.20
9.94
2.55
0.64
0.16
0.04
0.01
ENERGY(keV)
491.015
496.983
M. E. T. (s)
Run on 26-MAY-1990 16:52:34.59

89

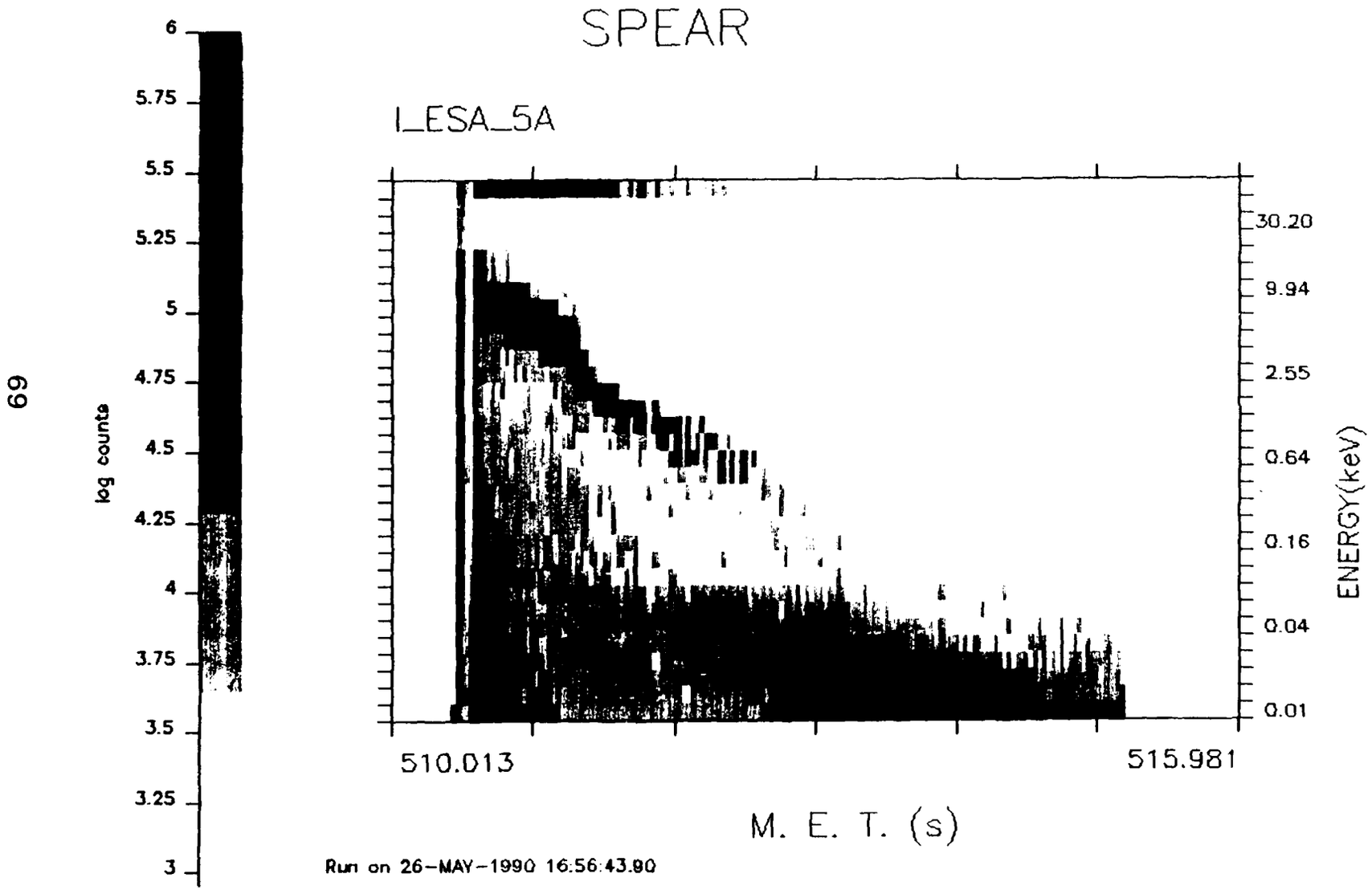
SPEAR
I_ESA_5A
log counts
6
5.75
5.5
5.25
5
4.75
4.5
4.25
4
3.75
3.5
3.25
3
30.20
9.94
2.55
0.64
0.16
0.04
0.01
ENERGY(keV)
510.013
515.981
M. E. T. (s)
Run on 26-MAY-1990 16:56:43.90

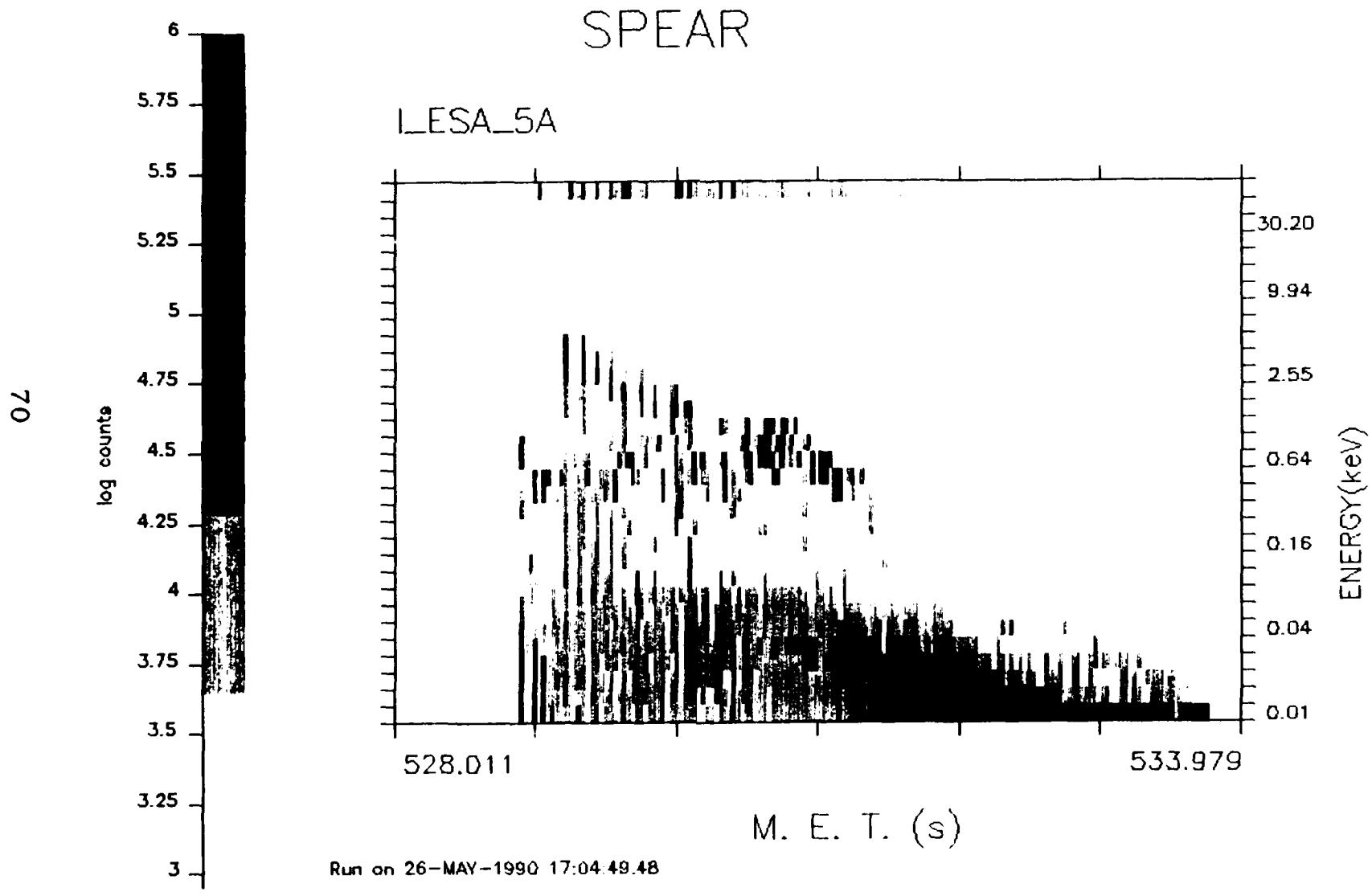
SPEAR
I_ESA_5A
log counts
6
5.75
5.5
5.25
5
4.75
4.5
4.25
4
3.75
3.5
3.25
3
30.20
9.94
2.55
0.64
0.16
0.04
0.01
ENERGY(keV)
528.011
533.979
M. E. T. (s)
Run on 26-MAY-1990 17:04:49.48

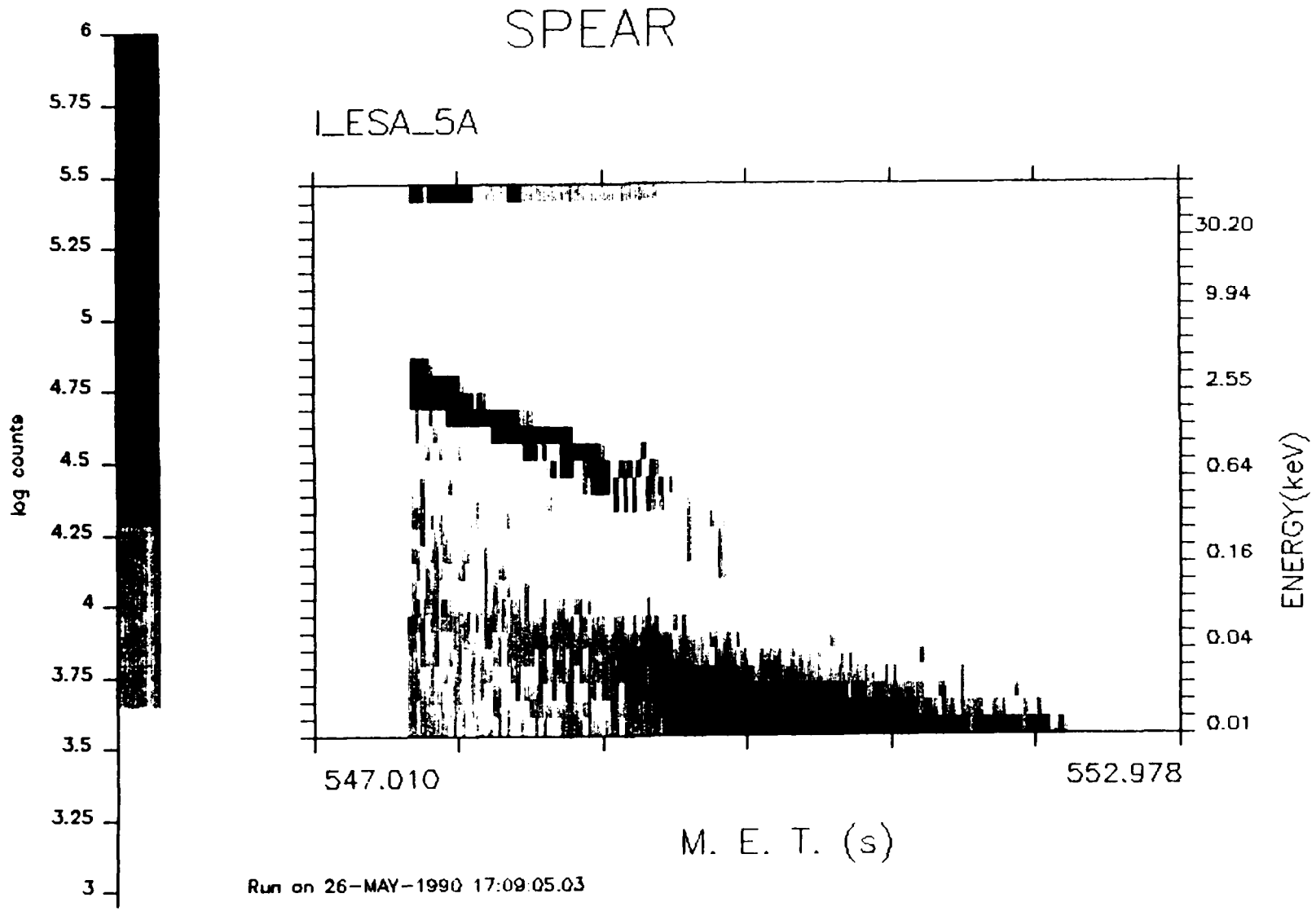
SPEAR
I_ESA_5A
log counts
6
5.75
5.5
5.25
5
4.75
4.5
4.25
4
3.75
3.5
3.25
3
30.20
9.94
2.55
0.64
0.16
0.04
0.01
ENERGY(keV)
547.010
552.978
M. E. T. (s)
Run on 26-MAY-1990 17:09:05.03

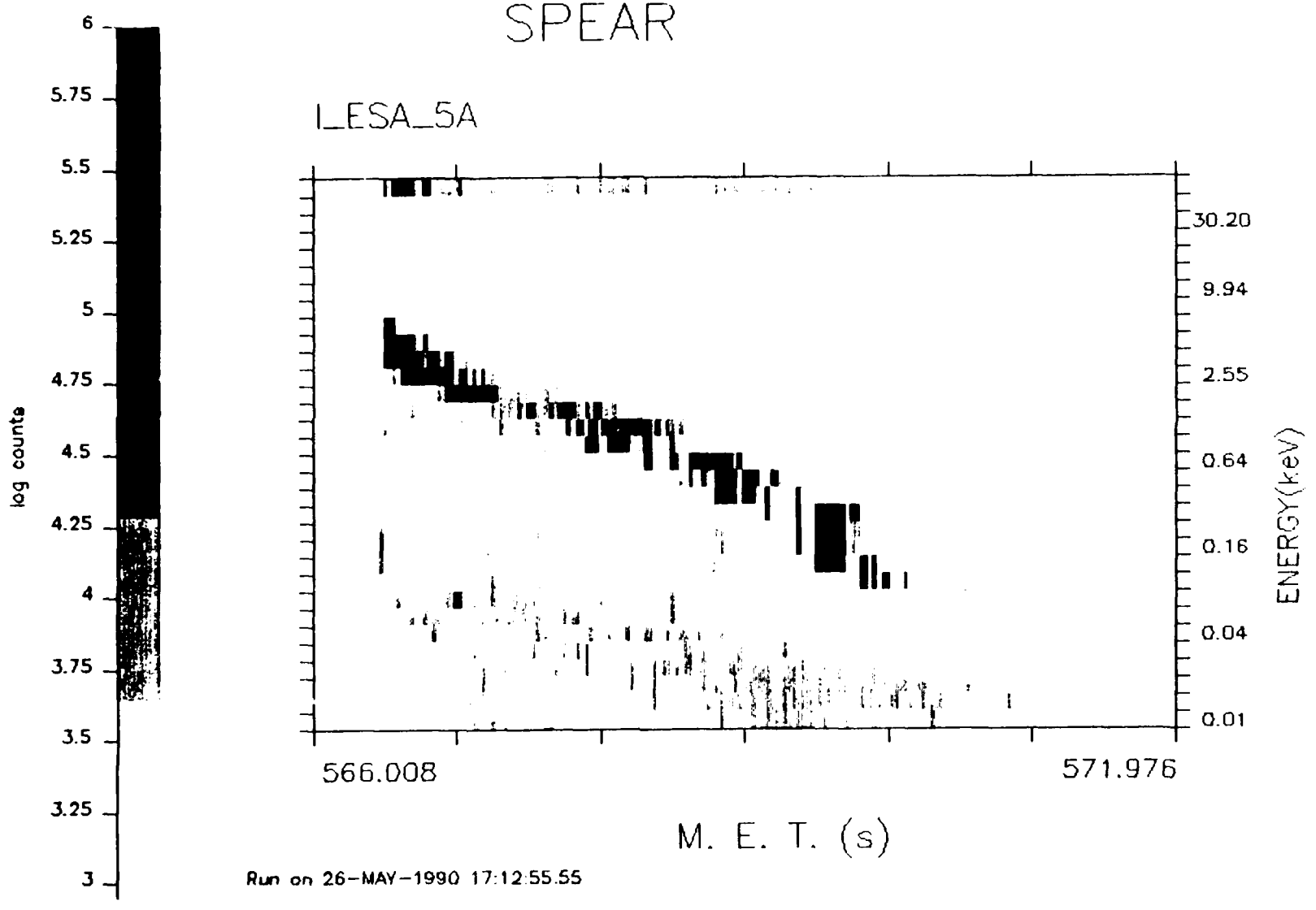
SPEAR
I_ESA_5A
log counts
6
5.75
5.5
5.25
5
4.75
4.5
4.25
4
3.75
3.5
3.25
3
30.20
9.94
2.55
0.64
0.16
0.04
0.01
ENERGY(keV)
566.008
571.976
M. E. T. (s)
Run on 26-MAY-1990 17:12:55.55

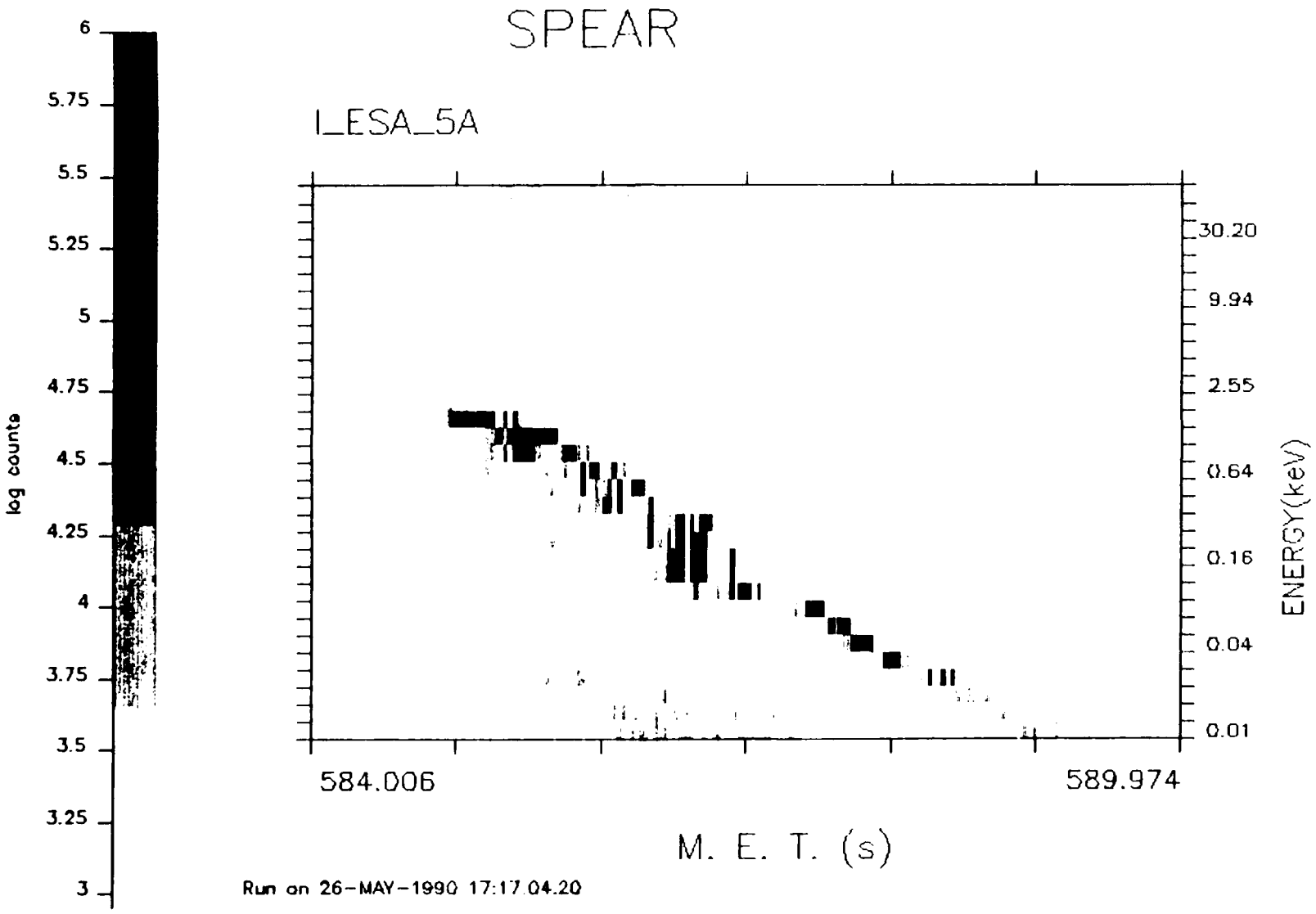
SPEAR
I_ESA_5A
log counts
6
5.75
5.5
5.25
5
4.75
4.5
4.25
4
3.75
3.5
3.25
3
30.20
9.94
2.55
0.64
0.16
0.04
0.01
ENERGY(keV)
584.006
589.974
M. E. T. (s)
Run on 26-MAY-1990 17:17.04.20

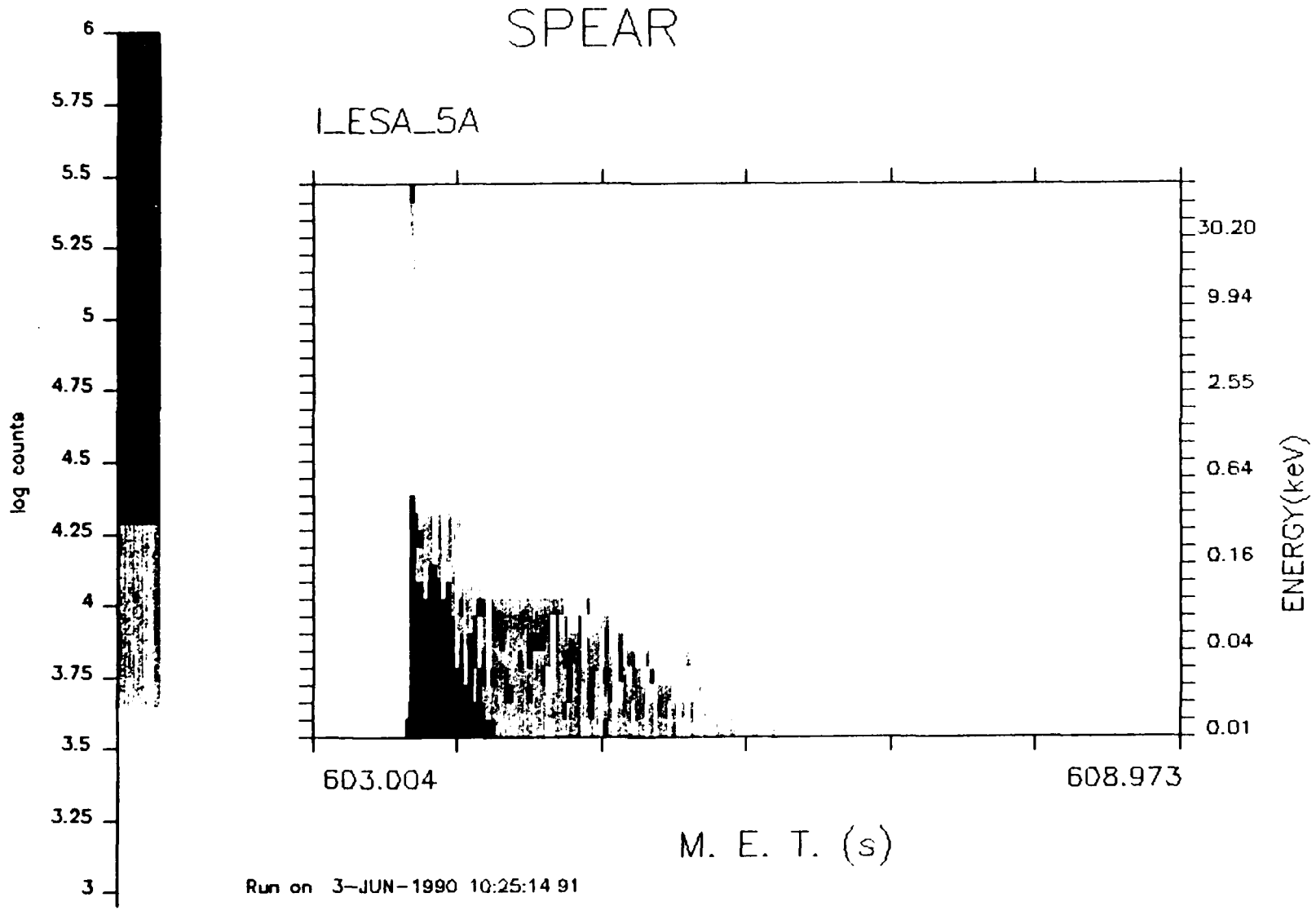
SPEAR
I_ESA_5A
log counts
6
5.75
5.5
5.25
5
4.75
4.5
4.25
4
3.75
3.5
3.25
3
30.20
9.94
2.55
0.64
0.16
0.04
0.01
ENERGY(keV)
603.004
608.973
M. E. T. (s)
Run on 3-JUN-1990 10:25:14 91

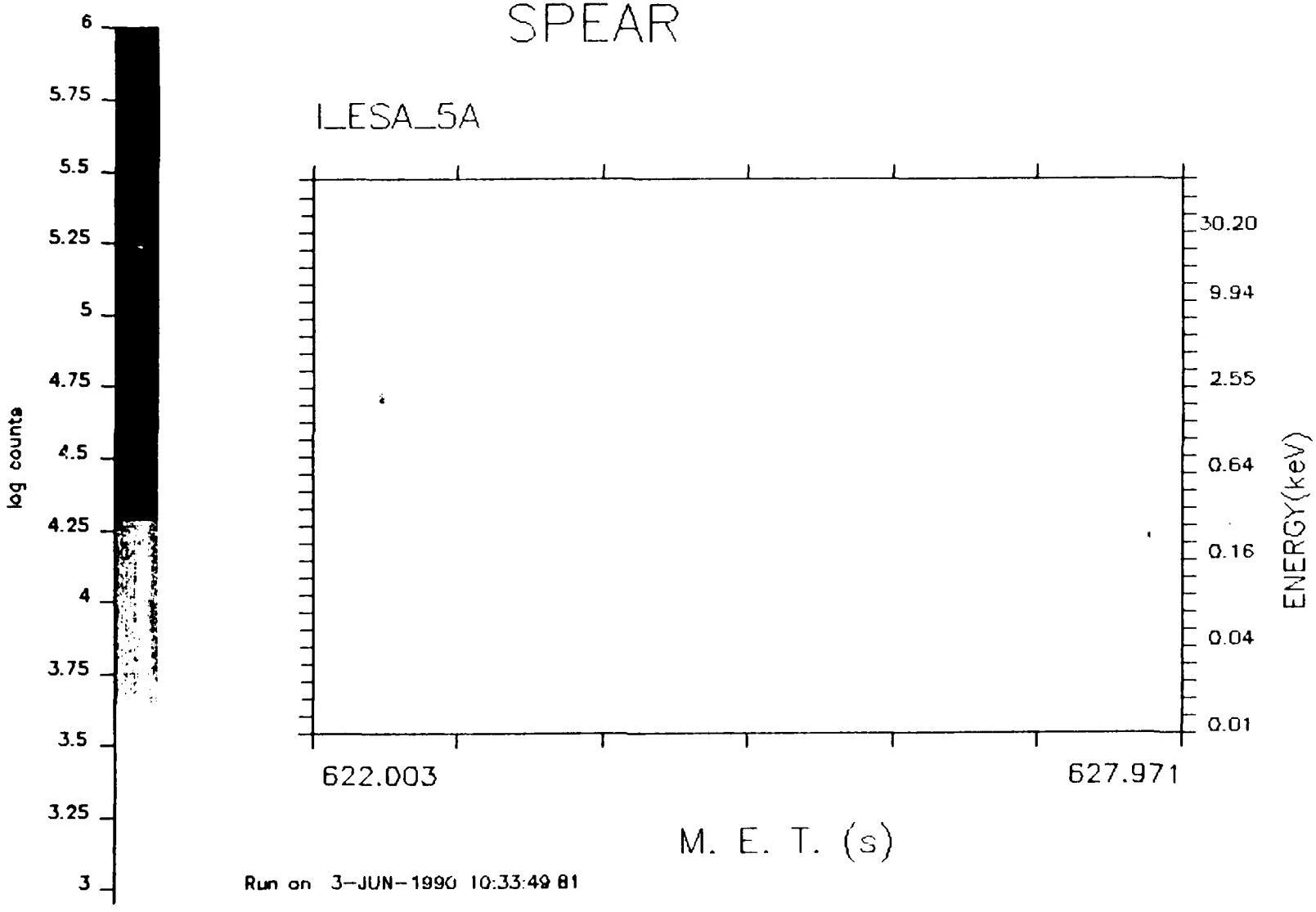
SPEAR
I_ESA_5A
log counts
6
5.75
5.5
5.25
5
4.75
4.5
4.25
4
3.75
3.5
3.25
3
30.20
9.94
2.55
0.64
0.16
0.04
0.01
ENERGY(keV)
622.003
627.971
M. E. T. (s)
Run on 3-JUN-1990 10:33:49.81

APPENDIX B

ION ESA 4B SPECTROGRAMS

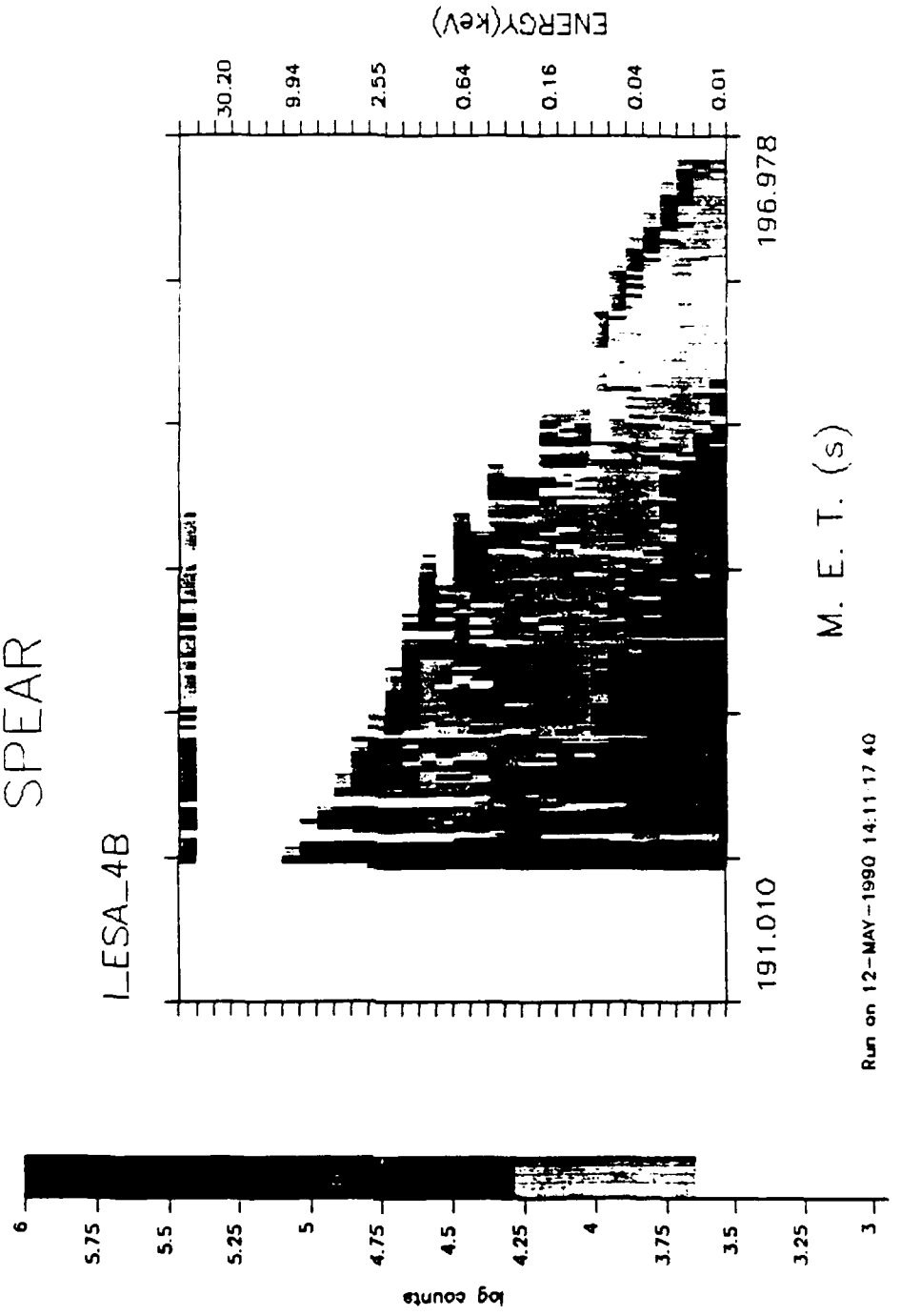

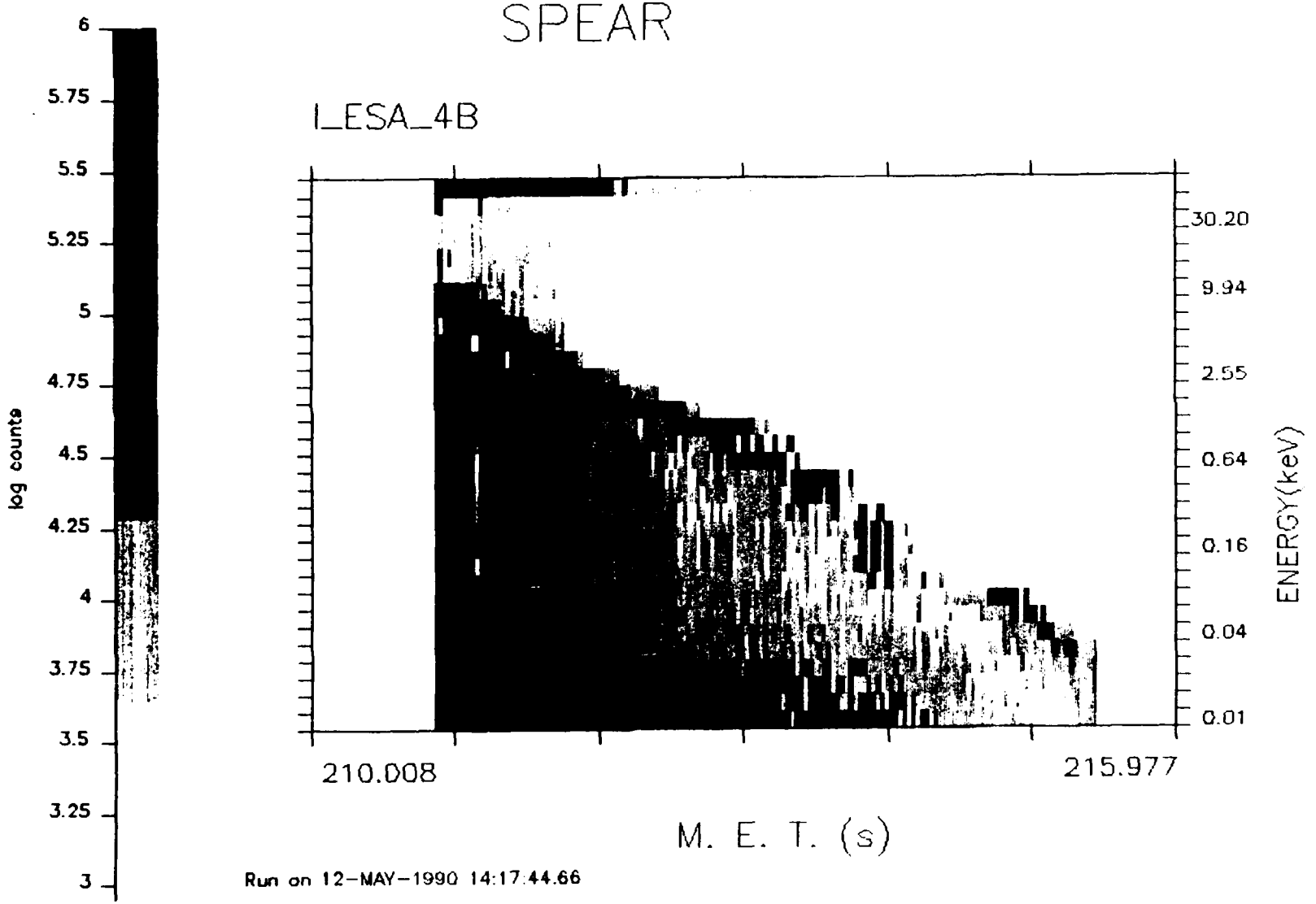
SPEAR
I_ESA_4B
log counts
6
5.75
5.5
5.25
5
4.75
4.5
4.25
4
3.75
3.5
3.25
3
30.20
9.94
2.55
0.64
0.16
0.04
0.01
ENERGY(keV)
210.008
215.977
M. E. T. (s)
Run on 12-MAY-1990 14:17:44.66

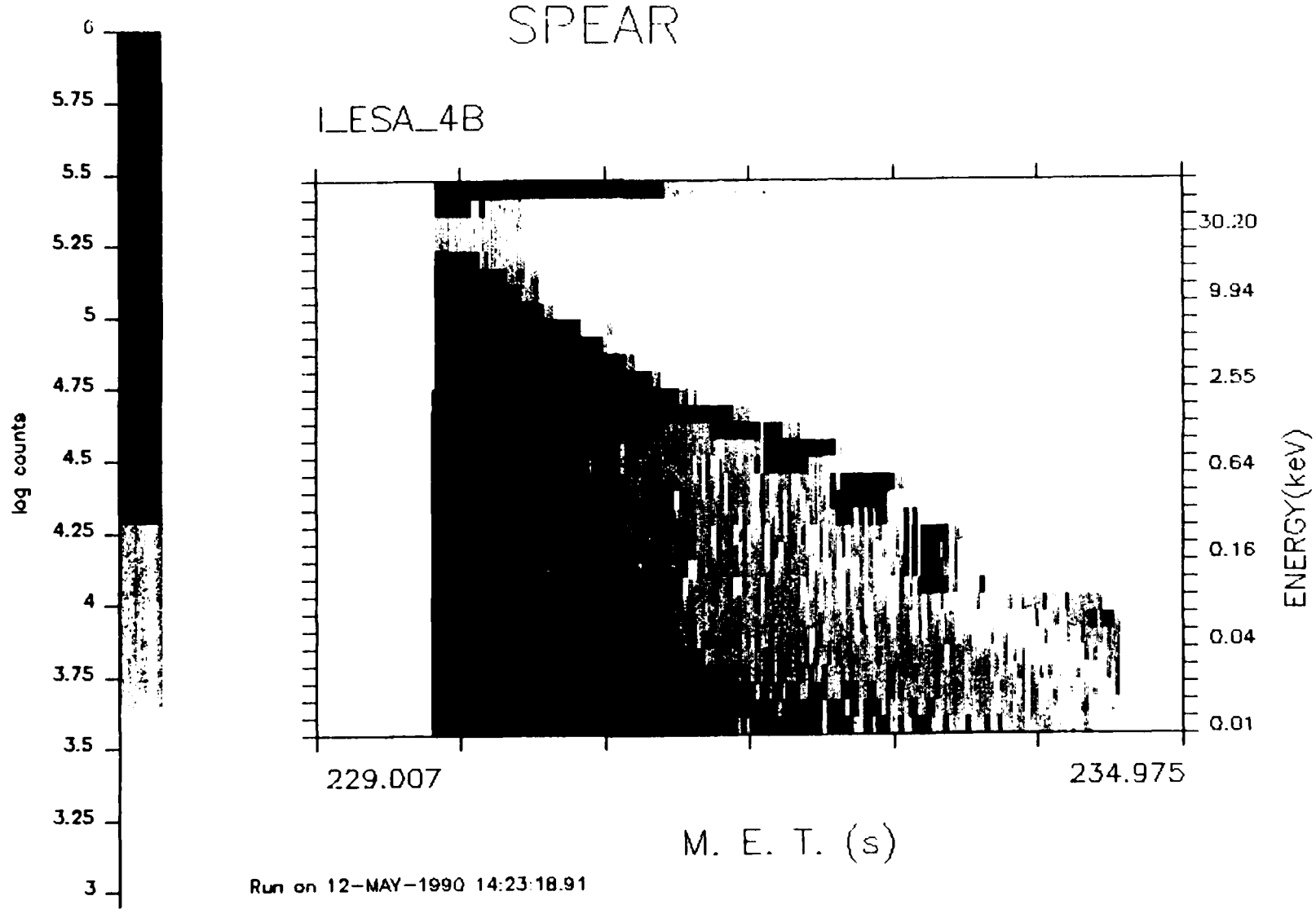
SPEAR
I_ESA_4B
log counts
6
5.75
5.5
5.25
5
4.75
4.5
4.25
4
3.75
3.5
3.25
3
30.20
9.94
2.55
0.64
0.16
0.04
0.01
ENERGY(keV)
229.007
234.975
M. E. T. (s)
Run on 12-MAY-1990 14:23:18.91

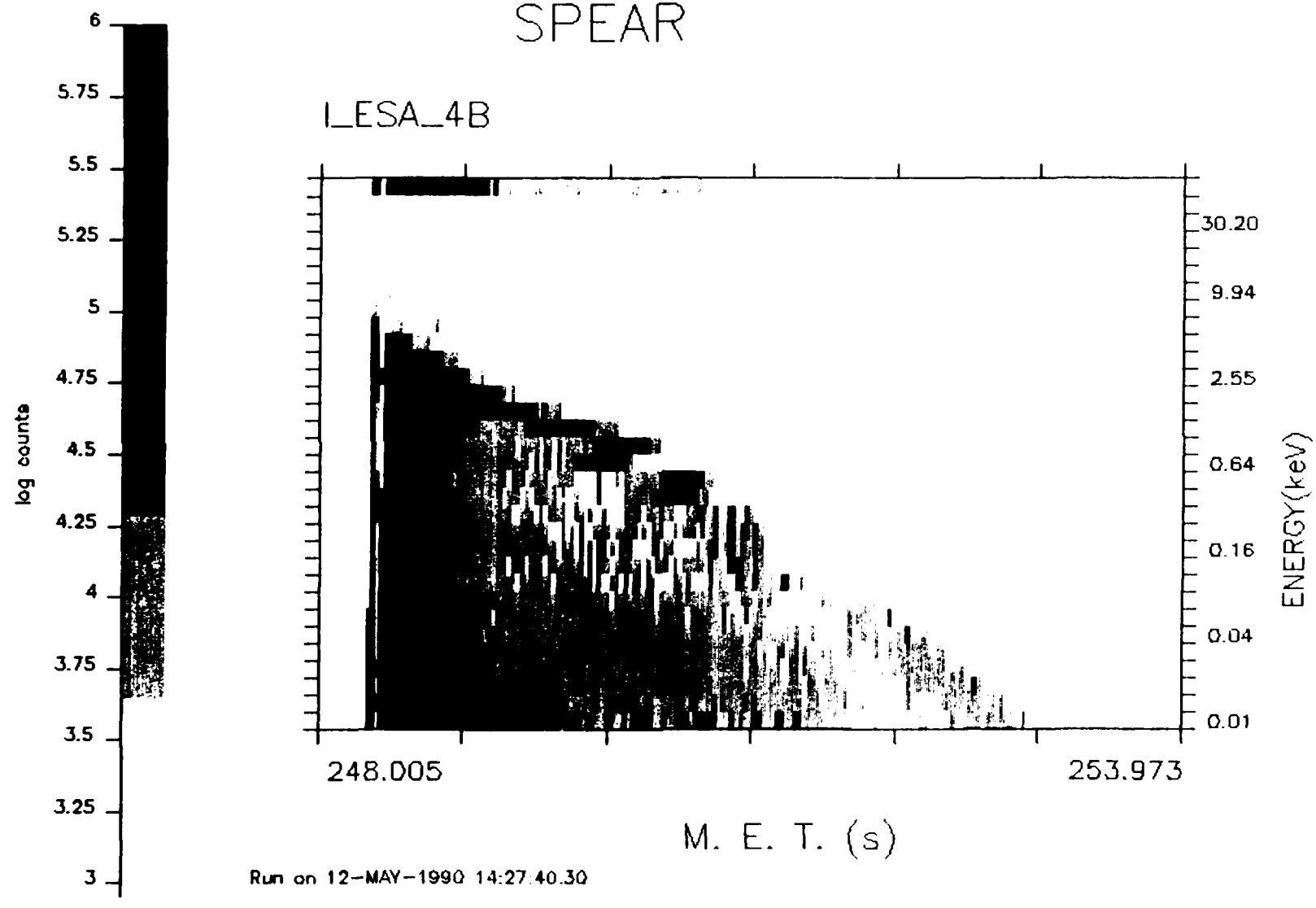
SPEAR
I_ESA_4B
6
5.75
5.5
5.25
5
4.75
4.5
4.25
4
3.75
3.5
3.25
3
log counts
30.20
9.94
2.55
0.64
0.16
0.04
0.01
ENERGY(keV)
248.005
253.973
M. E. T. (s)
Run on 12-MAY-1990 14:27:40.30

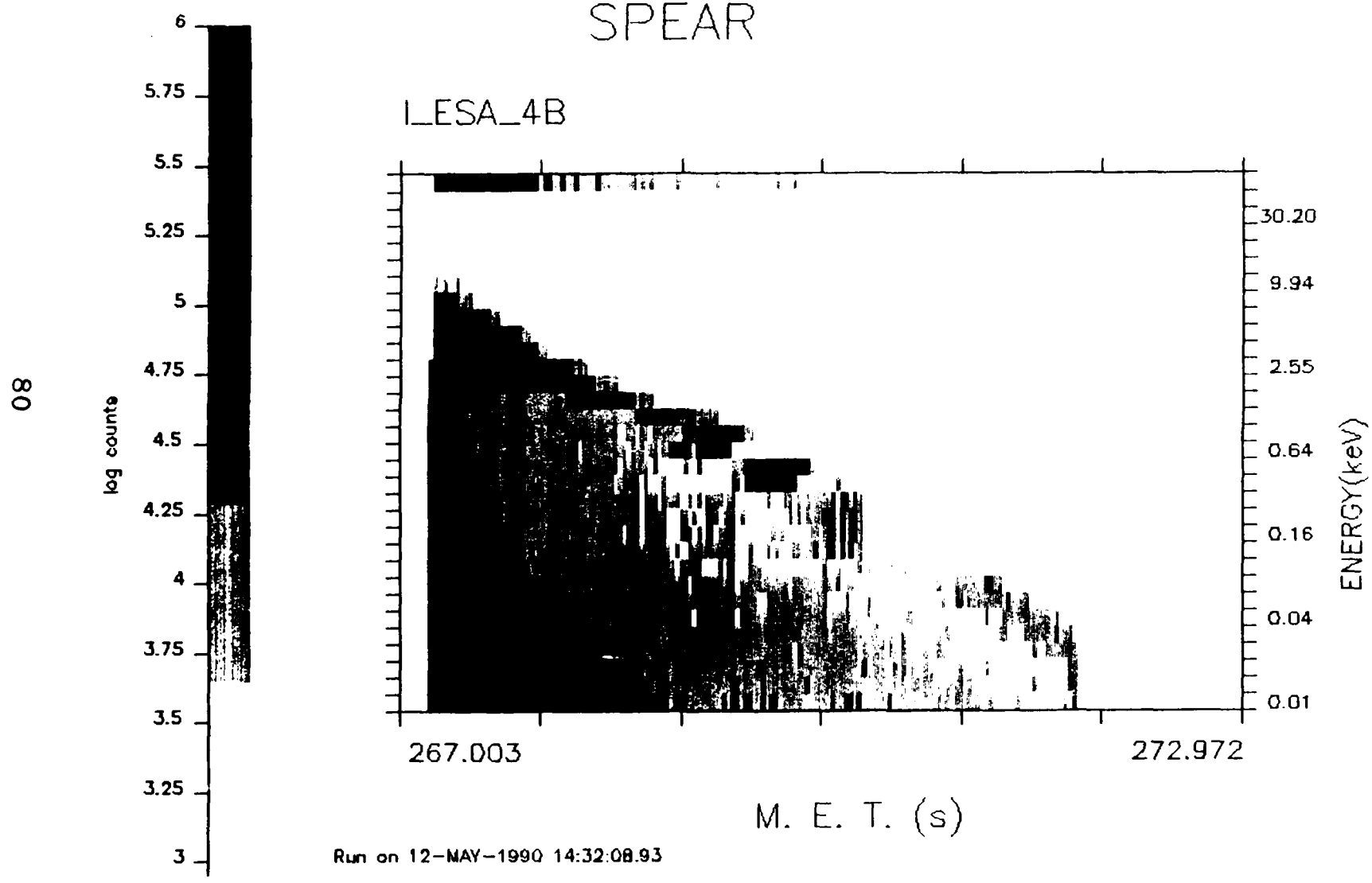
SPEAR
I_ESA_4B
6
5.75
5.5
5.25
5
4.75
4.5
4.25
4
3.75
3.5
3.25
3
log counts
30.20
9.94
2.55
0.64
0.16
0.04
0.01
ENERGY(keV)
267.003
272.972
M. E. T. (s)
Run on 12-MAY-1990 14:32:08.93

08

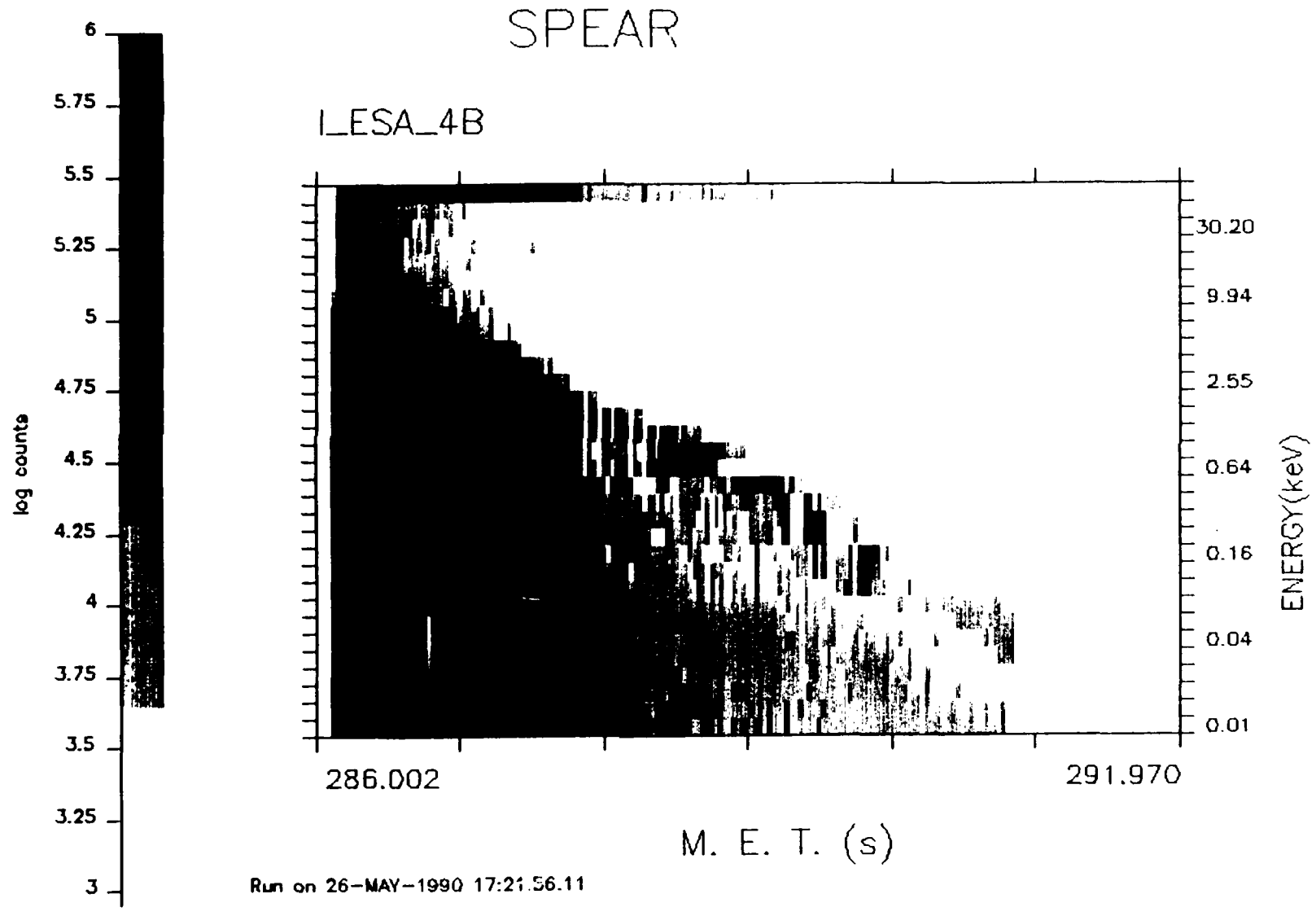
SPEAR
I_ESA_4B
log counts
6
5.75
5.5
5.25
5
4.75
4.5
4.25
4
3.75
3.5
3.25
3
30.20
9.94
2.55
0.64
0.16
0.04
0.01
ENERGY(keV)
286.002
291.970
M. E. T. (s)
Run on 26-MAY-1990 17:21:56.11

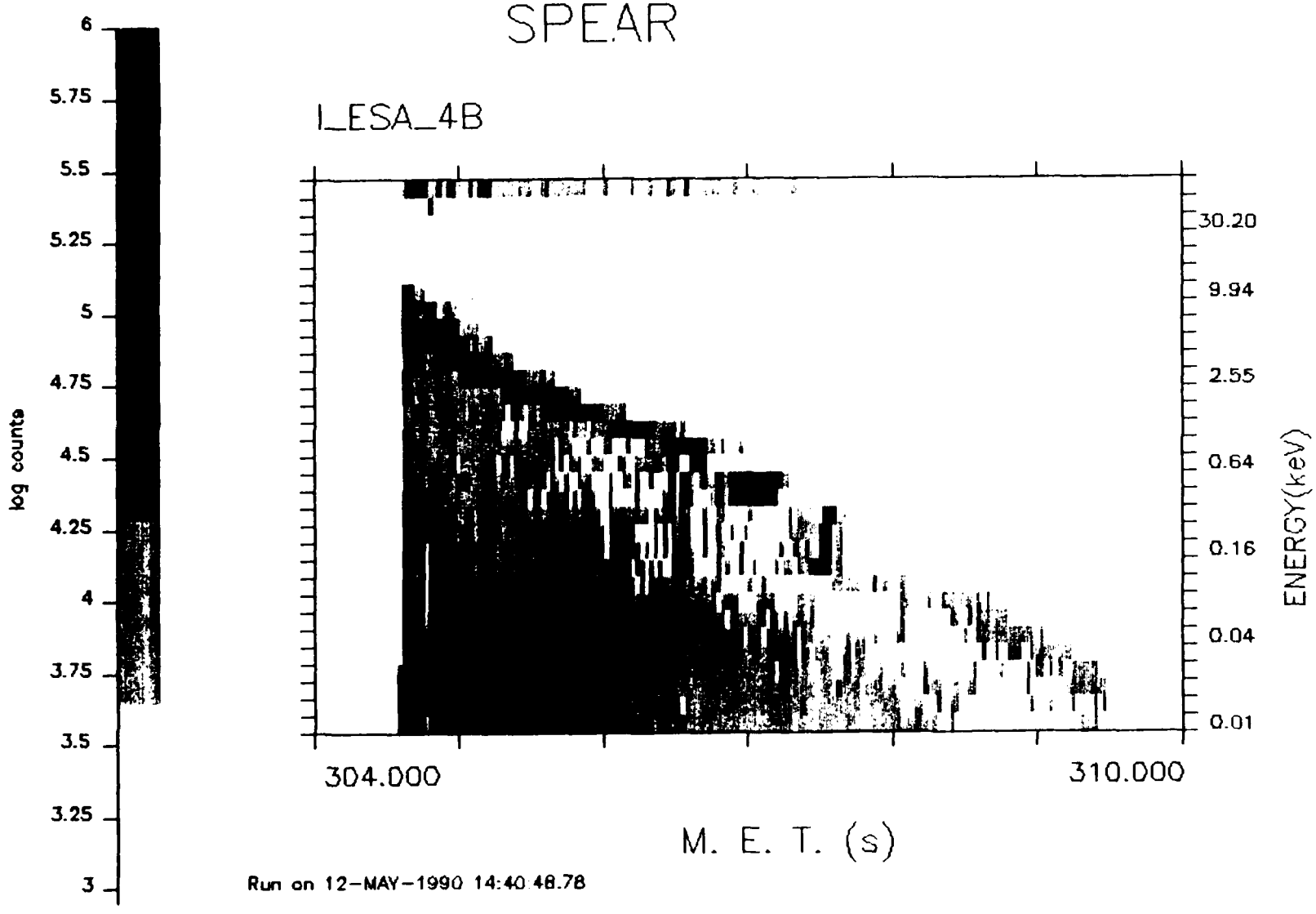
SPEAR
I_ESA_4B
log counts
6
5.75
5.5
5.25
5
4.75
4.5
4.25
4
3.75
3.5
3.25
3
30.20
9.94
2.55
0.64
0.16
0.04
0.01
ENERGY(keV)
304.000
310.000
M. E. T. (s)
Run on 12-MAY-1990 14:40:48.78

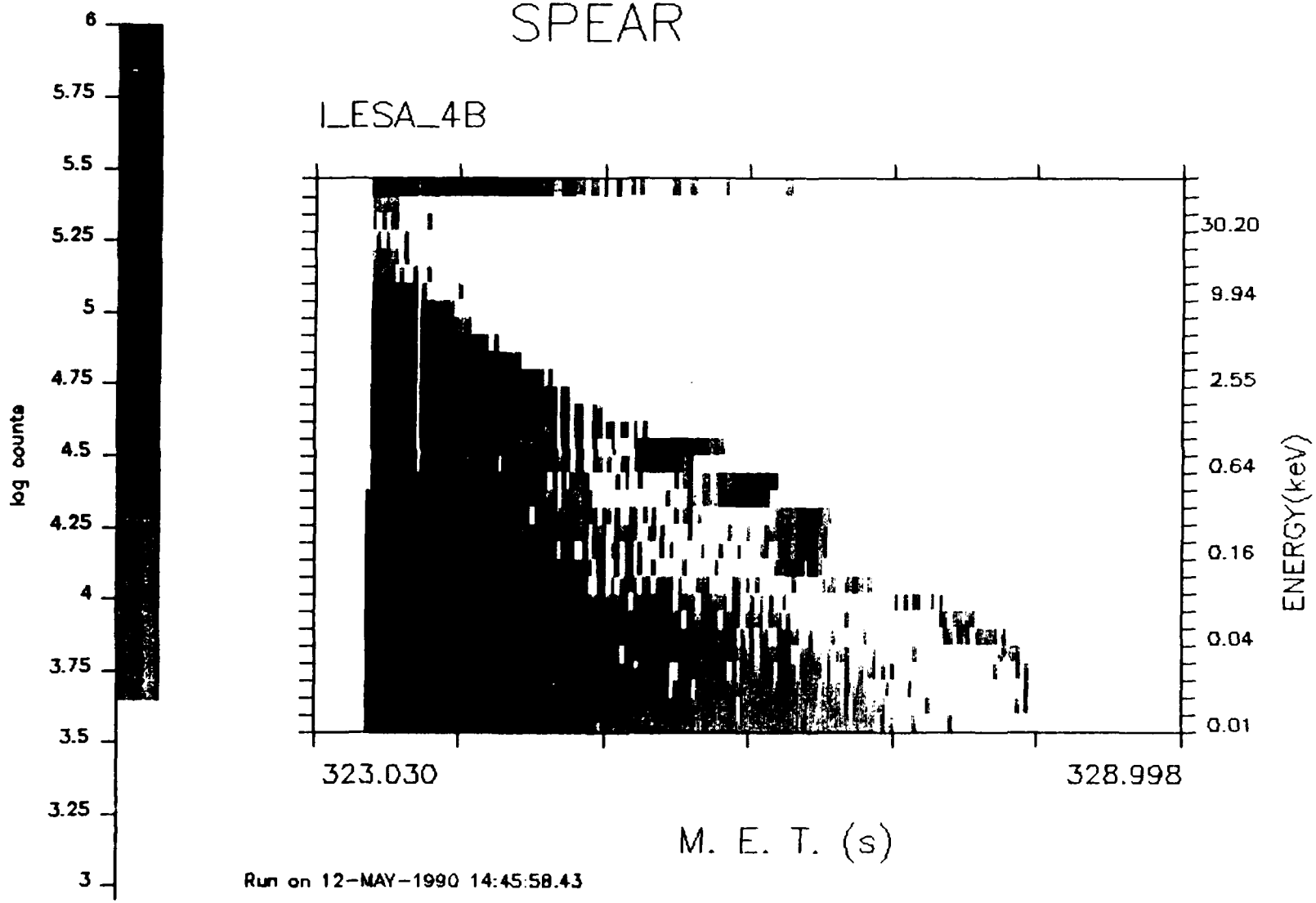
SPEAR
I_ESA_4B
log counts
6
5.75
5.5
5.25
5
4.75
4.5
4.25
4
3.75
3.5
3.25
3
30.20
9.94
2.55
0.64
0.16
0.04
0.01
ENERGY(keV)
323.030
328.998
M. E. T. (s)
Run on 12-MAY-1990 14:45:58.43

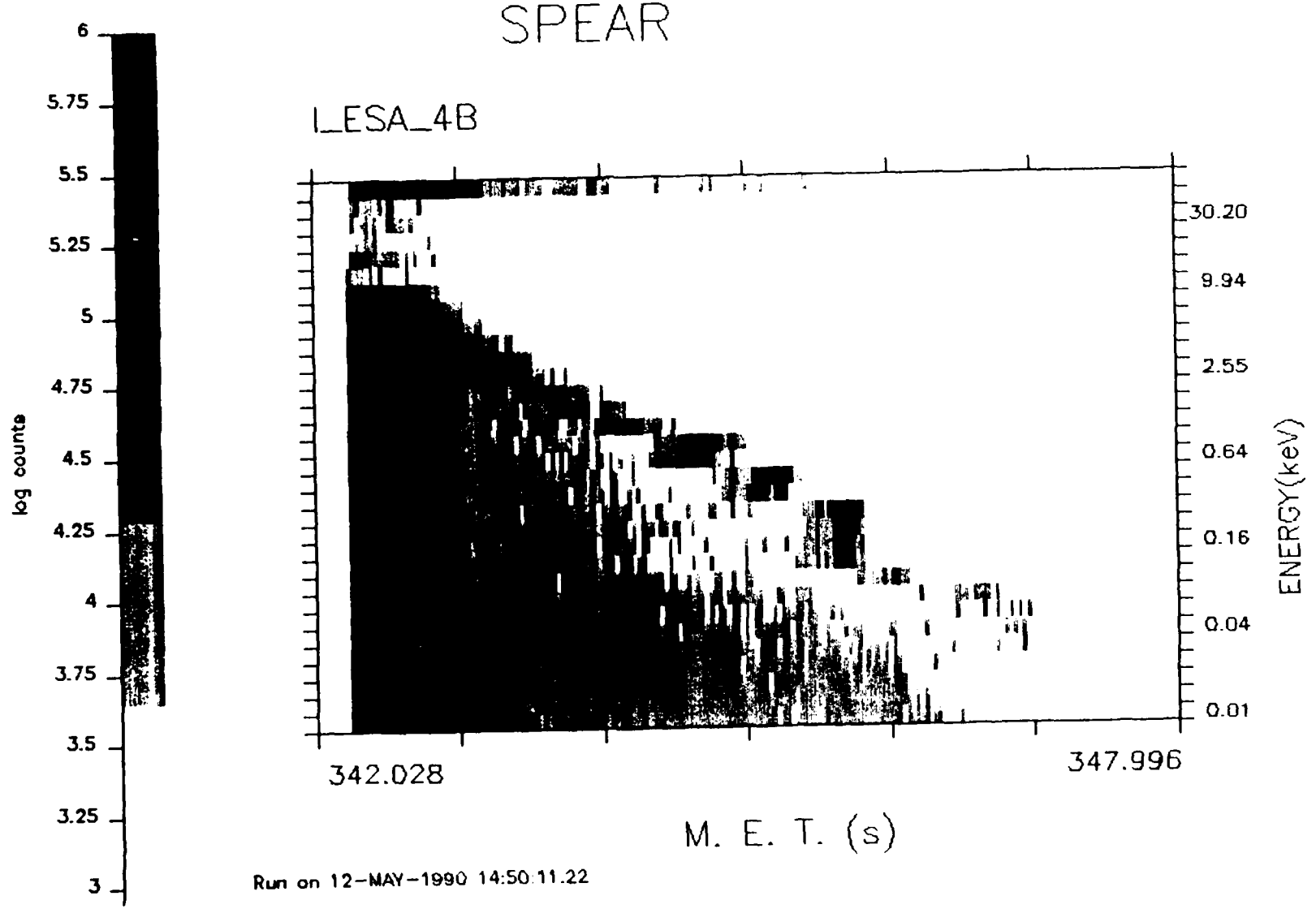
SPEAR
I_ESA_4B
log counts
6
5.75
5.5
5.25
5
4.75
4.5
4.25
4
3.75
3.5
3.25
3
30.20
9.94
2.55
0.64
0.16
0.04
0.01
ENERGY(keV)
342.028
347.996
M. E. T. (s)
Run on 12-MAY-1990 14:50:11.22

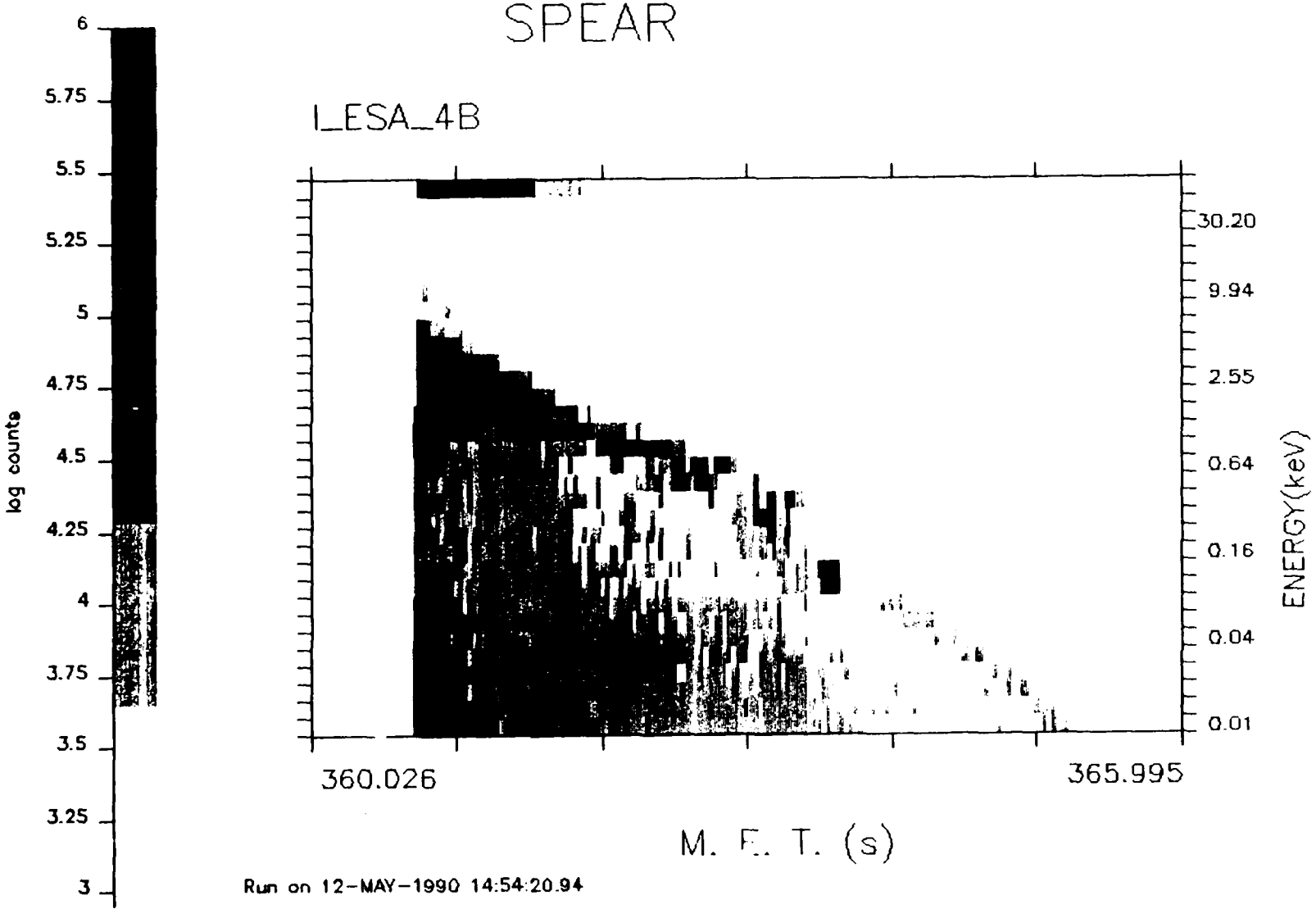
SPEAR
I_ESA_4B
log counts
6
5.75
5.5
5.25
5
4.75
4.5
4.25
4
3.75
3.5
3.25
3
30.20
9.94
2.55
0.64
0.16
0.04
0.01
ENERGY(keV)
360.026
365.995
M. E. T. (s)
Run on 12-MAY-1990 14:54:20.94

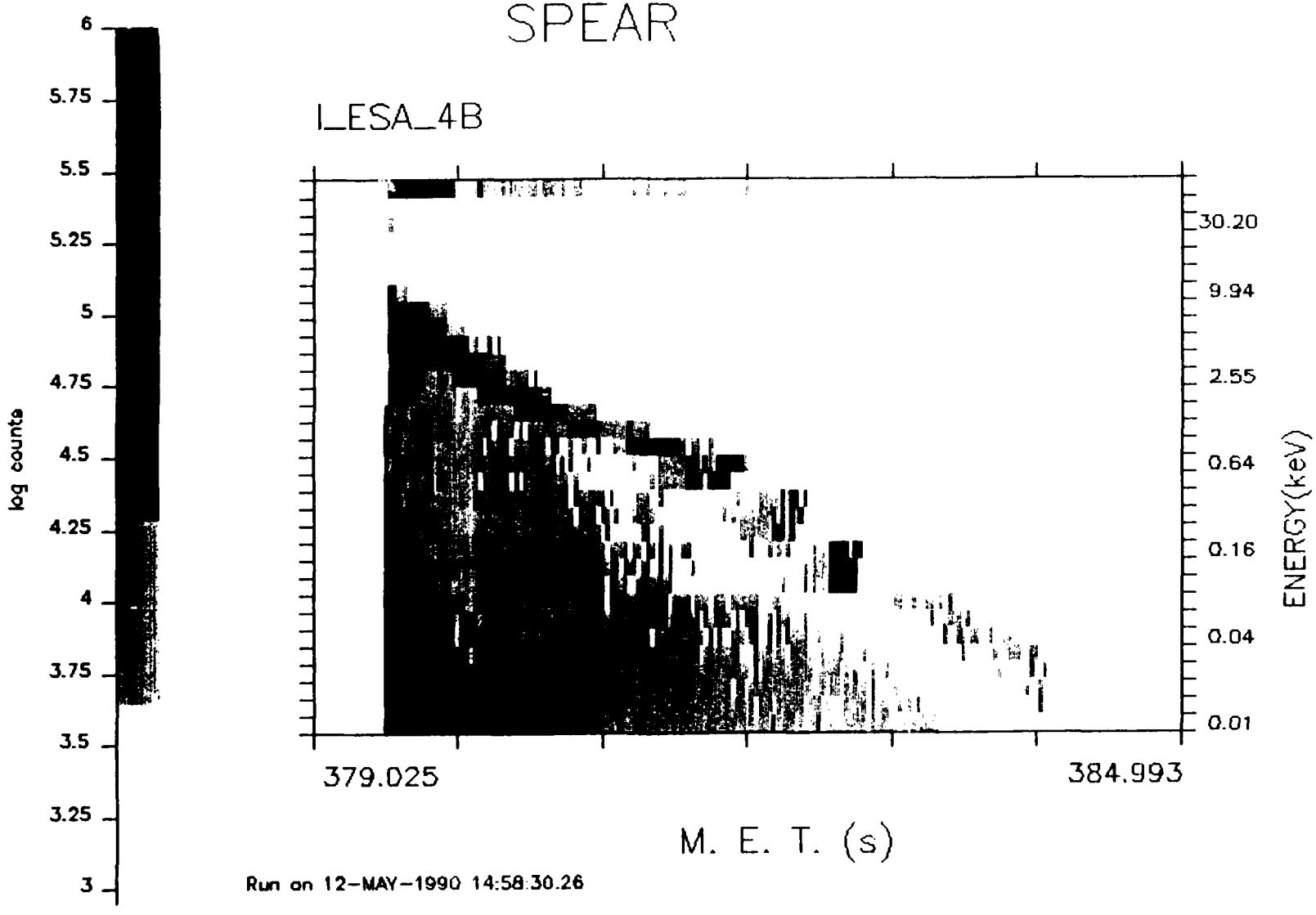
SPEAR
I_ESA_4B
log counts
6
5.75
5.5
5.25
5
4.75
4.5
4.25
4
3.75
3.5
3.25
3
30.20
9.94
2.55
0.64
0.16
0.04
0.01
ENERGY(keV)
379.025
384.993
M. E. T. (s)
Run on 12-MAY-1990 14:58:30.26

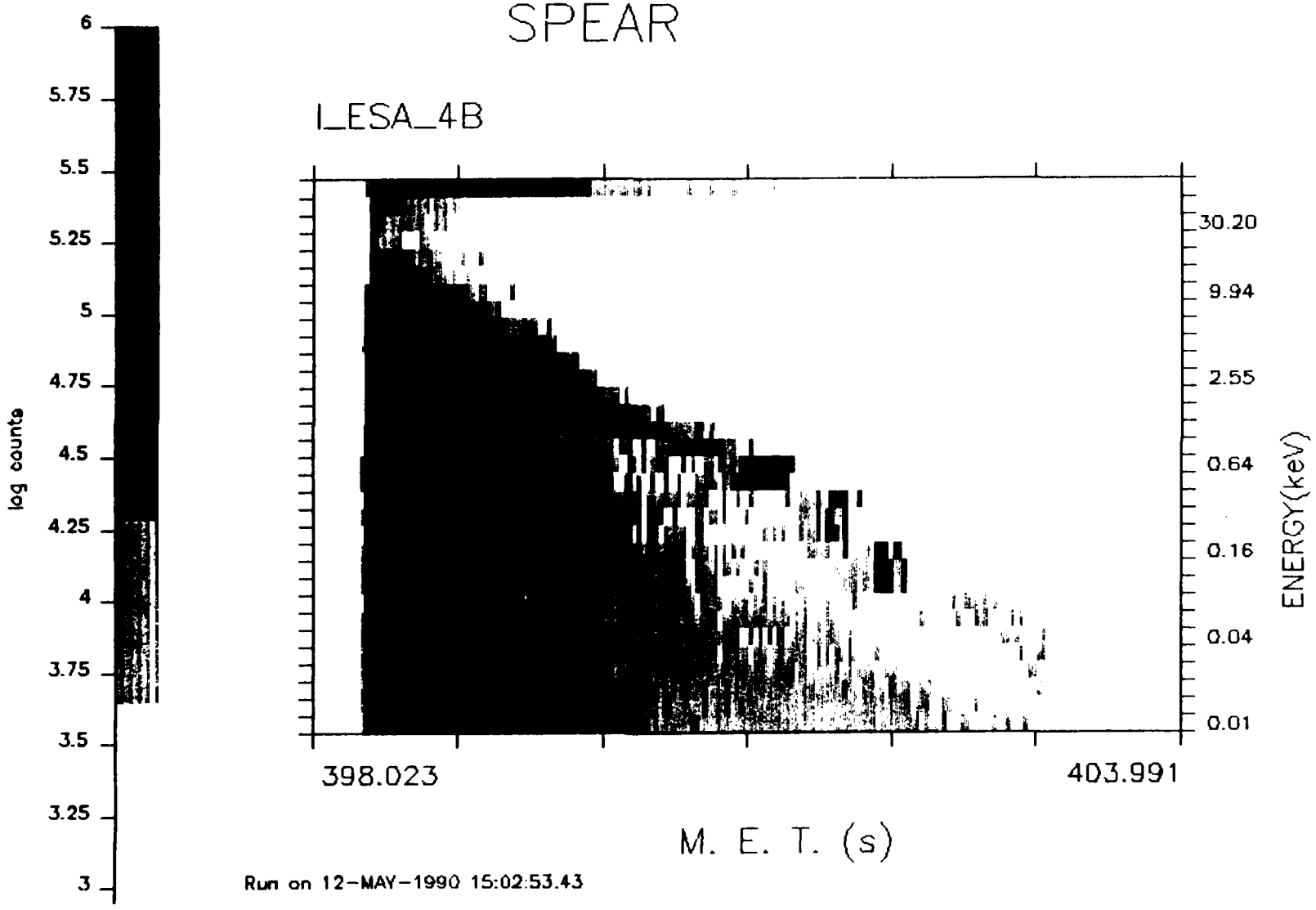
SPEAR
I_ESA_4B
log counts
6
5.75
5.5
5.25
5
4.75
4.5
4.25
4
3.75
3.5
3.25
3
30.20
9.94
2.55
0.64
0.16
0.04
0.01
ENERGY(keV)
398.023
403.991
M. E. T. (s)
Run on 12-MAY-1990 15:02:53.43

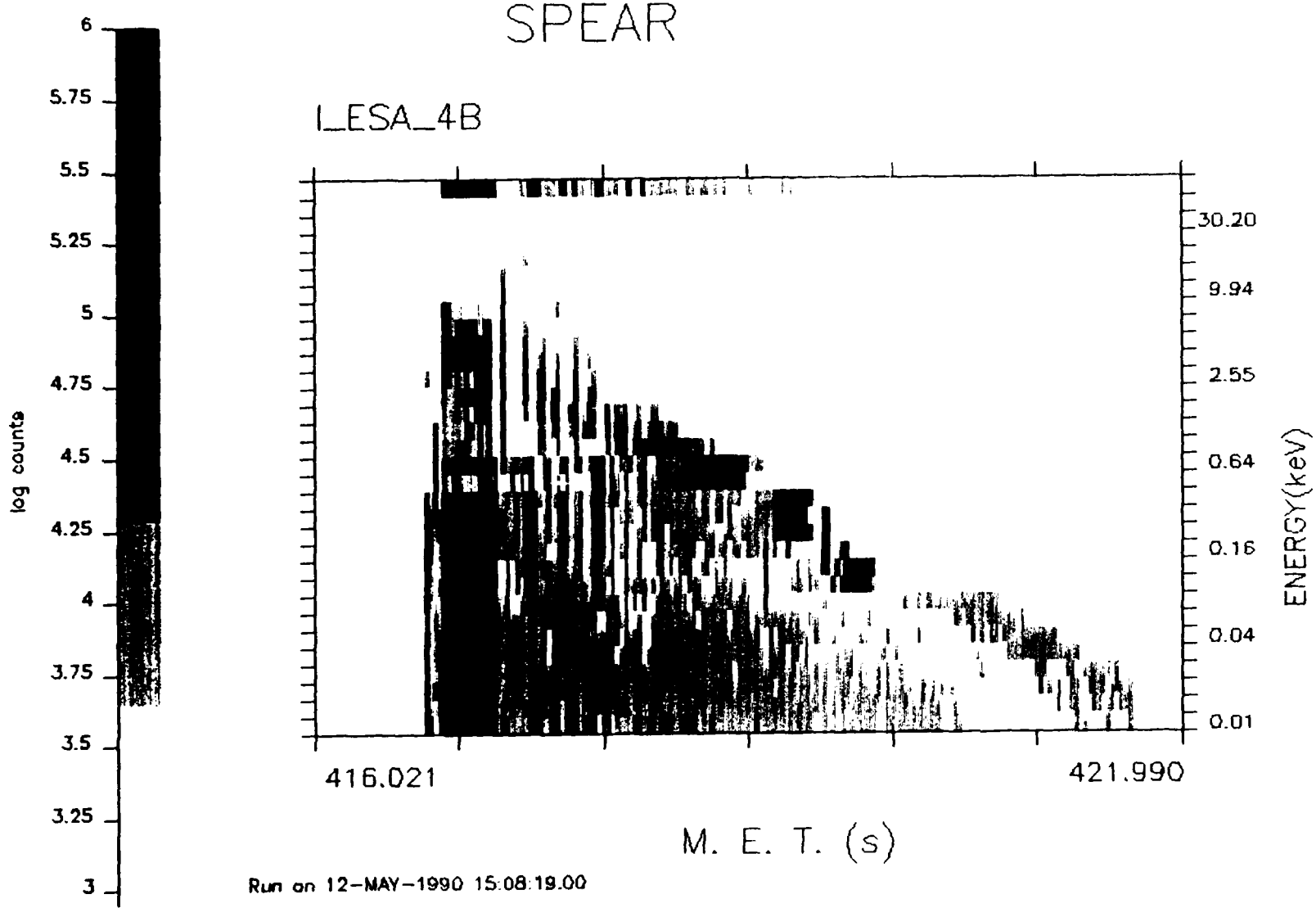
SPEAR
I_ESA_4B
log counts
6
5.75
5.5
5.25
5
4.75
4.5
4.25
4
3.75
3.5
3.25
3
30.20
9.94
2.55
0.64
0.16
0.04
0.01
ENERGY(keV)
416.021
421.990
M. E. T. (s)
Run on 12-MAY-1990 15:08:19.00

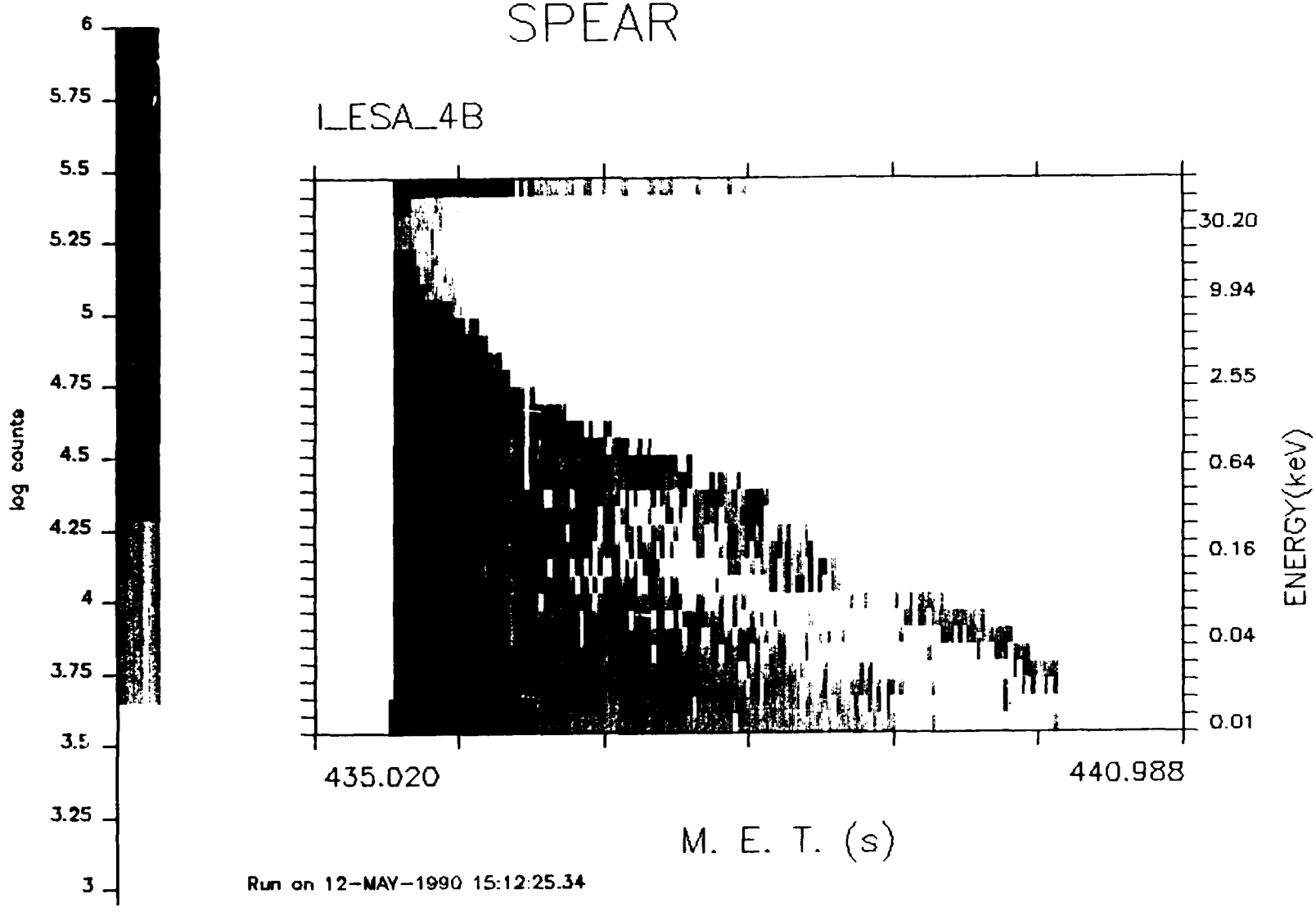
SPEAR
I_ESA_4B
log counts
6
5.75
5.5
5.25
5
4.75
4.5
4.25
4
3.75
3.5
3.25
3
30.20
9.94
2.55
0.64
0.16
0.04
0.01
ENERGY(keV)
435.020
440.988
M. E. T. (s)
Run on 12-MAY-1990 15:12:25.34

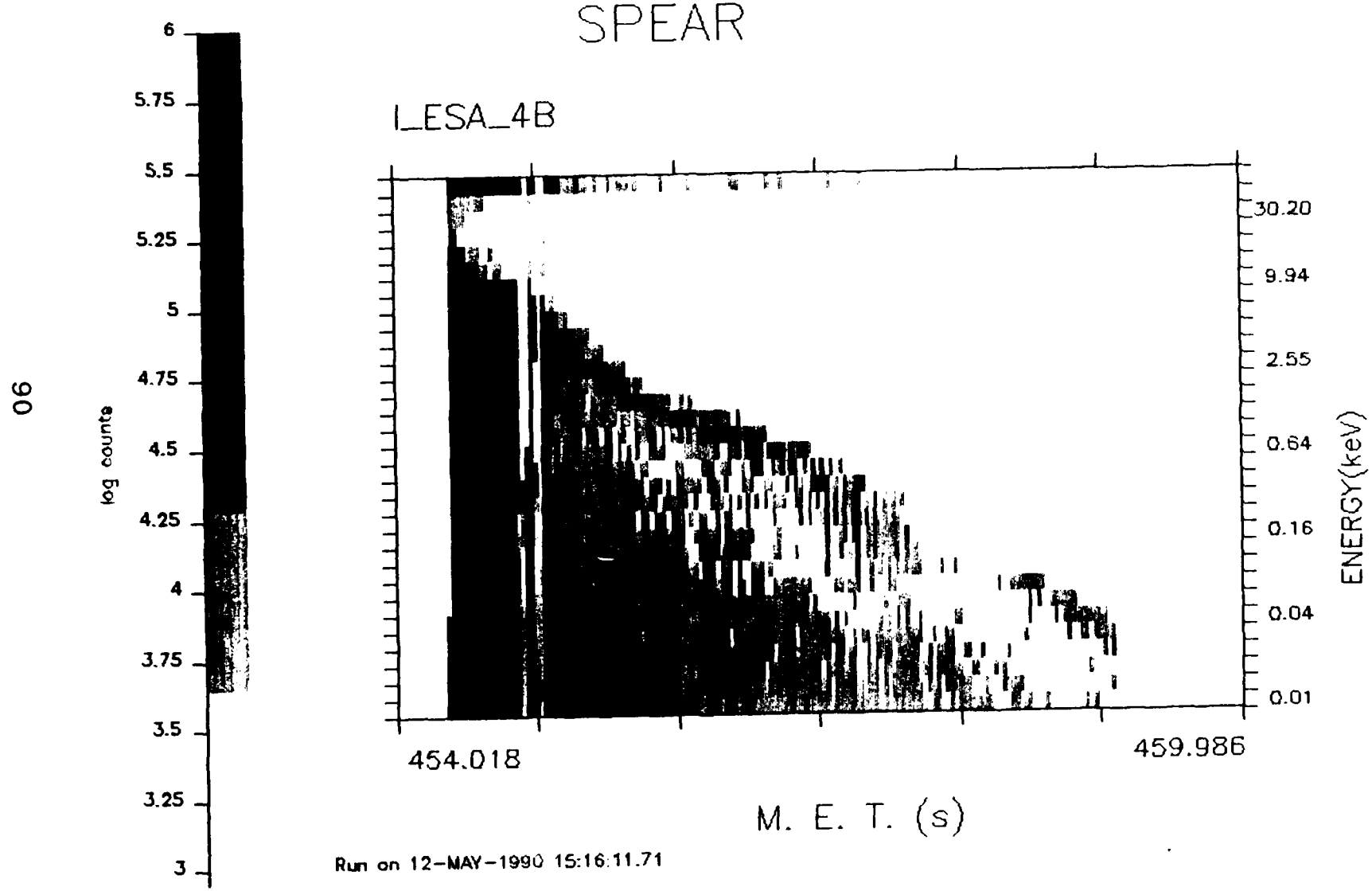
SPEAR
I_ESA_4B
06
log counts
6
5.75
5.5
5.25
5
4.75
4.5
4.25
4
3.75
3.5
3.25
3
30.20
9.94
2.55
0.64
0.16
0.04
0.01
ENERGY(keV)
454.018
459.986
M. E. T. (s)
Run on 12-MAY-1990 15:16:11.71

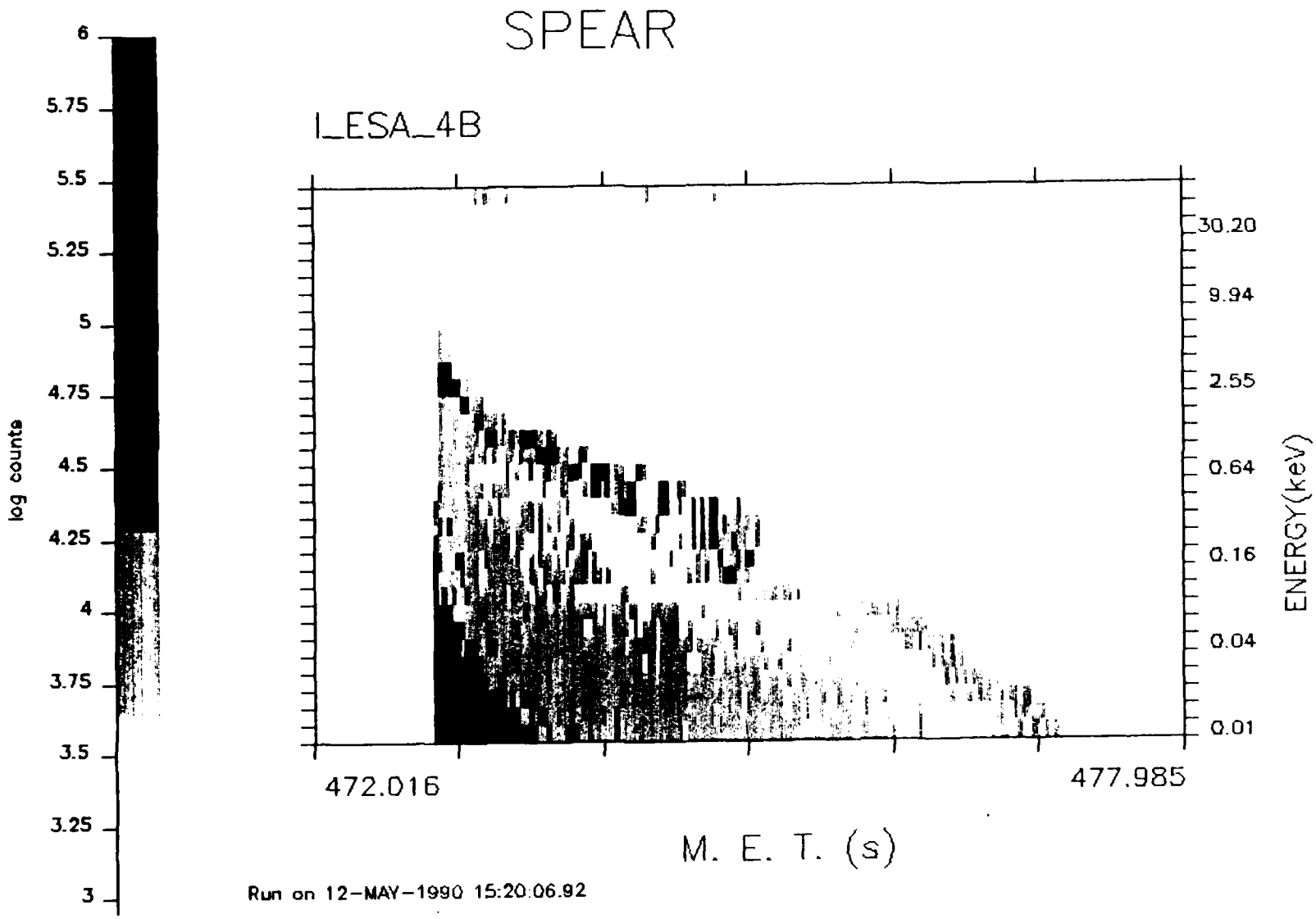
SPEAR
I_ESA_4B
log counts
6
5.75
5.5
5.25
5
4.75
4.5
4.25
4
3.75
3.5
3.25
3
30.20
9.94
2.55
0.64
0.16
0.04
0.01
ENERGY(keV)
472.016
477.985
M. E. T. (s)
Run on 12-MAY-1990 15:20:06.92

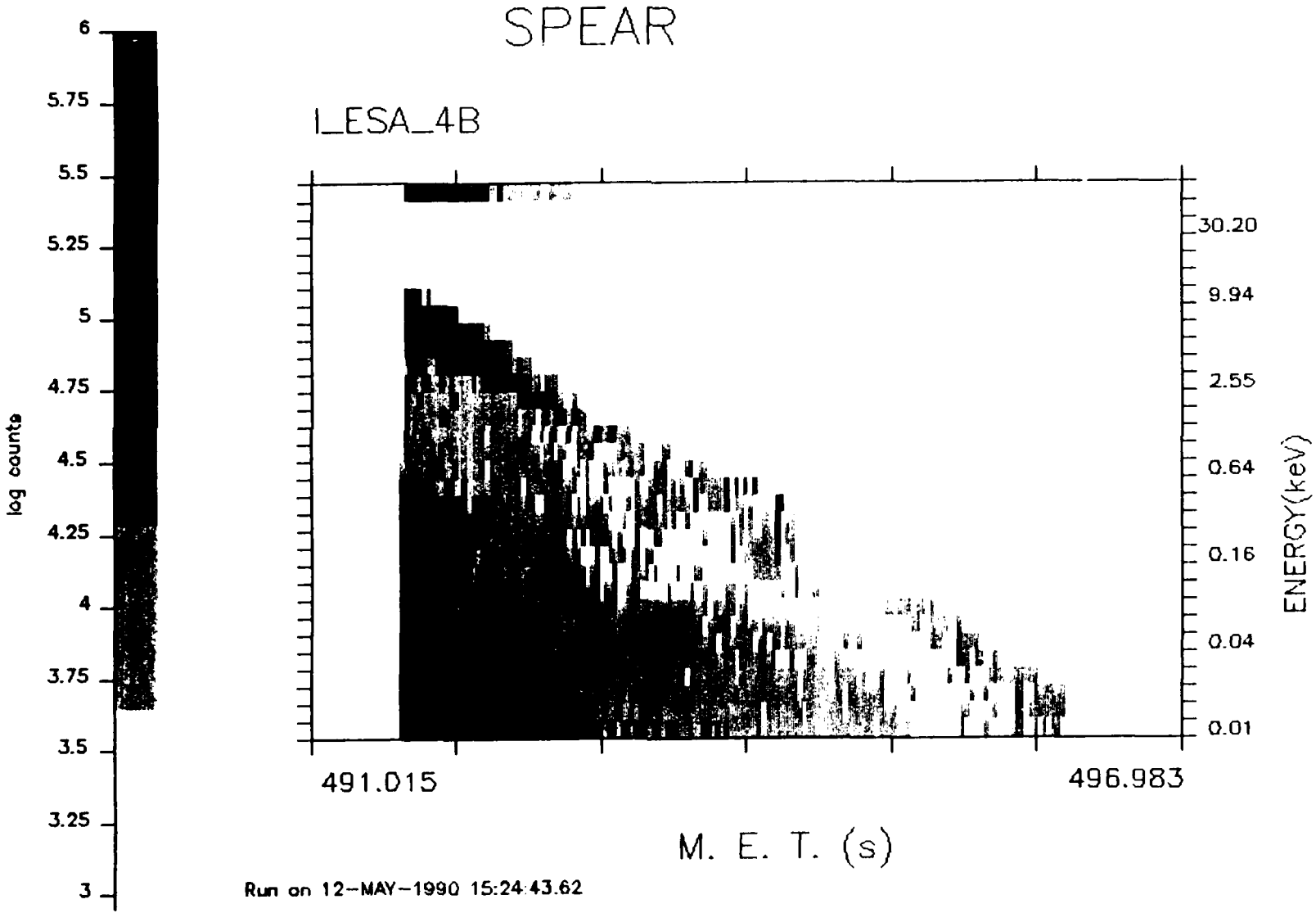
SPEAR
I_ESA_4B
log counts
6
5.75
5.5
5.25
5
4.75
4.5
4.25
4
3.75
3.5
3.25
3
30.20
9.94
2.55
0.64
0.16
0.04
0.01
ENERGY(keV)
491.015
496.983
M. E. T. (s)
Run on 12-MAY-1990 15:24:43.62

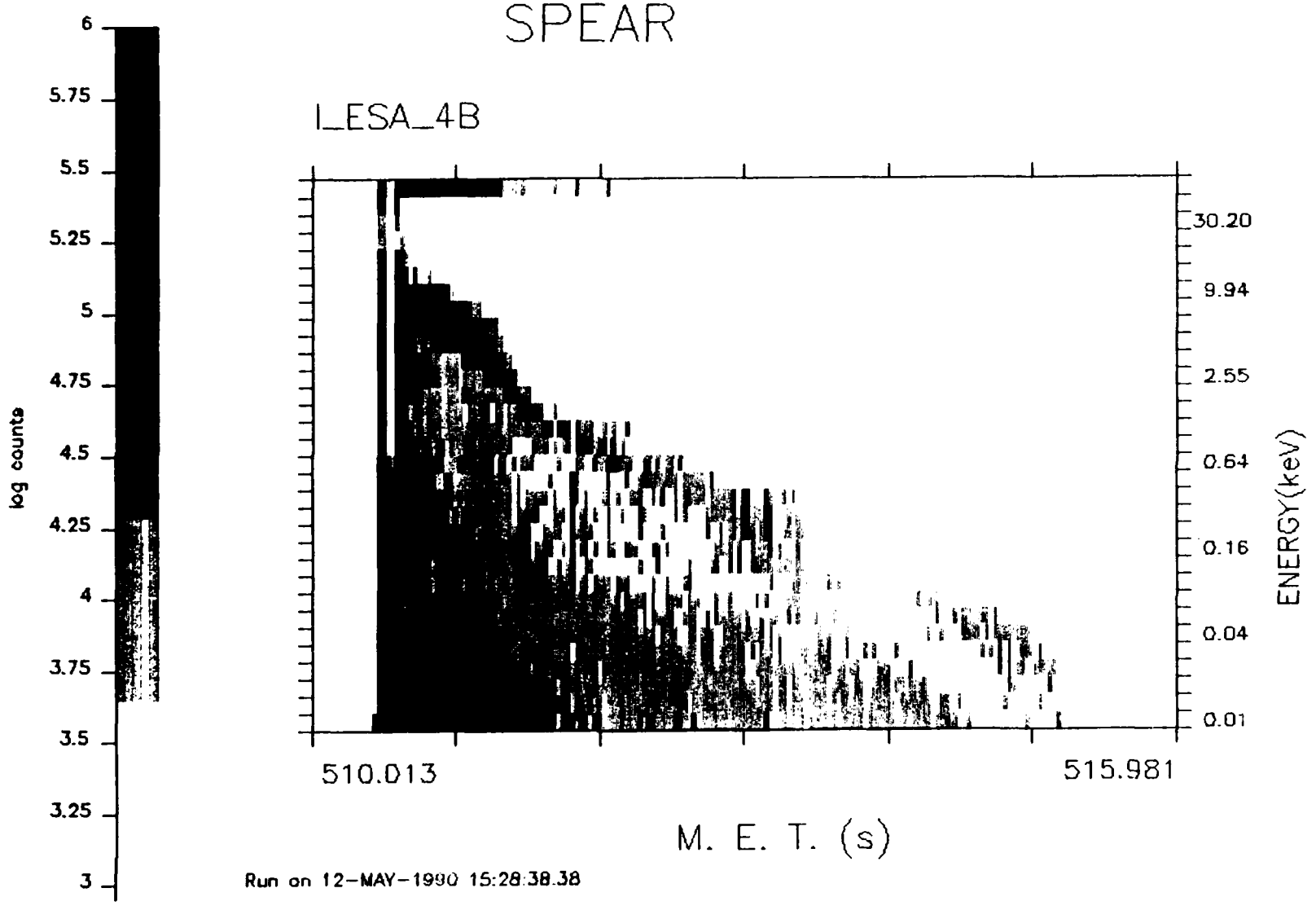
SPEAR
I_ESA_4B
log counts
6
5.75
5.5
5.25
5
4.75
4.5
4.25
4
3.75
3.5
3.25
3
30.20
9.94
2.55
0.64
0.16
0.04
0.01
ENERGY(keV)
510.013
515.981
M. E. T. (s)
Run on 12-MAY-1990 15:28:38.38

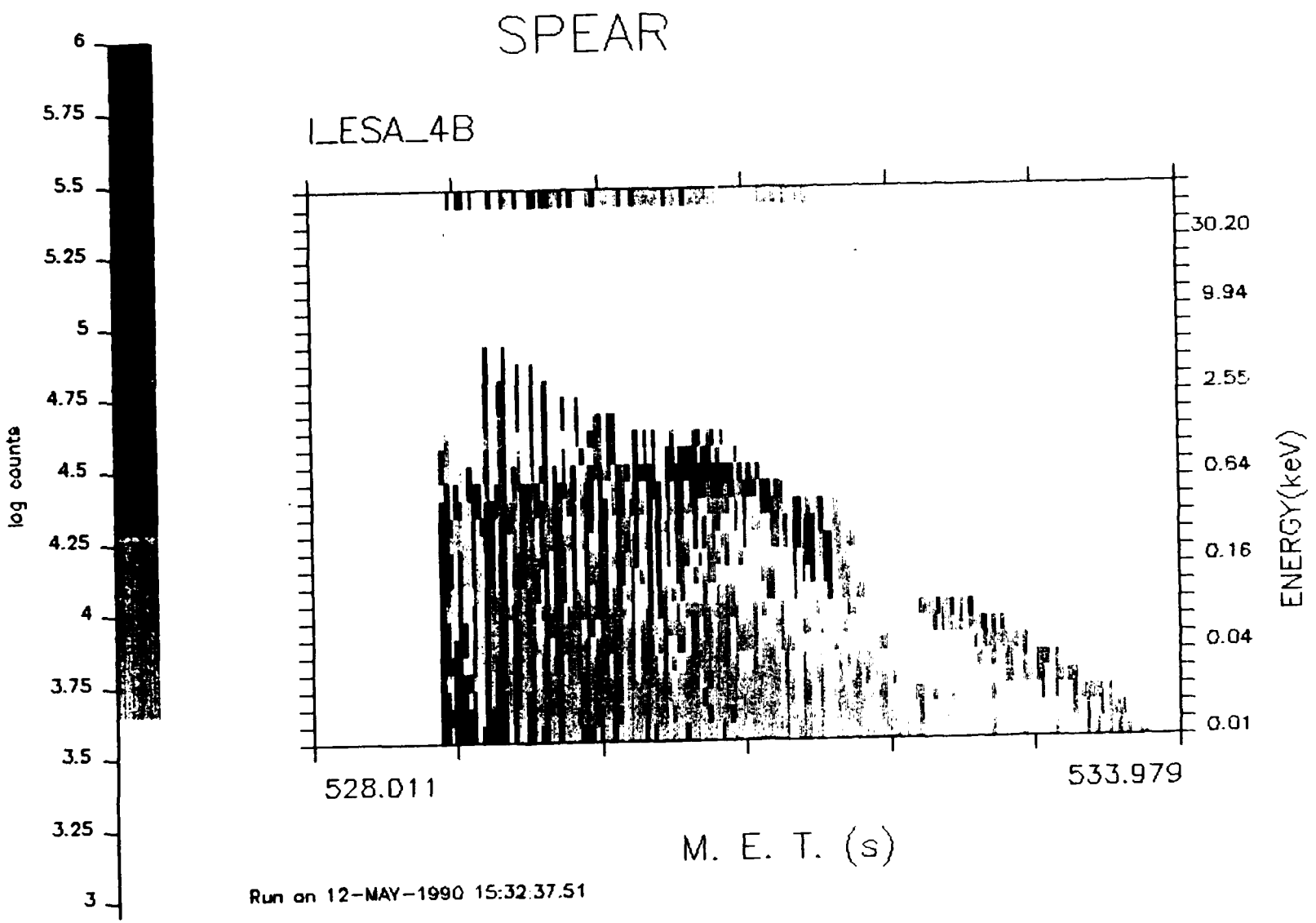
SPEAR
I_ESA_4B
log counts
6
5.75
5.5
5.25
5
4.75
4.5
4.25
4
3.75
3.5
3.25
3
30.20
9.94
2.55
0.64
0.16
0.04
0.01
ENERGY(keV)
528.011
533.979
M. E. T. (s)
Run on 12-MAY-1990 15:32:37.51

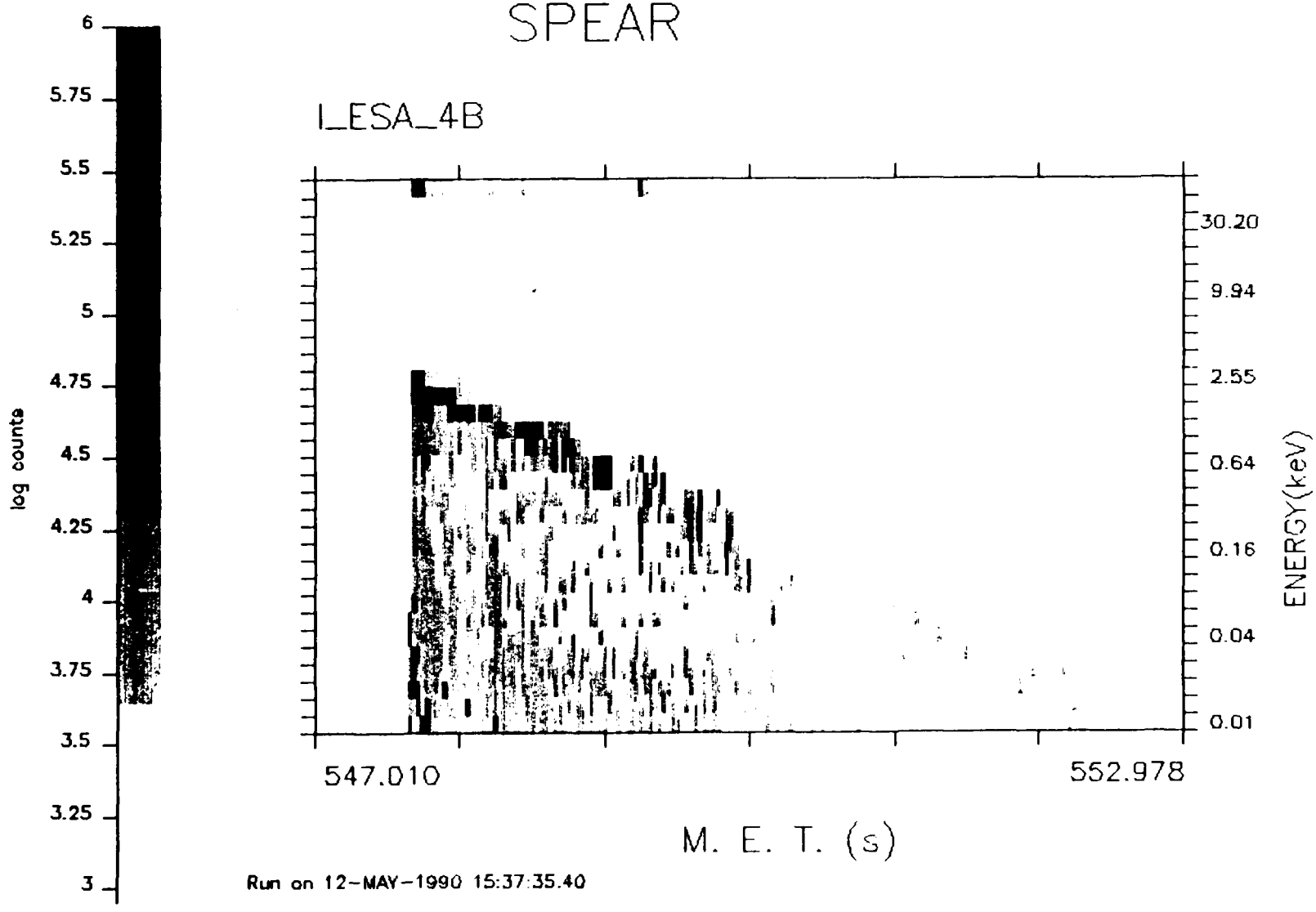
SPEAR
I_ESA_4B
log counts
6
5.75
5.5
5.25
5
4.75
4.5
4.25
4
3.75
3.5
3.25
3
30.20
9.94
2.55
0.64
0.16
0.04
0.01
ENERGY(keV)
547.010
552.978
M. E. T. (s)
Run on 12-MAY-1990 15:37:35.40

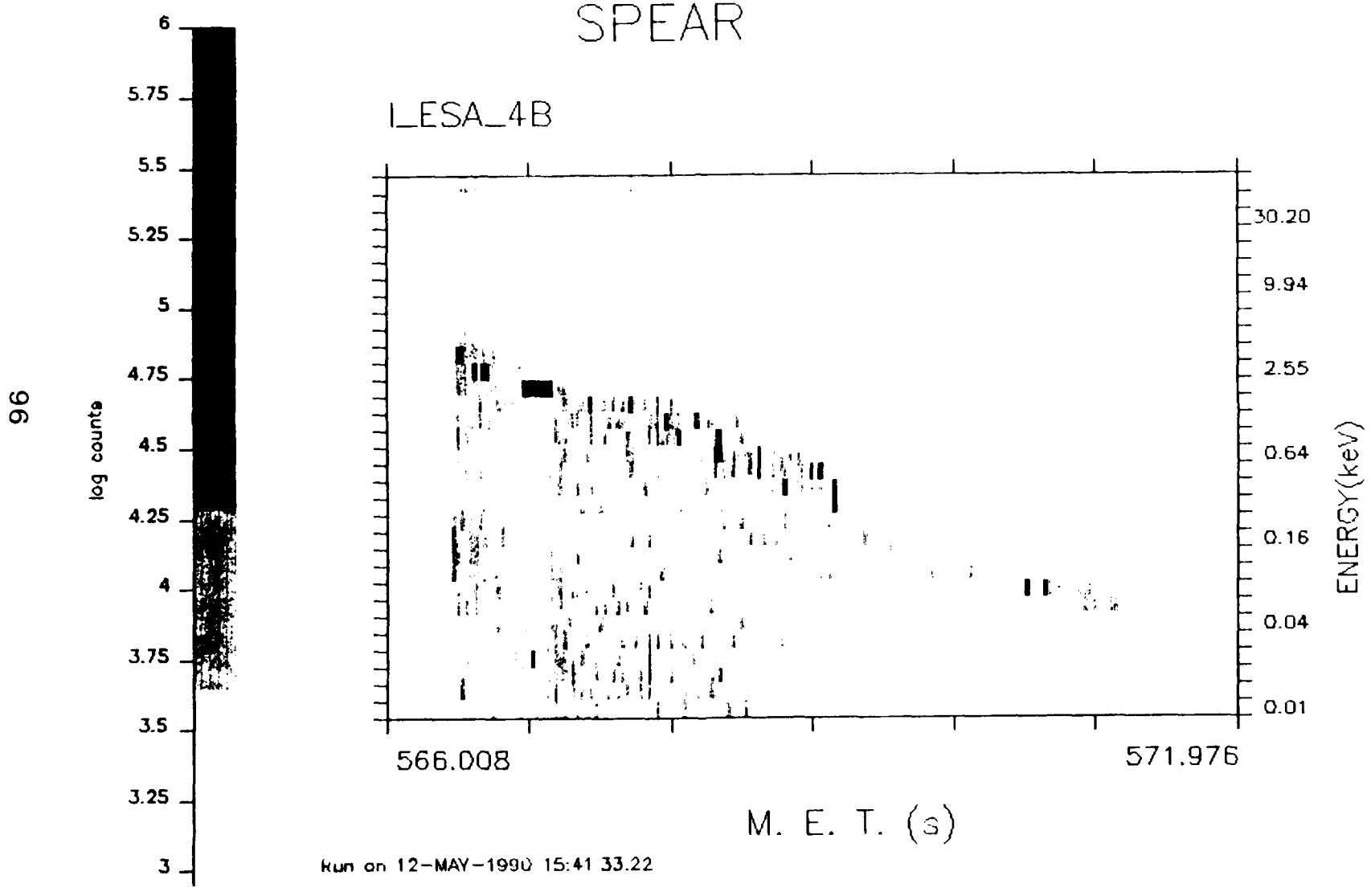
SPEAR
I_ESA_4B
log counts
6
5.75
5.5
5.25
5
4.75
4.5
4.25
4
3.75
3.5
3.25
3
30.20
9.94
2.55
0.64
0.16
0.04
0.01
ENERGY(keV)
566.008
571.976
M. E. T. (s)
Run on 12-MAY-1990 15:41 33.22

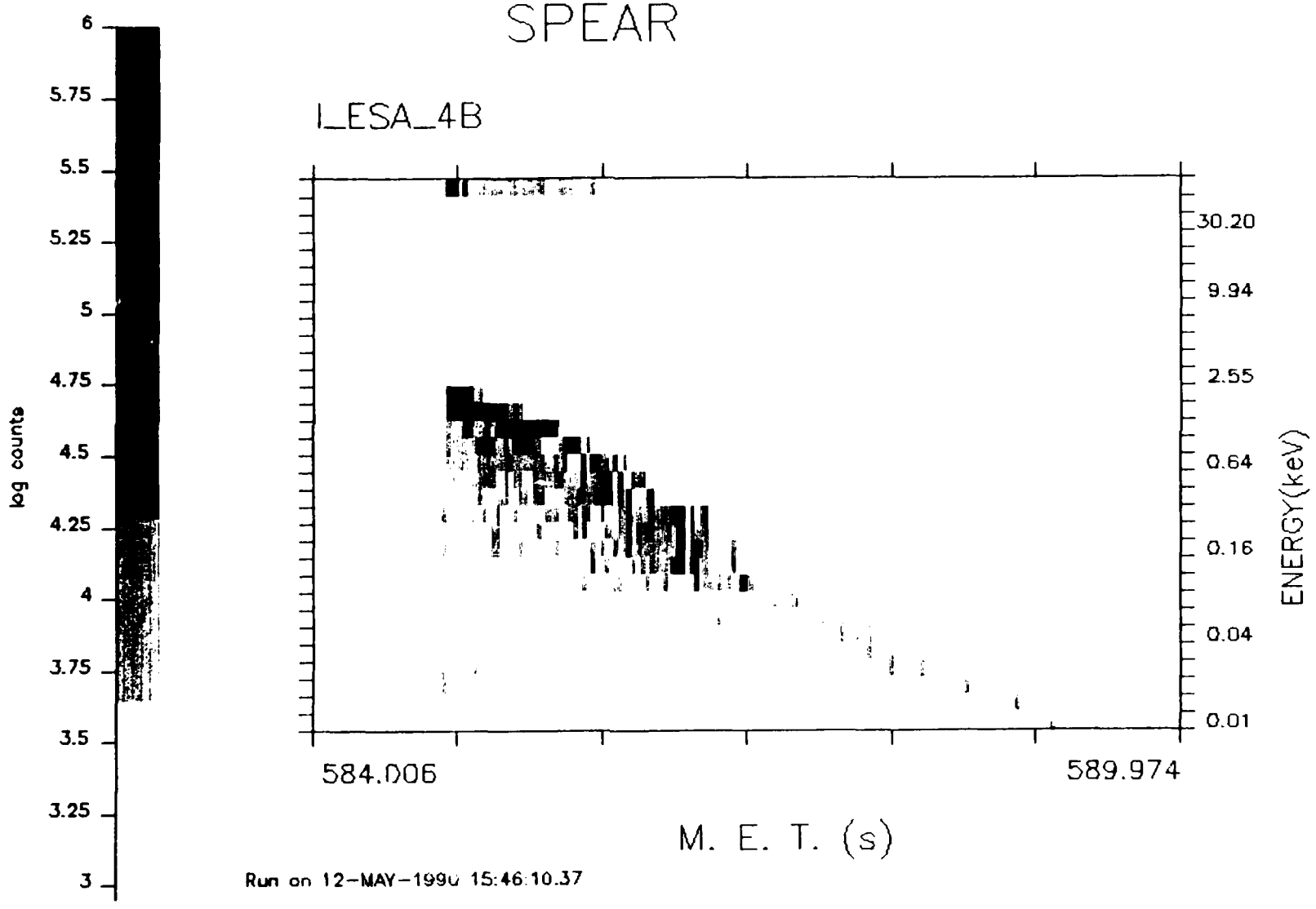
SPEAR
I_ESA_4B
log counts
6
5.75
5.5
5.25
5
4.75
4.5
4.25
4
3.75
3.5
3.25
3
30.20
9.94
2.55
0.64
0.16
0.04
0.01
ENERGY(keV)
584.006
589.974
M. E. T. (s)
Run on 12-MAY-1990 15:46:10.37

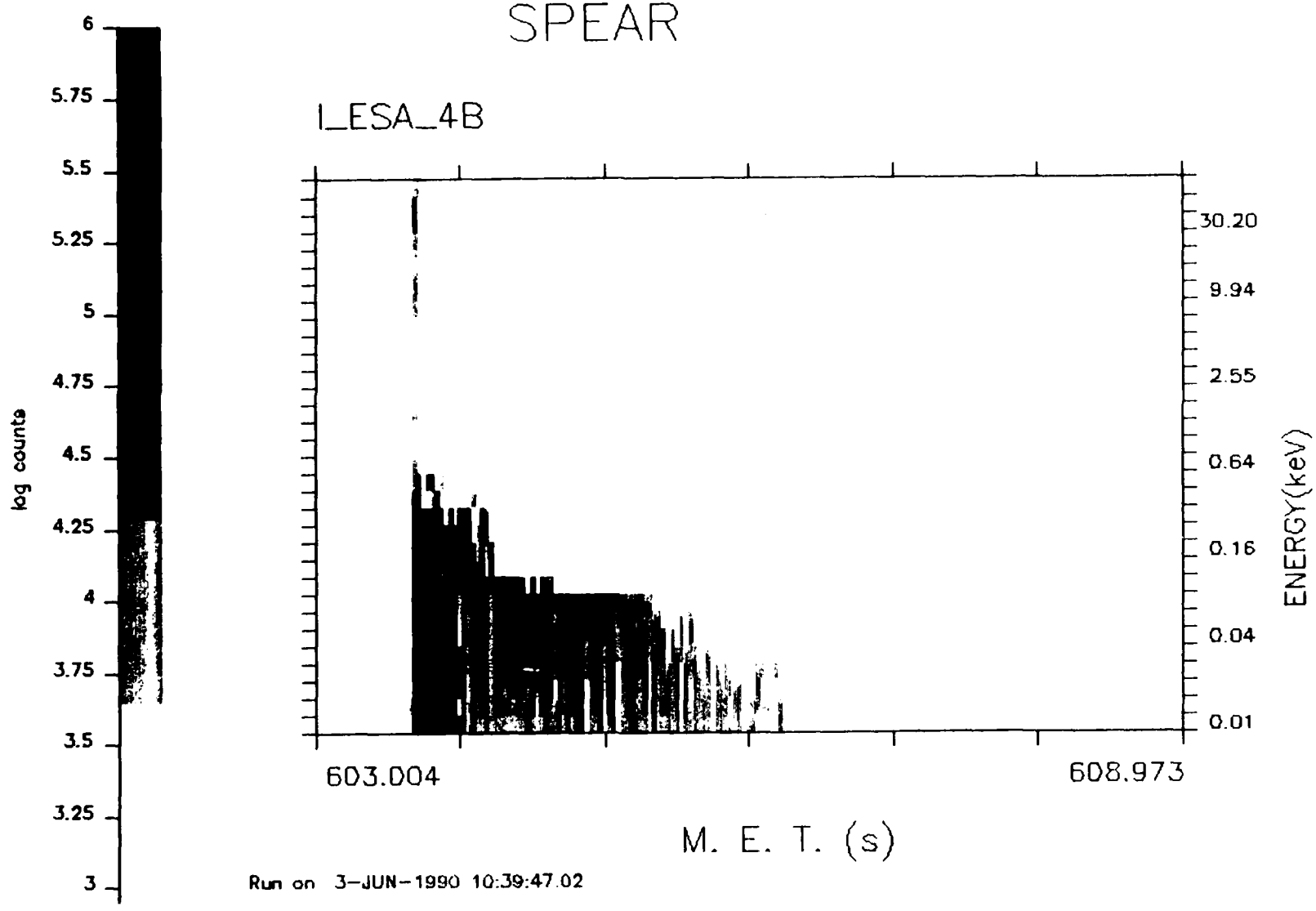
SPEAR
I_ESA_4B
log counts
6
5.75
5.5
5.25
5
4.75
4.5
4.25
4
3.75
3.5
3.25
3
30.20
9.94
2.55
0.64
0.16
0.04
0.01
ENERGY(keV)
603.004
608.973
M. E. T. (s)
Run on 3-JUN-1990 10:39:47.02

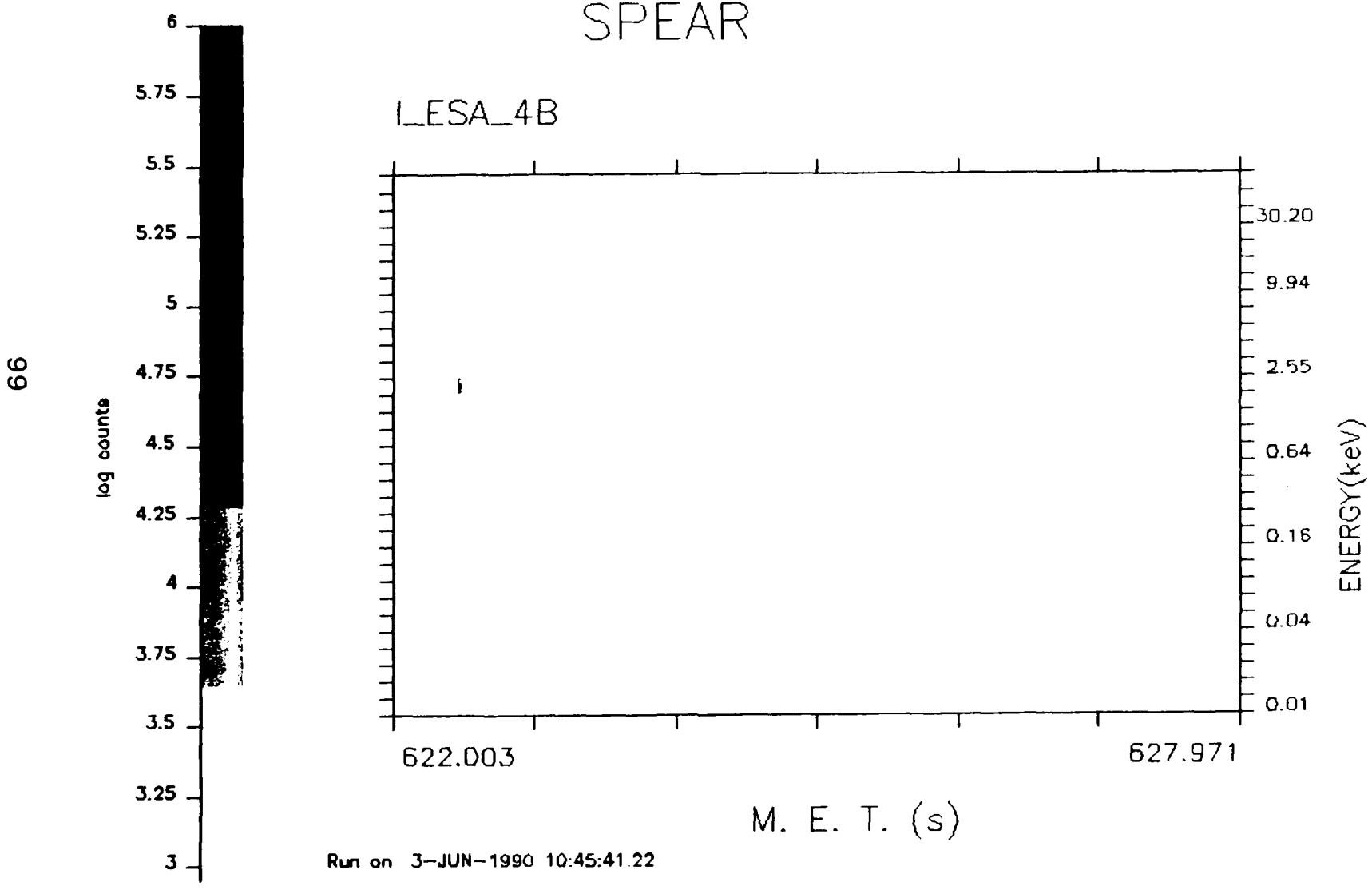
SPEAR
I_ESA_4B
log counts
6
5.75
5.5
5.25
5
4.75
4.5
4.25
4
3.75
3.5
3.25
3
30.20
9.94
2.55
0.64
0.16
0.04
0.01
ENERGY(keV)
622.003
627.971
M. E. T. (s)
Run on 3-JUN-1990 10:45:41.22

APPENDIX C

ROCKET BODY POTENTIAL PLOTS

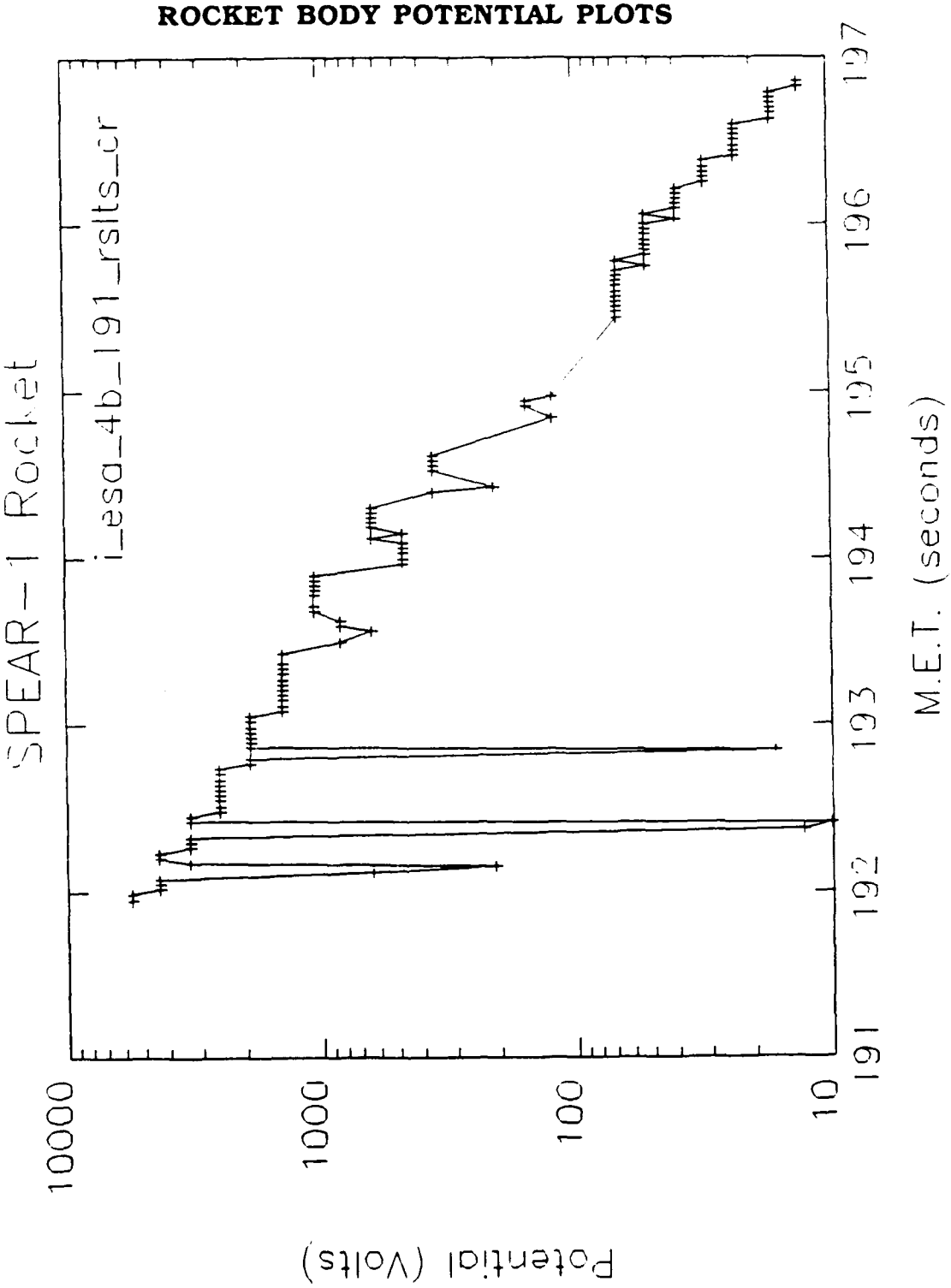

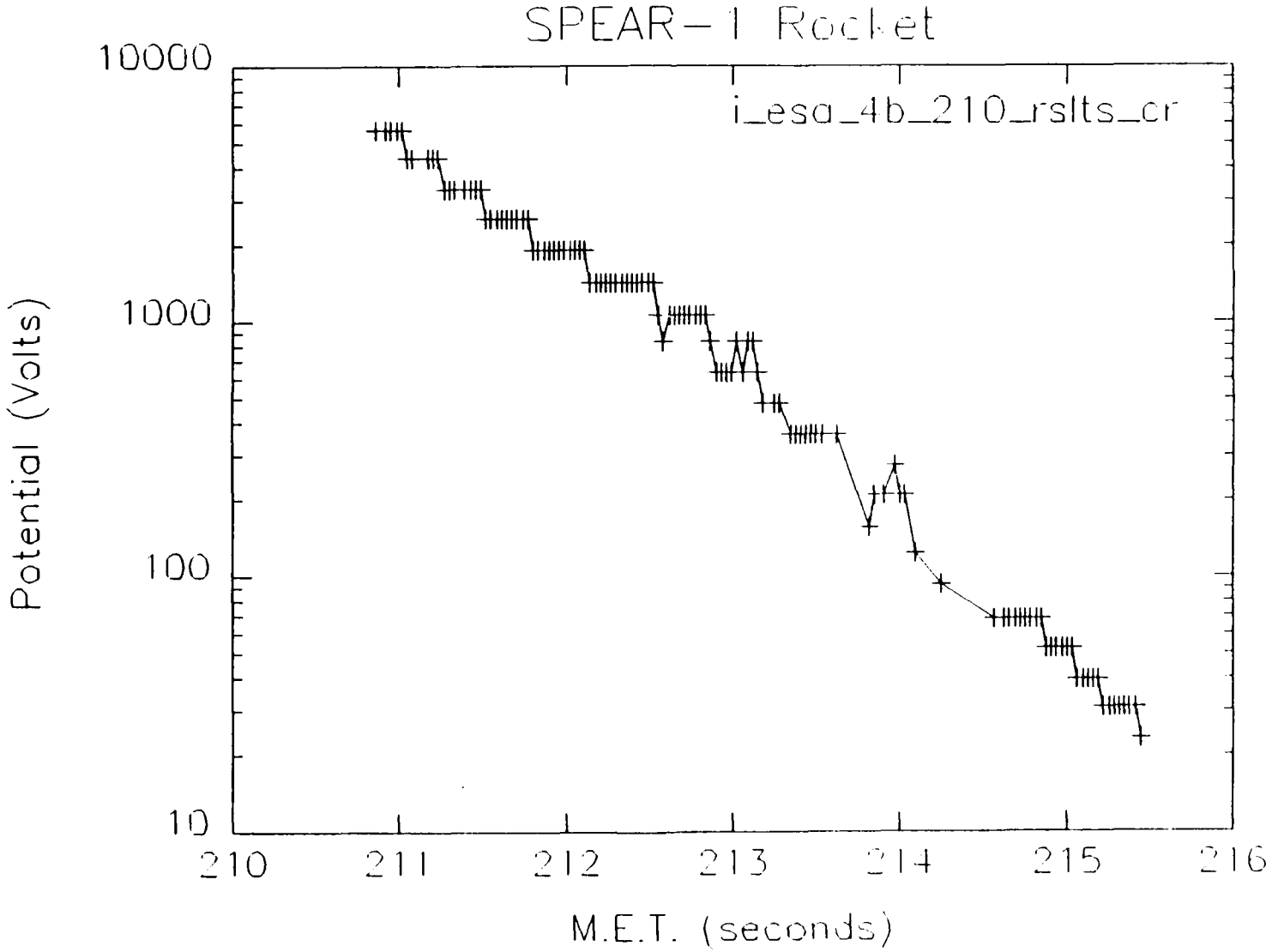
SPEAR-1 Rocket
i_esa_4b_210_rslts_cr
10000
1000
100
10
Potential (Volts)
210
211
212
213
214
215
216
M.E.T. (seconds)

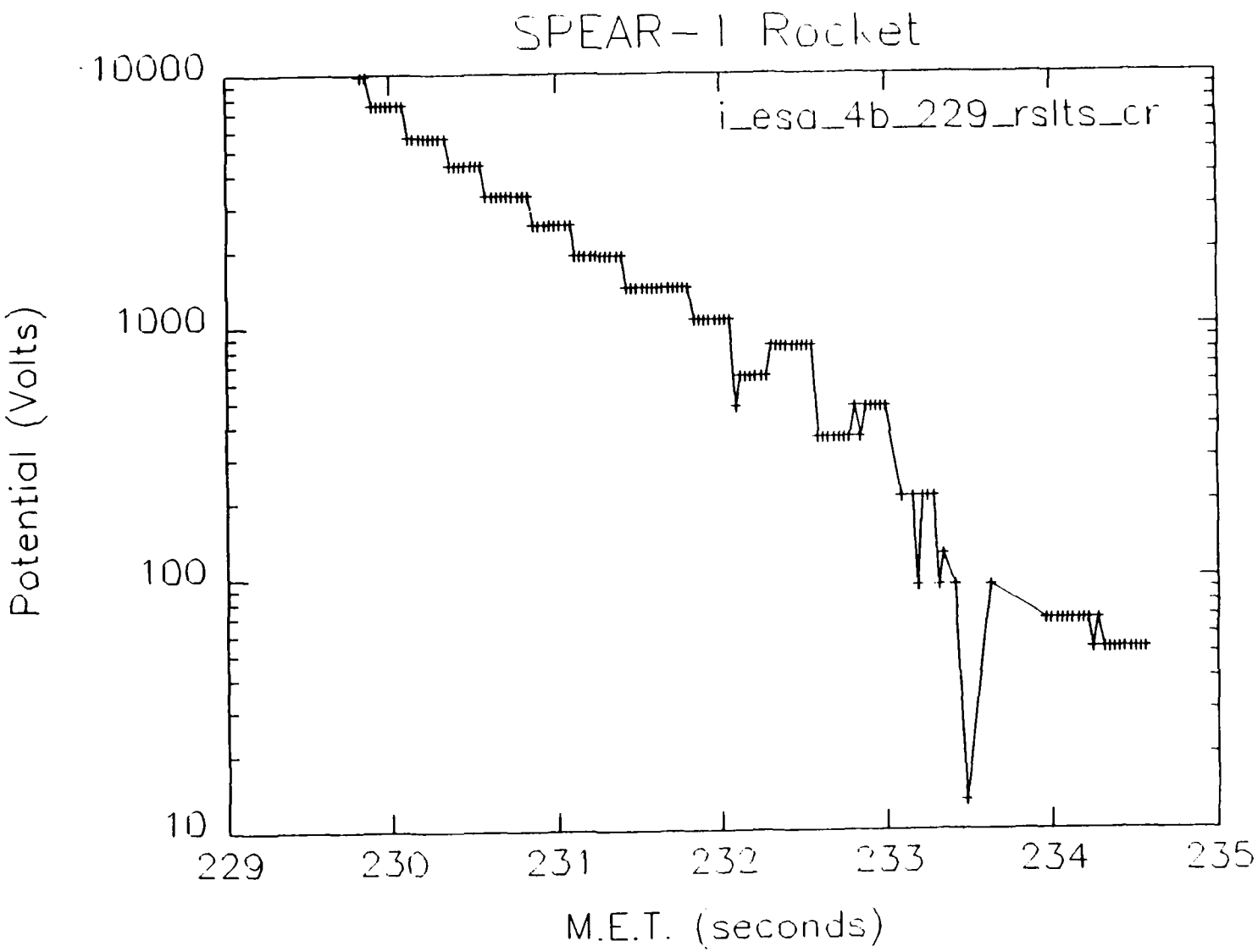
SPEAR-1 Rocket
i_esa_4b_229_rslts_cr
10000
1000
100
10
Potential (Volts)
229
230
231
232
233
234
235
M.E.T. (seconds)

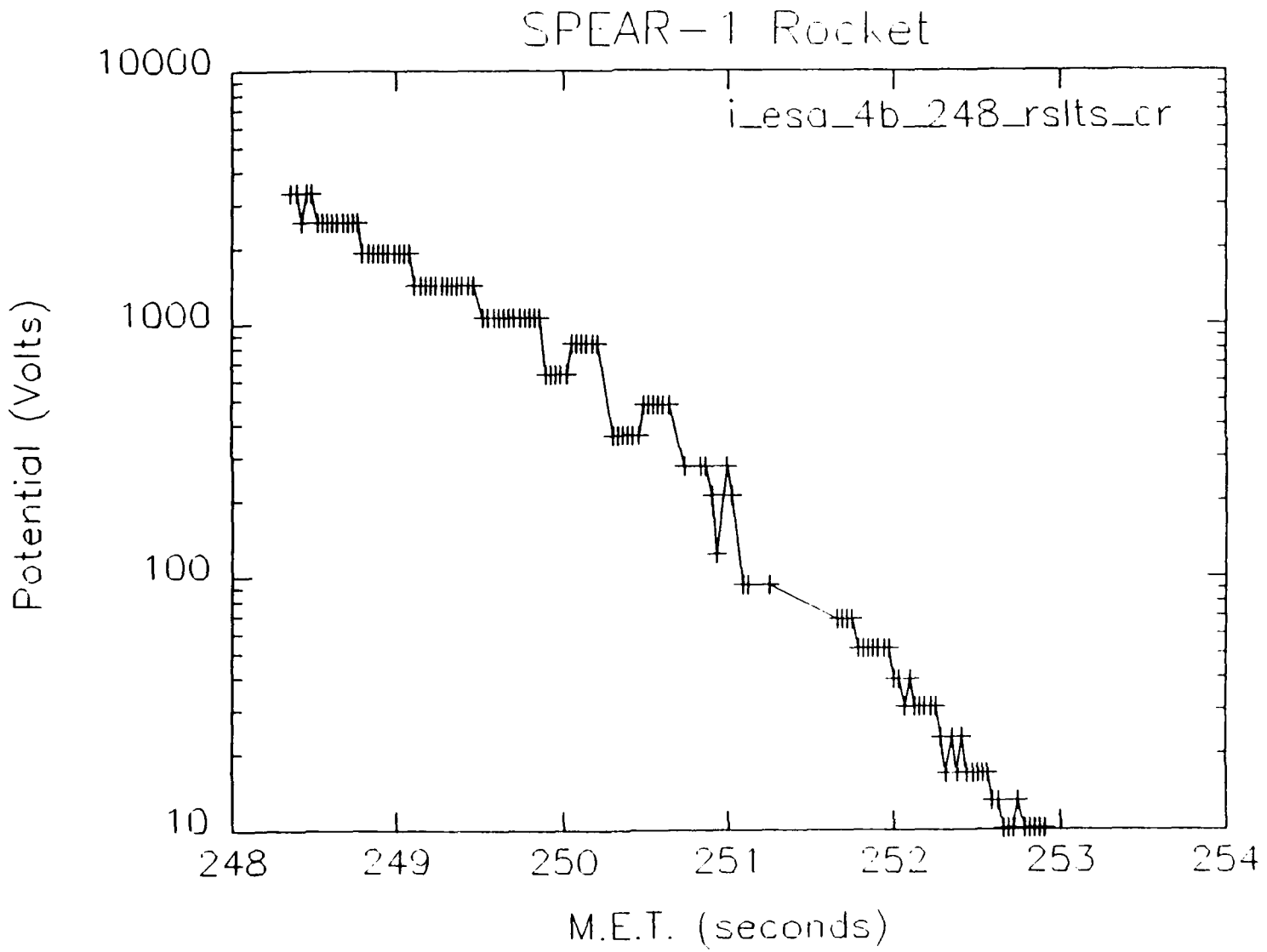
SPEAR-1 Rocket
i_esa_4b_248_rslts_cr
10000
1000
100
10
Potential (Volts)
248
249
250
251
252
253
254
M.E.T. (seconds)

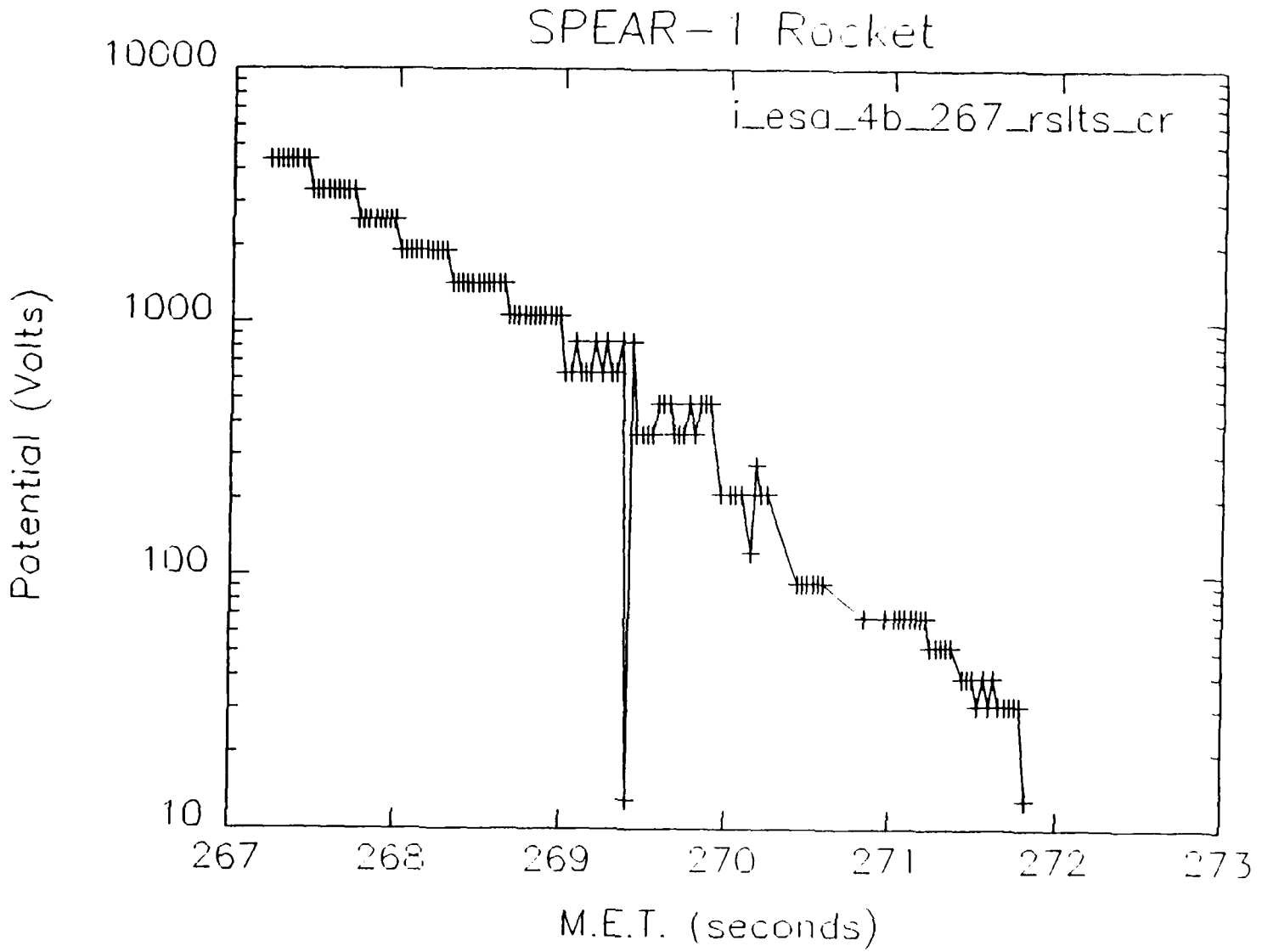
SPEAR-1 Rocket
i_esa_4b_267_rslts_cr
10000
1000
100
10
Potential (Volts)
267
268
269
270
271
272
273
M.E.T. (seconds)

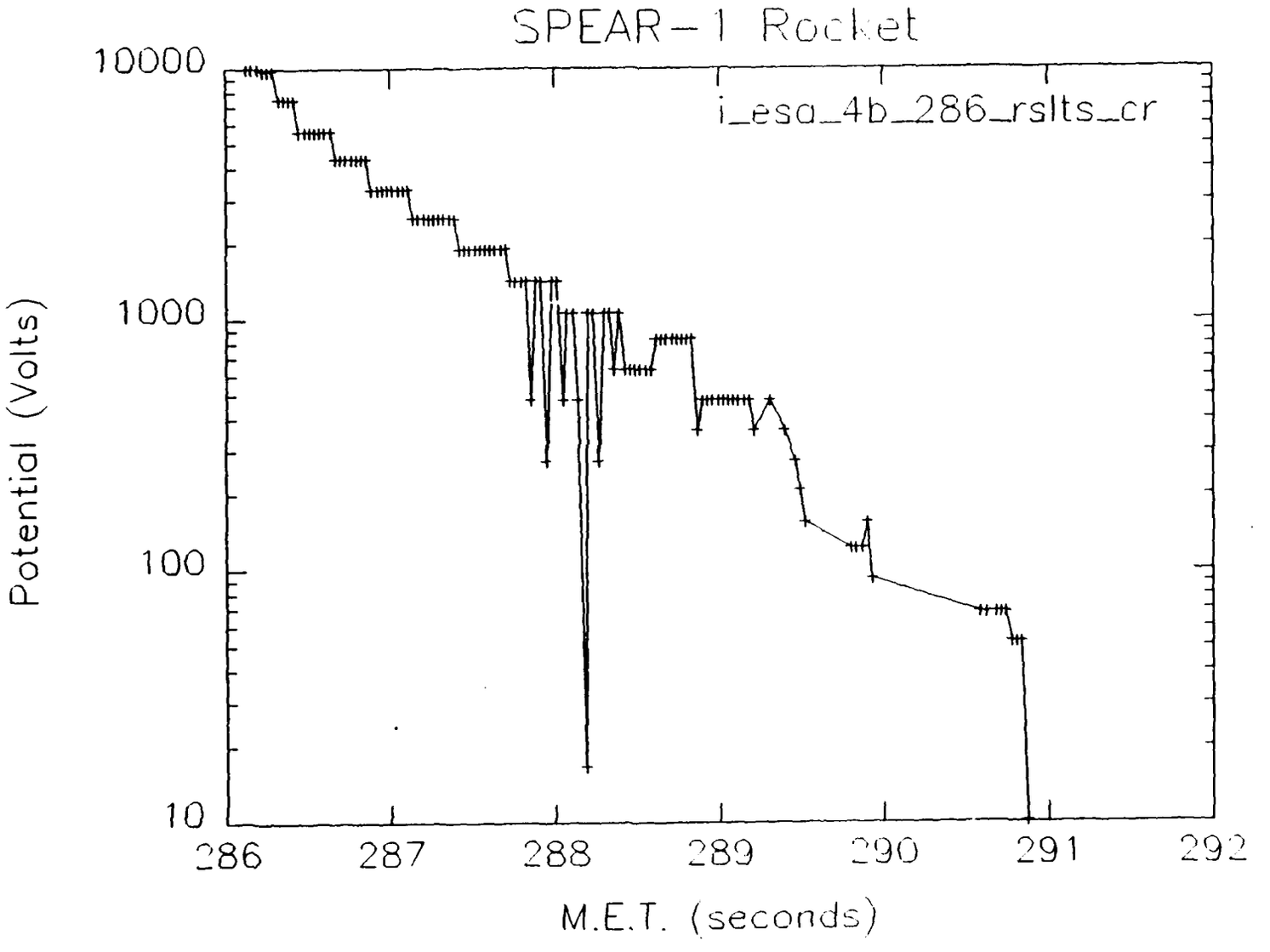
SPEAR-1 Rocket
i_esa_4b_286_rslts_cr
10000
1000
100
10
Potential (Volts)
286
287
288
289
290
291
292
M.E.T. (seconds)

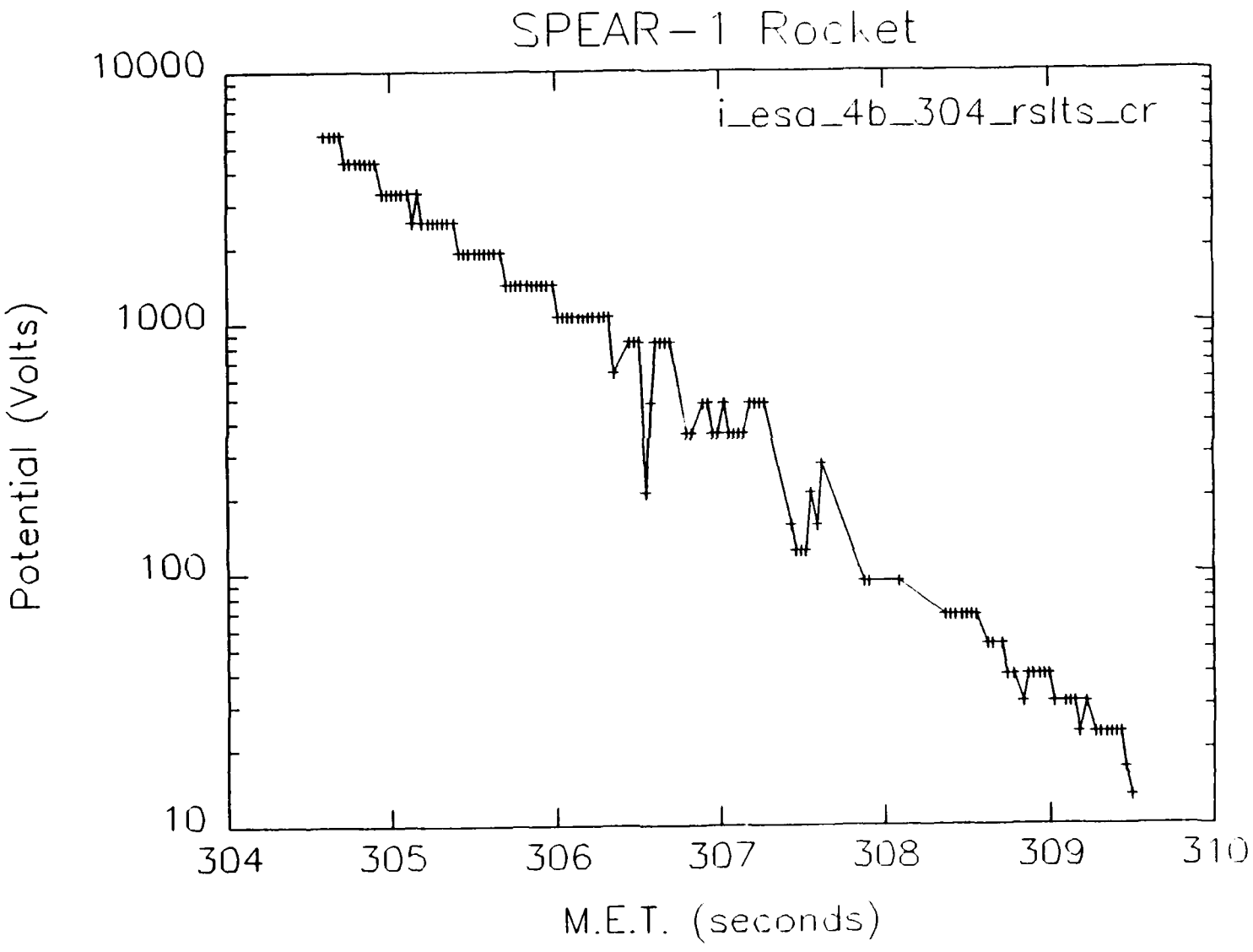
SPEAR-1 Rocket
i_esa_4b_304_rslts_cr
10000
1000
100
10
Potential (Volts)
304
305
306
307
308
309
310
M.E.T. (seconds)

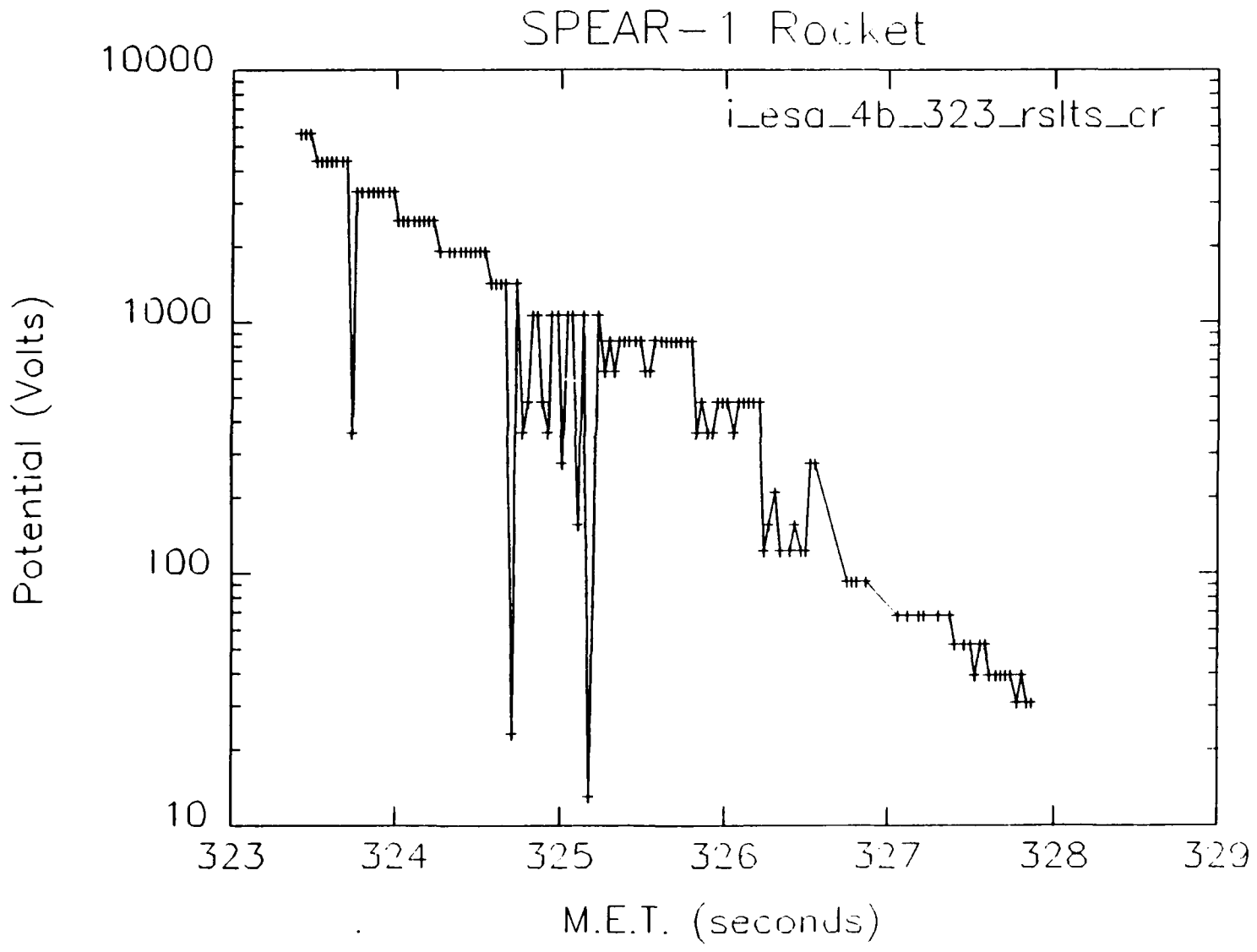
SPEAR-1 Rocket
i_esa_4b_323_rslts_cr
10000
1000
100
10
Potential (Volts)
323
324
325
326
327
328
329
M.E.T. (seconds)

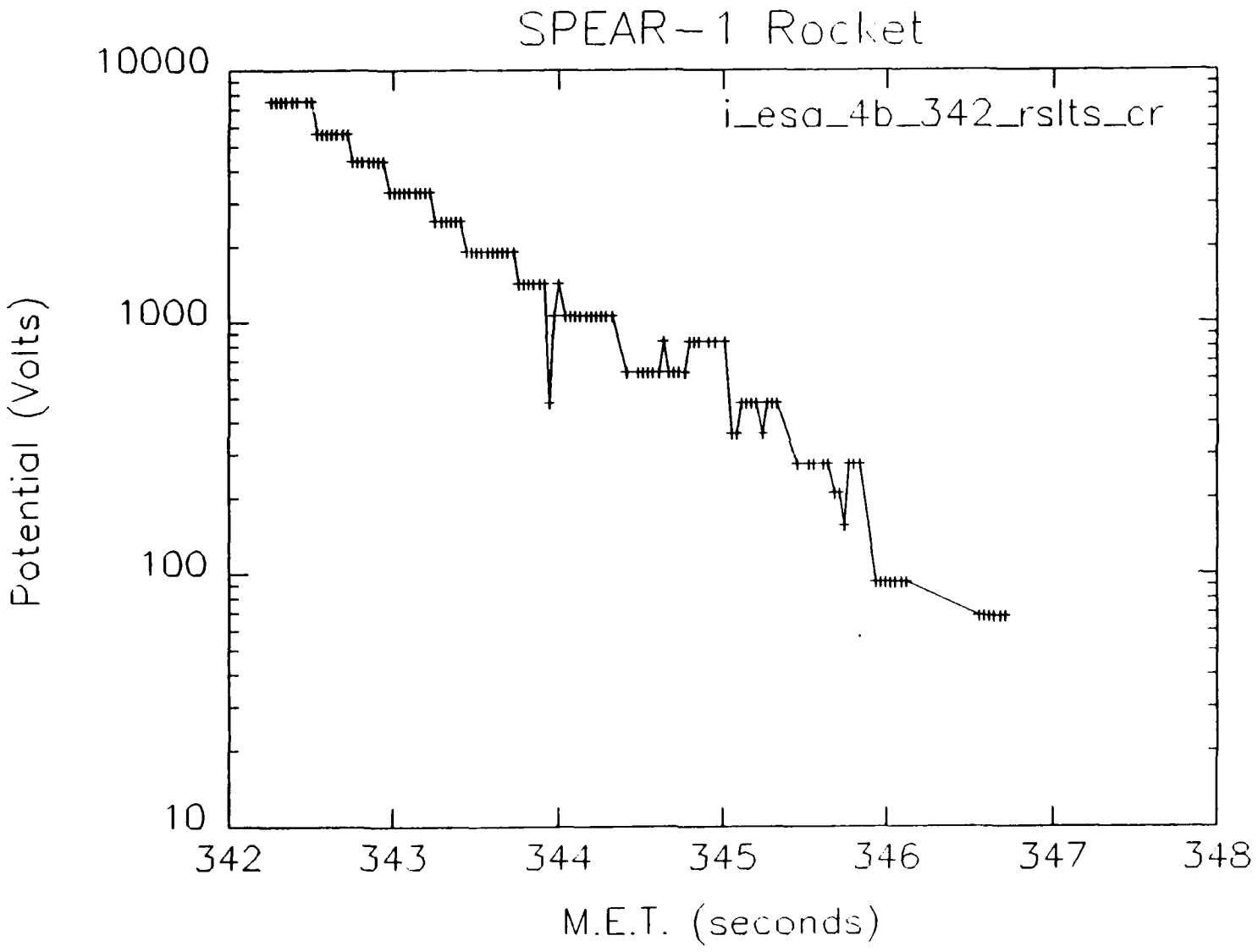
SPEAR-1 Rocket
i_esa_4b_342_rslts_cr
10000
1000
100
10
Potential (Volts)
342
343
344
345
346
347
348
M.E.T. (seconds)

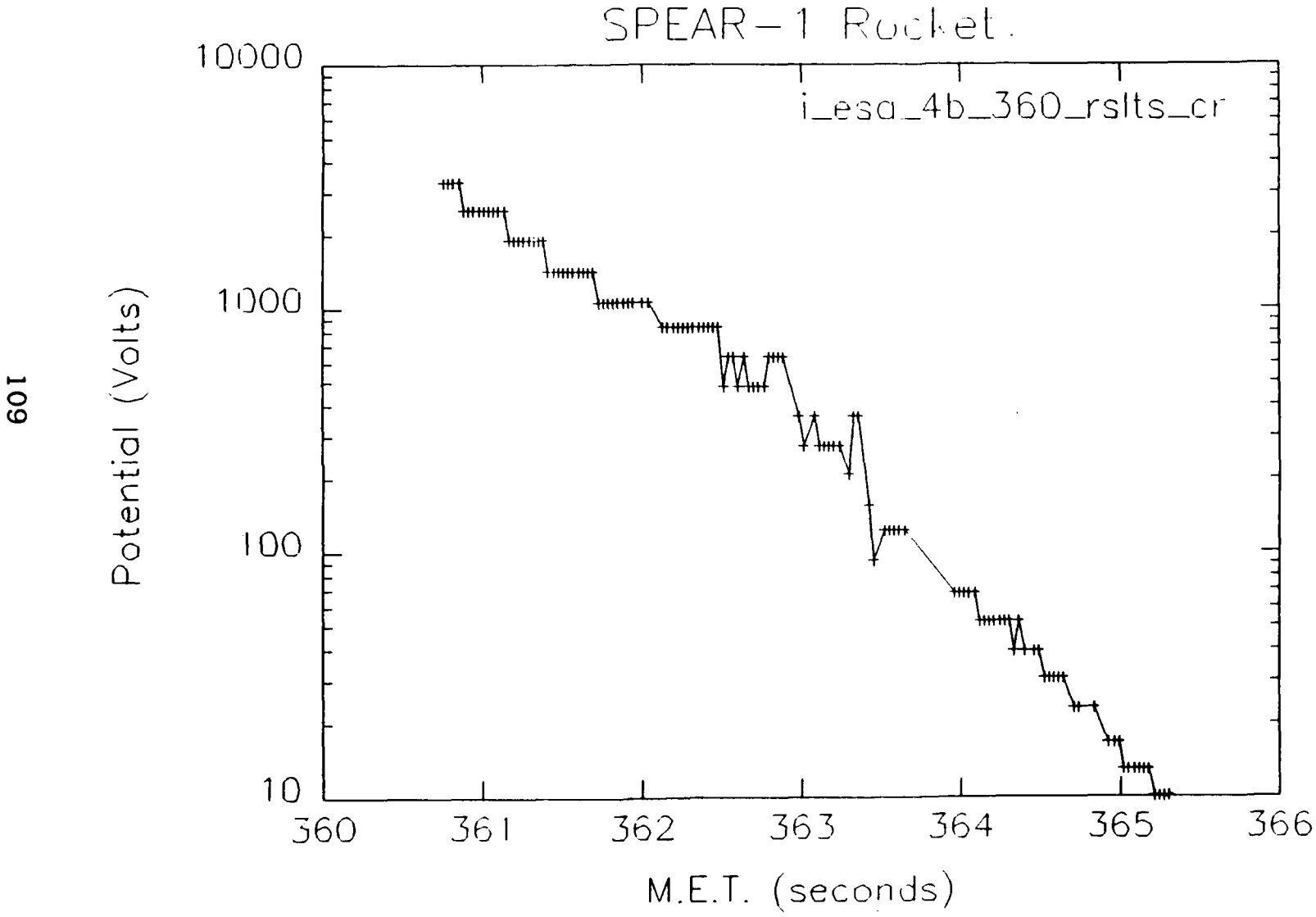
SPEAR-1 Rocket
i_esa_4b_360_rslts_cr
10000
1000
100
10
Potential (Volts)
360
361
362
363
364
365
366
M.E.T. (seconds)

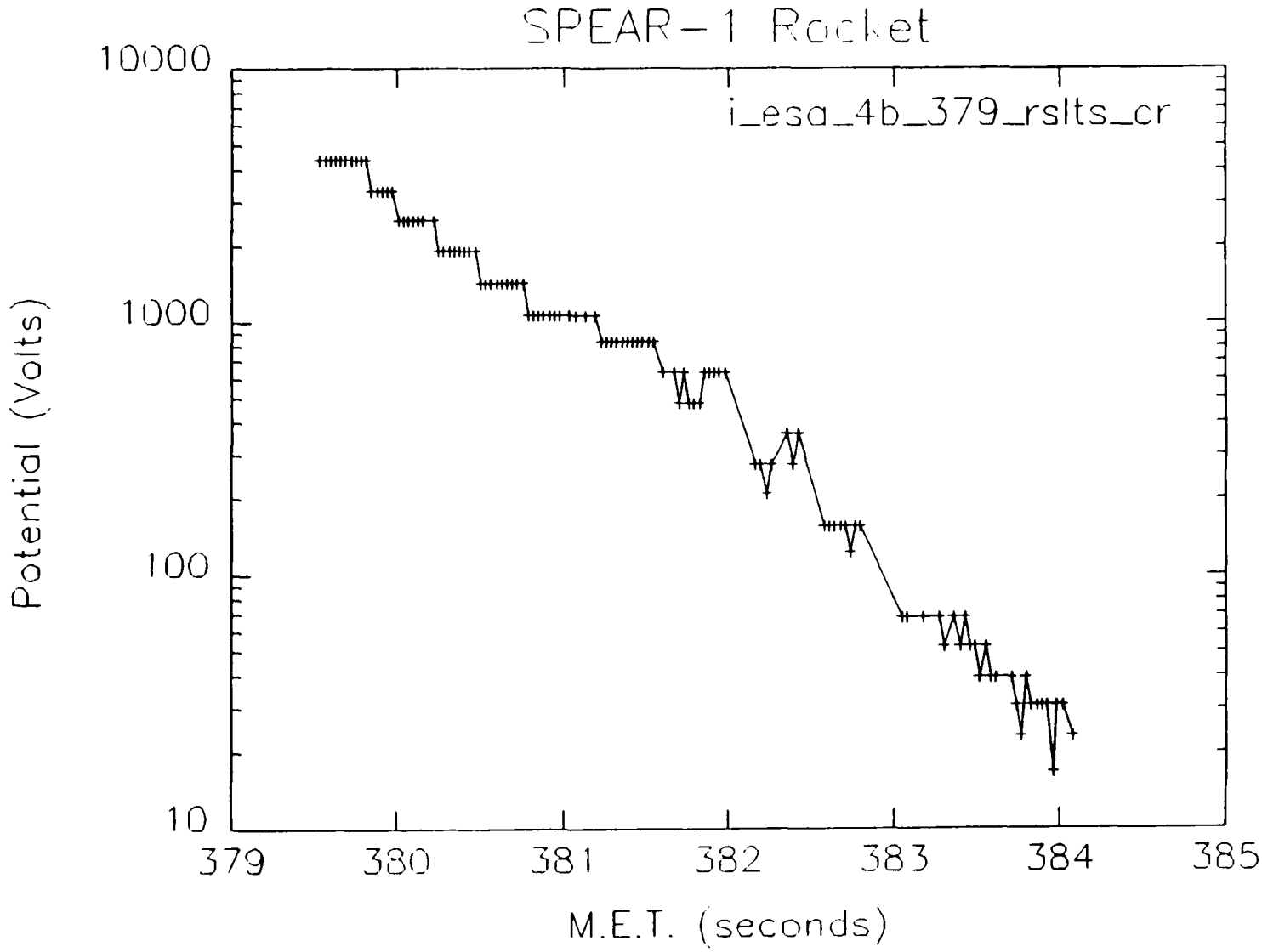
SPEAR-1 Rocket
i_esa_4b_379_rslts_cr
10000
1000
100
10
Potential (Volts)
379
380
381
382
383
384
385
M.E.T. (seconds)

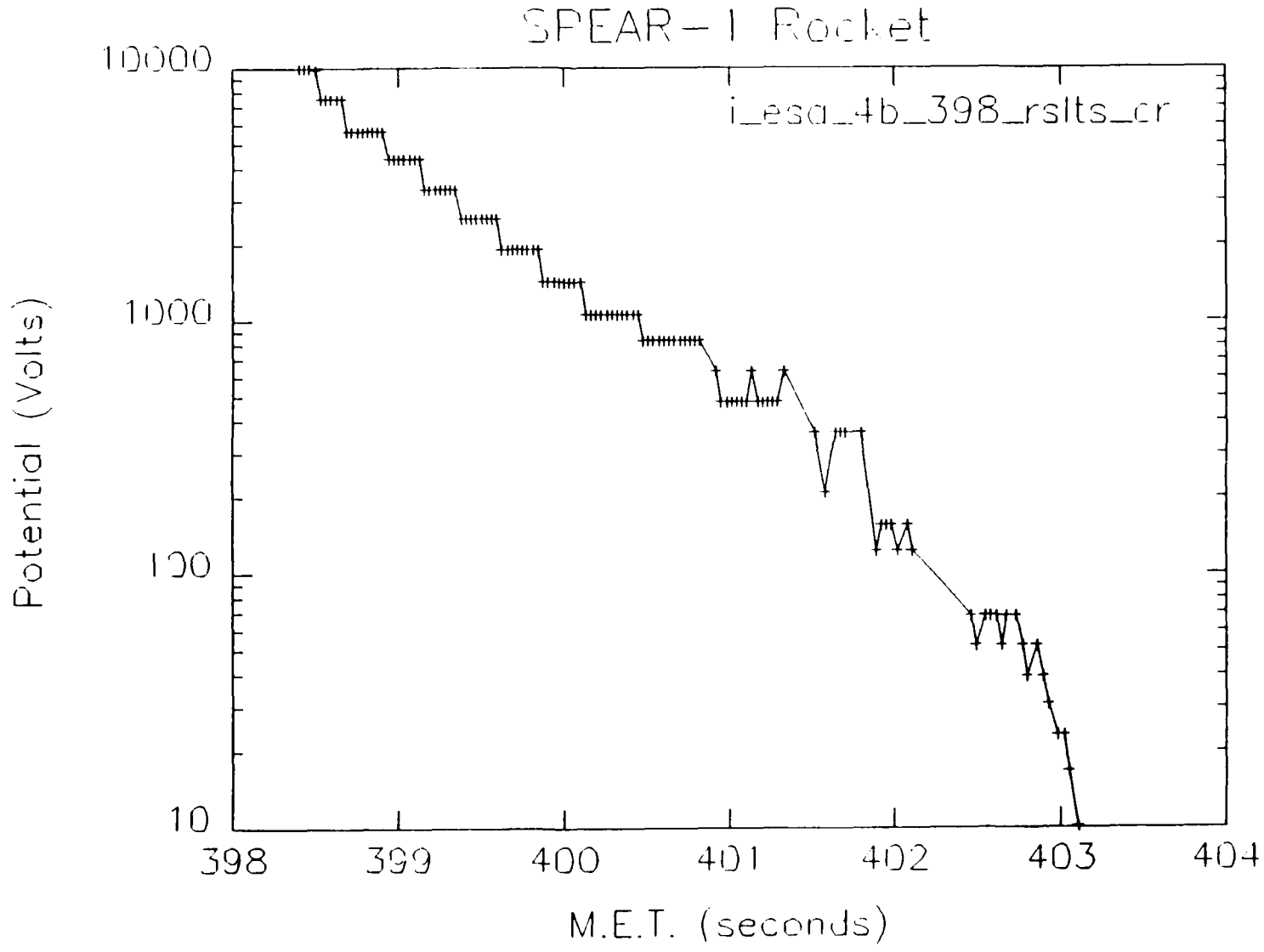
SPEAR-1 Rocket
i_esa_4b_398_rslts_cr
10000
1000
100
10
Potential (Volts)
398
399
400
401
402
403
404
M.E.T. (seconds)

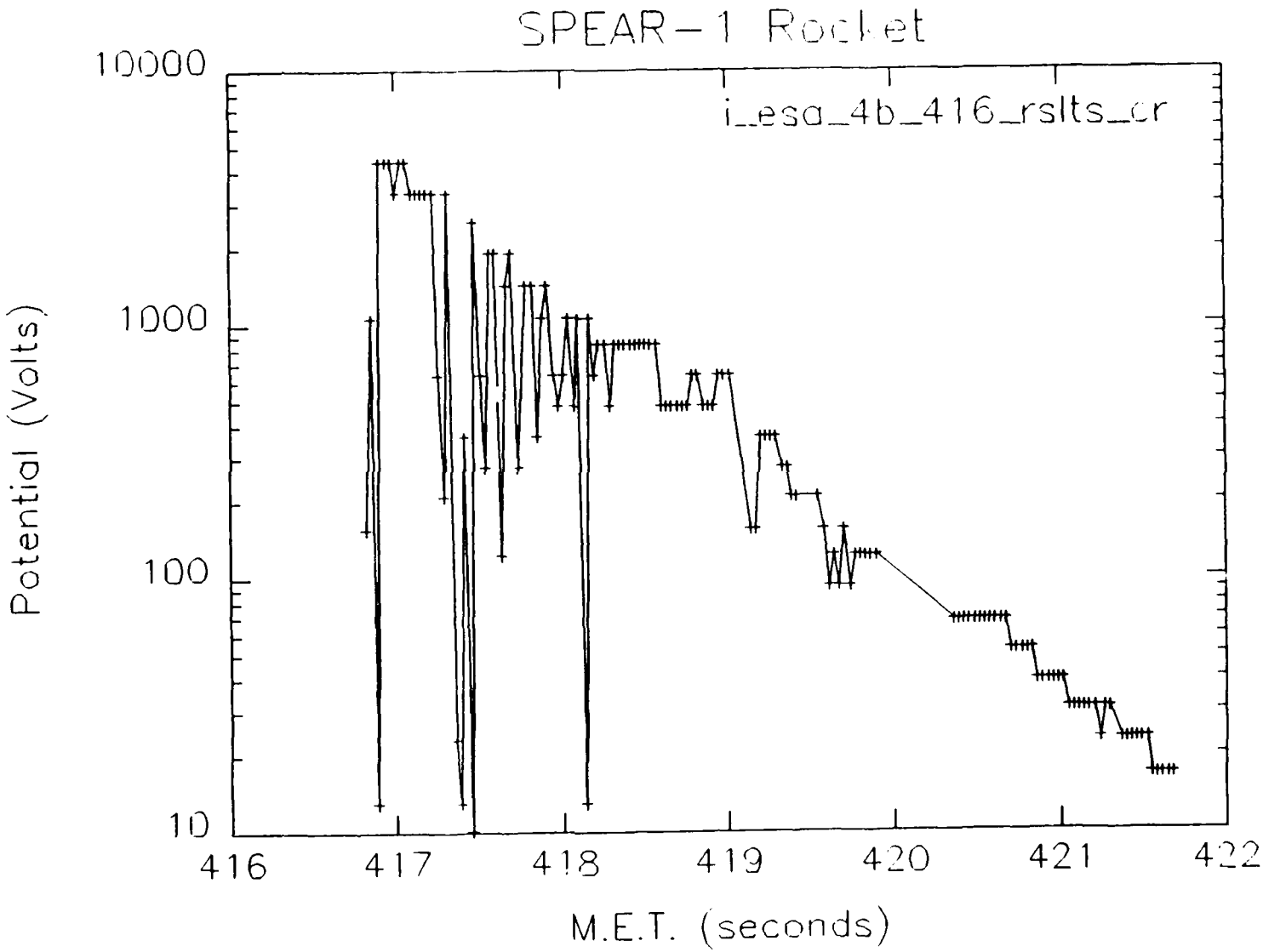
SPEAR-1 Rocket
i_esa_4b_416_rslts_cr
10000
1000
100
10
Potential (Volts)
416
417
418
419
420
421
422
M.E.T. (seconds)

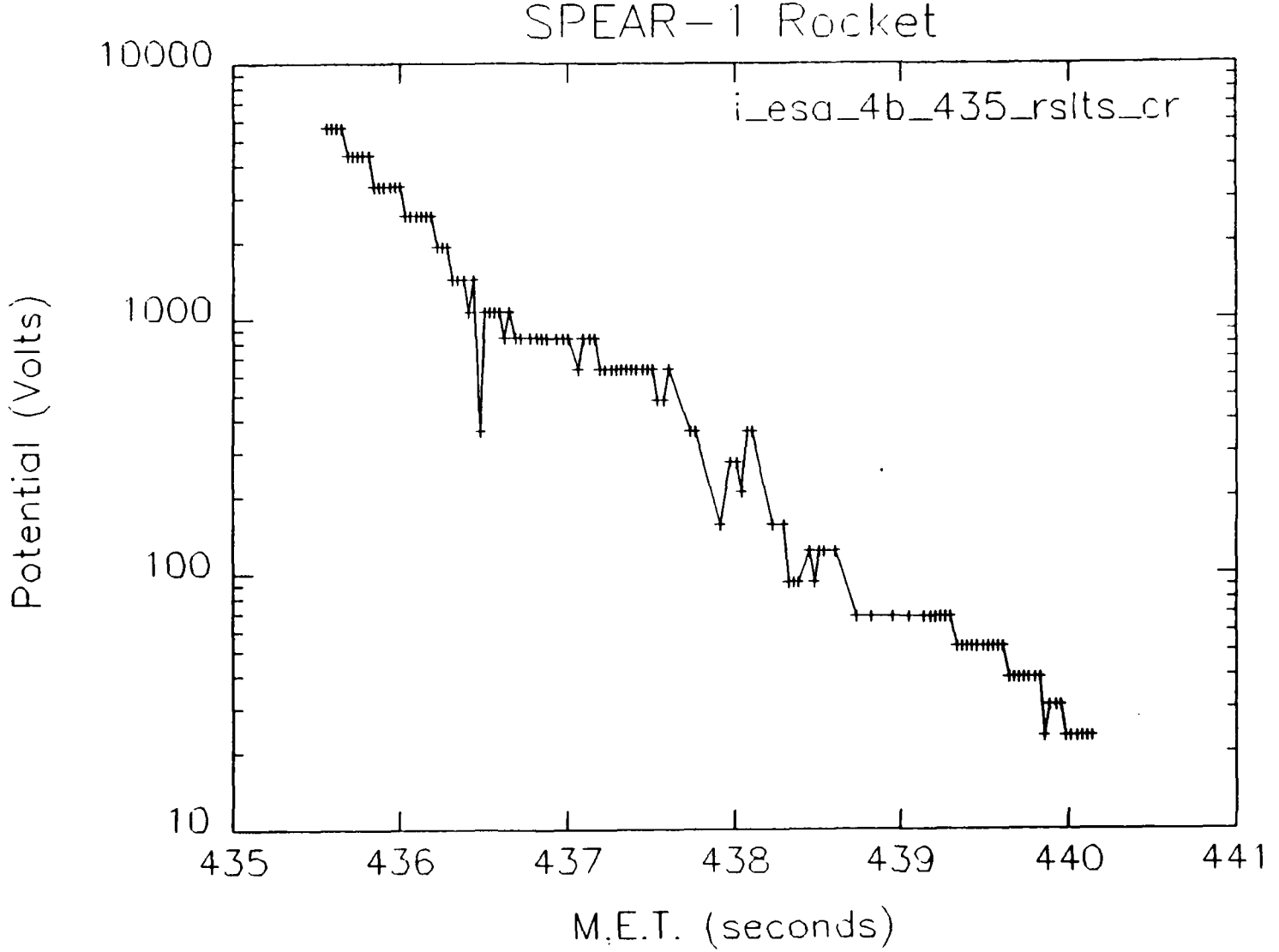
SPEAR-1 Rocket
i_esa_4b_435_rslts_cr
10000
1000
100
10
Potential (Volts)
435
436
437
438
439
440
441
M.E.T. (seconds)

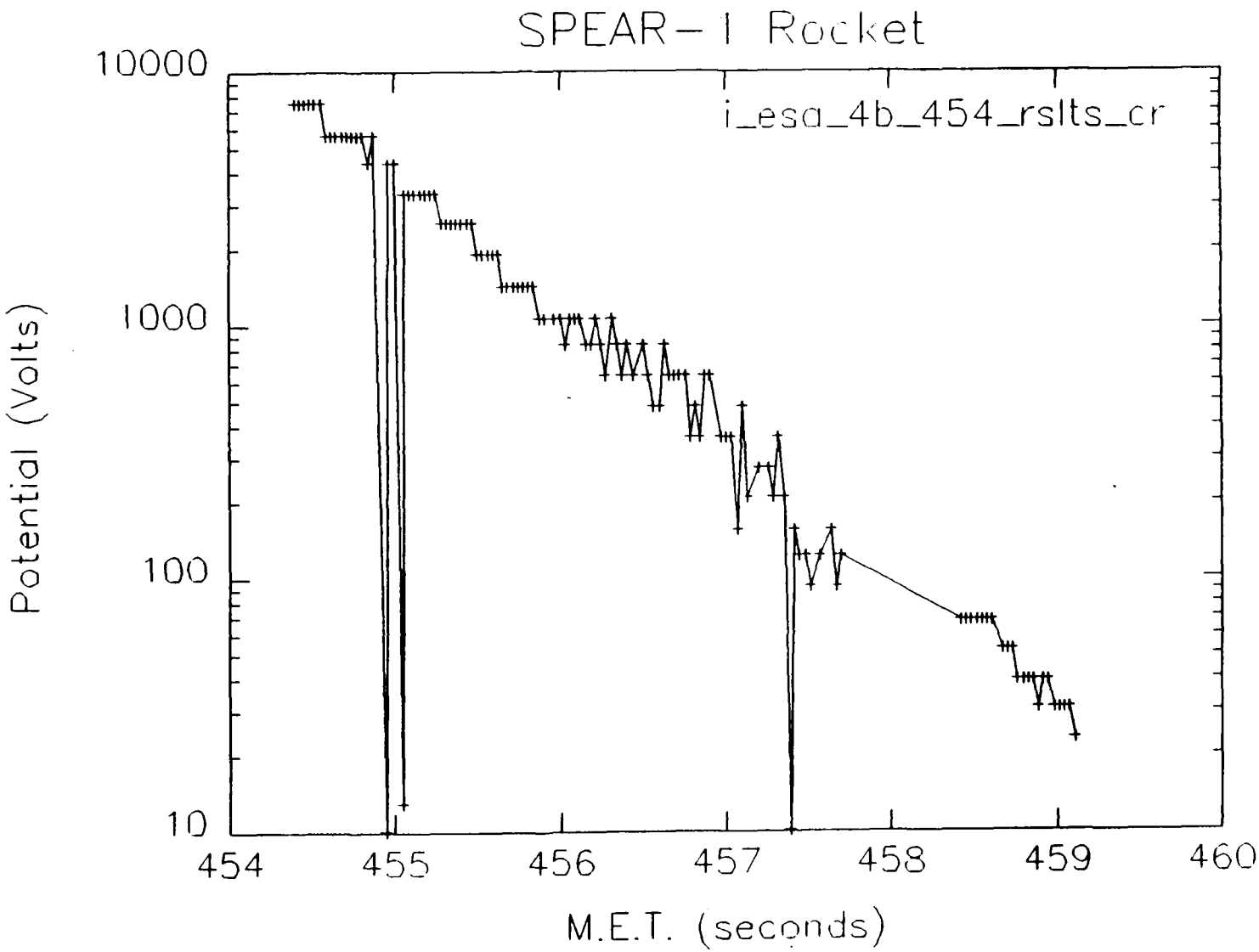
SPEAR-1 Rocket
i_esa_4b_454_rslts_cr
10000
1000
100
10
Potential (Volts)
454
455
456
457
458
459
460
M.E.T. (seconds)

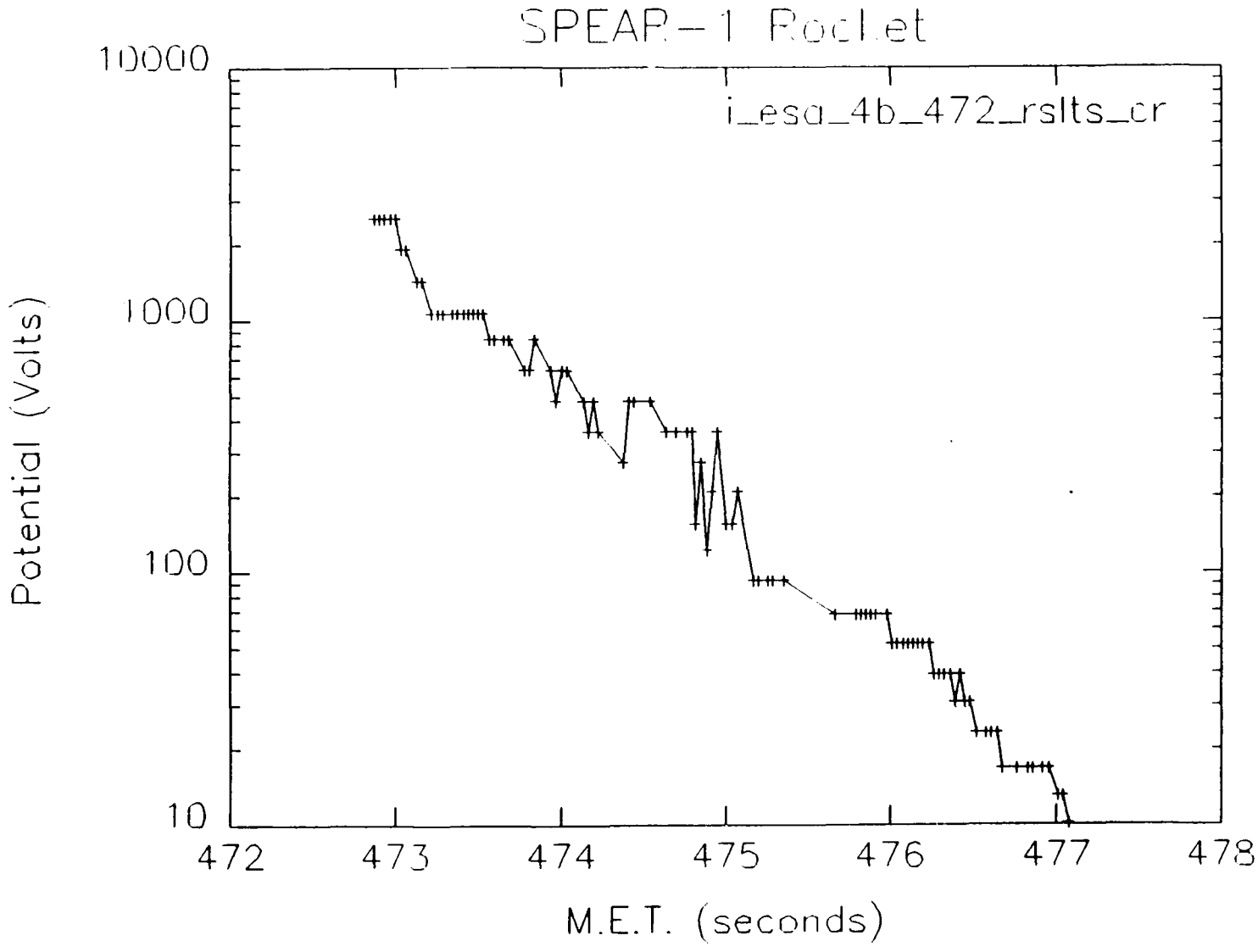
SPEAR-1 RocLet
i_esa_4b_472_rslts_cr
10000
1000
100
10
Potential (Volts)
472
473
474
475
476
477
478
M.E.T. (seconds)

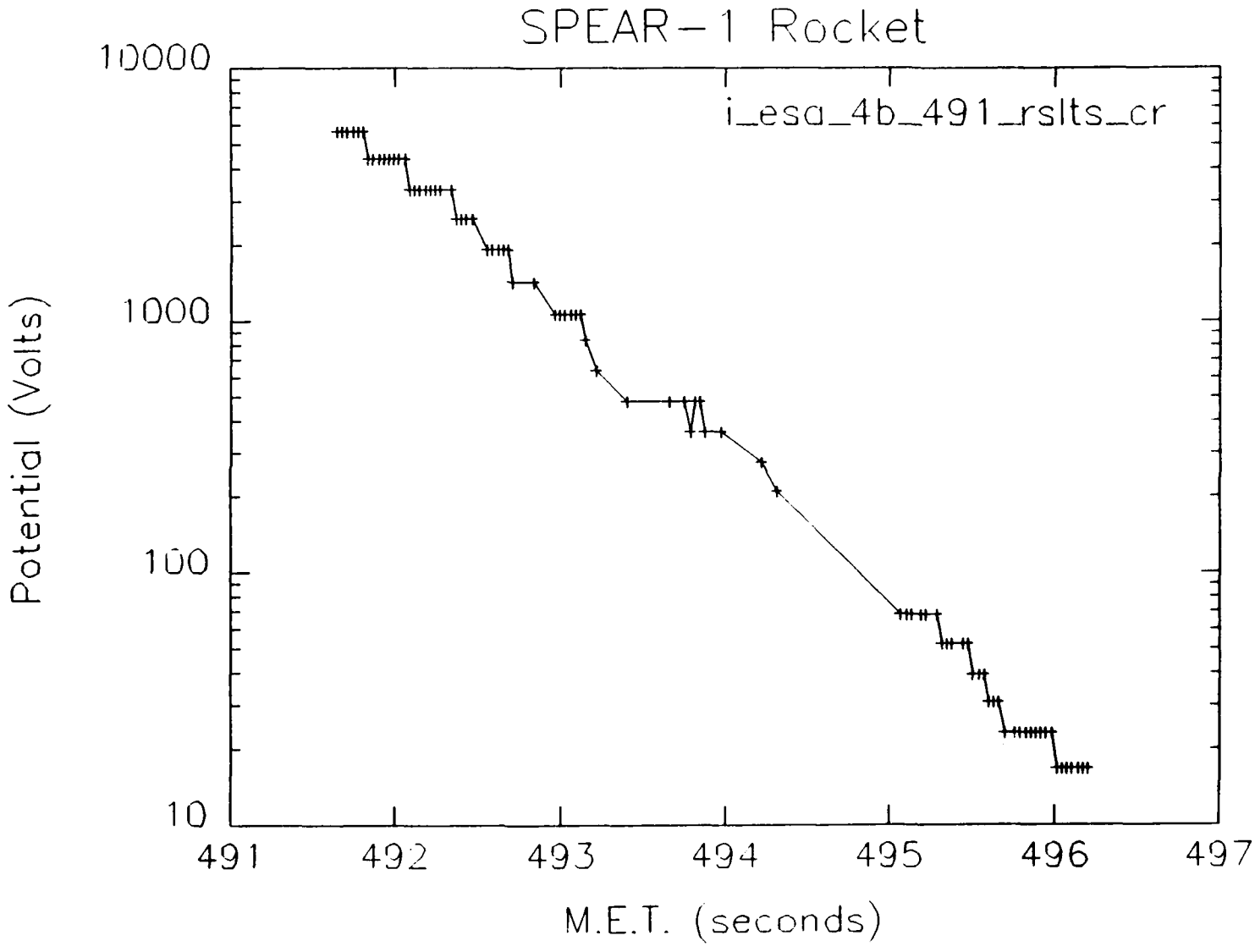
SPEAR-1 Rocket
i_esa_4b_491_rslts_cr
10000
1000
100
10
Potential (Volts)
491
492
493
494
495
496
497
M.E.T. (seconds)

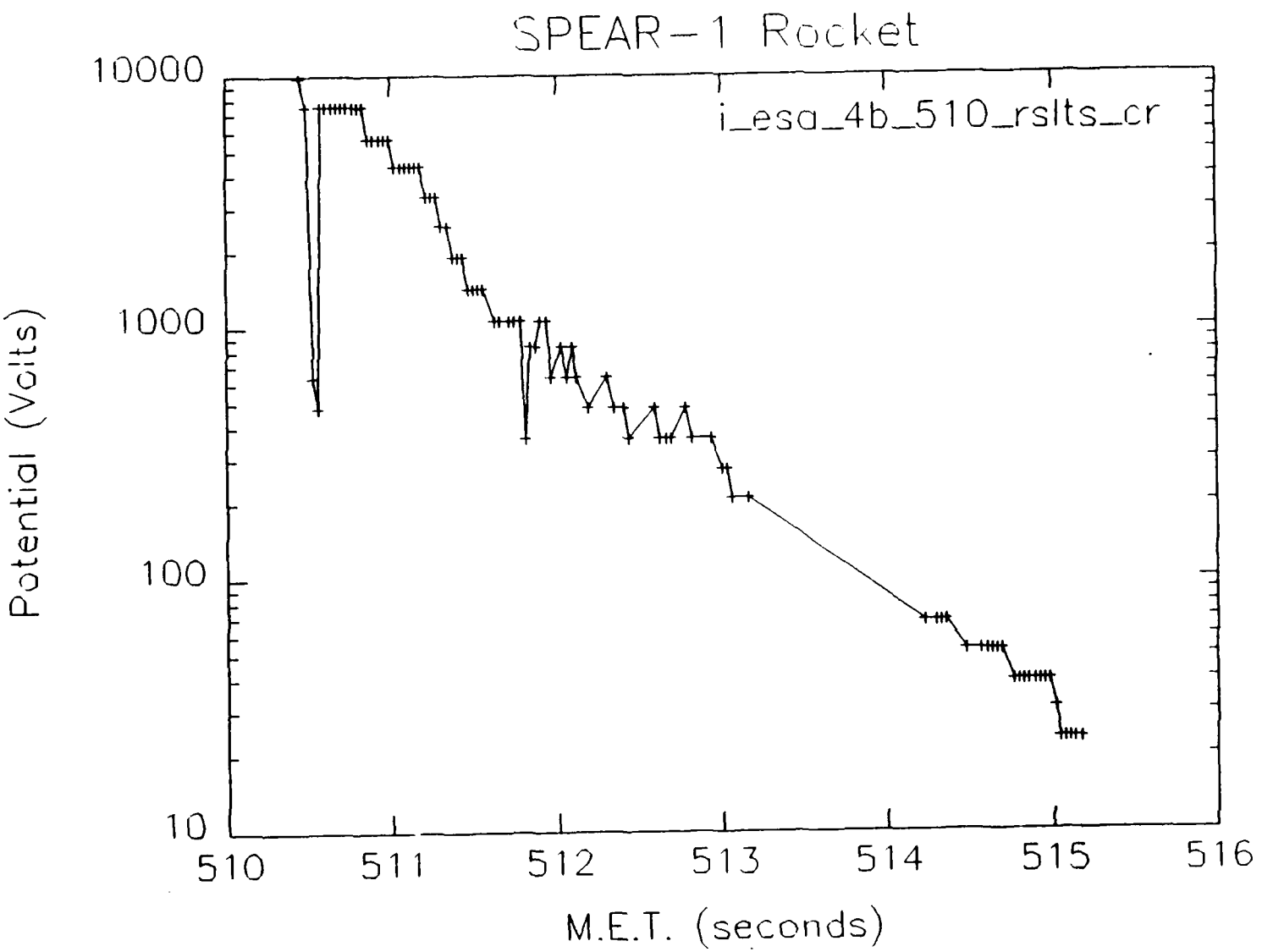
SPEAR-1 Rocket
i_esa_4b_510_rslts_cr
10000
1000
100
10
Potential (Volts)
510
511
512
513
514
515
516
M.E.T. (seconds)

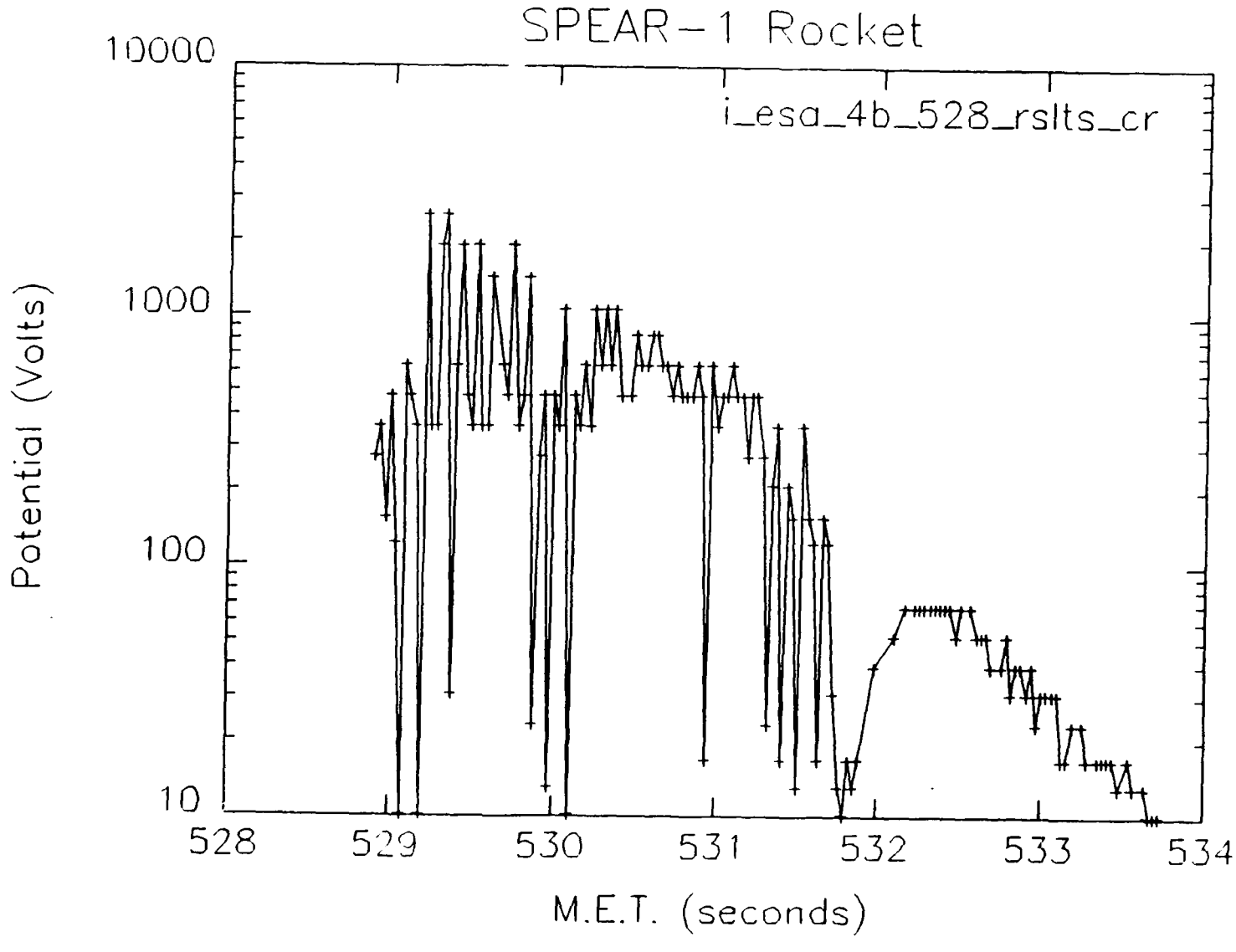
SPEAR-1 Rocket
i_esa_4b_528_rslts_cr
10000
1000
100
10
Potential (Volts)
528
529
530
531
532
533
534
M.E.T. (seconds)

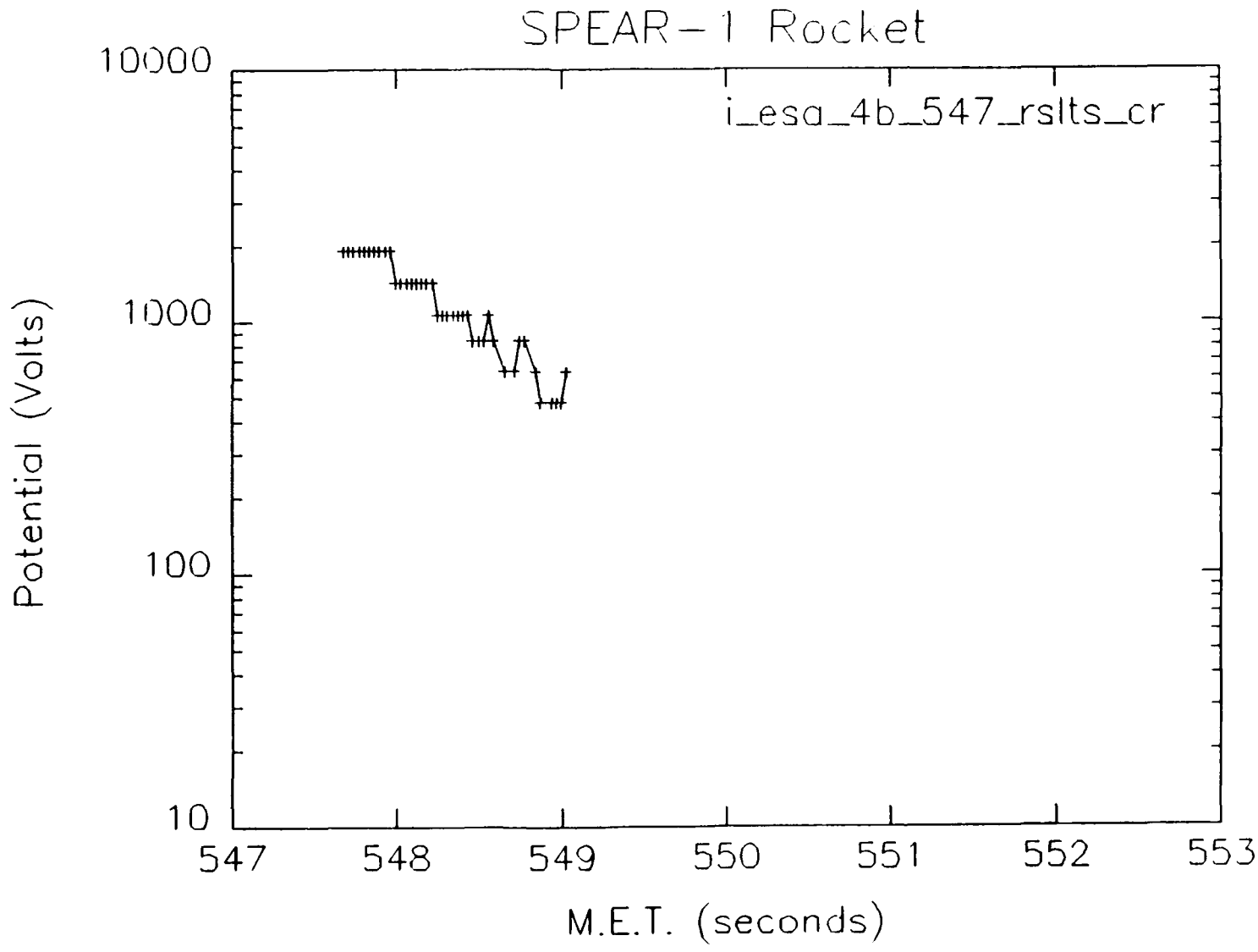
SPEAR-1 Rocket
i_esa_4b_547_rslts_cr
10000
1000
100
10
Potential (Volts)
547
548
549
550
551
552
553
M.E.T. (seconds)

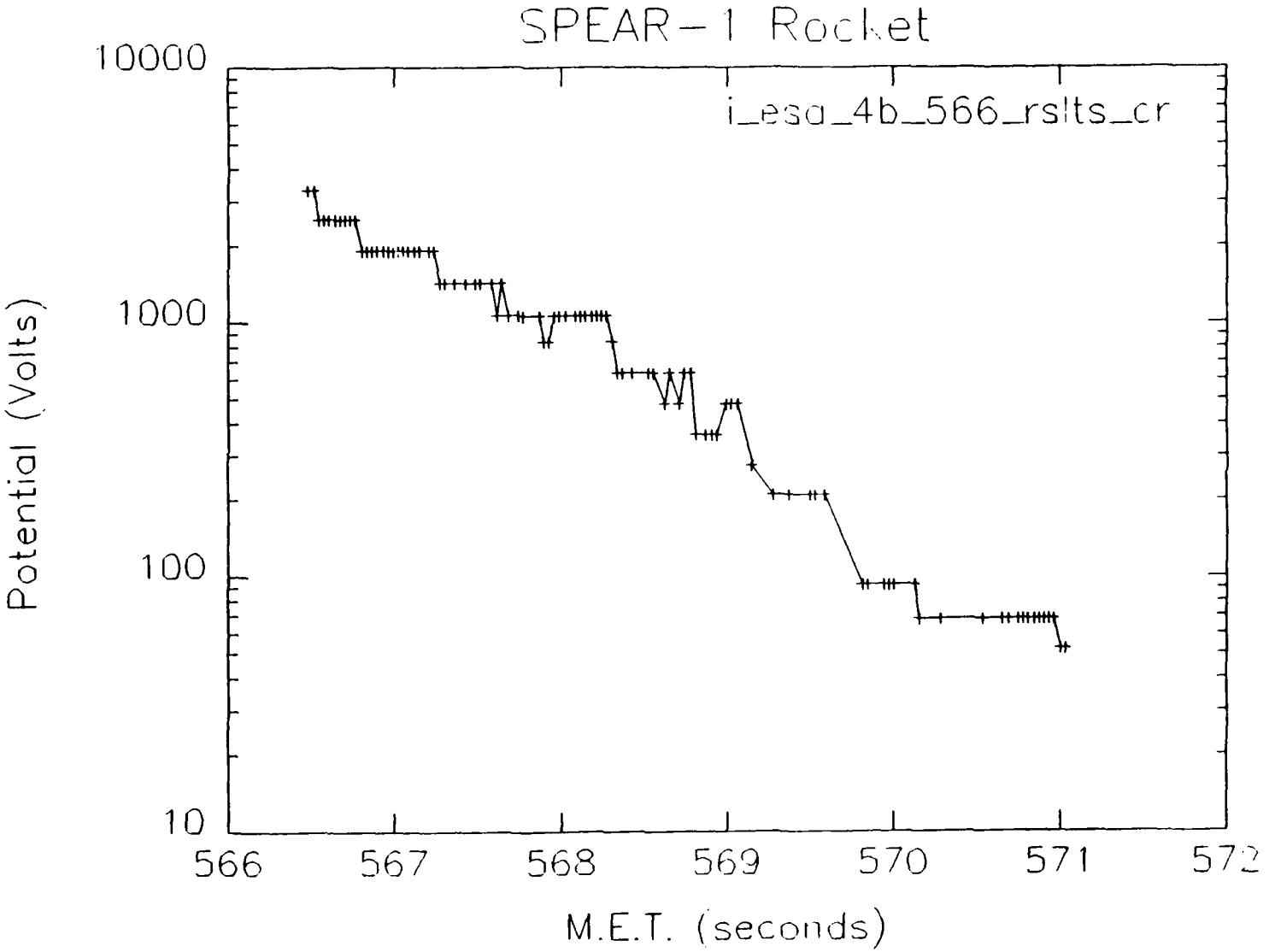
SPEAR-1 Rocket
i_esa_4b_566_rslts_cr
10000
1000
100
10
Potential (Volts)
566
567
568
569
570
571
572
M.E.T. (seconds)

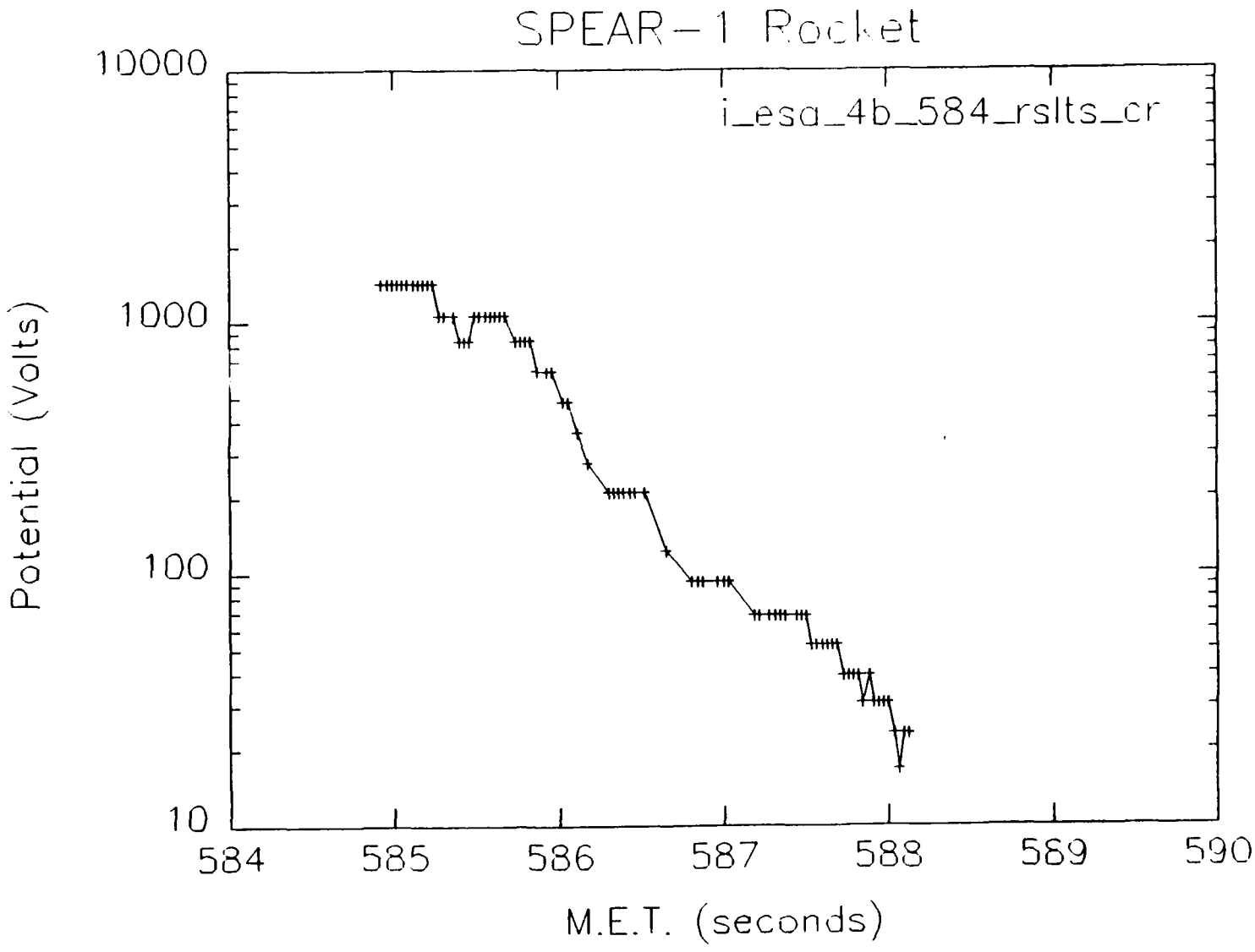
SPEAR-1 Rocket
i_esa_4b_584_rslts_cr
10000
1000
100
10
Potential (Volts)
584
585
586
587
588
589
590
M.E.T. (seconds)

APPENDIX D

SPHERE VS. ROCKET POTENTIALS

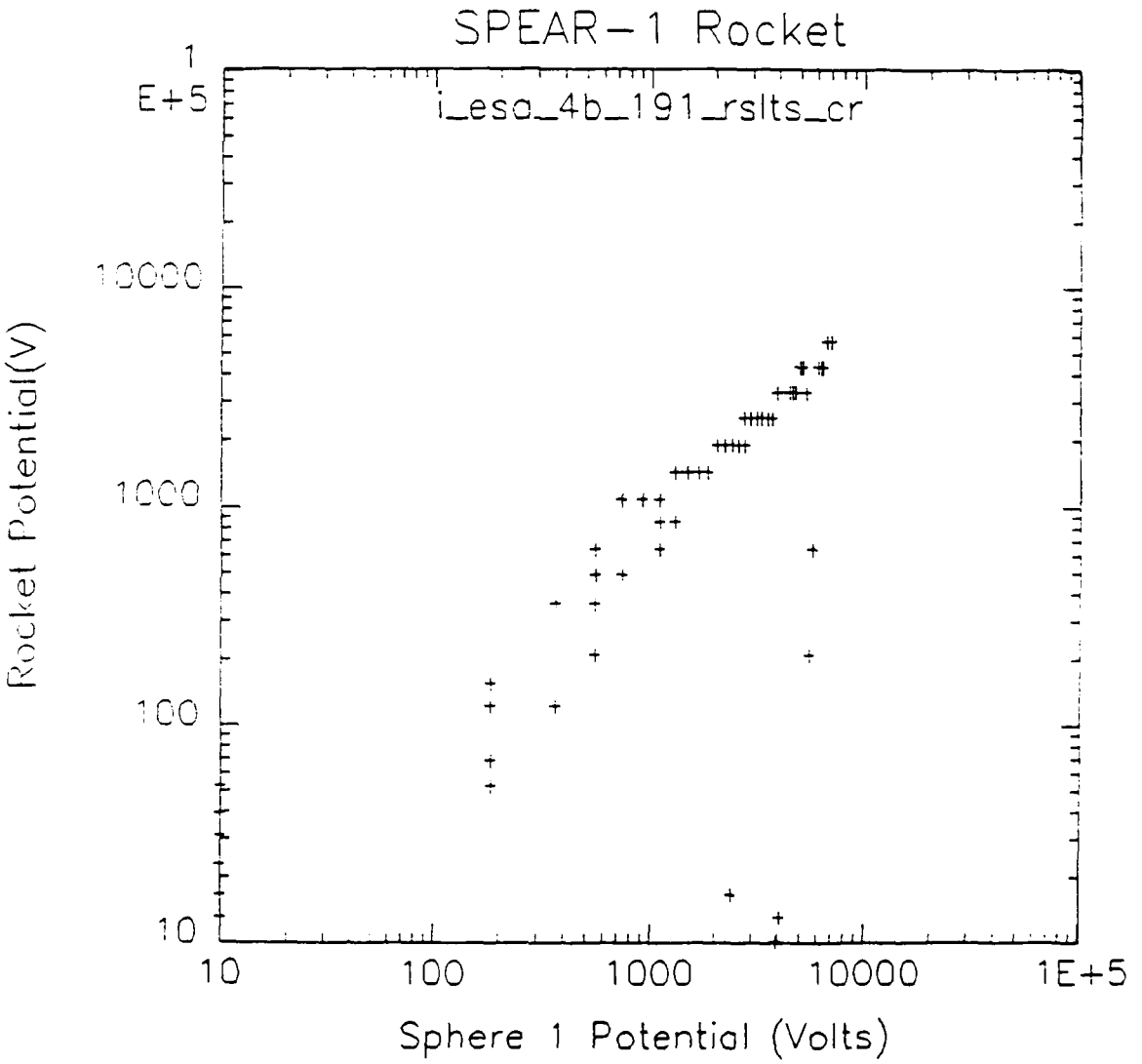

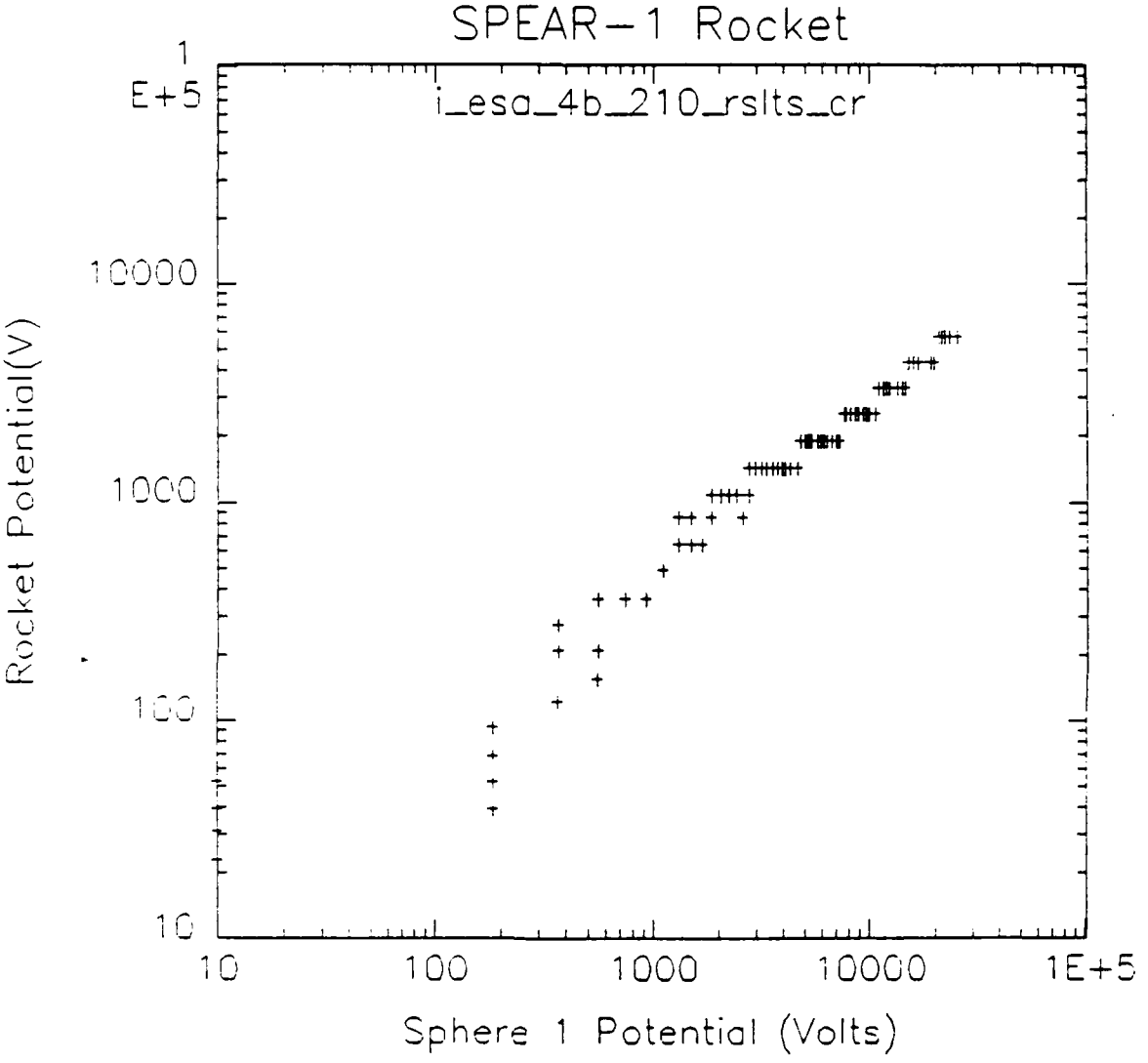
SPEAR–1 Rocket
i_esa_4b_210_rslts_cr
Rocket Potential(V)
Sphere 1 Potential (Volts)
1
E+5
10000
1000
100
10
10
100
1000
10000
1E+5

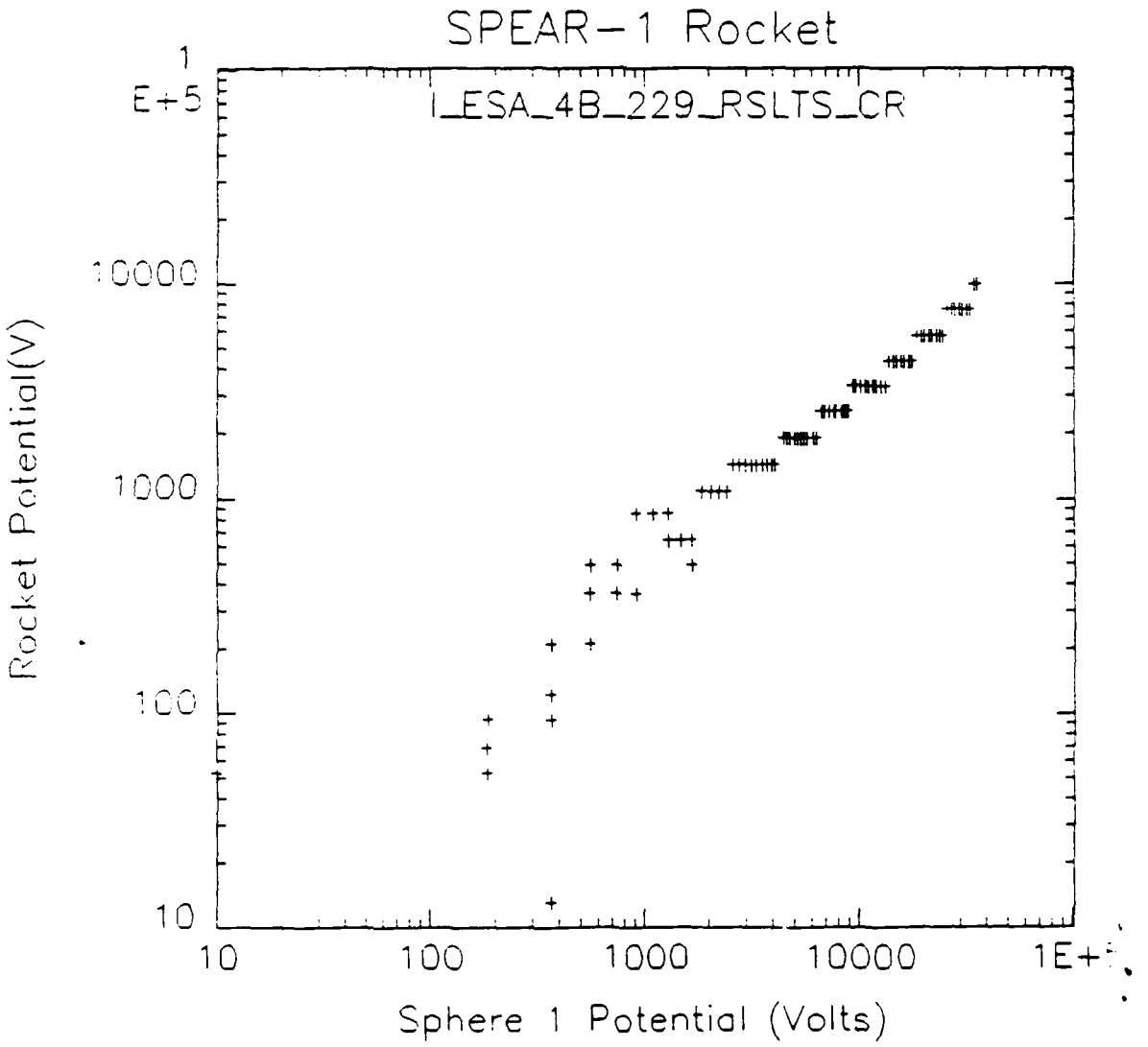
SPEAR-1 Rocket
I_ESA_4B_229_RSLTS_CR
Rocket Potential(V)
1
E+5
10000
1000
100
10
10
100
1000
10000
1E+
Sphere 1 Potential (Volts)

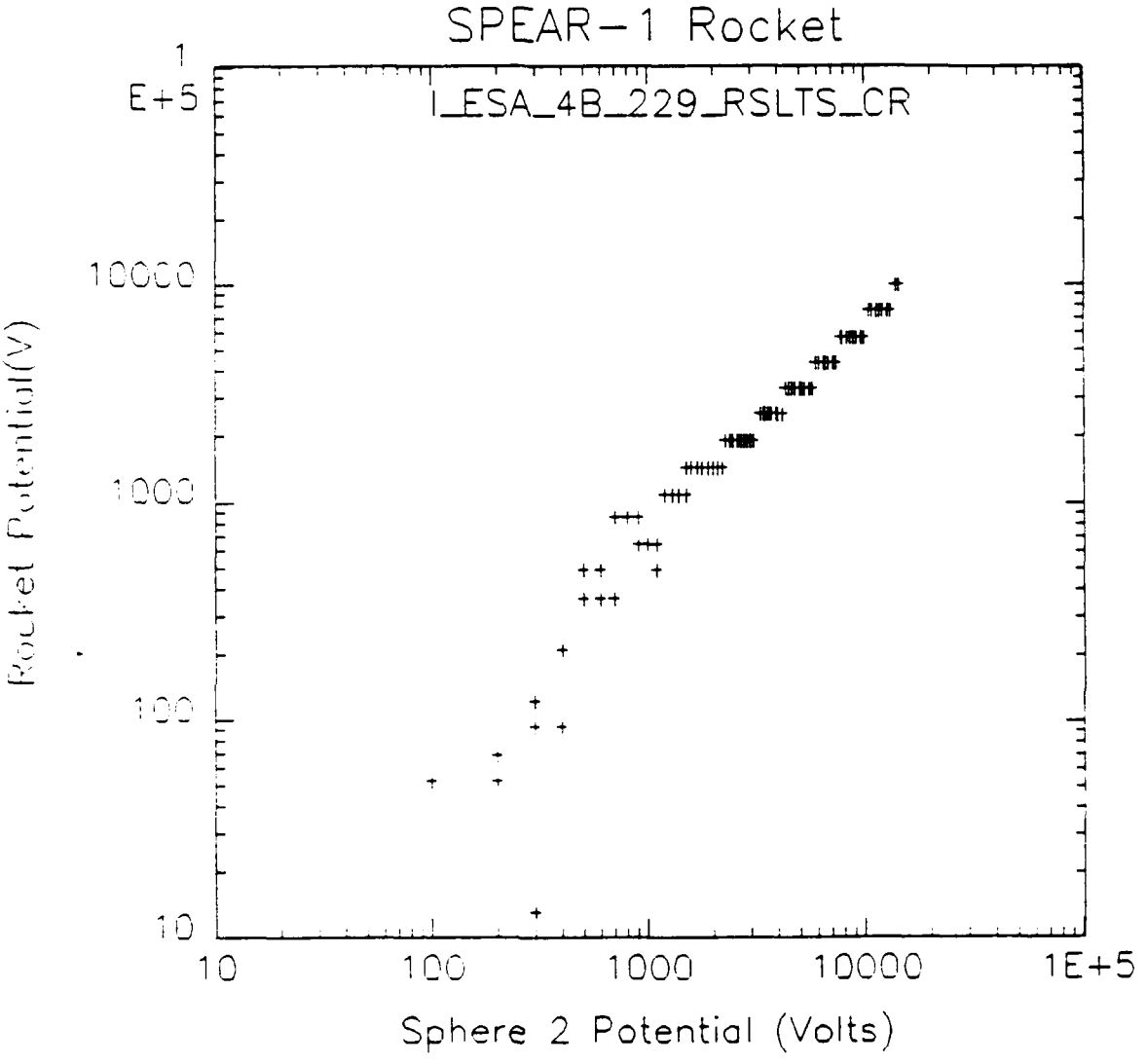
SPEAR-1 Rocket
I_ESA_4B_229_RSLTS_CR
Rocket Potential(V)
1
E+5
10000
1000
100
10
10
100
1000
10000
1E+5
Sphere 2 Potential (Volts)

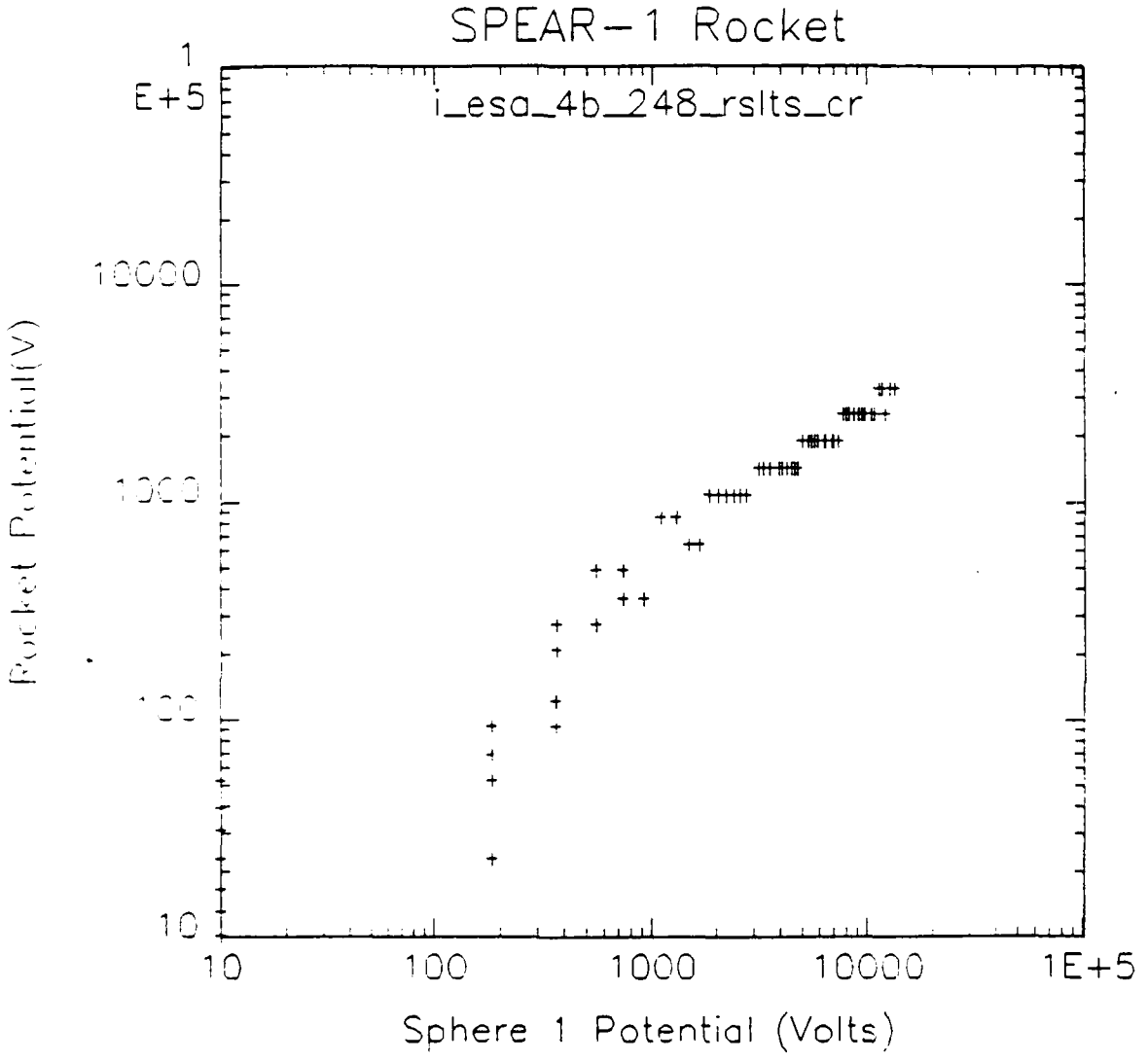
SPEAR-1 Rocket
i_esa_4b_248_rslts_cr
1
E+5
10000
1000
100
10
Rocket Potential(V)
10
100
1000
10000
1E+5
Sphere 1 Potential (Volts)

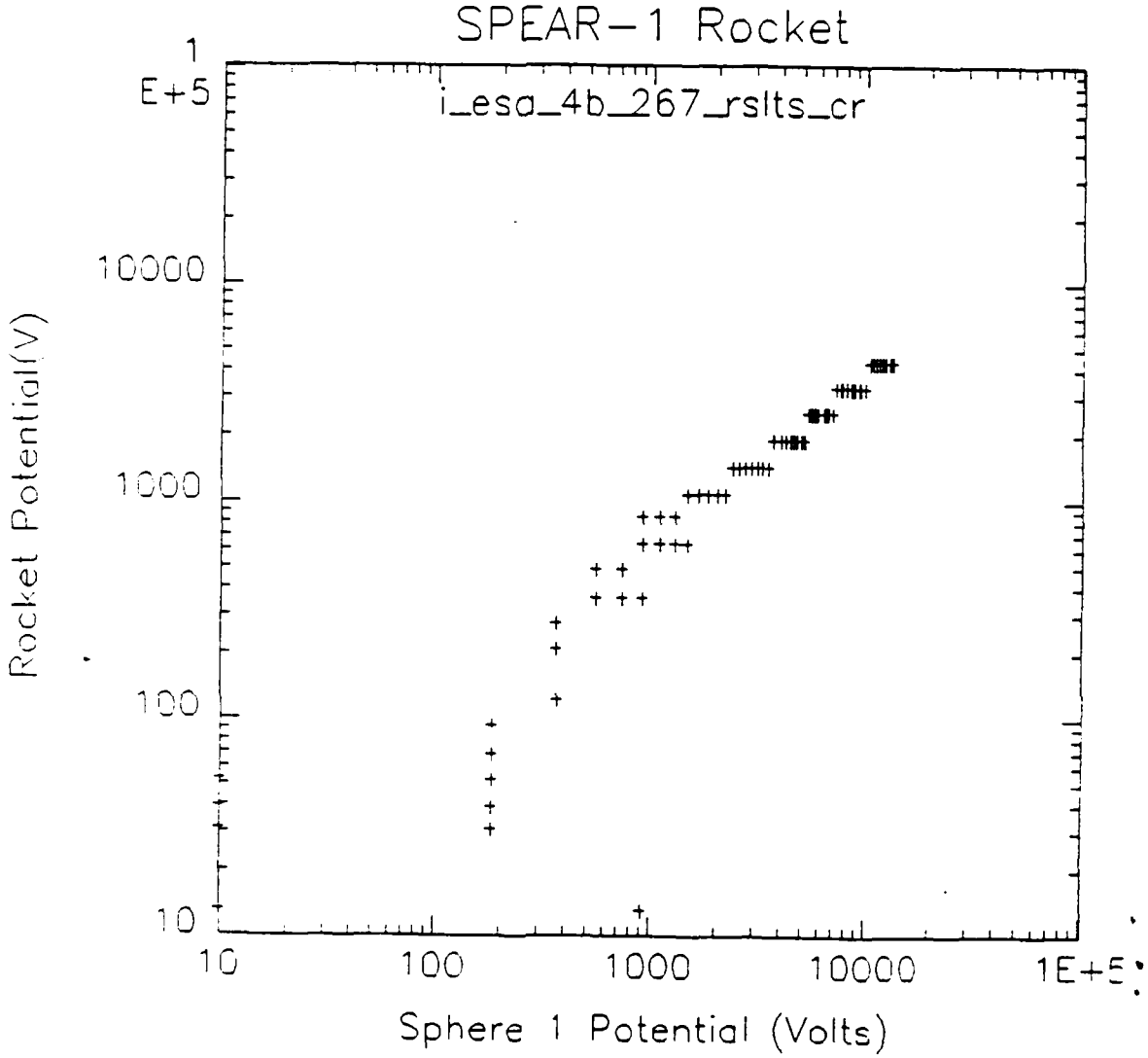
SPEAR-1 Rocket
i_esa_4b_267_rslts_cr
Rocket Potential(V)
1
E+5
10000
1000
100
10
10
100
1000
10000
1E+5
Sphere 1 Potential (Volts)

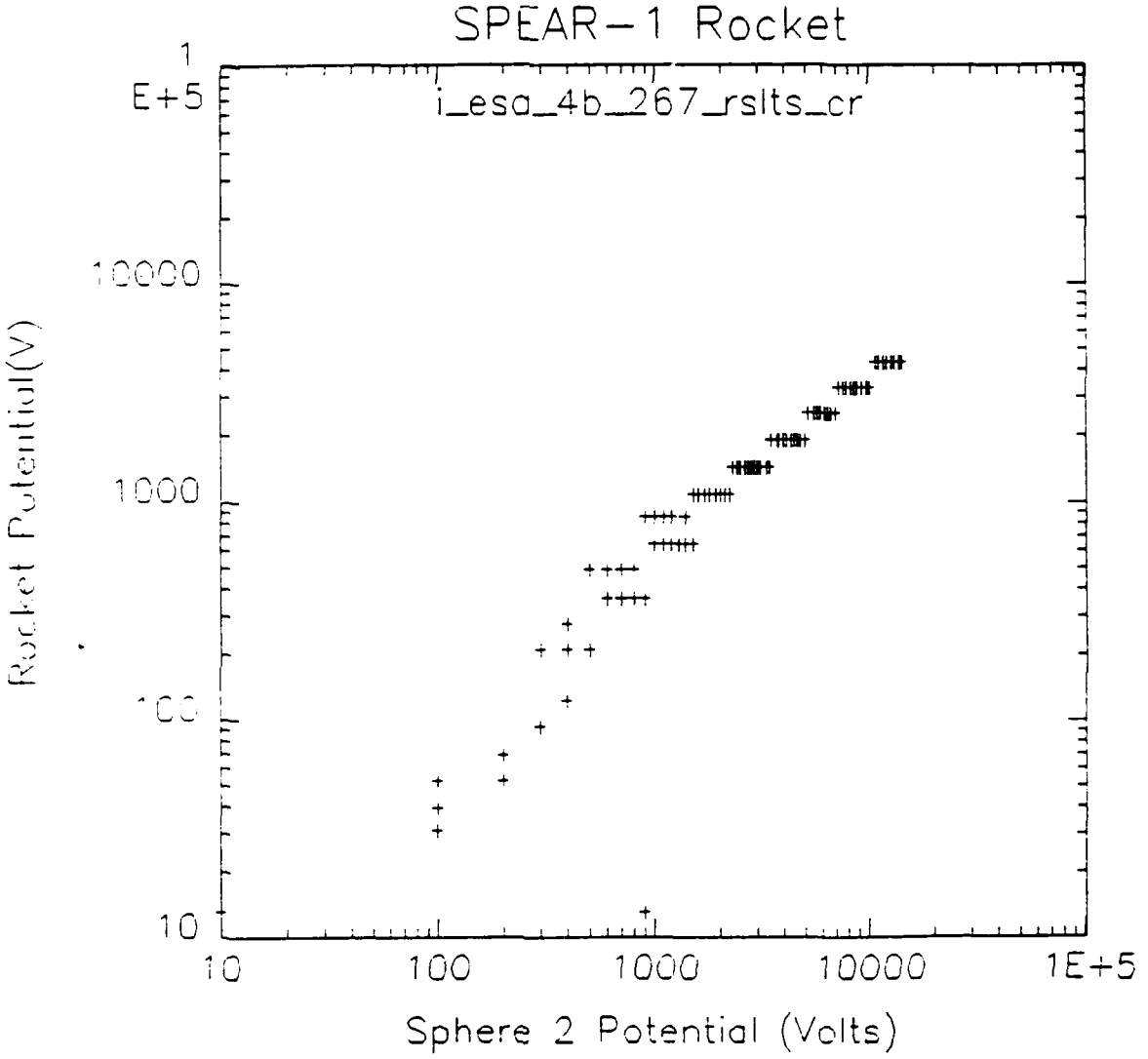
SPEAR-1 Rocket
i_esa_4b_267_rslts_cr
1
E+5
10000
1000
100
10
Rocket Potential(V)
10
100
1000
10000
1E+5
Sphere 2 Potential (Volts)

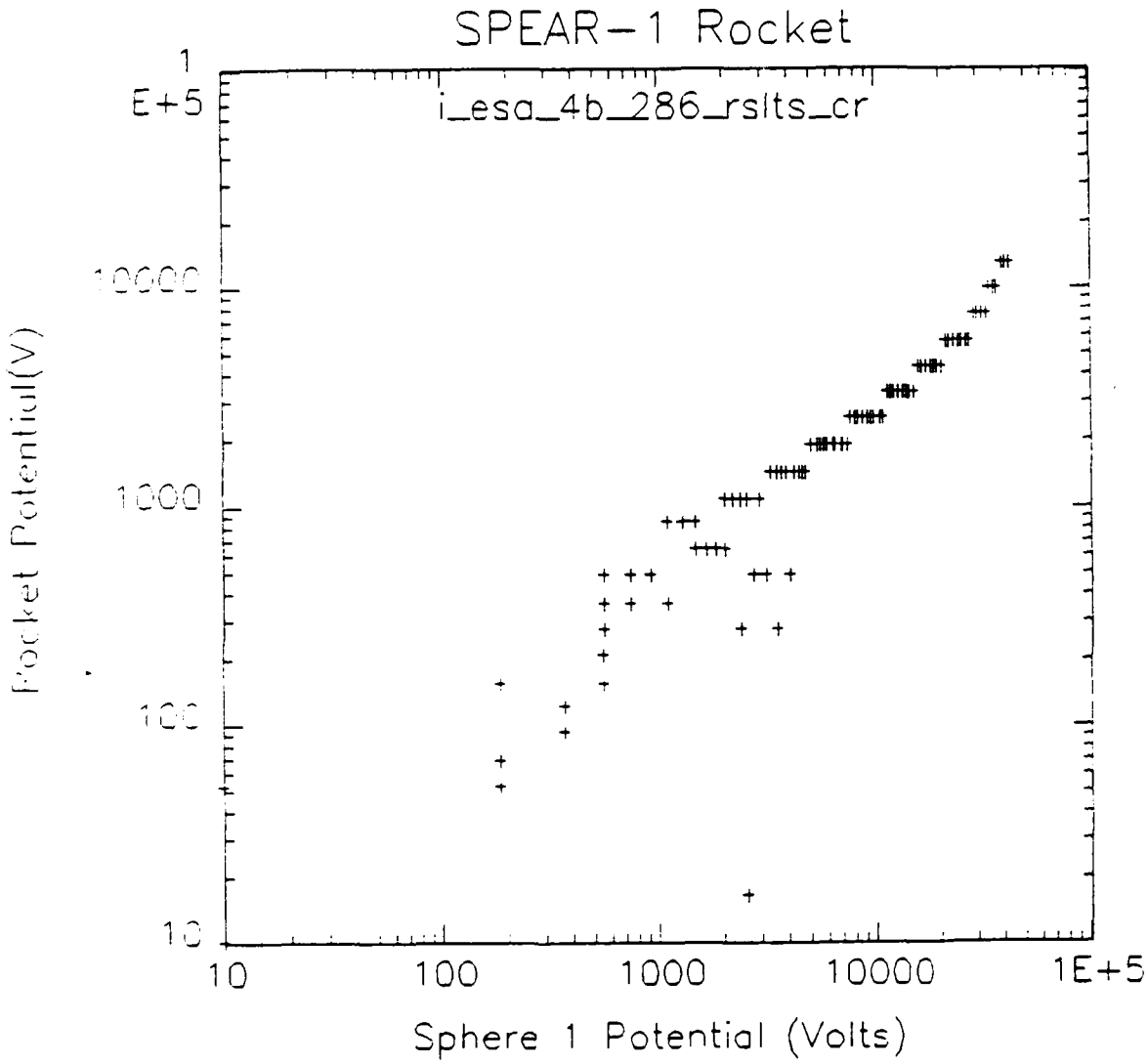
SPEAR-1 Rocket
i_esa_4b_286_rslts_cr
Rocket Potential(V)
1
E+5
10000
1000
100
10
10
100
1000
10000
1E+5
Sphere 1 Potential (Volts)

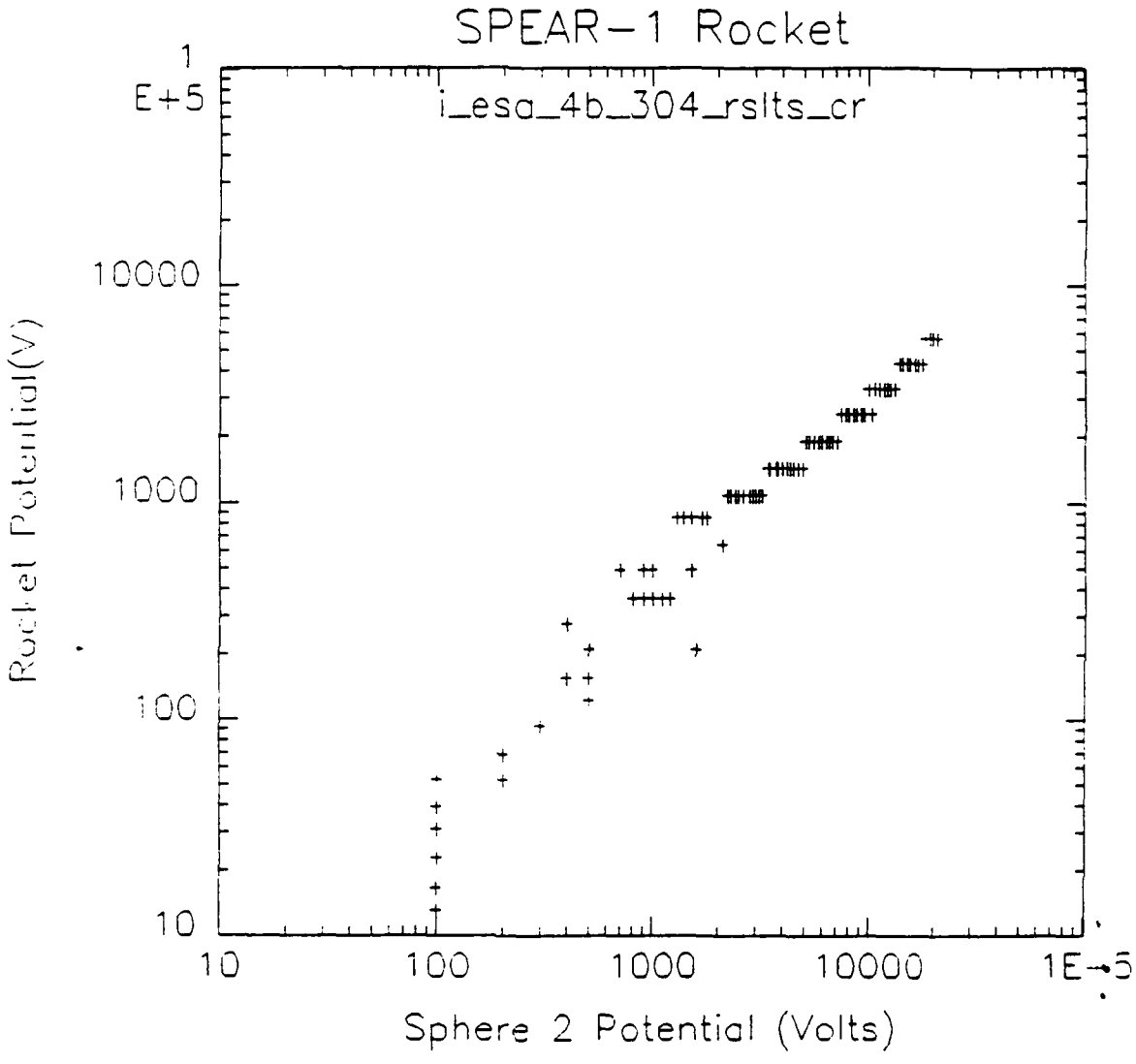
SPEAR-1 Rocket
i_esa_4b_304_rslts_cr
Rocket Potential(V)
1
E+5
10000
1000
100
10
10
100
1000
10000
1E+5
Sphere 2 Potential (Volts)

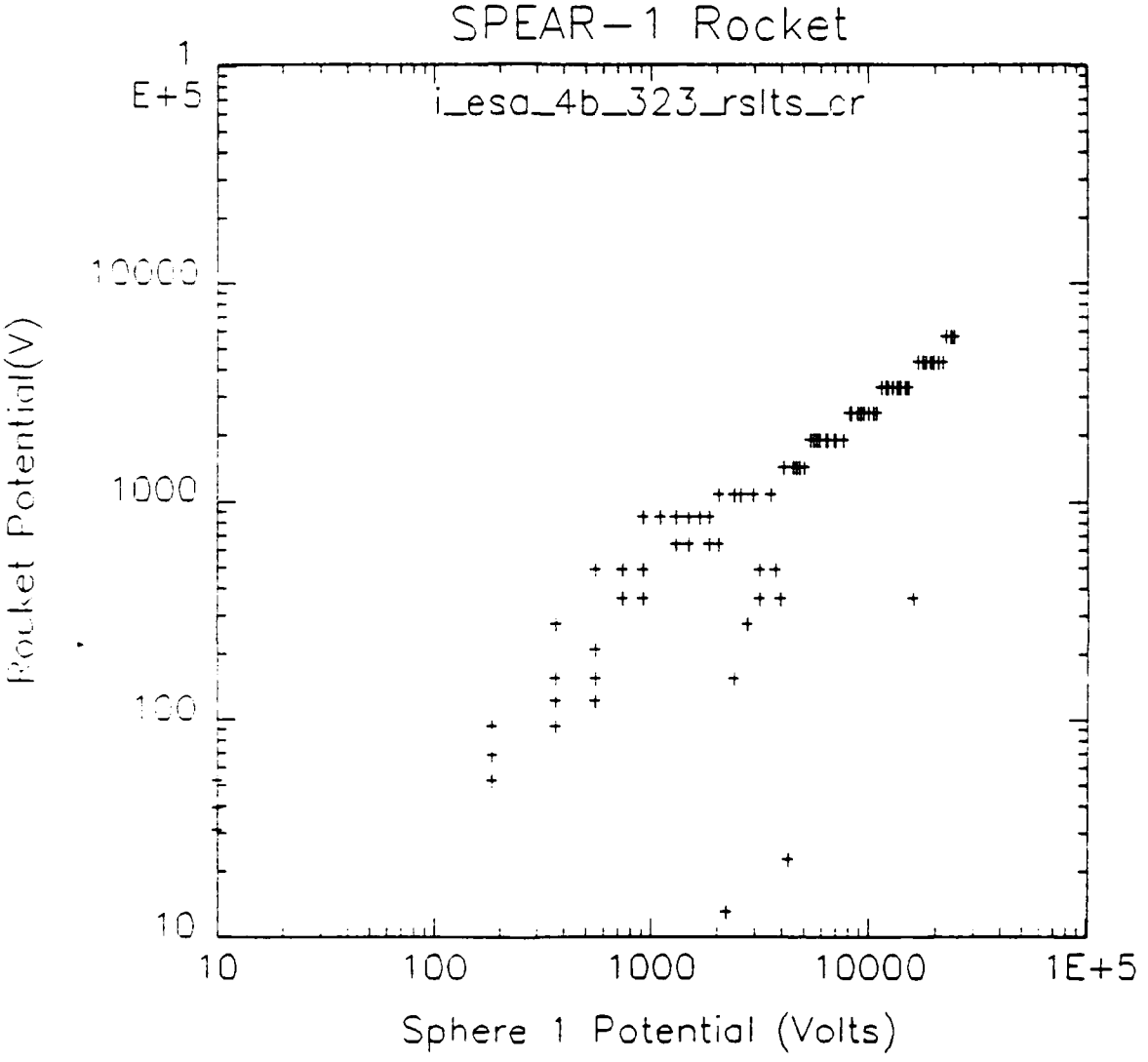
SPEAR–1 Rocket
i_esa_4b_323_rslts_cr
Rocket Potential(V)
1
E+5
10000
1000
100
10
10
100
1000
10000
1E+5
Sphere 1 Potential (Volts)

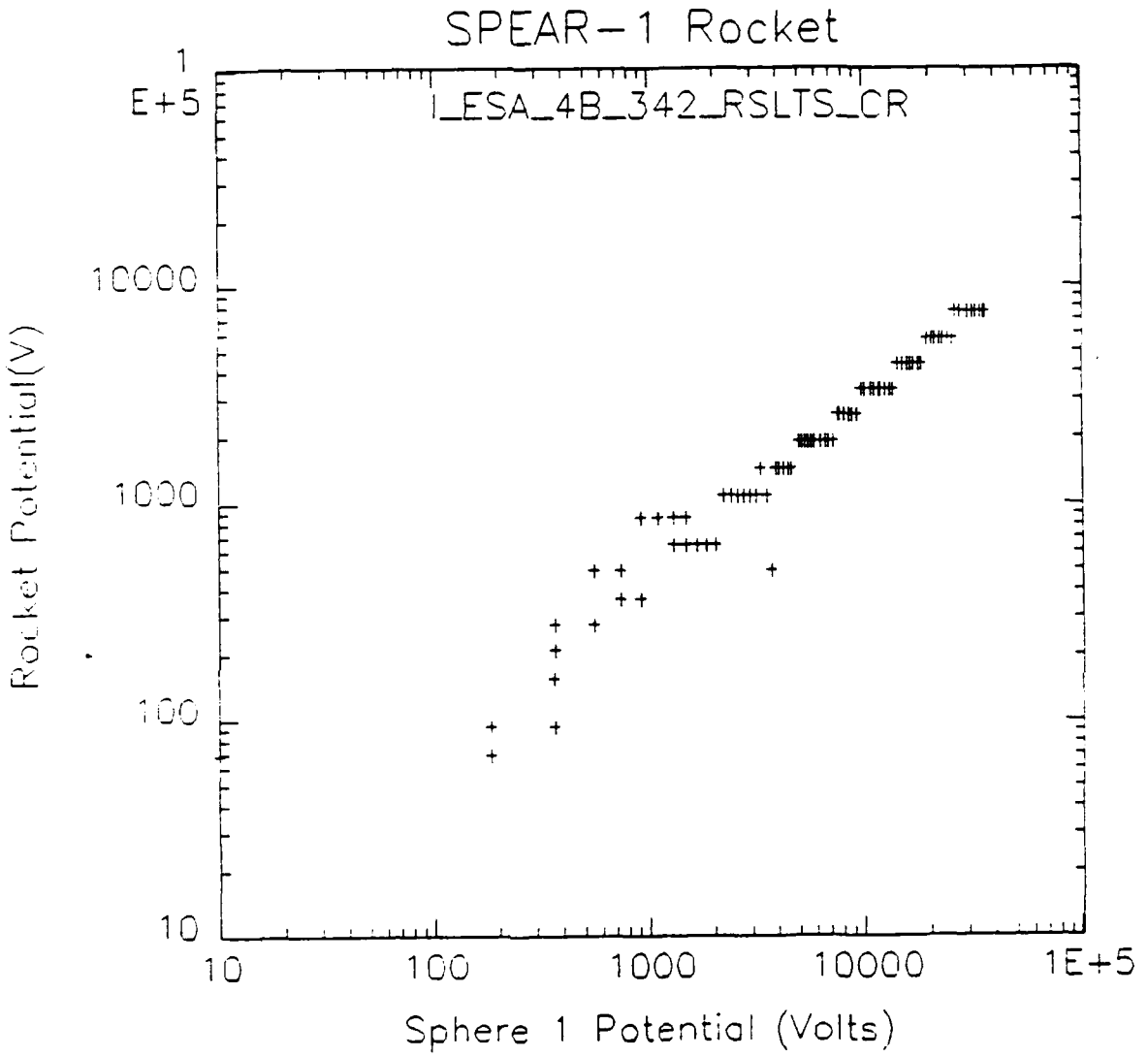
SPEAR-1 Rocket
I_ESA_4B_342_RSLTS_CR
Rocket Potential(V)
1
E+5
10000
1000
100
10
10
100
1000
10000
1E+5
Sphere 1 Potential (Volts)

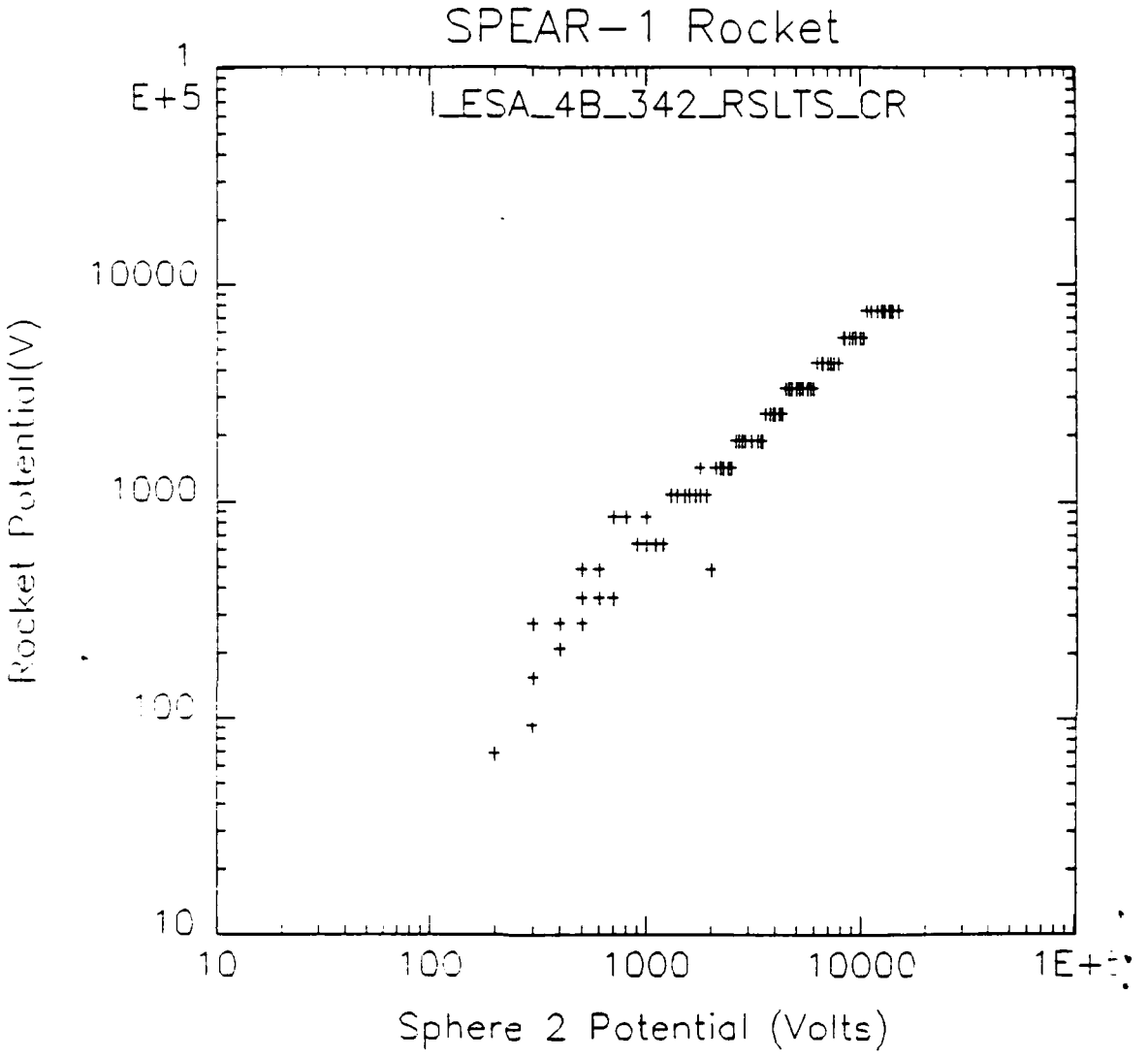
SPEAR-1 Rocket
I_ESA_4B_342_RSLTS_CR
Rocket Potential(V)
1
E+5
10000
1000
100
10
10
100
1000
10000
Sphere 2 Potential (Volts)

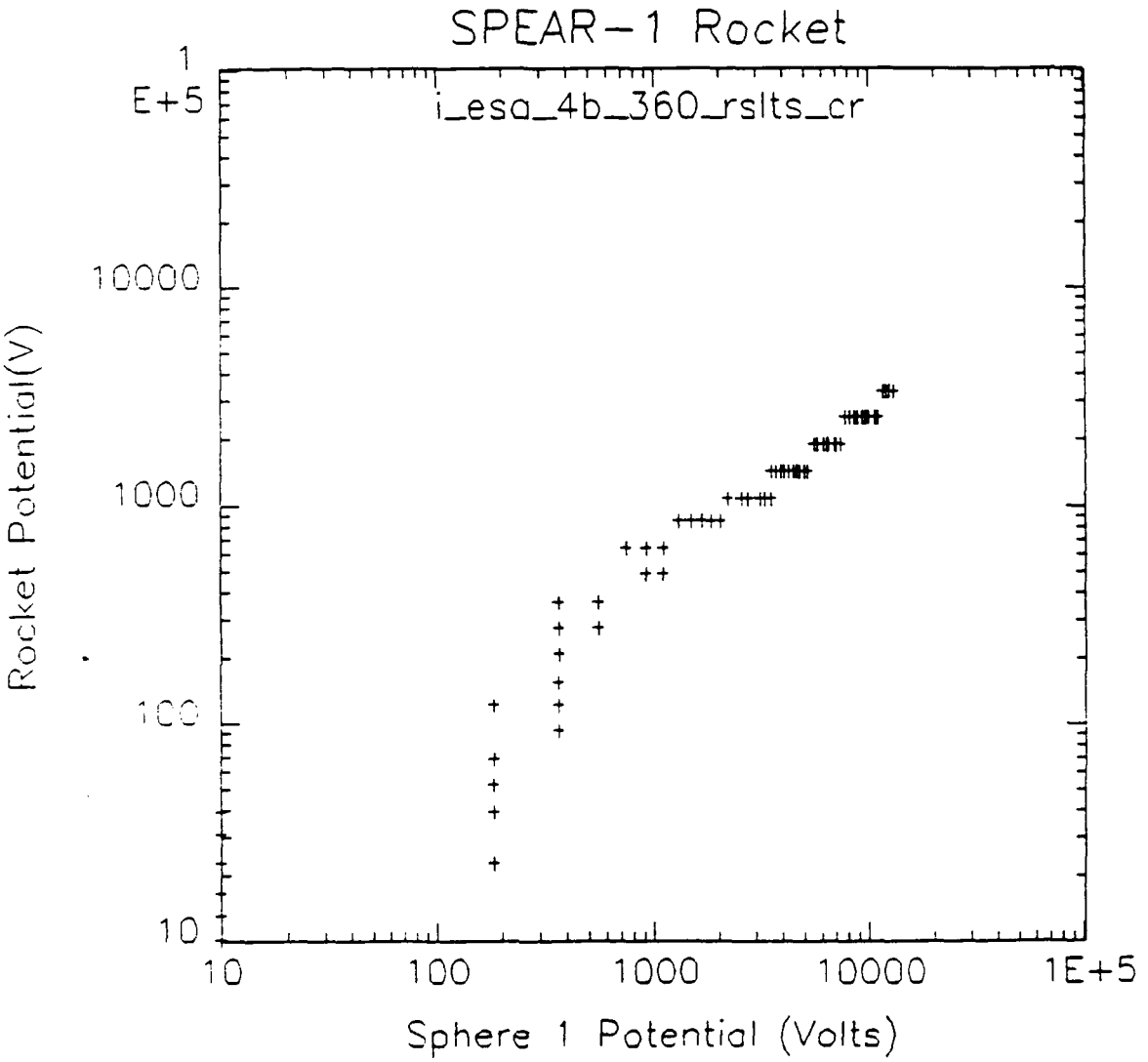
SPEAR-1 Rocket
i_esa_4b_360_rslts_cr
Rocket Potential(V)
1
E+5
10000
1000
100
10
10
100
1000
10000
1E+5
Sphere 1 Potential (Volts)

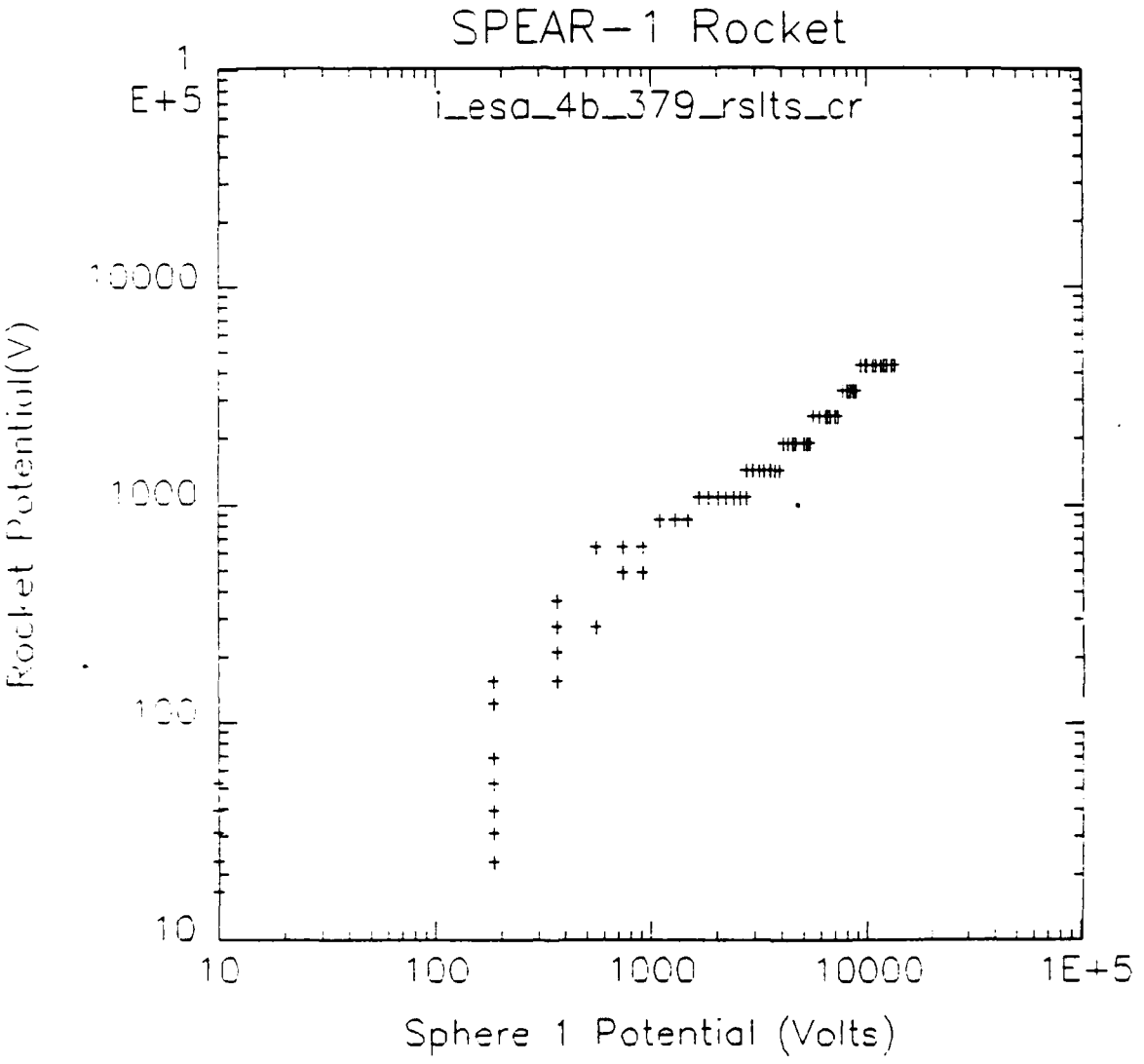
SPEAR-1 Rocket
i_esa_4b_379_rslts_cr
Rocket Potential(V)
1
E+5
10000
1000
100
10
10
100
1000
10000
1E+5
Sphere 1 Potential (Volts)

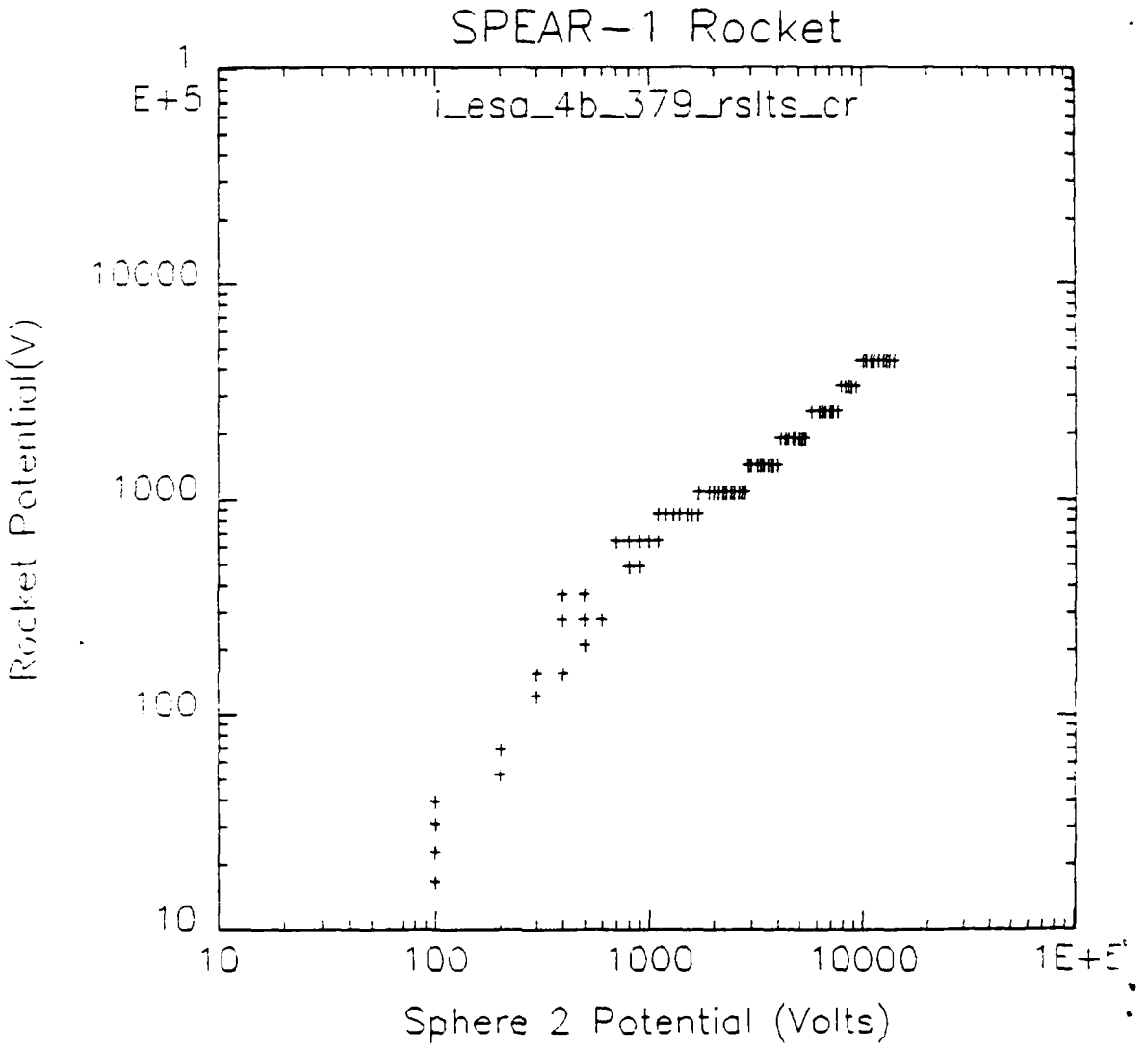
SPEAR-1 Rocket
i_esa_4b_379_rslts_cr
Rocket Potential(V)
1
E+5
10000
1000
100
10
10
100
1000
10000
1E+5
Sphere 2 Potential (Volts)

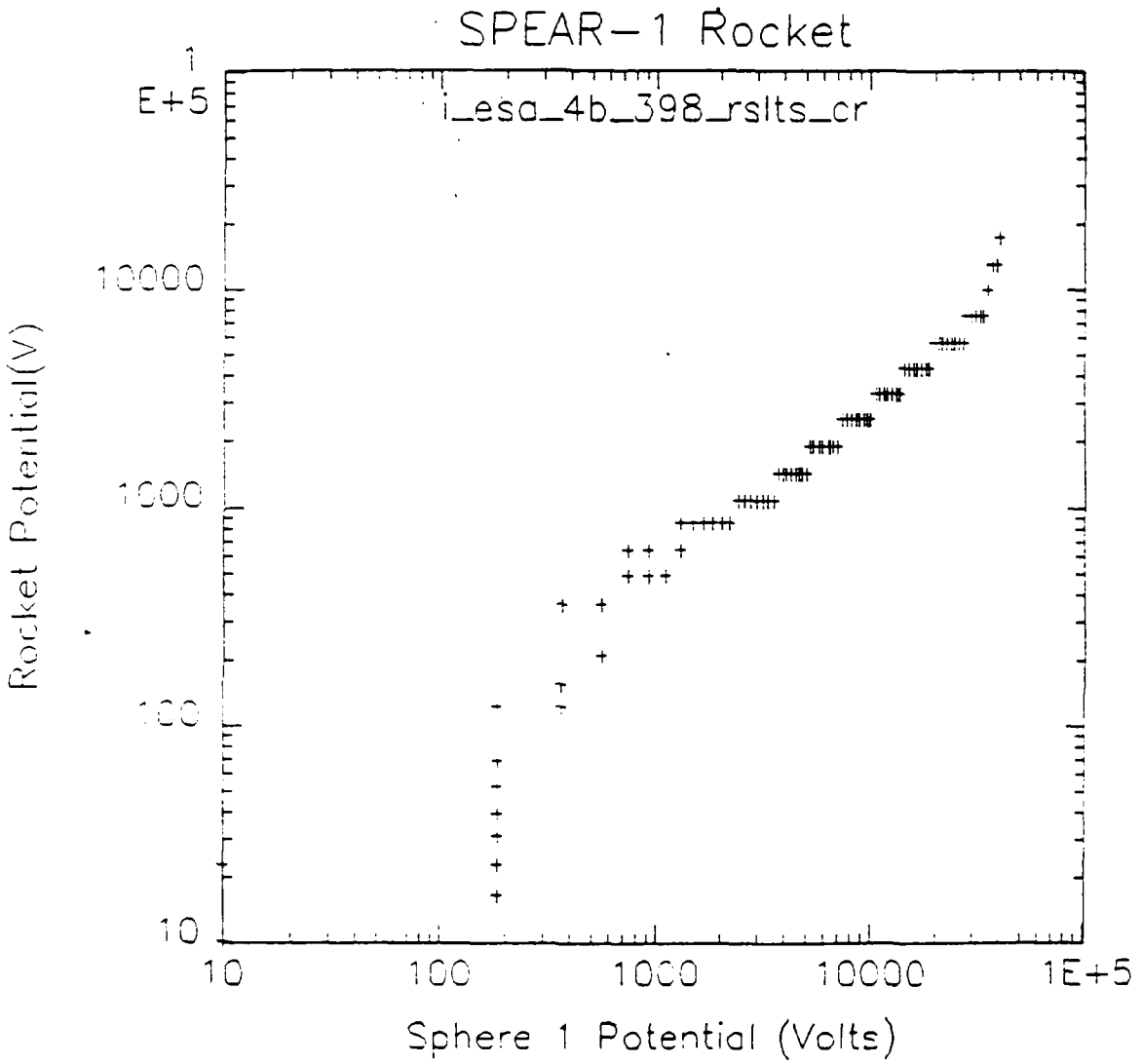
SPEAR–1 Rocket
i_esa_4b_398_rslts_cr
Rocket Potential(V)
1E+5
10000
1000
100
10
10
100
1000
10000
1E+5
Sphere 1 Potential (Volts)

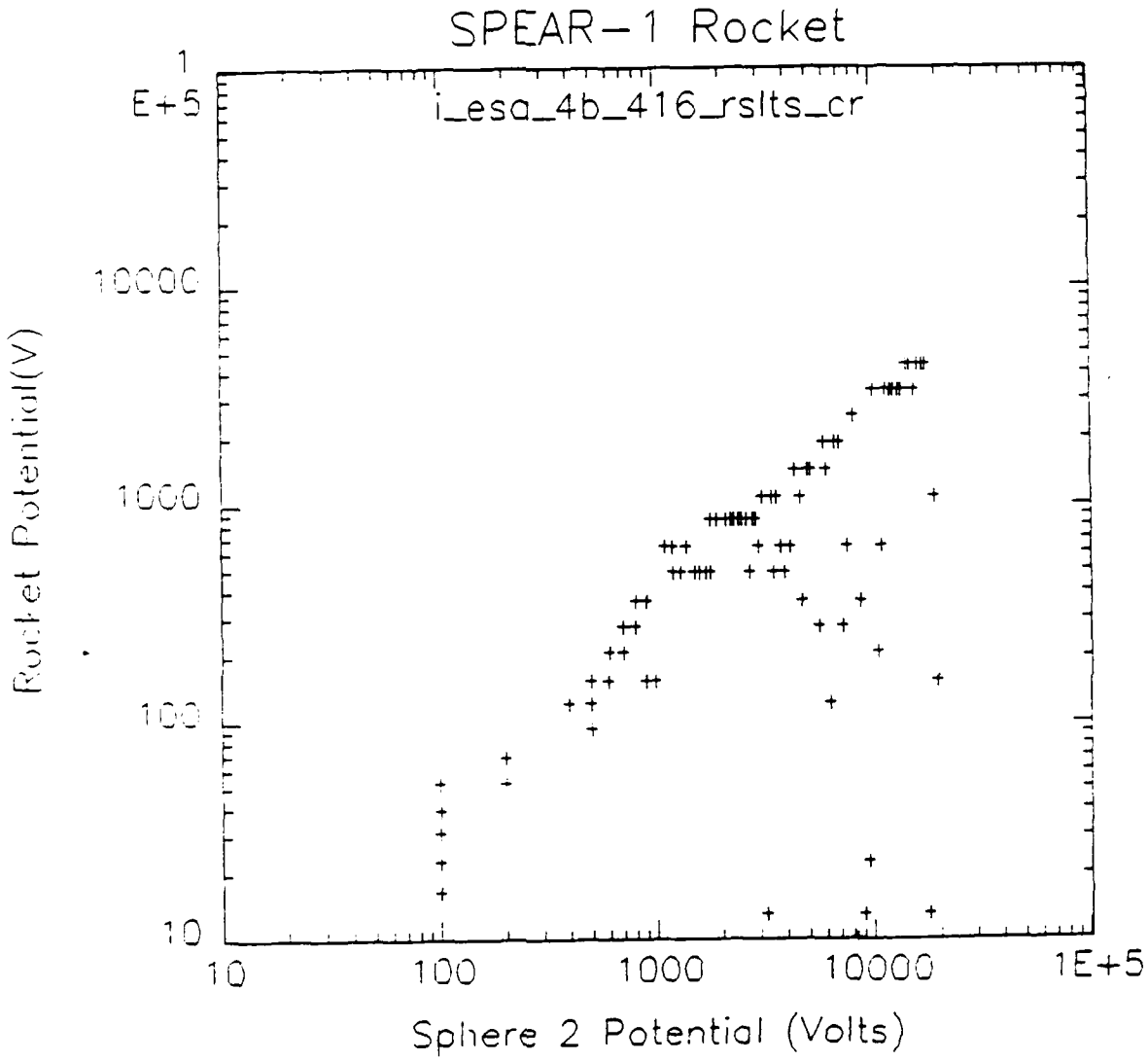
SPEAR-1 Rocket
i_esa_4b_416_rslts_cr
Rocket Potential(V)
1
E+5
10000
1000
100
10
10
100
1000
10000
1E+5
Sphere 2 Potential (Volts)

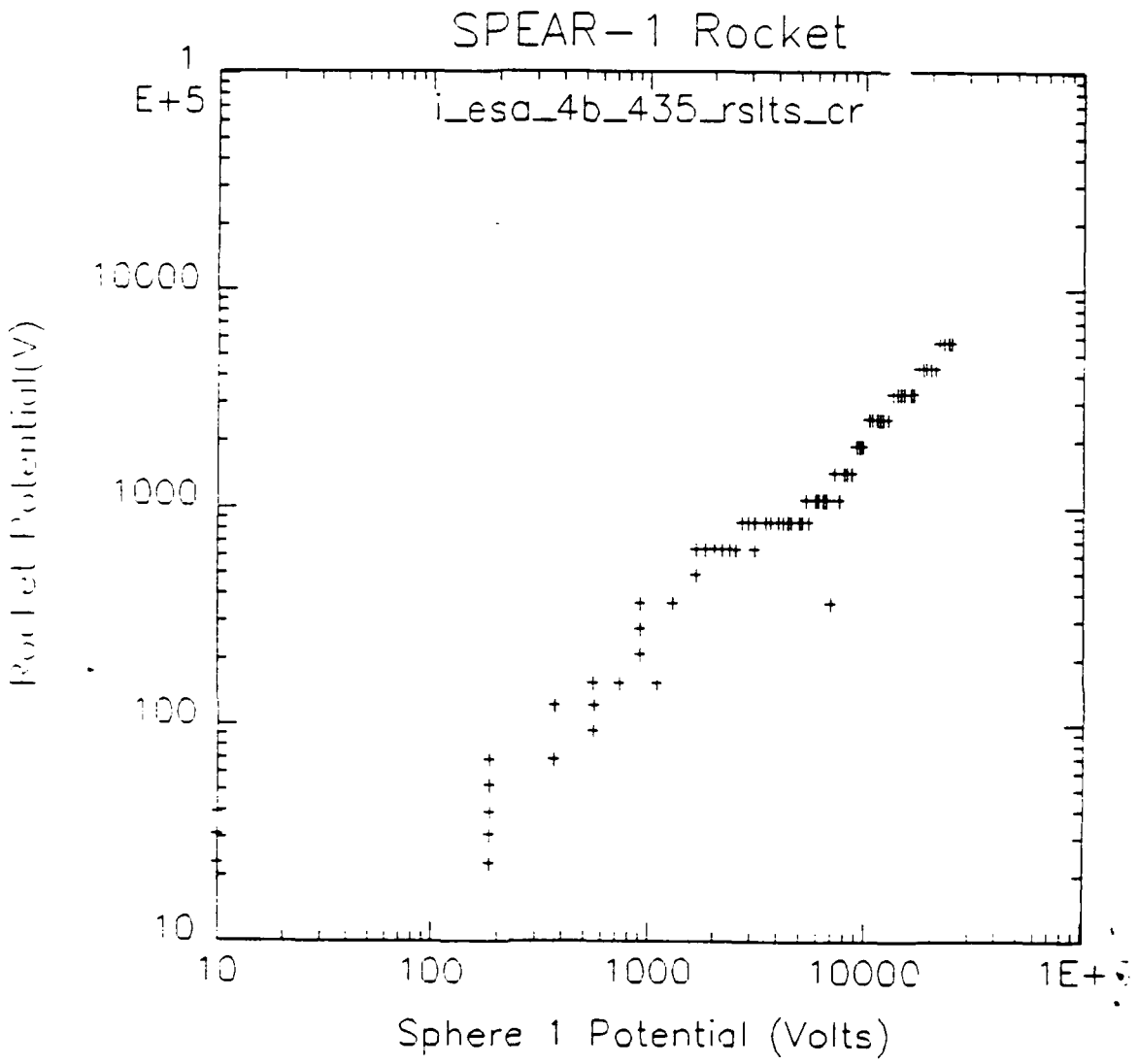
SPEAR-1 Rocket
i_esa_4b_435_rslts_cr
Rocket Potential(V)
1
E+5
10000
1000
100
10
10
100
1000
10000
1E+5
Sphere 1 Potential (Volts)

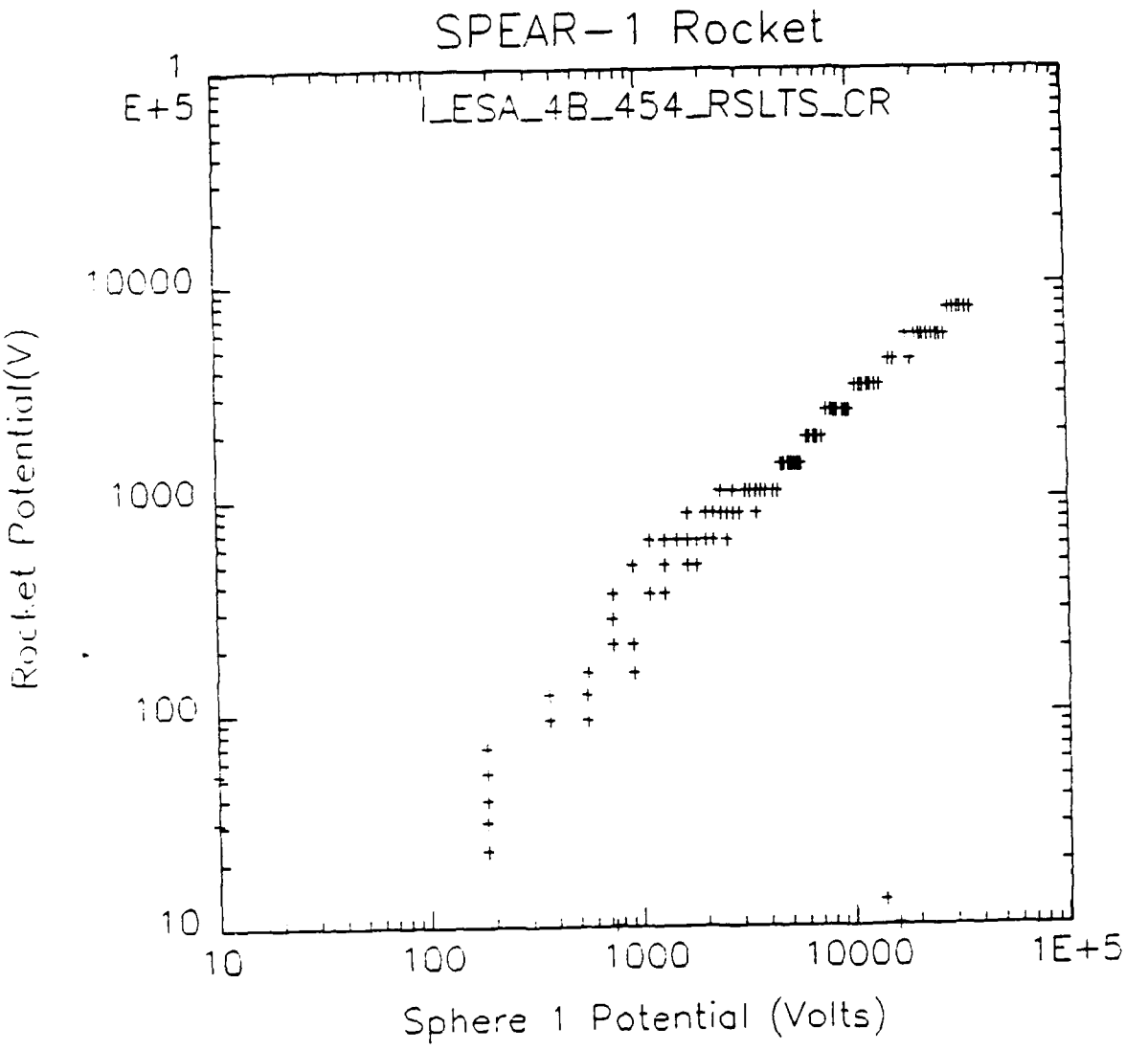
SPEAR-1 Rocket
I_ESA_4B_454_RSLTS_CR
Rocket Potential(V)
1E+5
10000
1000
100
10
10
100
1000
10000
1E+5
Sphere 1 Potential (Volts)

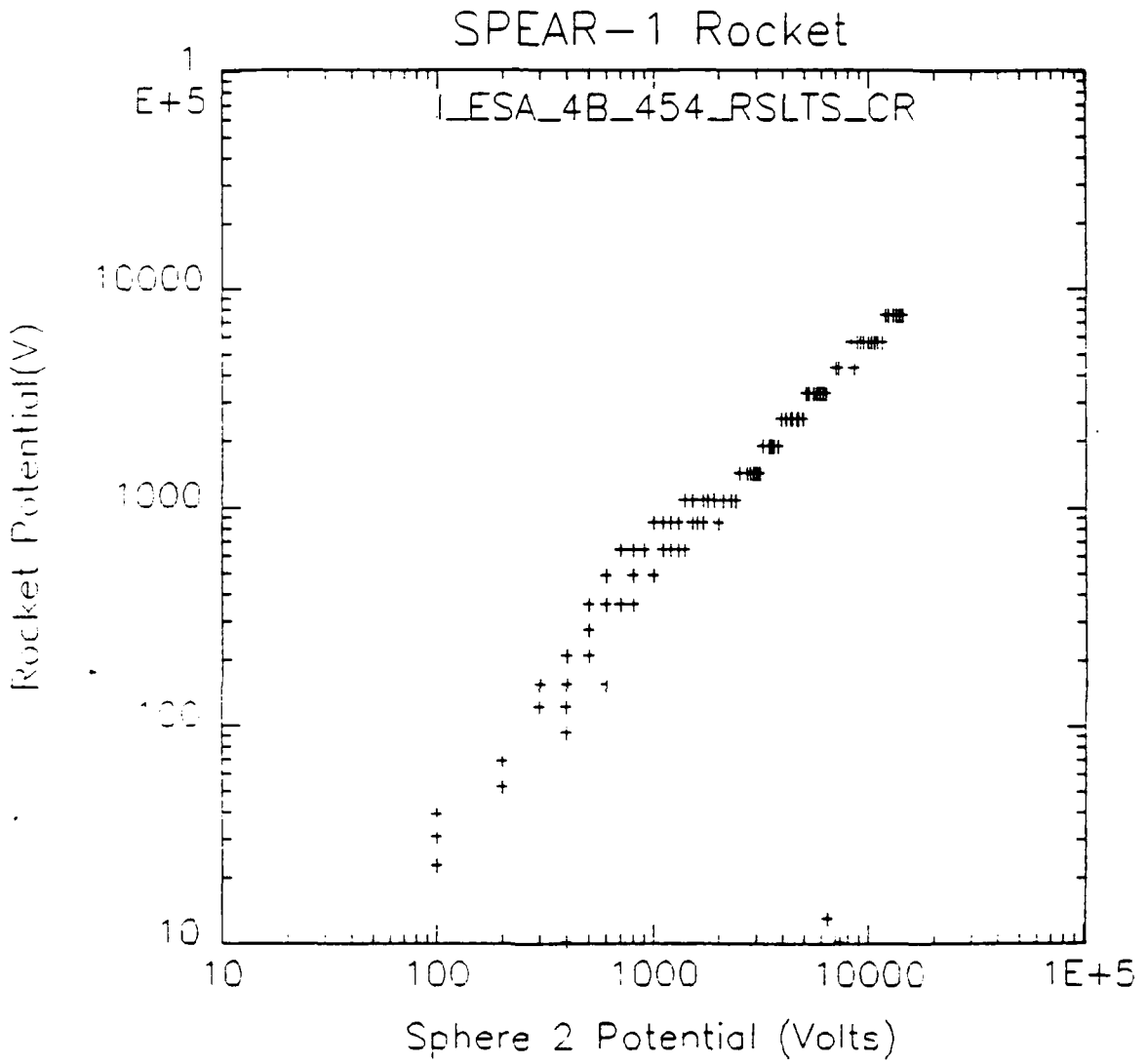
SPEAR–1 Rocket
I_ESA_4B_454_RSLTS_CR
Rocket Potential(V)
1
E+5
10000
1000
100
10
10
100
1000
10000
1E+5
Sphere 2 Potential (Volts)

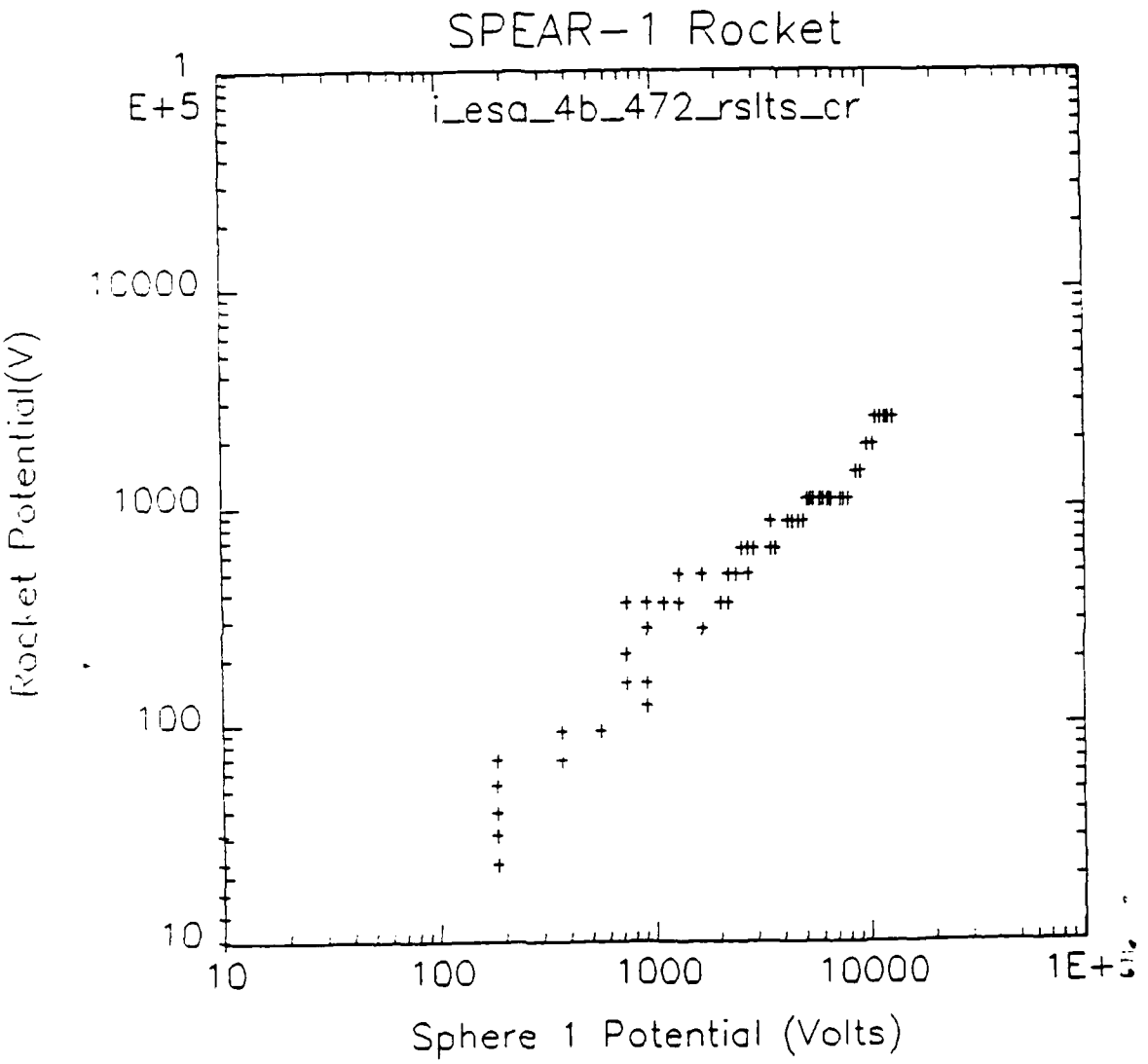
SPEAR–1 Rocket
i_esa_4b_472_rslts_cr
Rocket Potential(V)
1
E+5
10000
1000
100
10
10
100
1000
10000
Sphere 1 Potential (Volts)

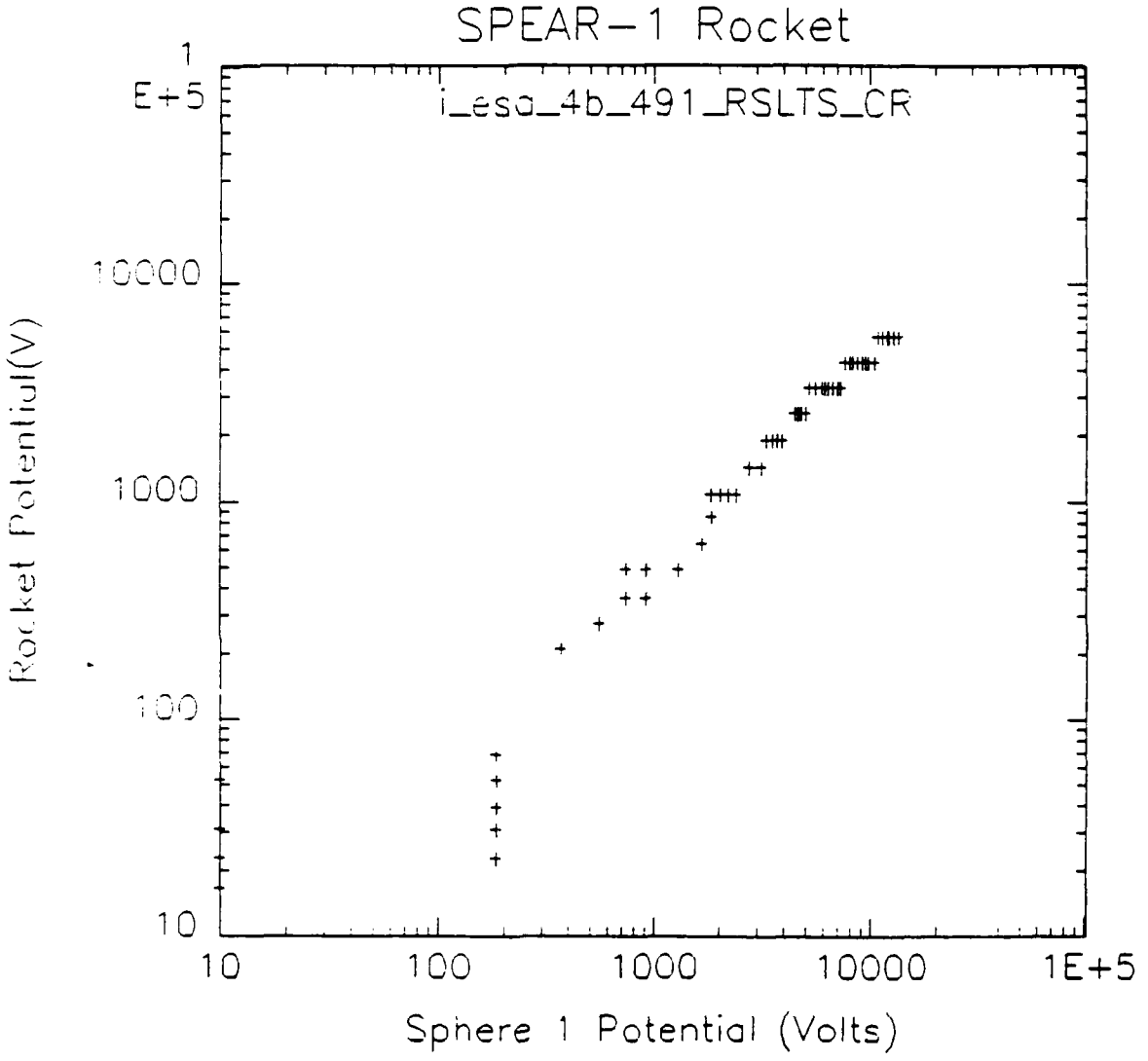
SPEAR-1 Rocket
i_esa_4b_491_RSLTS_CR
Rocket Potential(V)
1E+5
10000
1000
100
10
10
100
1000
10000
1E+5
Sphere 1 Potential (Volts)

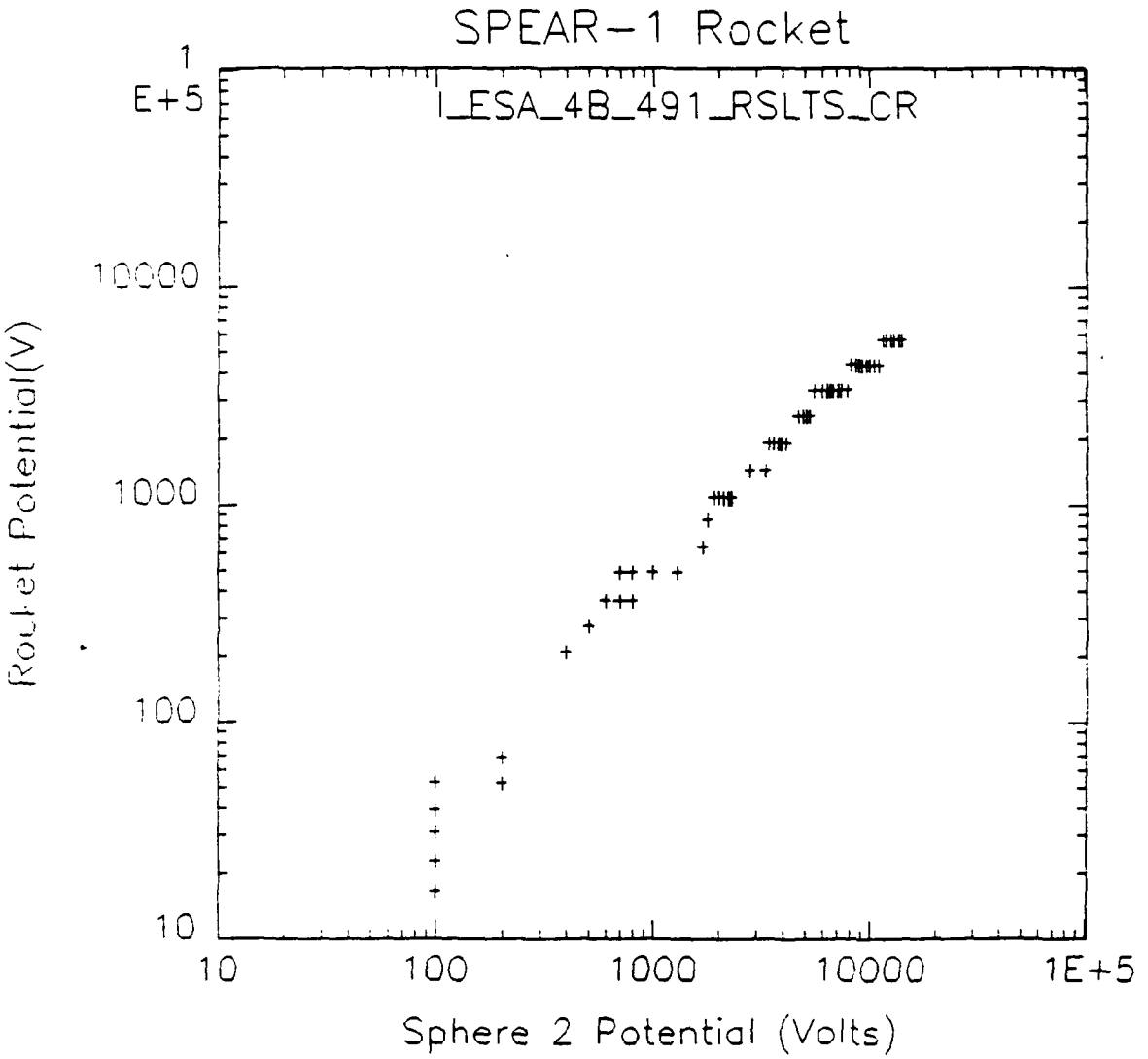
SPEAR-1 Rocket
I_ESA_4B_491_RSLTS_CR
1
E+5
10000
1000
100
10
Rocket Potential(V)
10
100
1000
10000
1E+5
Sphere 2 Potential (Volts)

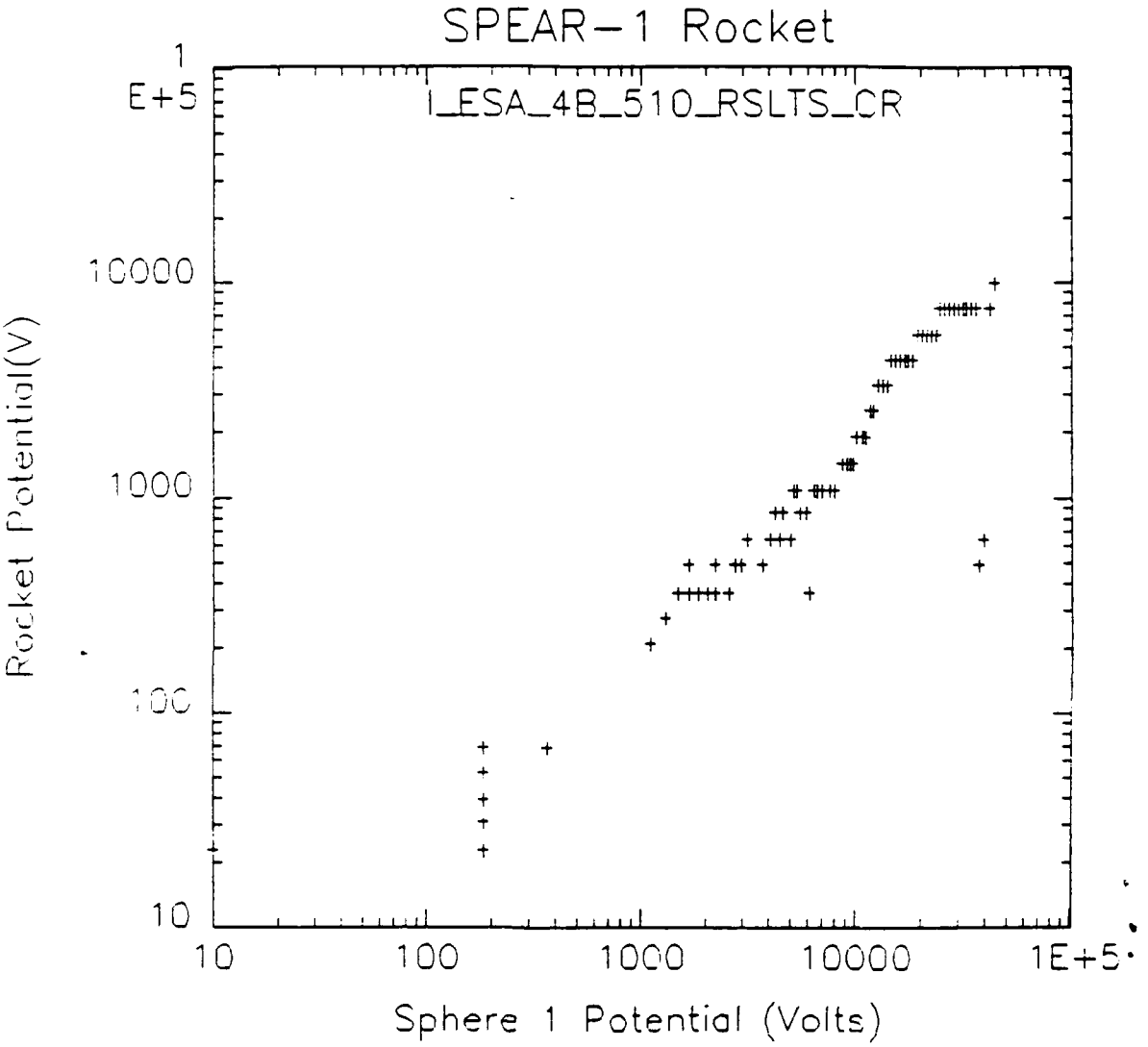
SPEAR-1 Rocket
I_ESA_4B_510_RSLTS_CR
Rocket Potential(V)
1
E+5
10000
1000
100
10
10
100
1000
10000
1E+5
Sphere 1 Potential (Volts)

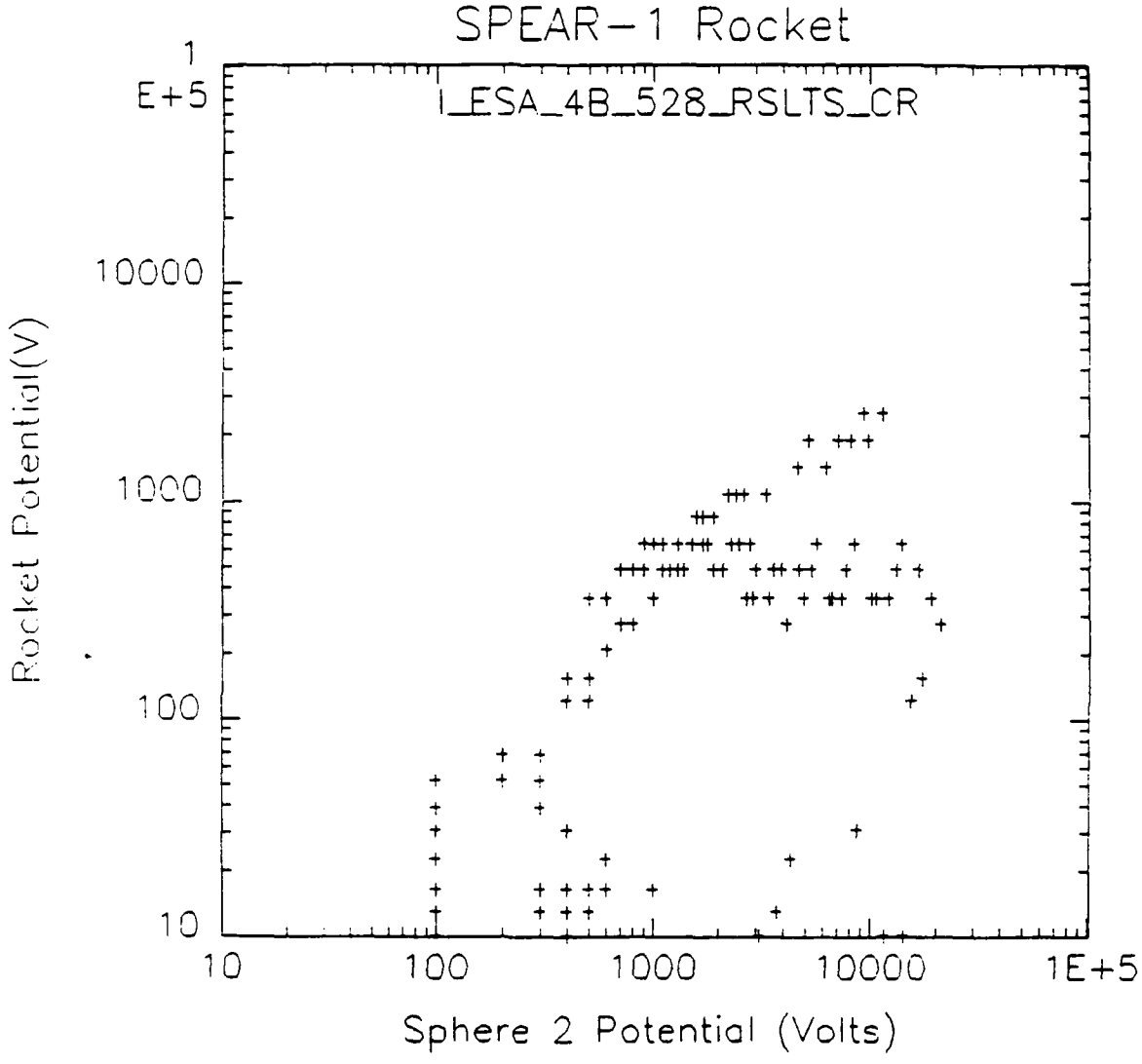
SPEAR-1 Rocket
I_ESA_4B_528_RSLTS_CR
Rocket Potential(V)
1
E+5
10000
1000
100
10
10
100
1000
10000
1E+5
Sphere 2 Potential (Volts)

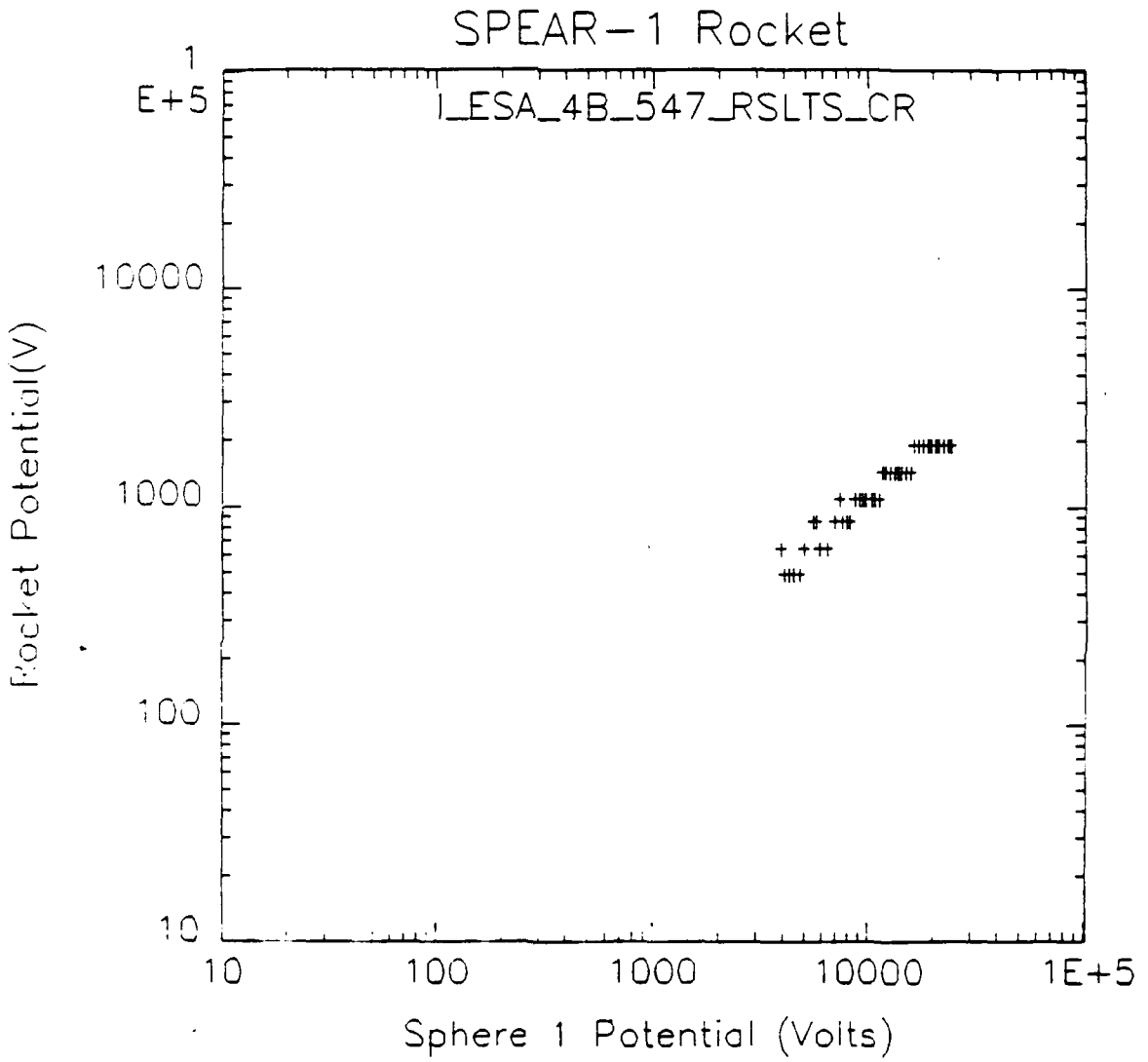
SPEAR–1 Rocket
I_ESA_4B_547_RSLTS_CR
Rocket Potential(V)
1
E+5
10000
1000
100
10
10
100
1000
10000
1E+5
Sphere 1 Potential (Volts)

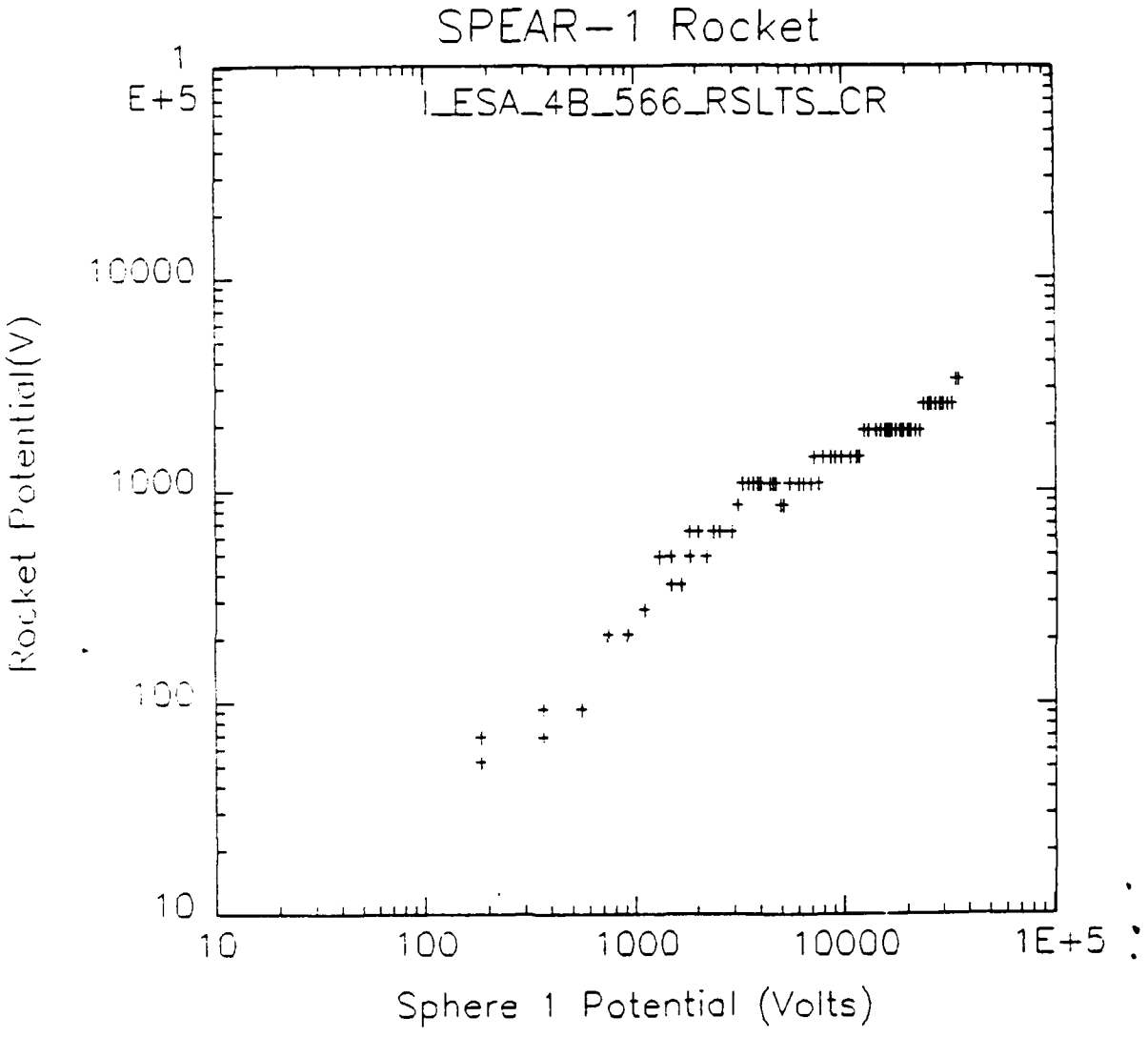
SPEAR-1 Rocket
I_ESA_4B_566_RSLTS_CR
Rocket Potential(V)
1E+5
10000
1000
100
10
10
100
1000
10000
1E+5
Sphere 1 Potential (Volts)

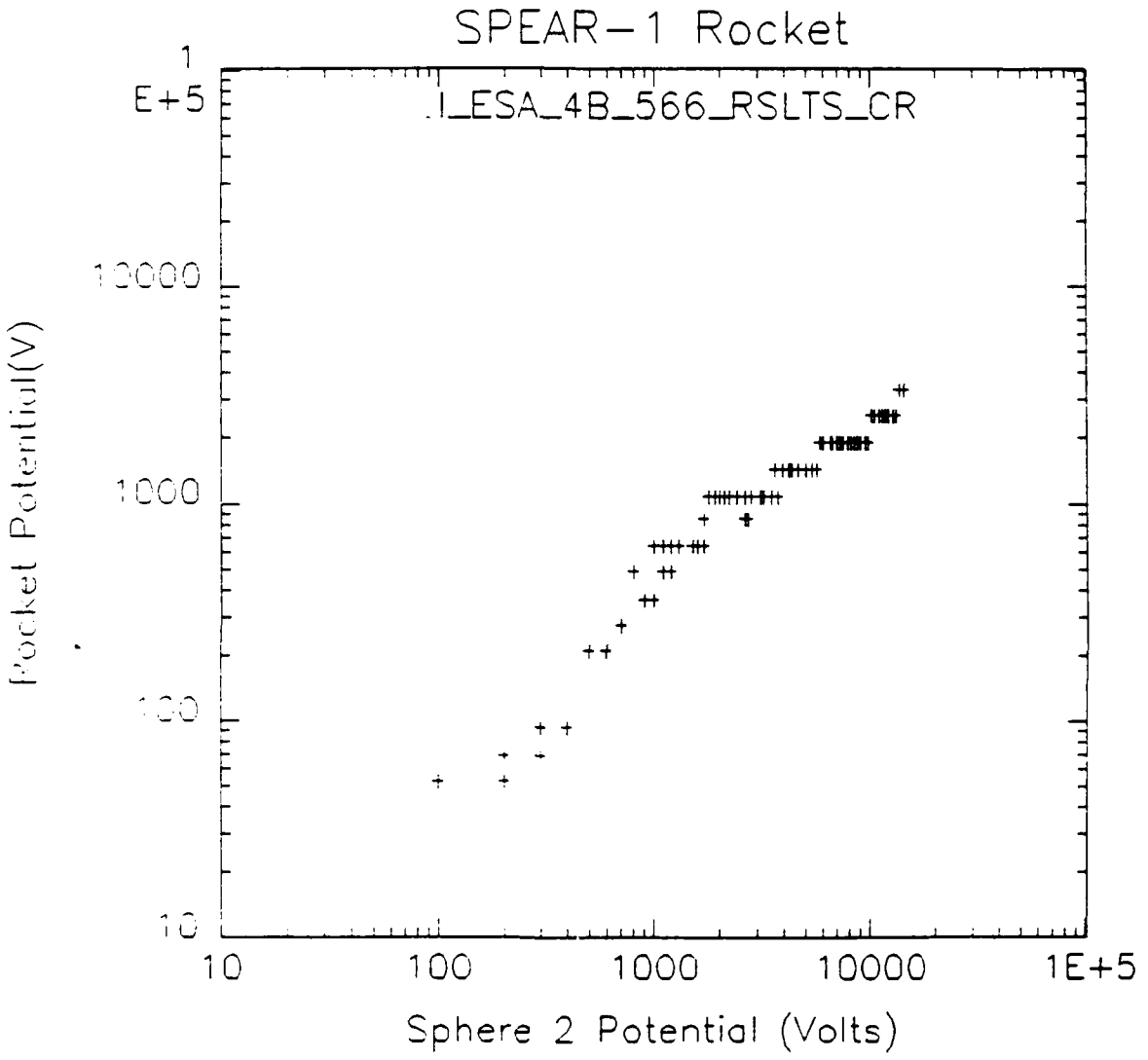
SPEAR-1 Rocket
I_ESA_4B_566_RSLTS_CR
Rocket Potential(V)
1
E+5
10000
1000
100
10
10
100
1000
10000
1E+5
Sphere 2 Potential (Volts)

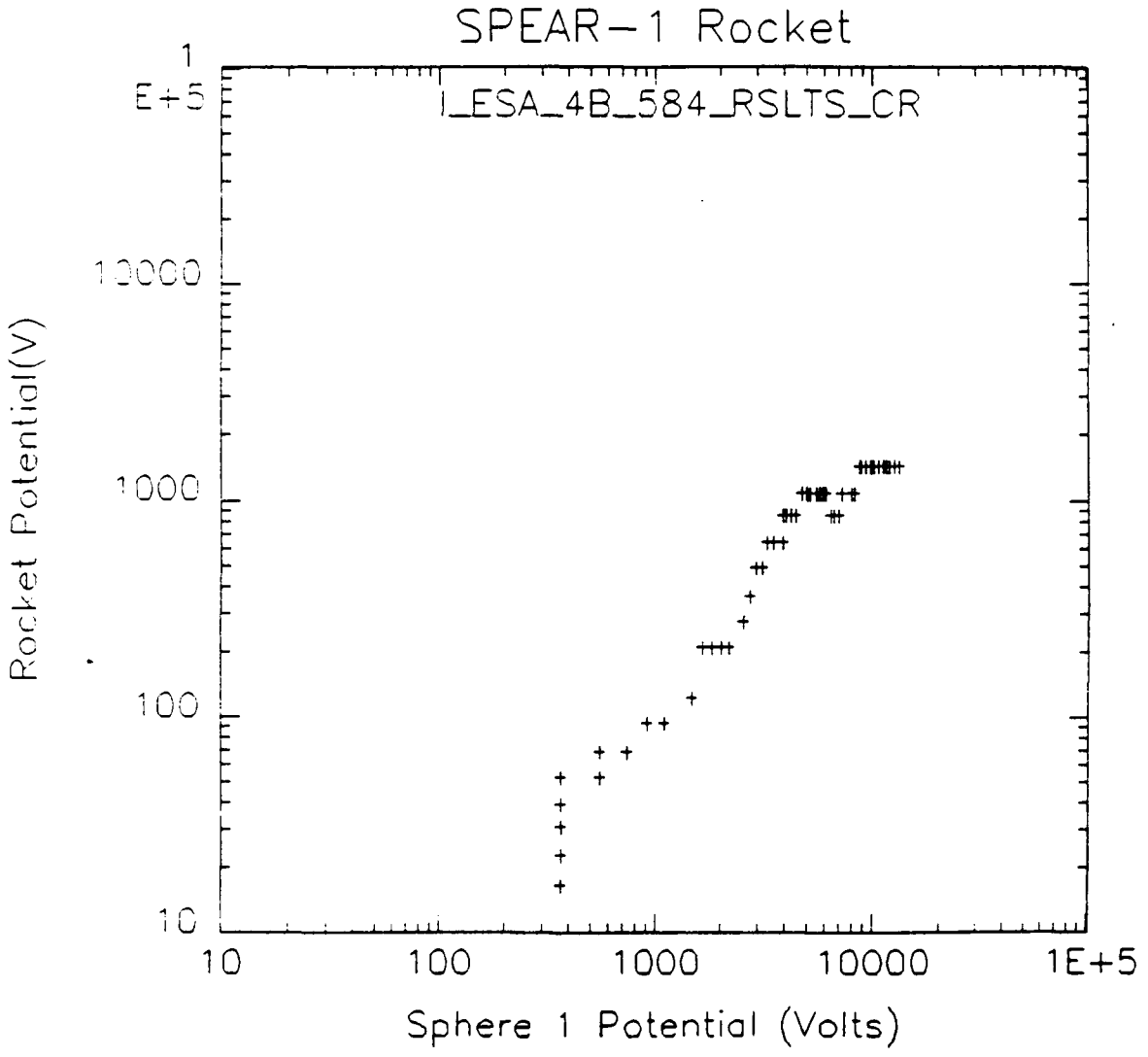
SPEAR–1 Rocket
I_ESA_4B_584_RSLTS_CR
Rocket Potential(V)
1
E+5
10000
1000
100
10
10
100
1000
10000
1E+5
Sphere 1 Potential (Volts)

APPENDIX E

CHARGING PEAK CHARACTERISTICS

The ambient ion distribution function (f) in the ionosphere is nominally a 0.1 eV 0^+ Maxwellian. This is illustrated in Figure E-1.

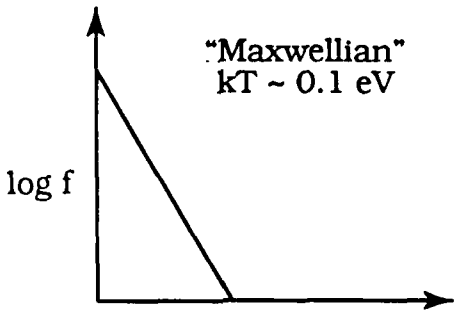

Figure E-1. **Ambient Distribution**

When the plasma is accelerated through a potential difference, the distribution function which should be observed at the rocket is illustrated by Figure E-2.

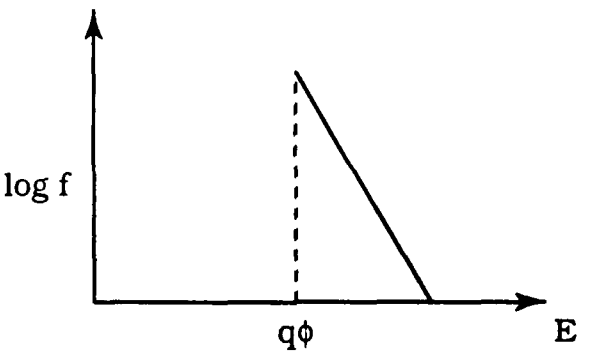

Figure E-2. **Accelerated Distribution**

In the absence of ions generated by some secondary source, there should be no ions at energies below the "cut-off" potential ($q\phi$).

The electrostatic analyzer (ESA) response to the accelerated, cold, ionospheric plasma is determined by the wide energy "window," set by the 11 percent $\Delta E/E$ detector characteristic. For example, at 6 keV, the energy window is approximately 660 eV wide. This should lead to a near delta function response by the ESA shown in Figure E-3. Data like this are shown in Figure 12e.

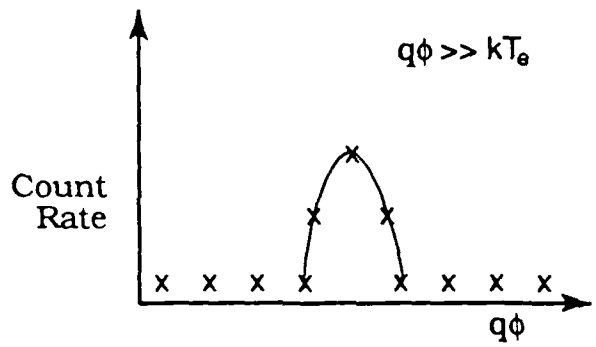

Figure E-3. **Delta Distribution**

The actual data does not always have this appearance. A much broader peak is reflected in the ESA response, as illustrated in Figure 12a. This is a result of one or all of the following:

1. The peak is missed due to incomplete energy sampling (primarily due to telemetry limitations). The modulation in Figure 9 is caused by this incomplete sampling.
2. Ionization of neutral gas(es) near the rocket.
3. Oscillation in the rocket potential at frequencies greater than 1 kHz.

In addition, ion fluxes well below the peak can be observed as a result of sputtering induced by 1-10 keV ambient O^+. [Ref. 11]

LIST OF REFERENCES

1. Rait, W. J., and Allred, Cpt. D. B., *Space Power Experiments Aboard Rockets SPEAR-1 Final Report to Defense Nuclear Agency*, Utah State University, Logan, Utah, October 1988.

2. Raitt, W.; Myers, N.; Roberts, J. A.; and Thompson, D. C., *SPEAR-1, An Experiment to Measure Current Collection in the Ionosphere by High Voltage Biassed Conductors*, Center for Atmospheric and Space Science, Utah State University, Logan, Utah. To be published in the NASA Conference Publication on "Workshop on Current Collection from Space Plasmas."

3. Gilchrist, B. E., et al., "Electron Collection Enhancement Arising from Neutral Gas Jets on a Charged Vehicle in the Ionosphere," *Journal of Geophysical Research*, v. 95, n. A3 (March 1, 1990).

4. Extract of the Statement of Work on the particle detector design for SPEAR-1. A copy was provided to the author by Dr. Roy Torbert during a meeting with him at the University of New Hampshire, May 17, 1990.

5. Conversation between the author and Dr. Roy Torbert, University of New Hampshire, May 17, 1990.

6. Allred, D. B., et al., "The SPEAR-1 Experiment: High Voltage Effects on Space Charging in the Ionosphere," *IEEE Transactions on Nuclear Science*, v. 35, n. 6 (December 1988).

7. Alport, M. J.; Antoniades, J. A.; Boyd, D. A.; Greaves, R. G.; and Ellis, R. F., "Electrical Breakdown at Low Pressure in the Presence of a Weak Magnetic Field," *Journal of Geophysical Research*, v. 95, n. A5 (May 1990).

8. Modeling was conducted by Ira Katz and co-workers of S-Cubed, San Diego, California.

9. Conversation between Dr. R. C. Olsen, Naval Postgraduate School, and Dr. Roy Torbert, University of New Hampshire. The energy sweep began 2 ms prior to the capacitor reaching peak voltage, so the first two steps in the sweep occurred during charging vice discharging.

10. Conversation among the author, Dr. R. C. Olsen, Dr. Roy Torbert, and Dr. Torbert's co-workers conducted at the University of New Hampshire, May 17, 1990.

11. Norwood, C. W., "Ions Generated on or Near Satellite Surfaces," Master's Thesis, Naval Postgraduate School, Monterey, California, June 1988, pp. 66–80.

12. Conversation between the author and Dr. R. C. Olsen, 1 June 1990.

BIBLIOGRAPHY

Katz, I., D. L. Cooke, D. E. Parks, M. J. Mandell, and A. L. Rubin, "Three-Dimensional Wake Model for Low Earth Orbit," *Journal of Spacecraft and Rockets*, 21, 125, 1984.

Katz, I., et al., "Structure of the Bipolar Plasma Sheath Generated by SPEAR-1, *Journal of Geophysical Research*, v. 94, n. A2 (February 1, 1989), pp. 1450–1458.

Langmuir, I., and K. B. Blodgett, "Currents Limited by Space Charge Between Concentric Spheres," *Physics Review*, v. 24, 49, 1924.

Mandell, M. J., I. Katz, and D. L. Cooke, "Potentials on Large Spacecraft in LEO," *IEEE Transactions in Nuclear Science*, NS-29, 1584, 1982.

Mandell, M. J., J. R. Lilley, Jr., I. Katz, T. Neubert, and N. B. Myers, "Computer Modeling of Current Collection by the CHARGE-2 Mother Payload," *Geophysical Research Letters*, v. 17, n. 2 (February 1990), pp. 135–138.

INITIAL DISTRIBUTION LIST

		No. Copies
1.	Defense Technical Information Center Cameron Station Alexandria, VA 22304-6145	2
2.	Library, Code 0142 Naval Postgraduate School Monterey, CA 93943-5002	2
3.	Department Chairman, Code Ph Department of Physics Naval Postgraduate School Monterey, CA 93943-5000	2
4.	Dr. R. C. Olsen, Code Ph/Os Department of Physics Naval Postgraduate School Monterey, CA 93943-5000	20
5.	Dr. S. Gnanalingham, Code Ph/Gm Department of Physics Naval Postgraduate School Monterey, CA 93943-5000	1
6.	Dr. J. Fennell M2/259 Aerospace Corporation P. O. Box 92957 Los Angeles, CA 90009	1
7.	Dr. J. B. Reagan Lockheed Palo Alto Research Laboratories 3251 Hanover Street Palo Alto, CA 94304	1
8.	Dr. D. Baker Code 609 NASA/GSFC Greenbelt, MD 20771	1

9. Dr. E. C. Whipple — 1
Center for Astrophysics and Space Science
University of California at San Diego
La Jolla, CA 92093

10. Dr. C. E. McIlwain — 1
Center for Astrophysics and Space Science
University of California at San Diego
La Jolla, CA 92093

11. Dr. I. Katz — 1
S-Cubed
P. O. Box 1620
La Jolla, CA 92038-1620

12. Dr. M. Mandell — 1
S-Cubed
P. O. Box 1620
La Jolla, CA 92038-1620

13. Dr. V. Davis — 1
S-Cubed
P. O. Box 1620
La Jolla, CA 92038-1620

14. Mr. Gracen Joiner — 1
Code 1114SP
Office of Naval Research
800 N. Quincy Street
Arlington, VA 22217

15. United States Space Command — 1
Attn: Technical Library
Peterson AFB, CO 80914

16. Space Systems Academic Group, Code 72 — 1
Naval Postgraduate School
Monterey, CA 93943-5000

17. Space Systems Curricular Office, Code 39 — 1
Naval Postgraduate School
Monterey, CA 93943-5000

18. MAJ Dan Allred — 1
HQ/DNA/RAEV
6801 Telegraph Road
Alexandria, VA 22310

19. Dr. Roy Torbert — 1
Space Science Center–IEOS
Science and Engineering Research Building
University of New Hampshire
Durham, NH 03824

20. Dr. Craig Kletzing — 1
Space Science Center–IEOS
Science and Engineering Research Building
University of New Hampshire
Durham, NH 03824

21. Mr. David Rau — 1
Space Science Center–IEOS
Science and Engineering Research Building
University of New Hampshire
Durham, NH 03824

22. Dr. David Cooke — 1
AFGL
Hanscom AFB, MA 01731

23. Dr. W. John Raitt — 1
CASS
Utah State University
Logan, UT 84322

24. Dr. Neil Myers — 1
Rome Air Development Center
Hanscom AFB, MA 01731

25. Dr. John Antoniades — 1
Laboratory for Plasma Research
University of Maryland
College Park, MD 20742

26. Dr. Ken Wright — 1
NASA/MSFC
Huntsville, AL 35812

27. Nagendra Singh — 1
Department of Electrical Engineering
University of Alabama
Huntsville, AL 35899

28. Dr. Henry Radoski 1
AFOSR/NP
Building #410, Bolling AFB
Washington, DC 20332

29. Dr. Nobie Stone 1
NASA/MSFC
Huntsville, AL 35812

30. Dr. Roger Williamson 1
Starlab
Stanford University
Palo Alto, CA 94305

31. Mr. Brian Gilchrist 1
Starlab
Stanford University
Palo Alto, CA 94305

32. Torston Neubert 1
Starlab
Stanford University
Palo Alto, CA 94305

33. Dr. Peter Banks 1
Starlab
Stanford University
Palo Alto, CA 94305

34. Dr. Hugh R. Anderson 1
SAIC
13400B Northrup Way, Suite 36
Bellevue, WA 98005

35. Dr. Douglas W. Potter 1
SAIC
13400B Northrup Way, Suite 36
Bellevue, WA 98005

36. Dr. W. F. Denig 1
Geophyics Laboratory (AFSC)
Hanscom AFB, MA 01731-5000

37. Dan Hastings 1
Department of Aero. and Astro.
MIT
Cambridge, MA 02139

38. Thurston Van Horn
P. O Box 425
Colby, KS 67701

5